Modeling of Static and Dynamic Components of Cutting Force in Sawing

By

RODRIGO ECHEVERRI

B.A.Sc., Universidad de Norte, Colombia, 1998

A THESIS SUBMITTED IN PARTIAL FULFILMENT OF

THE REQUIREMENTS FOR THE DEGREE OF

MASTER OF APPLIED SCIENCE

in

THE FACULTY OF GRADUATE STUDIES

(Department of Mechanical Engineering)

We accept this thesis as conforming

to the required standard

THE UNIVERSITY OF BRITISH COLUMBIA

June 2003

(Rodrigo Echeverri)

Department of Mechanical Engineering

The University of British Columbia

Vancouver, Canada

Date June 19th/2003.

ABSTRACT

The research presented in this thesis is directed towards the development of models for the calculation of cutting forces in bandsaws. The motivation for this work is the search for a solution to the washboarding problem in sawing. Washboarding is a cutting accuracy problem that is often found in sawmills which causes losses in material and labor.

The first chapter of this thesis presents a literature review of previous research conducted both in cutting mechanics and the washboarding problem. The references consulted indicate that the presence of lateral cutting forces is caused by unbalanced chip loads on the saw teeth during vibration. A survey in the literature in wood cutting reveals that no previous research is available which can be directly applied for the estimation of these lateral cutting forces in bandsawing. Therefore a series of models from metal cutting are studied and their application to wood cutting considered.

The body of the work divides the cutting process in two major, independent components. The first part is the static process that would occur under unbalanced chip loads but no tool vibration. The second part is the portion of the process that creates components of force which depend upon the kinematics of the cutting process.

A series of cutting models to estimate the forces under static conditions in bandsawing are proposed in the second chapter of the thesis. The third part of the work shows the development of a series of fundamental models that cover the analysis of the dynamics of the simple orthogonal cutting process. The theories proposed in that section are compared to the findings of other researchers and it is concluded that the model improves the understanding of the cutting process during tool vibrations. The fourth section of the work provides a series of experimental results that support the developments achieved for the static portion of the cutting force model for bandsawing. Finally, the last chapter of the thesis presents a series of conclusions and suggestions for reducing the washboarding problem by decreasing the magnitude of the lateral forces exerted in a vibrating bandsaw tooth.

TABLE OF CONTENTS

LIST OF FIGURES

LIST OF TABLES

NOMENCLATURE

C:	Bandsaw blade speed
V_f:	Feed speed of the log into the saw
K_w:	Kerf width
γ:	Rake angle
F_m:	Main cutting force
F_L:	Lateral cutting force
F_f:	Feed cutting force
α_R:	Radial angle
α_T:	Tangential angle
b:	Bite
K_L	Lateral cutting force coefficient
T	Period between consecutive teeth
β:	Friction angle
ϕ:	Shear angle
τ	Shear stress
k_1	Chip thickness coefficient
k_2	Chip thickness rate of change coefficient
h:	Chip thickness
h_o:	Mean uncut chip thickness
h_c:	Cut chip thickness
δ_o:	Outer surface slope
δ_i:	Inner surface slope

A_i	Inner surface amplitude
A_o	Outer surface amplitude
C_s:	Multiplying factor to relate shear angle and surface slope
V_o:	Cutting velocity
ψ:	Chip flow angle
Δ:	Lateral displacement of the sawblade
P_x	Washboarding pitch in the feed direction
P_y	Washboarding pitch in the cutting direction
A_c	Uncut chip area
K_{fc}:	Orthogonal cutting constant due to shearing in the feed direction
K_{fe}:	Orthogonal cutting constant due to edge effects in the feed direction
K_{mc}:	Orthogonal cutting constant due to shearing in the main cutting direction
K_{me}:	Orthogonal cutting constant due to edge effects in the main cutting direction
V_s:	Shear velocity
w	Power spent in the cutting process
V_c:	Chip velocity
k	Shear cutting stress
C_f	Friction multiplier
ϕ_s:	Side shear angle
ϕ_m:	Main shear angle
A_T:	Total area of shear
F_c:	Cutting force due to shear
F_e:	Cutting force due to edge effects
P:	Depth of ploughing penetration
L:	Length of the projection of the tool face in ploughing
κ:	Negative hook created by the presence of a nose radius in a tool

ε:	Angle of flow in the intermediate region in ploughing
σ:	Angle made by the back shear plane in ploughing
R	Resultant cutting force
F_s	Shear force
L_f	Length of plastic friction region on the face of the tool
r	Radius of the nose of the tool
f	Frequency of tool vibration

ACKNOWLEDGEMENTS

I wish to sincerely thank Dr. Ian Yellowley for providing me with this unique research opportunity and helping me with invaluable guidance, excellent suggestions, encouragement, care and attention throughout my studies at UBC.

I would also like to thank Dr. Stanley Hutton for his guidance and support during my studies. I believe he has made me a better professional in all respects by encouraging me to put my best efforts in my research and by teaching me how to think independently and question my own ideas and work.

My deepest love and gratitude is felt for my mother and family for their never ending encouragement and support. This would not have been possible without them.

I must also thank my colleagues and lab mates Zhusan Luo, Haocheng Wang, Kevin Oldknow, Chris Mytting, Michael Dalziel and Mathieu Bouvier for their company, advice, support and unconditional friendship.

CHAPTER I

"If a fool persists in his folly, he would become wise."

- William Blake

1. INTRODUCTION AND OVERVIEW

1.1. Background

The invention of the bandsaw was first claimed by William Newbury in 1808. Early bandsaw machines and their blades were plagued with every problem imaginable, and many which could not be imagined. Changes were continuously implemented during the several years that it took to develop the knowledge to make the wide bandsaw practical. In spite of the difficulties encountered, bandsaws have many advantages such as their continuous cutting action. Bandsaws are used extensively in the wood cutting industry from primary log break down to various resawing operations in sawmills. This extensive use of wide bandsaws results from their ability to cut a wide range of primary log sizes, to operate at high cutting speeds, and to remove a minimum amount of material during cutting. Due to the relatively thin saw-blades used, bandsaws are also more suitable for making deeper cuts than are circular saws since less wood is lost.

Even though many of the difficulties associated with sawblades have been overcome, some key problems still remain. Most of the problems encountered today are related to the dynamic characteristics of the sawblade as well as the cutting process itself. One such problem commonly known as "washboarding" is particularly problematic in the wood sawing industry, and has been a topic of ongoing research for several years [1]. This problem is characterized by a washboard-like pattern in the finished sawn surfaces, and is caused by resonant vibration of the sawblade at high frequencies. This pattern can be easily seen in the sawn boards and it requires planning in order to be removed. This is of course undesirable because of the associated wood loss and additional secondary operations required.

The major problems involved in the study of the washboarding phenomenon are:

1) To develop a better understanding of the dynamics of the sawblade and bandmill systems

2) To understand the forces acting upon the blade which are responsible for the deviation from its intended path

3) To identify potential improvements that can be implemented in sawblade design in order to eliminate the washboarding problem

This thesis deals with the last two points above. The discussion concentrates on an experimental and analytical study of the factors that influence the cutting forces in sawing including saw tooth geometry, dynamics of the cutting process and geometry of the chip loads applied upon vibrating saw teeth.

1.1.1. Bandsawing Process

A schematic representation of the bandsawing process is shown in Figure 1-1. The blade moves downward into the log with cutting velocity *C*, the log is fed horizontally into the blade with a feed velocity V_f. The solid wood in the path of the teeth is severed into tiny chips. The bottom wheel is driven by an electric or hydraulic motor through a belt drive. The top wheel is lifted by a hydraulic system which tightens or 'strains' the blade. This blade 'straining' process is performed before operating the mill and its purpose is to stiffen the blade.

Two pressure guides made of reinforced rubber are supported on two guide arms connected with the vertical column of the mill frame. The purpose of these guides is to stabilize the blade in the cutting region. During cutting the wood is supported by the carriage and passes through this span of blade.

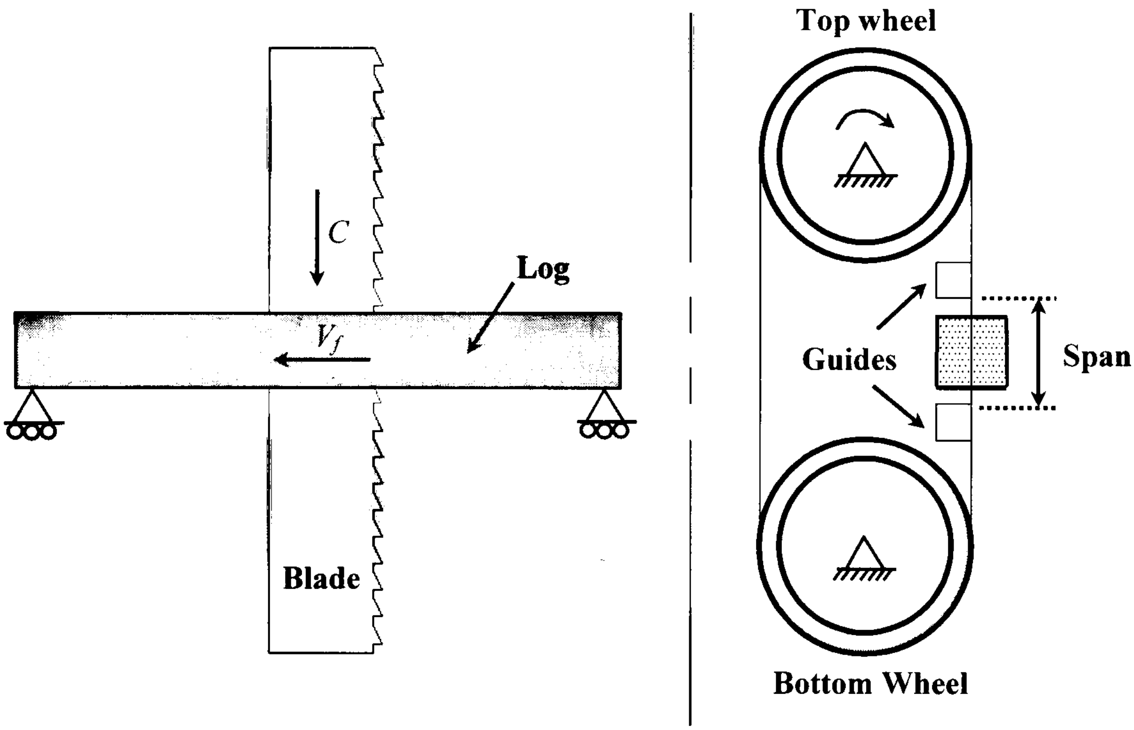

Figure 1-1. Schematic representation of the bandsawing process

1.1.2. Washboarding Problem

As mentioned in Section 1.1, washboarding is a sinusoidal pattern that can be often found on the surface of sawn wood like the one shown in Figure 1-2. Lumber with washboarding is not acceptable since this pattern increases the deviation of the board thickness from the target size, which is a parameter of sawing quality in the lumber industry. As a result, boards have to be cut thicker than the target size and then planed, which transforms into material losses, additional labor and the need for more machining equipment.

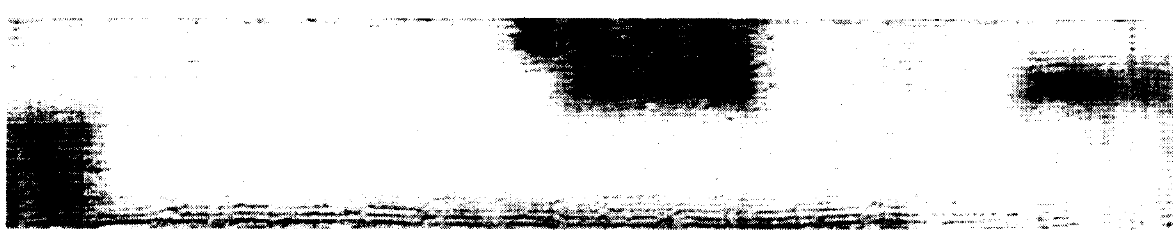

Figure 1-2. Washboarding pattern

Washboarding is a problem that sawmills have always dealt with but one for which a solution has still to be found. Most sawmills experience at least some degree of washboarding, and although in practice different measures are taken to decrease the problem, such as changing the feed speed, the blade speed or even the blade itself, these modifications are often time consuming and limited in effectiveness. The main reason for the lack of success in finding a practical solution to the problem is that the washboarding phenomenon is still poorly understood.

1.1.3. Bandsaw Blade Geometry

A bandsaw blade is a toothed strip of steel welded to form a continuous loop with teeth along one or both edges. The toothed region of a saw blade is shown in Figure 1-3. The open space in front of a tooth is called the gullet. This space holds sawdust when the tooth is cutting. The sawdust produced will be stored in the gullet and released at the bottom of the log. If more sawdust is produced than the gullet can accommodate it will be spilled between the sawn surfaces and the blade. Bandsaw blades with deep gullets are used for cutting soft wood and can be run at higher feed speeds than blades with smaller gullets, which are used for hard wood and can only handle low feed speeds. Deeper tooth gullets are used when high feed speeds are required but increasing the depth of the gullet has also been found to increase washboarding.

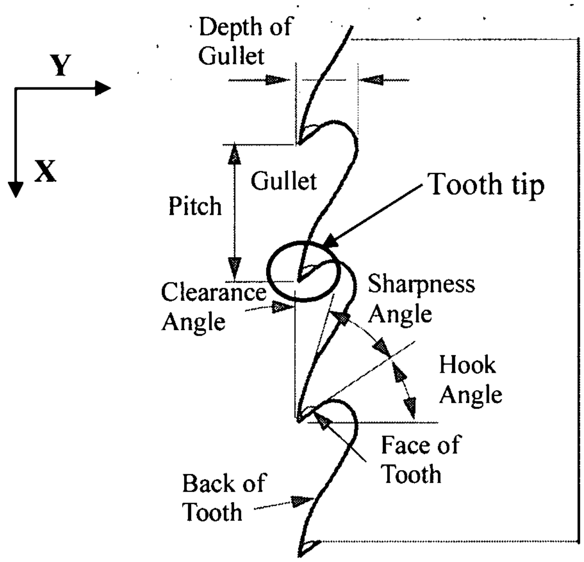

Figure 1-3. Wide bandsaw blade geometry [1]

Pitch is the distance between two consecutive teeth. It ranges from 44 to 76 mm. In practice, small pitches are found to produce smoother surface finish but only allow for low feed speeds as mentioned above [2]. Hook is the angle of the tooth face with respect to the feed direction as shown in Figure 1-3. A generally accepted rule is that softwoods require a greater hook angle than hardwoods. Typical values are 25 to 30 degrees for softwood, 20 degrees for medium density wood and 15 degrees for hard wood [2].

In order to prevent the back of the tooth tip from rubbing the wood during cutting there must be a certain amount of clearance. This is provided by the clearance angle, measured between the line made by the tooth tips and the back of the tooth.

In practice, the type of blade used has been found to have great impact in the presence of washboarding. Thicker blades are known to produce less washboarding. However, they produce wider kerf, which leads to material waste and therefore are not desired.

1.1.4. Saw Tooth Tip Geometry

Only a small part of the blade shown will come in contact with the wood during the cutting process. This part corresponds to the encircled region labeled "Tooth tip" in Figure 1-3. This portion of the tooth contains a number of geometrical parameters that affect the cutting forces during bandsawing. This geometry is shown in detail in Figure 1-4 with some typical values for the variables.

Figure 1-4 shows the thickness of the chip being removed from the workpiece, called *bite* in the lumber industry; the *gauge* or thickness of the sawblade; the *kerf,* which corresponds to the width of the main cutting edge; α, the back clearance angle and γ, the hook angle of the tooth.

Three orthogonal components of force act on the saw tooth, the main force F_m, also called tangential force, the feed force F_f in the plane of the blade, and the lateral force perpendicular to this plane. The direction of the forces acting on the tooth is shown with respect to a local coordinate system placed in the middle of the main edge of one tooth.

Region ABCDEF in Figure 1-4 is the portion of the tooth that is in contact with the wood during cutting. Points ABCD and ABF define two regions of importance. The plane ABCD is located on the face of the tooth and contains all three cutting edges. The geometry and orientation of these edges influences the cutting forces applied to the tooth. The plane ABF corresponds to the lateral face of the tooth, which is the one being pushed sideways towards and from the wood while the tooth vibrates.

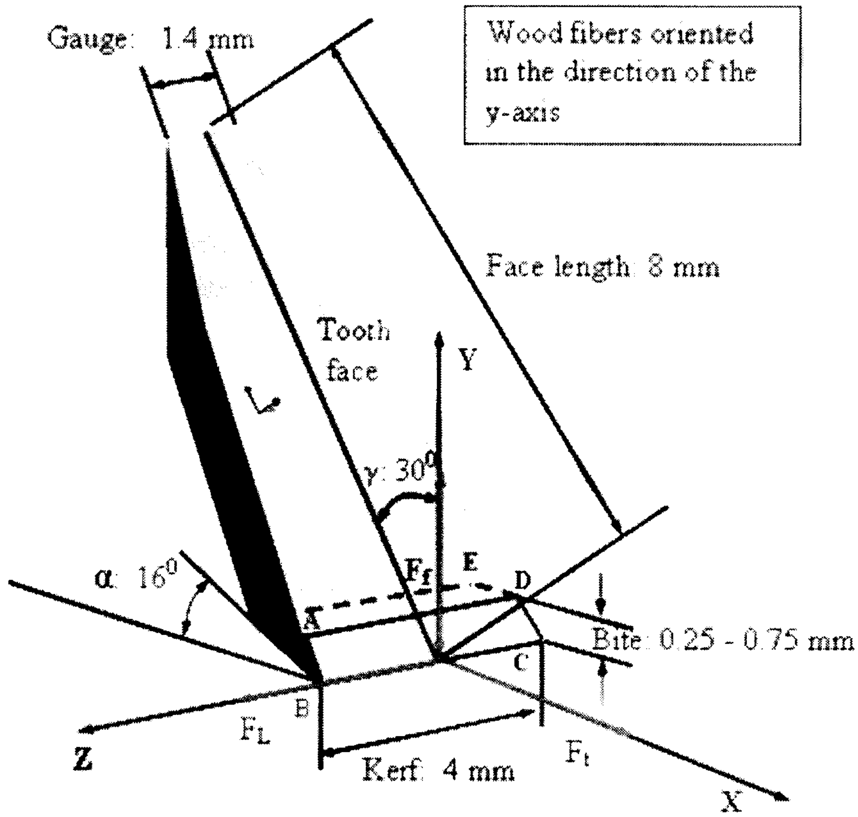

Figure 1-4. Three-dimensional view of a saw tooth and typical values of variables

When examining the saw tooth, three clearance angles are found. The clearance angle α, has already been defined above. Two other angles cannot be clearly seen in Figure 1-4 and therefore two more views are required to thoroughly describe the geometry.

As shown in Figure 1.5, the plane of the face of the tooth, ABCD, differs from a rectangle by virtue of a clearance angle called the *radial angle*, which will be noted as α_R in this thesis. Typical values for this variable range between 5 and 7 degrees in wood bandsaws. Another important variable that can be seen on this plane is the distance between the side of the tooth tip and the side of the blade, which is called *side clearance*. This distance helps avoid rubbing between the saw tooth and the sides of the kerf.

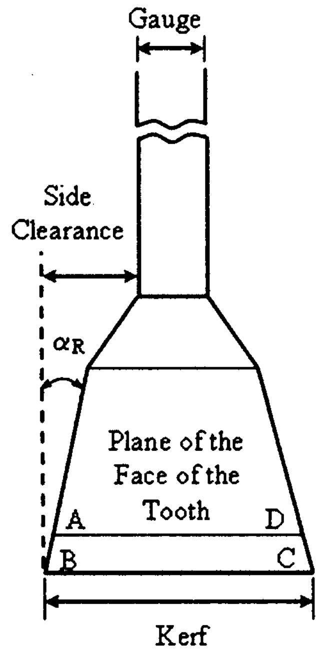

Figure 1-5. View of the plane that lies on the face of the tooth

The plane that crosses points ADEF, parallel to plane XZ, contains the tangential angle, which provides clearance with respect to the flank conducted by edges AB and CD. This angle is shown in Figure 1-6 and will be noted as α_T in this work.

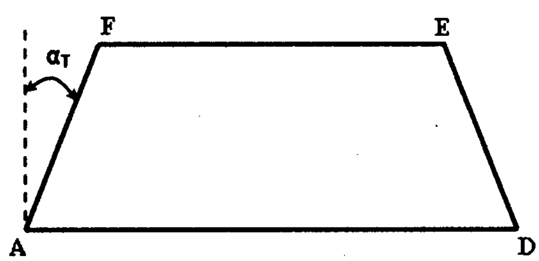

Figure 1-6. Cut-away view of the tooth through the plane ADEF

1.1.5. Saw Tooth Defects

In the process of saw manufacturing and preparation, a large amount of effort is devoted to swaging and setting of the teeth and also to the leveling, tensioning and straightening of the blade. One of the goals of this process is to make all the teeth in a sawblade identical and follow each other in a straight line in order to avoid unbalanced chip loads. However, it is evident that this goal is quite ambitious and is not fully achieved in practice. Saw tooth defects have been identified to cause unbalanced lateral forces acting on saw teeth [12]. Also, sawblades are often subjected to extreme operating conditions during use, which can distort their original geometry. There is a need to understand how these defects affect cutting accuracy in order to improve the sawing process. The following table presents a summary of common tooth and preparation defects.

Table 1-1. Saw Tooth Defects

Defect	Possible Causes	Figure
Tooth face obliquity	Under ideal conditions, the face of the grinding wheel should be perpendicular to the centerline of the sawblade during sharpening. If the wheel is swiveled by an amount θ_G, the face of all teeth will become oblique with respect to the direction of the cut. This defect will cause a consistent lateral force applied to all teeth on the blade.	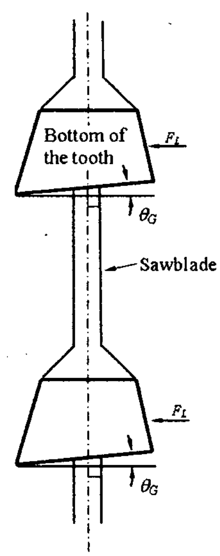
Bent tooth	Improper punching of the teeth in a new sawblade can produce localized tooth bending. This defect is not corrected automatically during leveling, tensioning or straightening and therefore it must be corrected manually and it might not be detected before the blade is put in operation.	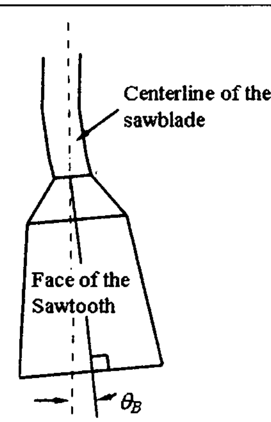

	A bent tooth will cut an unsymmetrical chip load that yields lateral forces. The presence of bent teeth can be tracked on the cut wood boards since a visible mark will be left behind by the bent tooth for every revolution of the band.	
Broken corners	In practice, after a sawblade is put in operation, it is found that some saw teeth present damaged corners. This defect is produced when the teeth impact knots or could also be caused by imperfections in the manufacturing of the blade.	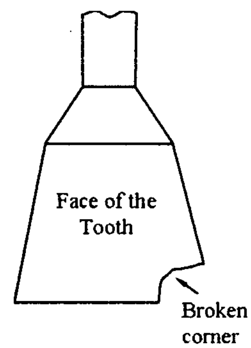
Tooth misalignment	One of the steps in sawblade preparation is the straightening of the saw teeth. A misalignment error as small as a fraction of a millimeter is likely to produce unbalanced chip loads on the saw teeth that will produce lateral forces.	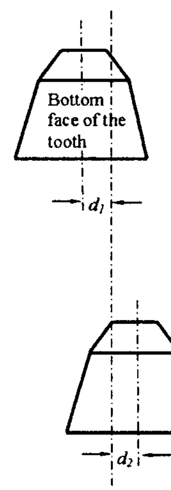
Tooth face asymmetry	The radial angle in sawblades is set during swaging. The shaping dies that produce these angles must have the same setting and angle during the process. However misalignment and wear on the swage can cause the face of the tooth to be asymmetrical.	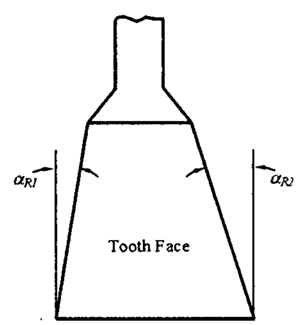

1.2. Previous Research

The dynamics and stability of a sawblade during washboarding have been investigated quite thoroughly by a number of authors [1, 3, and 7]. This work has provided some understanding of the mechanisms that produce washboarding. However, the problem also presents the challenge of modeling the forces applied to the blade during cutting, which has not yet been addressed. These forces need to be included in the models for the stability analysis of the sawing process as the forcing function component of the equation of motion of the blade. The development of such a force model for bandsawing requires a high degree of understanding of the wood cutting process, which is not available at this time. Due to this fact, the review provided here considers in detail previous developments in the area of metal cutting, which have been applied to the analysis of the stability of the turning and milling processes. These models can provide some understanding of the physics of the cutting force functions in washboarding but need to be expanded in order to be applicable to wood machining processes such as sawing.

1.2.1. Washboarding

Tian [3] studied the washboarding phenomenon in unguided circular saws. He investigated the instability of the saws subjected to multiple regenerative and follower cutting forces. In his work, Tian conducted a series of tests, which showed that the maximum amplitude of vibration of the saw blade during washboarding decreased as the feed speed of the wood increased. This finding ruled out the tangential and feed forces as being the cause for the washboarding pattern that was produced since these forces will most likely increase with the feed rate. The conclusion for his experiments was that lateral regenerative cutting forces were the cause of the problem. A regenerative force is one that depends upon the displacement of the tooth currently in the cut compared to the displacement of the previous tooth. Regenerative forces have been found before to be the cause of instabilities in the chatter problem in machine tools [4, 5 and 6].

In order to illustrate this idea, two consecutive teeth are shown in Figure 1-7. Case (b) shows a larger bite than case (a) but the same lateral displacement for two consecutive teeth. It can be seen how the extra lateral cutting area is smaller when the bite is larger and therefore the lateral force should also be smaller.

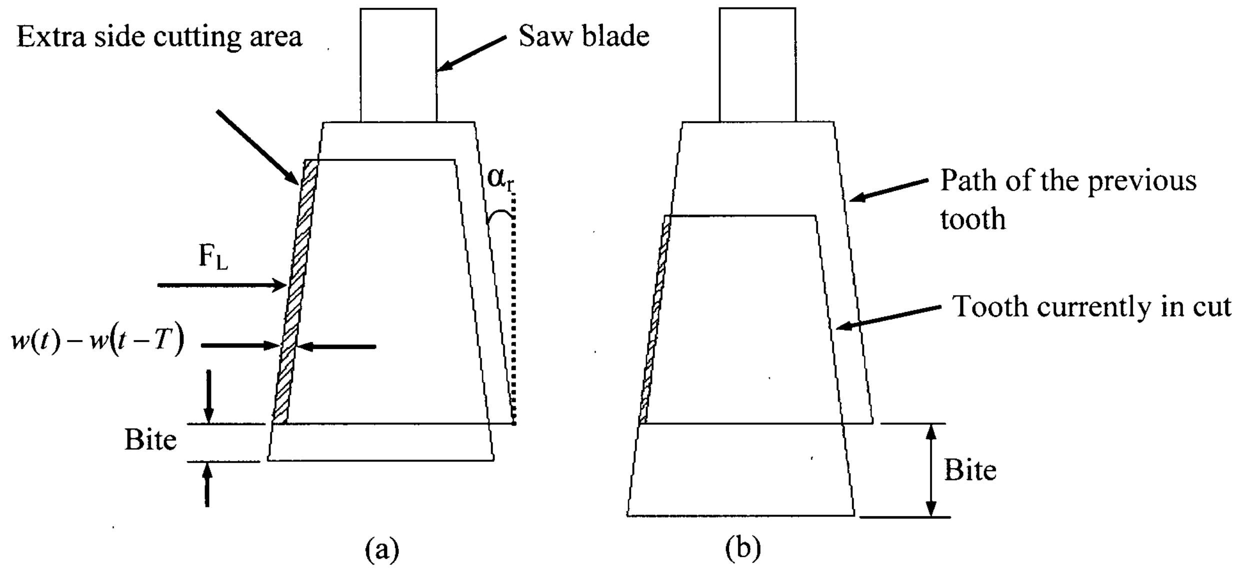

Figure 1-7. Effect of the bite on the lateral cutting forces

Luo [1] studied the washboarding problem in bandsaws. He determined the stability regions of the saw blade subjected to the regenerative lateral cutting forces and the system damping. The regenerative forces in Luo's work were defined as:

$$F_L = -K_L\left[w(t) - w(t-T)\right] \tag{1.1}$$

Where K_L is the regenerative cutting force coefficient, $w(t)$ is the lateral displacement of the current tooth, T the period between teeth and $w(t-T)$ is the lateral displacement of the previous tooth. The difference $w(t)-w(t-T)$ corresponds to the lateral chip thickness at time t as shown in Figure 1-7.

In Luo's study, the regenerative cutting force coefficient was not determined. Also, the influence of the lateral velocity of the blade on the flank cutting force was not taken into account. It will be seen later in this chapter that researchers in metal cutting have found that the surface slopes have an important impact on the characteristics of the dynamic cutting forces. Consequently, an experimental investigation into bandsaw lateral cutting forces will be conducted in order to gain thorough understanding of the mechanism of washboarding.

1.2.2. Wood Cutting

Franz [8] conducted one of the first pieces of fundamental research in wood cutting mechanics. He concentrated his study on the forces produced in cutting along the grain. His main finding was that in this direction, one of three different types of chips would be formed depending upon the cutting conditions. He called these chips types I, II and III. Chip type I is formed when positive rake angles over 20 degrees and large bites (more than 0.5 mm) are used. The wood splits ahead of the tool by cleavage until failure in bending as a cantilever beam occurs. Chip type II is a continuous type chip that is produced when the wood fails along a single plane that extends from the tool edge to the workpiece surface. This type of cutting mechanism is similar to the one in metal cutting and is desirable in wood machining because it produces excellent surface finish. Chip type III occurs when the tool forces cause compression and shear failure of the material ahead of the cutting edge. These conditions arise when negative or small rake angles are used in combination with small bites.

Franz also found that when chips type I and III are formed, the cutting forces are cyclic in nature. In contrast, he observed that continuous type chips produced constant forces, which reflect the homogeneity of this type of cutting process. Under these conditions, the chip typically assumes the form of a smooth spiral with a radius that depends upon the uncut chip thickness.

A model for the prediction of the chip type formation was proposed in [8] based upon an evaluation of the applicability of metal cutting theories to wood cutting. Franz questioned the assumption made in metal cutting that the resultant force system applied to the face of the tool is collinear with the one applied on the fracture plane in the workpiece. If this assumption is not valid in wood, then the force moment acting in the cutting region could determine the failure mechanism by which the chip is created. Franz validated this theory against his experimental data and found that the chip type to be produced in planning of wood can be predicted. The only information necessary for this prediction is the rake angle of the tool, the coefficient of friction between the tool face and the chip and the intended chip thickness.

McKenzie [9] studied the effect of cutting velocity on the wood cutting forces. He found that in the range of practical wood machining the effect of speed on the cutting forces is negligible.

This researcher also conducted experimental and analytical studies of the cutting process in the direction perpendicular to the grain. This type of operation is usually called ripsawing in the wood working industry. The experiments showed that a series of different chip formation mechanisms take place when cutting perpendicular to the grain. Depending upon the rake angle of the tool, the wood species and the moisture content of the wood sample, failure was found to take place either below or above the plane of cutting. When the wood below the cutting edge has been damaged, the next pass of a tool on that surface will create forces that are much lower than the ones found for the first pass since the workpiece has partially failed already. This phenomenon is produced by the fact that the wood fibers separate and bend under the cutting plane, causing localized failure regions. A series of analytical models to predict the cutting forces for ripsawing given the material properties and the cutting parameters were presented and validated in this work.

A shortcoming for the applicability of the work reported in [9] is that the models presented were validated in a series of orthogonal cutting tests in which there is no material surrounding the cutting region (i.e. the cutting edge is wider than the workpiece). However, in most ripsawing processes, the material around the cut provides resistance to the fibers below the cutting plane against bending. This in effect means that the cutting forces for a constrained workpiece will be most likely lower than those estimated by McKenzie since a portion of the work is wasted on the bending of the fibers in the non-constrained case.

St. Laurent [12] studied the effects of sawtooth edge defects on the cutting forces in bandsawing. He conducted a series of experiments using damaged saw teeth attached to a force transducer. A wood specimen was placed on a guided holder and pushed onto the saw tooth traveling in a linear slow motion and the cutting forces were measured. The results showed that small defects on the corners of teeth resulted in lateral forces values of up to 27% of the main cutting force when the size of the defect was about one bite. It was also found that the departure of the main edge of the tooth from perfect orthogonal cutting conditions produced consistent lateral forces. These forces became about 20% of the main cutting force when the angle of deviation reached about 10 degrees.

1.2.3. Metal Cutting

Extensive research has been conducted in metal cutting since the 19th century. One of the most important contributions in this area is the analysis of the orthogonal cutting process conducted by Merchant [14]. Orthogonal cutting occurs when a tool wider than the workpiece removes material with its main edge perpendicular to the cutting velocity. Even though this is the simplest cutting case possible, it provides an important understanding of the physics involved in the cutting process.

When the tool vibrates during orthogonal cutting, a more complex situation than that of orthogonal cutting arises. This process is known as dynamic cutting and it has received great attention for being of fundamental importance for the understanding of the self-induced vibration problem in machine tools, called *"Chatter"*. In this case, the forces produced on the tool are not only dependant upon the chip thickness but also on the instantaneous cutting velocity of the tool and other factors such as the instantaneous tool velocity.

Even though the orthogonal and dynamic cutting analyses provide force models for the most simple chatter cases, the situation in bandsawing involves a tool that has multiple cutting edges. The static forces produced in cutting with a multi-edged tool have been studied in the past usually with the aim of developing models for the chip flow in turning.

In order to develop an understanding of the cutting forces produced during washboarding, a thorough analysis of the three-dimensional dynamic cutting process is needed. No previous attempts to solve this complex problem have been found at this point by the author.

1.2.3.1. Orthogonal Cutting

Although the most common cutting operations are three dimensional and geometrically complex, the simple case of two-dimensional orthogonal cutting is used to explain the general mechanics of metal removal. Merchant [14] developed an analysis of the orthogonal static metal cutting process based on the assumption that all the deformation in the process occurs in a thin layer zone called shear plane. This process is shown in Figure 1-8.

A metal chip with a width of cut b (normal to the paper) and chip thickness h is being sheared away from the workpiece. In the orthogonal case, cutting is assumed to be uniform along the cutting edge; therefore the process can be considered to be a two-dimensional plane strain deformation process without side spreading of material. R is the resultant force applied to the chip by the tool and it can be resolved in main and feed force components as shown in Figure 1-8. These forces are given by the following expressions:

$$F_m = hb\tau \frac{\cos(\beta - \gamma)}{\sin(\phi)\cos(\phi + \beta - \gamma)} \tag{1.2}$$

$$F_f = hb\tau \frac{\sin(\beta - \gamma)}{\sin(\phi)\cos(\phi + \beta - \gamma)} \tag{1.3}$$

Where τ is the shear stress assumed to be uniform over the shear plane AB, ϕ is the shear angle, γ is the hook angle and β is the apparent friction angle on the face of the tool. From the above expressions the cutting forces may be determined, provided that the shear stress, friction angle and shear angle are all known. Initially, Merchant considered that τ would have the same value as the yield stress for the work material and that β would have the usual value for dry sliding friction. Later he identified that τ would have to be measured from cutting tests because the high strain rates in metal cutting invalidate the static test data found in material handbooks. Also, β has to be measured from cutting tests since the friction condition on the tool face is a combination of plastic and elastic friction. Therefore just a sliding friction model does not yield good results.

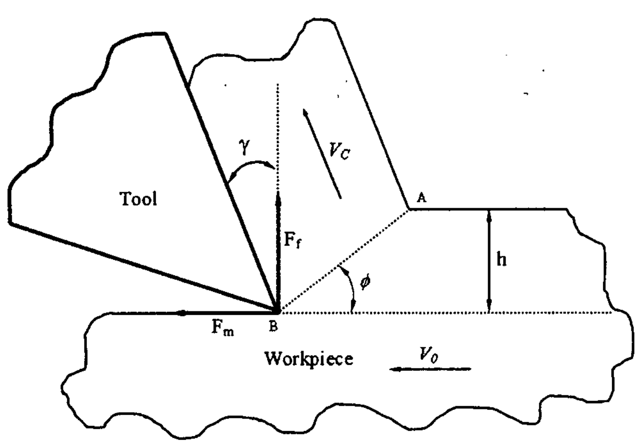

Figure 1-8. Orthogonal cutting process

The shear angle is a metal cutting characteristic that defines the geometry of the deformation within the metal being cut. Merchant applied the principle of minimum energy, which implies that ϕ adjusts itself so that the power consumed in the process is a minimum. He derived the following equation for ϕ:

$$\phi = \frac{\pi}{4} - \frac{1}{2}\beta + \frac{1}{2}\gamma \qquad (1.4)$$

This theory has been criticized in the metal cutting research community because there is no physical evidence for it even though the concept is intuitively appealing [15].

Lee and Schaffer [16] applied the theory of plasticity for an ideal rigid-plastic material, and assumed, like Merchant, that the deformation occurred within a constantly stressed zone. They considered that there must be a stress field within the chip to transmit the cutting forces from the shear plane to the tool face. This was represented as a slip-line field in which no deformation occurs although it was stressed up to the yield point. They proposed the following shear angle relationship:

$$\phi = \frac{\pi}{4} - \beta + \gamma \qquad (1.5)$$

None of the equations proposed above yields quantitatively accurate predictions for the shear angle due to the oversimplified assumptions embedded in them. However, they provide some understanding of the factors that influence the forces in the static cutting process.

Researchers in the metal cutting area concluded that since the number of unknown factors in the cutting process is large, a unique value of the shear angle might not exist [15]. Thus it has been suggested that any analysis should not be directed at establishing a single relationship, but instead should locate the possible bounds within which the shear angle must lie.

1.2.3.2. Dynamic Cutting

The effect of tool vibrations on the cutting forces has been studied extensively in metal cutting in a search for the solution of the machine tool chatter problem. The research efforts by Tobias [19], Albrecht [20], Tlusty [21], Wu [22, 23] and Wallace and Andrew [24, 25] towards the understanding and modeling of this dynamic cutting process showed that the forces depend on the instantaneous chip thickness and the slope of the inner and outer surfaces. The dynamic cutting process is illustrated in Figure 1-9 and will be considered in this section.

The trajectory of the tool shown is defined by function $y(t)$, which corresponds to the inner surface of the cut as shown in Figure 1.9. The outer surface of the cut is defined by $y(t-T)$, which is the path of a previous tool pass. The instantaneous chip thickness is $dh(t) = y(t) - y(t-T)$ and the rate of change of the chip thickness is $d\dot{h} = \dot{y}(t) - \dot{y}(t-T)$. Assuming the vibration amplitude of the tool for the previous pass is A_o, the length of that wave λ_o and the slope of the surface created measured at the end of the shear plane, δ_o. At the instant shown, the tool also vibrates with amplitude A_i; the length of the corresponding wave left on the surface is λ_i and the slope of the inner surface is δ_i. F_m corresponds to the main cutting force and F_f to the feed force. ε is the phase shift between the inner and the outer wave, ϕ the instantaneous shear angle, γ the rake angle of the tool and V_0 the tangential speed of the cut.

The oscillating component of the cutting force was considered by Tobias [19] to be a function of two independent factors $F(h, \dot{h})$ for the case in which the tool only vibrates in the vertical direction Y shown and cuts at constant tangential speed V_0.

$$dF(t) = k_1 dh(t) + k_2 d\dot{h}(t) \tag{1.6}$$

Where $dF(t)$ is the oscillation of the cutting force, $dh(t)$ the instantaneous chip thickness, k_1 the chip thickness coefficient, $d\dot{h}$ the rate of chip thickness change and k_2 the chip thickness rate of change coefficient.

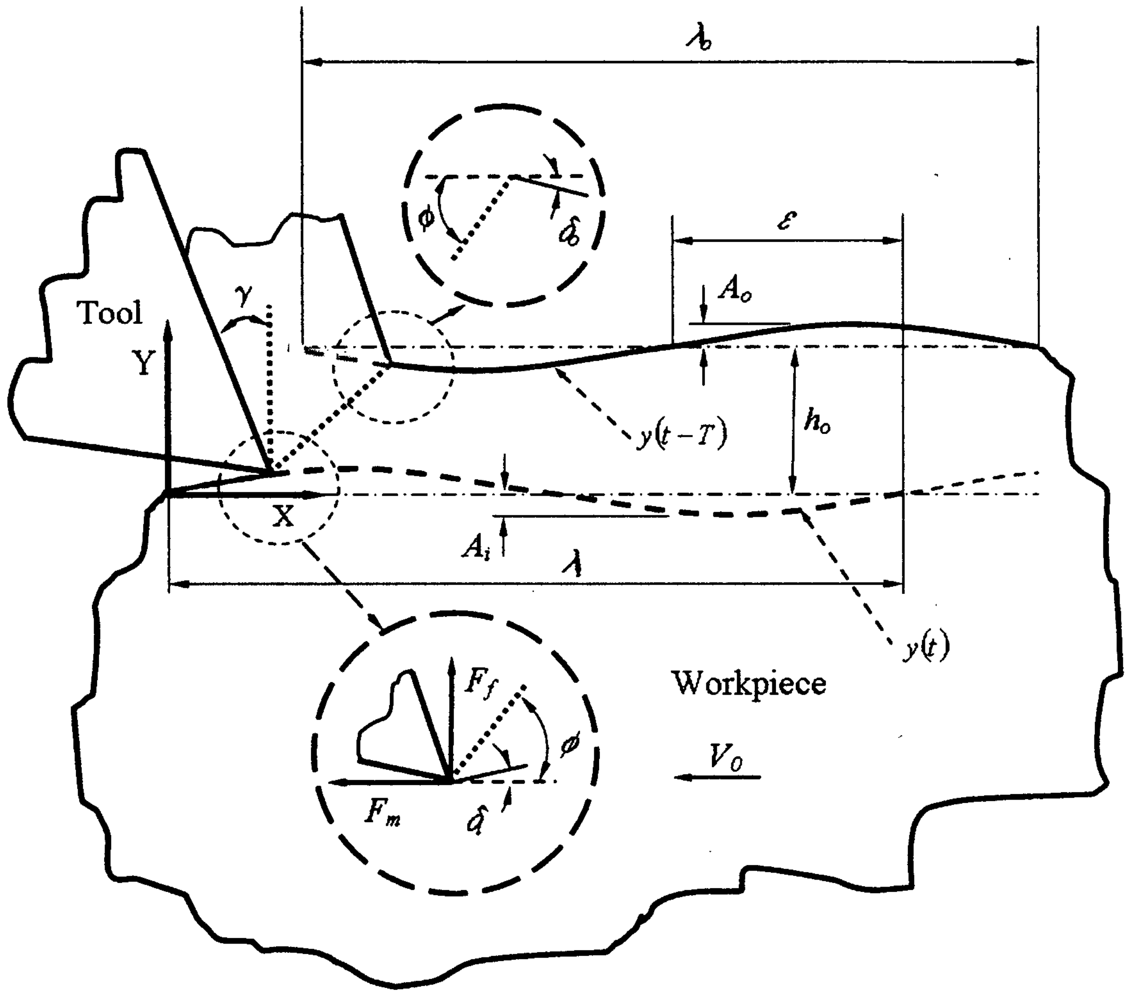

Figure 1-9. Dynamic cutting process

The dynamic cutting problem has been subdivided, by the researchers in the area, as the superposition of two different mechanisms called "Wave removing" and "Wave cutting" in order to separate the different factors that affect the cutting forces for each situation.

In wave removing, a rigid tool cuts a wavy surface. Albrecht [20] explained that the force in this case would be proportional to the chip thickness and the slope of the outer surface. Previous investigations into the dynamic metal cutting process by employing high-speed cameras have confirmed that the shear angle oscillates during cutting [26]. The process studied by Albrecht is shown in Figure 1-10.

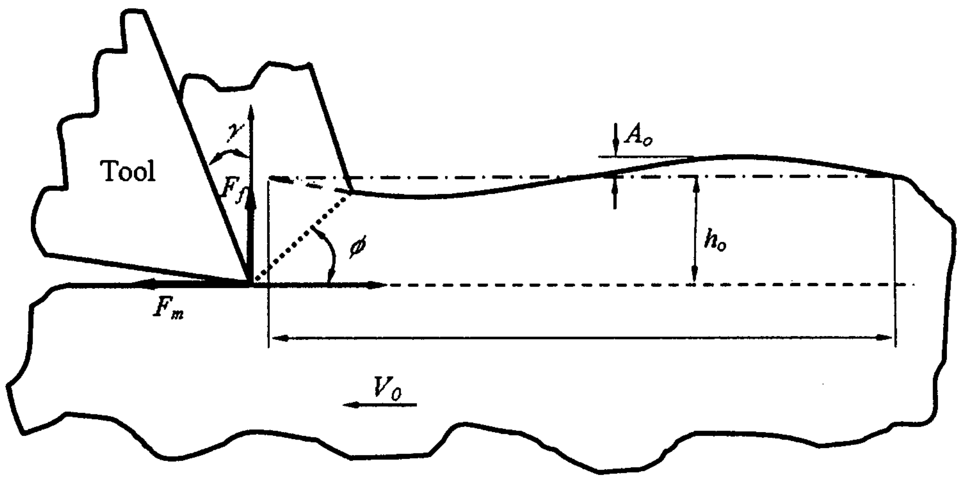

Figure 1-10. Wave removing process

Consider the case in which a tool is removing a chip from a surface, which has a slope δ at the free end of the shear plane with respect to the direction of the tangential cutting speed as shown in Figures 1-11b and 1-11c. The cutting force has been found to be different with respect to the case in which the tool is cutting a flat outer surface for the same instantaneous chip thickness. This change in the forces has been found by the researches in metal cutting to be caused by a variation of the position of the shear plane.

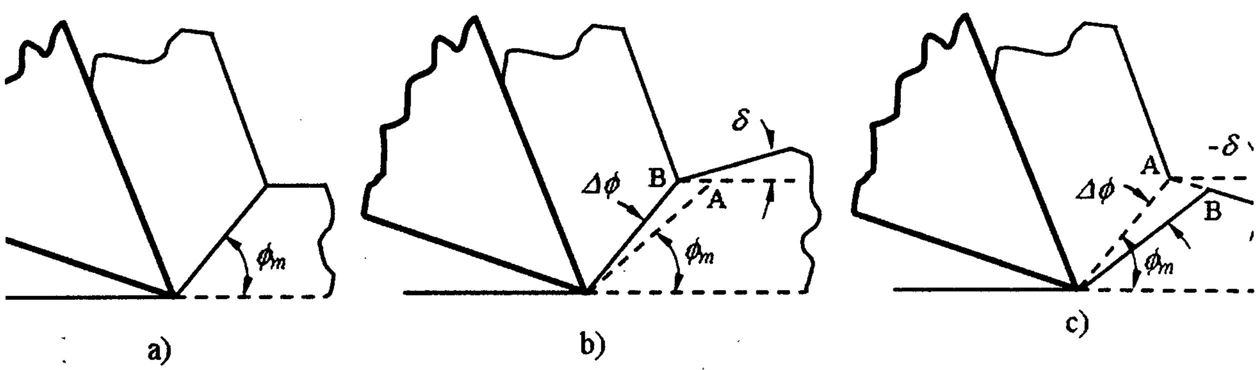

Figure 1-11. Oscillation of the shear angle during wave removing

A formula was given by Albrecht [20] for the instantaneous position of the shear plane as a function of the slope of the outer surface,

$$\phi = \phi_m + C_s\delta \tag{1.7}$$

Where C_s depends on the ratio between the chip thickness and the wavelength. The value of this constant has been found experimentally to be between 0.5 and 1.0. ϕ_m is the shear angle in the absence of the surface slope.

In Figures 1-11b and 1-11c the dashed line represents the original position of the shear plane, i.e. when cutting with no outer slope. The solid line shows the new position assumed by the plane under cutting with the surface slope. Point A is the position of the cut for the case in which a flat cutting surface is cut. Point B is the free end of the shear plane that is actually observed in dynamic cutting. This effect is considered by Tlusty [21] to introduce instability in the cutting process.

Wave cutting is the process of cutting with a tool vibrating in the direction normal to the tangential cutting speed while considering a non-undulated original surface.

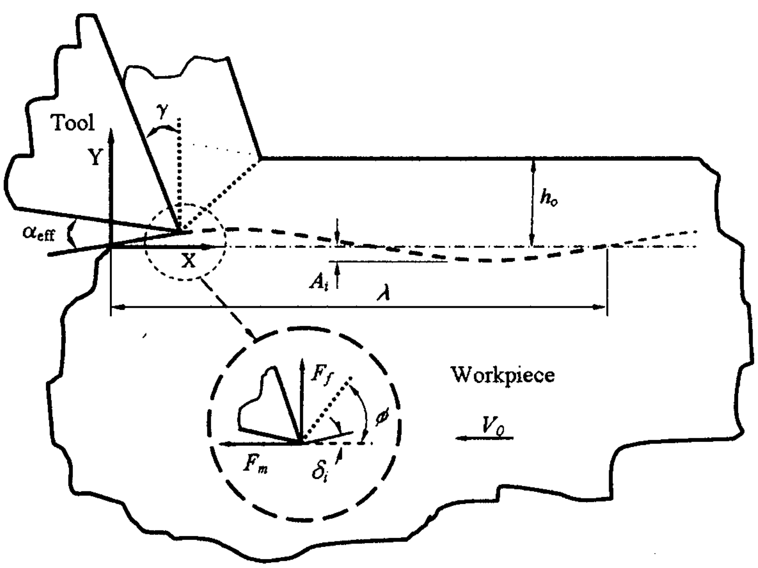

Figure 1-12. Wave cutting

The oscillating inner surface affects the instantaneous effective clearance angle as shown in Figure 1-12. Under these circumstances, the nose of the tool plays a role that has been considered to be very important for the process damping in dynamic cutting. However, this factor has proved difficult to model and an understanding of the localized process that occurs at this point still needs to be developed. It has been demonstrated experimentally [21] that if the clearance angle is decreased, the normal force is increased and therefore damping will be introduced. This factor will play a stabilizing role in the cutting process.

1.2.3.3. Three Dimensional Cutting

In the cutting models presented in the previous sections, only tools with one cutting edge are considered. As discussed before, during sawing three edges are involved in the cut. This makes bandsawing a three-dimensional cutting process. Figure 1-13 shows the same tooth as Figure 1.4 but in this case, the lateral vibrations present in the process are shown. The lateral velocity of the tooth is $\dot{w}$ and is collinear with the main edge of the tooth. The path left by a previous tooth is shown as well. The shape defined by points ABCDEFG and contained on the face of the tool, is being swept through the workpiece and its projection on the plane YZ defines the uncut chip geometry.

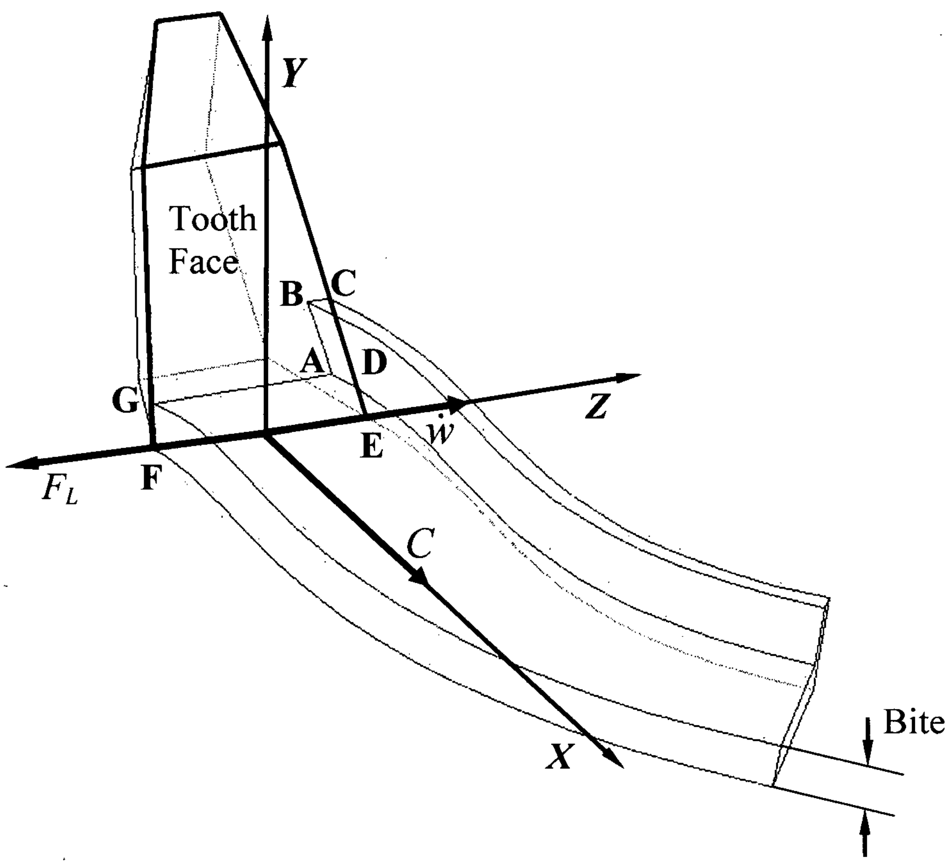

Figure 1-13. Geometry of cut in sawing

Usui, Hirota and Masuko [28] studied a three-dimensional cutting process similar to the one shown in Figure 1.13. The authors proposed a model in which the cutting of side and main cutting edges was taken into account for the prediction of the three components of cutting force and chip flow for turning operations in metal. Yellowley and Seethaler [29] developed an upper-bound model for the prediction of cutting forces and chip flow angles for turning tools of general geometry. This model included a prediction of rake face contact based upon force balance. Both of these models consider a geometry that is closer to the sawing case than the orthogonal cutting models but are developed for static operations and therefore need to be expanded in order to be applied in this work.

The following points summarize the findings of the literature review presented in this section:

1) The literature available in the area of cutting forces in wood cutting provides fundamental understanding of the chip formation mechanisms in different fundamental types of machining processes. However, no analytical development or experimental work has been found at this point which can be directly applied to the estimation of the cutting forces in a saw tooth under the conditions encountered in washboarding.

2) A number of research efforts in metal cutting are available, which are relevant for the analysis conducted in this thesis. These references cover conditions more similar to those in bandsawing than the literature found in wood cutting. However, it is identified that the direct applicability of this metal cutting knowledge might be limited and therefore a careful experimental investigation must be conducted in parallel with the analytical developments in order to provide evidence of the validity of the work presented.

1.3. Thesis Objectives and Scope

The main objective of the research reported in this thesis is to conduct an investigation into the lateral cutting forces generated in bandsawing. The motivation is the development of an overall model of the washboarding phenomena.

The scope of the work presented in the remainder of this thesis is:

- To develop models for cutting force calculation in bandsawing
- To design and conduct a series of experiments for the evaluation of the models presented
- To analyze the experimental data obtained
- To provide recommendations for improvement in saw tooth geometry in order to help minimize the washboarding problem

CHAPTER II

"I think and think for months and years, ninety-nine times, the conclusion is false. The hundredth time I am right."
- Albert Einstein

2. ANALYTICAL DEVELOPMENT OF A STATIC CUTTING FORCE MODEL FOR BANDSAWING

The first chapter of this thesis discussed that the sawing process is poorly understood and force models for the specific conditions in bandsawing need to be developed. The work reported in this chapter aims to create relations between sawtooth parameters and cutting forces for wood machining processes under static cutting conditions.

As a starting point for this study, the specific cutting conditions for a sawtooth during washboarding are discussed in the Section 2.1. The maximum lateral displacements of the saw tooth and the maximum surface slopes present in a typical washboarding pattern are also examined.

From the literature review presented in chapter one, it was seen that the dynamic cutting process can be divided primarily into static and dynamic force component analysis. The static component depends on the material and tool properties and the uncut chip geometry and is the object of study in this section. A series of models that allow the calculation of the cutting forces for multiple-edged tools such as a bandsaw tooth are presented. The force calculations require a combination of orthogonal cutting data obtained from tests and analytical estimates of the chip flow direction. This analytical portion of the models has been conducted using the upper-bound approach which has proven useful previously in the analysis of similar processes [28, 29].

The following models are presented:

1) Two-edge cutting process for a tool with zero hook angle and no obliquity

2) Three-edge cutting process with zero hook and no obliquity

3) Two-edge cutting process with side edge obliquity

These three cases cover most of the issues that require understanding in order to obtain a valid model for the static lateral cutting forces in bandsawing.

2.1. Analysis of the Cutting Conditions during Washboarding

Figure 2-1 shows the face of a bandsaw tooth during cutting. The convention used is consistent with the one established in Figure 1.4 in chapter one. The workpiece is represented by the shaded region in the figure. The boundary FEGH corresponds to a cut taken by a previous tooth. The representation has been simplified by only considering two consecutive teeth. The deviation Δ shows that there has been a relative lateral displacement between the teeth due to the vibrations of the sawblade.

The main edge of the tooth is BC and the side cutting edges are AB and CD. The region ABCDEF corresponds to the current uncut chip geometry. The chip load applied to the tooth determines the magnitude and direction of the instantaneous cutting forces. F_f is the force on the plane of the face of the tooth and is due to the friction produced by the chip sliding off the workpiece. This force is applied at angle ψ with respect to the main edge of the tool and is assumed collinear with the direction of chip flow.

Consider the top view of the bandsawing process presented in Figure 2-2. The convention again follows that of Figure 1.4 for the orientation of the axes. The two consecutive teeth shown are moving down towards the workpiece and cutting in the way shown in the process diagram in Figure 1.1. At the same time, a chip load like the one presented in fig. 2-1 is being removed by each tooth. The tooth represented in solid line is also vibrating sideways with speed $\dot{w}$ in the Z direction. The shaded regions presented correspond to the lateral chip loads that are exerted on the tooth and removed by the side flanks. At point O, the tooth leaves one side of the kerf to engage the other and the lateral chip load becomes zero.

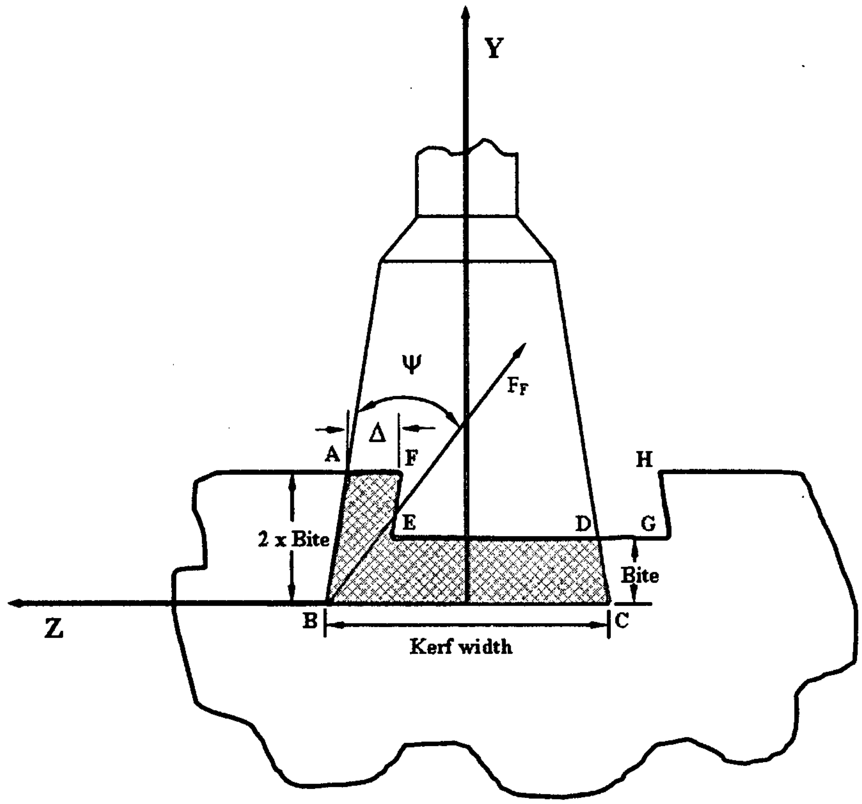

Figure 2-1. Unbalanced chip load in the bandsawing process

The trajectories of the sawteeth shown are assumed to be sinusoidal with length α being the distance between the maximum lateral displacements of adjacent teeth. The lateral chip thickness is variable, making this a dynamic cutting process similar to that encountered in the chatter problem in milling, turning and other machining operations [4]. However, a major difference between washboarding and other chatter cases previously studied by researchers is that the direction of the vibration of the tool is perpendicular to the feed velocity.

Both points A and D correspond to the projection of the lateral cutting edges of the saw tooth in this view. At the position presented, edge AE corresponds to the side clearance face of the tooth. The effective hook for the lateral cut is the angle between the face AD of the tooth and the Y axis (0° in the case shown).

It is important to establish the range of chip lateral thicknesses h_L, phases α and surface slopes that yield washboarding. The amplitude of the washboarding pattern and the phase between teeth can be used to determine the lateral chip thickness range that is applied to the sawteeth during the cut. Tlusty's classical analysis of the stability in the orthogonal chatter problem [5] assumes that regeneration will occur when the phase between waves is 180 degrees. It is considered in that reference that such a phase yields maximum force oscillation since maximums of the outer wave are aligned with minimums of the inner wave, creating maximum chip load variation. However, it will be seen later in this section that this is not the case in washboarding.

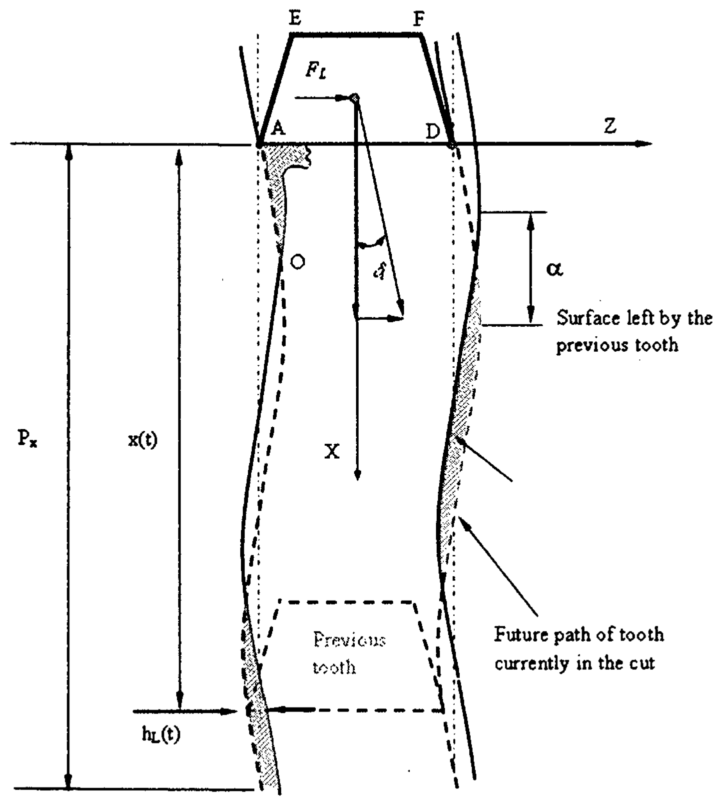

Figure 2-2. Top view of the dynamic cutting in bandsawing as the sawtooth

Luo [1] conducted several cutting experiments in bandsaws. He described the washboarding pattern in terms of two pitches, one along the feed direction, P_X and the other in the cutting direction, P_Y. Two types of washboarding pattern were studied in this reference. The first of them, called *"washboarding type I"* is shown in Figure 2-3 with typical values and following the convention for the axes established in the first chapter of this work. The main characteristic of this type I pattern is that the pitch is similar in both the feed and cutting direction.

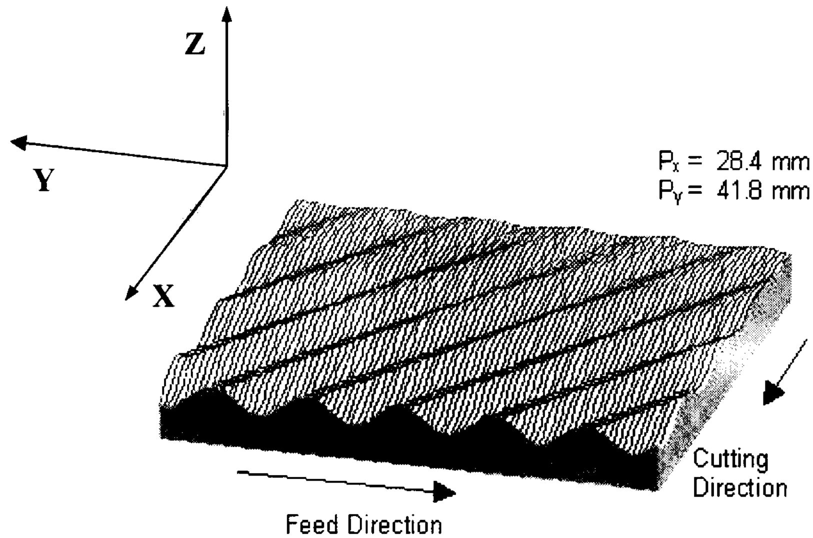

Figure 2-3. Washboarding pattern type I [1]

Another type of washboarding is shown in Figure 2-4. This pattern shows a shorter pitch in the feed direction when compared to the type I seen above. This is known as *"washboarding type II"*.

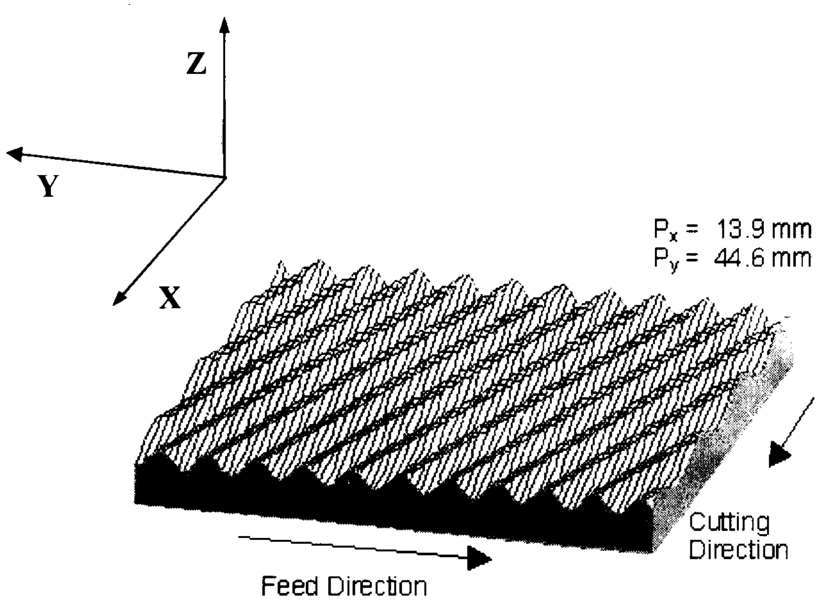

Figure 2-4. Washboarding pattern type II [1]

Consider the coordinate system shown in Figure 2-2. Assume that the trajectory of the current tooth is due to a single vibration mode and corresponds to a sinusoid with wave length P_x and that its position in the Y direction is given by,

$$y_i = A\sin\left(\frac{2\pi}{P_x}x\right) \tag{2.1}$$

Now, if the same amplitude is also considered for the previous tooth and the phase between the teeth is assumed to be α then the trajectory of that tooth can be expressed as,

$$y_o = A\sin\left(\frac{2\pi}{Px}x + \alpha\right) \tag{2.2}$$

The instantaneous lateral chip thickness will be the absolute value of the difference between the previous and current positions of the teeth,

$$h_L = A\left[\sin\left(\frac{2\pi}{P_x}x + \alpha\right) - \sin\left(\frac{2\pi}{P_x}x\right)\right] \tag{2.3}$$

Using trigonometric identities, equation 2.3 can be expressed as,

$$h_L = 2A\cos\left(\frac{2\pi}{P_x}x + \frac{\alpha}{2}\right)\sin\left(\frac{\alpha}{2}\right) \tag{2.4}$$

For variable x, the maximum possible value of h_L in equation 2.4 above is $h_L = 2A$ and occurs when $\alpha = \frac{\pi}{2}$. For a constant value of α, the maximum lateral chip load h_{Lmax} will occur when the argument of the cosine function in equation 2.4 is equal to $n\pi$, where n = 0, 2, 4...

The equation for the position at which the maximum lateral chip thickness occurs is,

$$x_{\max} = \frac{P_x}{2\pi}\left(n\pi - \frac{\alpha}{2}\right) \tag{2.5}$$

The value for the maximum lateral chip thickness can be found by evaluating equation 2.4 at any value x_{max} found from 2.5 for a given value of α.

Table 2-1 presents some experimental results reported by Luo [1]. The phase ε, in degrees, and the maximum chip thickness have been calculated from the information found on the pattern in the wood. The typical amplitude of washboarding varies from 0.13 mm to 0.5 mm and can be as large as 1.2 mm [1] therefore in Table 2.1 a typical value of 1.0 mm has been considered for illustration purposes.

Table 2-1. Phase ε, and Maximum Slope and Lateral Chip Thickness for Washboarding Type I.

Washboarding Type I					
Amplitude [mm]	Bite [mm]	Pitch X [mm]	ε [deg]	Maximum side chip thickness [mm]	Maximum surface slope in the X direction [deg]
1.00	0.64	71.00	3.22	0.0562	2.53
1.00	0.64	66.00	3.46	0.0604	2.72
1.00	0.61	40.00	5.51	0.0961	4.46
1.00	0.61	38.00	5.78	0.1008	4.69
1.00	0.61	36.00	6.10	0.1063	4.95

Table 2-2. Phase ε, and Maximum Slope and Lateral Chip Thickness for Washboarding Type II

Washboarding Type II					
Amplitude [mm]	Bite [mm]	Pitch X [mm]	ε [deg]	Maximum side chip thickness [mm]	Maximum surface slope in the X direction [deg]
1.00	0.40	11.00	12.99	0.4381	14.86
1.00	0.30	7.30	15.03	0.2616	20.36
1.00	0.28	5.70	17.65	0.3068	23.90
1.00	0.40	7.00	20.42	0.3545	20.95

The table above shows that washboarding occurs when the phase is either between 3 ~ 6 degrees for type I and 12 ~ 21 for type II. This is much different than the value of 180 degrees that is assumed in the classical analysis of the chatter problem. It can also be seen that the maximum lateral chip thickness involved in washboarding type II are at least twice that of that for type I.

2.2. Static Two-Edge Cutting Analysis for Bandsawing

In order to study the cutting process presented in Figure 2-1, the analysis of a simplified two-edge model has been conducted. The study aims to improve the understanding of the coupling of the cutting forces in multi-edged tools. The model requires the direction of chip flow of the cutting process to be predicted and it applies to a tool with zero hook. The final goal of this development is to achieve the prediction of lateral and feed cutting forces based upon a simple set of orthogonal cutting data for a given material.

2.2.1. Considerations Involved in an Upper-bound Analysis

It was discussed in Section 1.2.3.3 that previous research has been conducted in the prediction of the forces in three dimensional cutting using upper-bounds. This approach has been used extensively in the analysis of machining processes due to its simplicity [15]. The estimates using upper-bounds are often within 10% of the experimental values found by researchers in cutting [28, 29]. Based on these reasons, the models presented in the remainder of this chapter will be developed using this analysis technique.

Upper-bounds are based upon a limit theorem, which states that "any estimate of the collapse of a structure made by equating the internal rate of energy dissipation to the rate at which external forces do work in some assumed pattern of deformation will be greater than or equal to the correct load" [37]. This theorem implies that any proposed plastic deformation field that satisfies the external constraints imposed on the process can be used to estimate a force that is slightly higher or equal to the actual solution. Furthermore, no knowledge of the stress condition inside the material is required.

The first step in the development of an upper-bound is finding a deformation pattern that meets the kinematical constraints of the process. As an example of this procedure, consider the orthogonal cutting process shown in Figure 2.5. The magnitude and direction of the incoming velocity V_0 are known. The face of the tool constrains the outgoing flow and therefore the direction of the final velocity of the material is known as well. A velocity diagram is proposed in the figure which satisfies the kinematics of the problem. This diagram is known as a *hodograph.*

The hodograph represented is only one out of an infinite number of possible solutions for the plastic flow in this process. In the case presented, the deformation field chosen contains a single plane in which all the material collapses, reaching the final geometry. This deformation plane also known as a *shear plane* is an idealization of the real process, which might involve a larger deformation region. The material to the right and left of the shear plane shown in Figure 2.5 is considered to be two independent volumes.

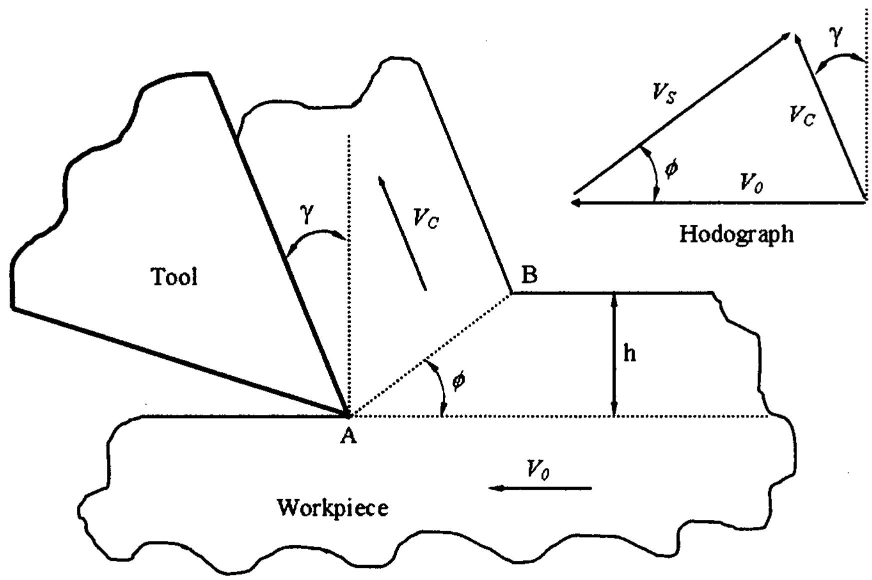

Figure 2-5. Front view of a two-edge cutting process

The location of the shear plane in the cutting process shown is determined by the *shear angle,* ϕ which is initially an unknown in the problem. The first goal of the analysis is to find an estimate for the geometry of the process by finding a value of the shear angle which minimizes the power expenditure. In order to achieve this, the energy spent in the process needs to be expressed in terms of ϕ considering all other parameters in the process constant.

The magnitude of the shear stress is considered to be constant over the entire shear plane. The value for this stress is assumed to be *k*, which is the yield shear stress for a continuous plastic deformation process. This value differs from τ obtained from static tests because it is dependent upon the strain rates and temperatures present in the process. In reality, the material might present certain work-hardening characteristics, which will be dependent upon these two factors.

The upper-bound approach does not consider these effects and therefore applies k as a simple constant.

Upper-bounds assume that the properties of the material in the process are non-directional and therefore they are mainly applicable to isotropic materials. The approach can also be used as a first approximation for the analysis of anisotropic materials if an appropriate value for the shear stress k is obtained experimentally.

2.2.2. Two-edge model geometry

Figure 2.6 presents the face of a two-edged tool removing material from a workpiece. The tool moves towards the workpiece in the direction out of the page with velocity C. The main edge, BC has length k_w and the side edge AB has length b.

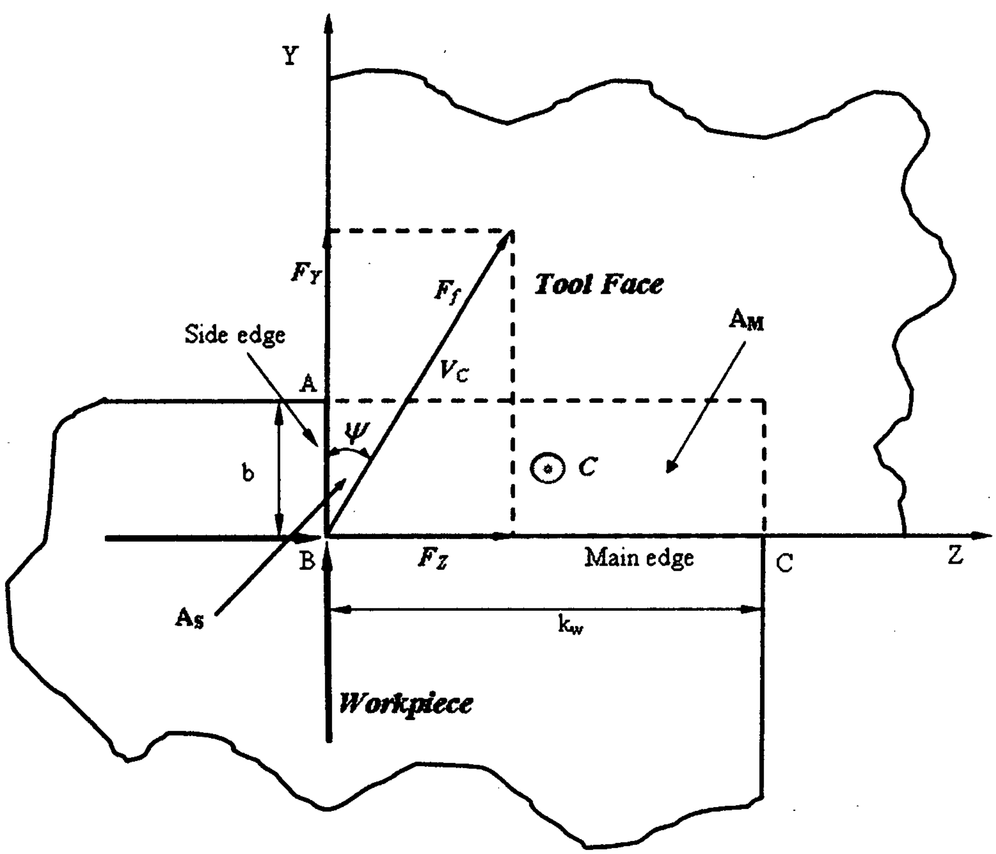

Figure 2-6. Front view of a two-edge cutting process

The chip flows away from the cutting region with chip velocity V_C and angle ψ on the plane of the face as shown. Force F_F shown is collinear with the direction of chip flow. The proposed deformation fields for this process are shown in Figure 2.7.

2.2.3. Forces Acting on the Tool in Two-edge Cutting

If quasi-static equilibrium of the chip is assumed, the cutting forces acting on the plane of the face of the tool shown in Figure 2-6 are the friction force from the chip, F_f and the edge forces F_{ex} and F_{ez}. These edge forces are assumed independent of the shear process occurring in the material and are due to secondary process of ploughing occurring on the cutting edge [15]. The total force in the Y and Z directions can be expressed as:

$$F_z = F_f \sin(\psi) + F_{ez} \tag{2.6}$$

$$F_y = F_f \cos(\psi) + F_{ey} \tag{2.7}$$

The forces F_f, F_{ex} and F_{ey} can be estimated from orthogonal cutting data as follows:

$$F_f = K_{fc} A_C = K_{fc} b k_w \tag{2.8}$$

Where K_{fc} is the specific cutting pressure for the given material and cutting tool, A_C is the uncut chip area, b is the depth of cut and k_w the width of cut as shown in Figure 2-6.

The edge forces can be obtained from:

$$F_{ez} = K_{fe} b \tag{2.9}$$

$$F_{ey} = K_{fe} k_w \tag{2.10}$$

Where K_{fe} is the edge constant for the given tool/workpiece combination

The constants K_{fc} and K_{fe} can be obtained from linear regression of the orthogonal cutting data, which will be presented in the third chapter of this thesis. Examining equations 2.6 through 2.10, it can be seen that the only missing parameter for the estimation of the lateral cutting forces is the chip flow angle ψ. It is possible to obtain a theoretical estimate of this angle by formulating an upper-bound solution for the 2-edge cutting process.

2.2.4. Upper Bound Solution for the Chip Flow Angle in Two-edge Cutting

The chip-flow angle ψ in the two edge cutting case shown in Figure 2-6 can be estimated by minimizing the power expression for a kinematically admissible model of the cutting process. It is assumed here that two shear angles are developed. The total power in the process is the result of the power spent on the shear planes and the friction on the face of the tool. The projection of the two shear planes present in the process on the face of the tool is shown in Figure 2.6. The total power is given by the following equation:

$$W = kV_m A_m + kV_s A_s + kV_f A_f \tag{2.11}$$

Where k is the cutting shear stress, V_m and V_s are the magnitudes of the respective velocities on the shear planes and A_S, A_M the areas of these planes. Friction has been introduced by assuming an area of plastic contact between the chip and the face of the tool; therefore V_f is the chip velocity and A_f is this assumed friction area.

The set of views shown in Figure 2-7 helps the visualization of this three-dimensional cutting process. The hodographs shown correspond to a solution for the flow of the material, which is admissible kinematically. That is, given that the incoming velocity and direction of the material is known as well as the direction of the outgoing flow, the hodograph represents a solution that does not violate any flow rules. These hodographs are shown for the main and side edges. The incoming velocity V_0 is constant and therefore irrelevant to the minimization of the power spent in the process. Considering this, the velocity of the chip on the X and Y directions is found from the hodographs as:

$$V_{CZ} = V_0 \tan\phi_m \tag{2.12}$$

$$V_{CX} = V_0 \tan\phi_s \tag{2.13}$$

The chip flow angle is given by:

$$\psi = \arctan\left(\frac{\tan\phi_s}{\tan\phi_m}\right) \tag{2.14}$$

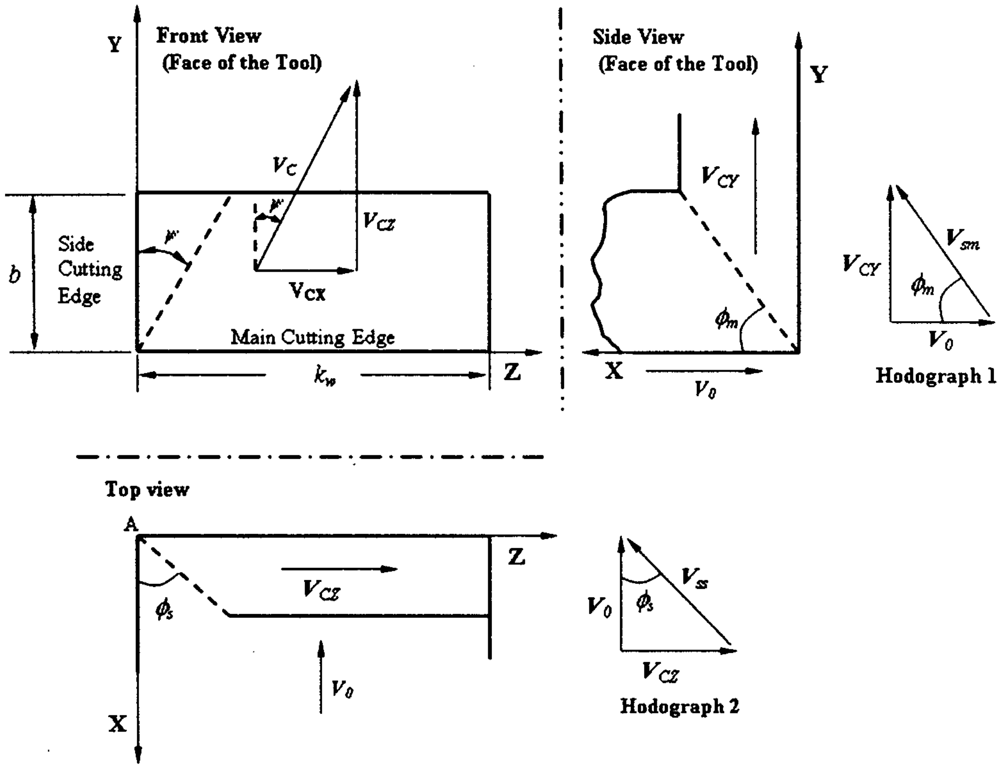

Figure 2-7. Geometry of the two-edge cutting process

The main and side edge contributions to the shear velocity are:

$$V_{sm} = \frac{V_0}{\cos\phi_m} \tag{2.15}$$

$$V_{ss} = \frac{V_0}{\cos\phi_s} \tag{2.16}$$

The friction velocity is the resultant of the components X and Y of the chip velocity as follows:

$$V_f = \sqrt{V_{CY}^2 + V_{CZ}^2} = V_0\sqrt{\tan\phi_m^2 + \tan\phi_s^2} \tag{2.17}$$

The resultant velocities on the shear planes are:

$$V_{smt} = \sqrt{V_{sm}^2 + V_{CZ}^2} = V_0\sqrt{\left(\frac{1}{\cos\phi_m}\right)^2 + (\tan\phi_s)^2} \tag{2.18}$$

And,

$$V_{sst} = \sqrt{V_{ss}^2 + V_{CY}^2} = V_0 \sqrt{\left(\frac{1}{\cos\phi_s}\right)^2 + (\tan\phi_m)^2} \tag{2.19}$$

The shear areas can be found from inspection and their expressions are,

$$A_m = \frac{1}{\sin\phi_m}\left[k_w b - \frac{d^2 \tan\phi_s}{2\tan\phi_m}\right] \tag{2.20}$$

$$A_s = \frac{b^2}{2\tan\phi_m \cos\phi_s} \tag{2.21}$$

The area of plastic friction contact on the face of the tool is difficult to estimate. However, a reasonable assumption often made in metal cutting analysis is that the areas of sticking friction on the face of the tool is proportional to the uncut chip thickness, that is,

$$A_f = C_f b k_w \tag{2.22}$$

Where C_f is a constant that can be found from force equilibrium and usually lies between 1 and 4. The power spent on the process becomes,

$$W = kV_0\sqrt{\left(\frac{1}{\cos\phi_m}\right)^2 + (\tan\phi_s)^2}\,\frac{1}{\sin\phi_m}\left[\frac{b}{k_w} - \left(\frac{b}{k_w}\right)^2 \frac{\tan\phi_s}{2\tan\phi_m}\right] + k\sqrt{\left(\frac{1}{\cos\phi_s}\right)^2 + (\tan\phi_m)^2}\ldots$$

$$\left(\frac{b}{k_w}\right)^2 \frac{1}{2\tan\phi_m \cos\phi_s} + kC_f \frac{b}{k_w}\sqrt{\tan\phi_m^2 + \tan\phi_s^2} \tag{2.23}$$

The upper bound formulation requires finding a minimum for 2.23 with respect to ϕ_m and ϕ_s as a function of $\frac{b}{k_w}$. This solution will yield the chip flow angle. A numerical solution has been obtained and is shown in the Figure 2.8.

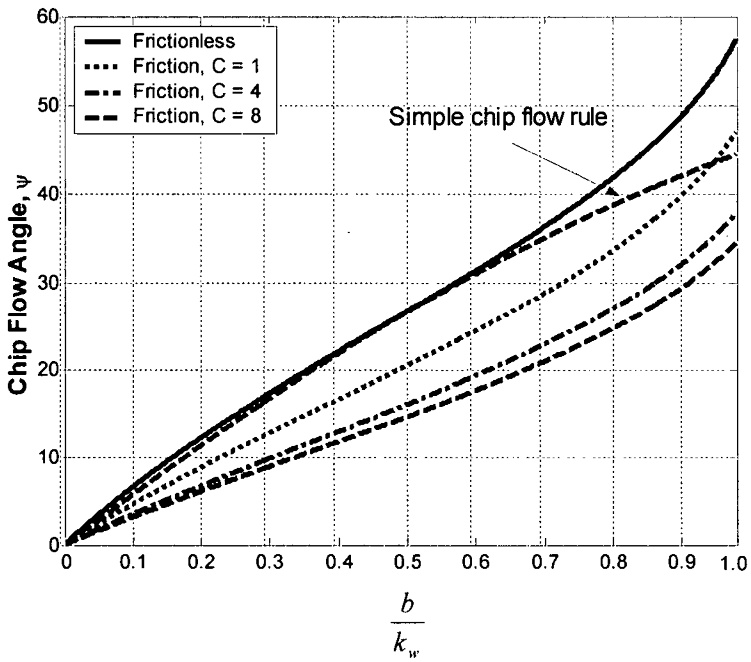

Figure 2-8. Solution for ψ as a function of the ratio between the depth and width of cut in two edge cutting

The solution presented in Figure 2-8 provides the value of ψ required for estimating the cutting force in the two-edge process from equations 2.1 and 2.2. A ratio $\frac{b}{k_w} = 0$ corresponds to orthogonal cutting. The model predicts that the chip will slide straight up on the face of the tool for that case, which is an expected result. As the ratio between the lengths of the edges increases, the chip deviates from the upward direction and starts flowing sideways. This sideways flow creates the lateral component of force on the tool.

A comparison with the simple chip flow rule is also shown in Figure 2-8. The chip flow rule is an empirical estimate of the flow direction. This rule states that the direction of the chip flow will be normal to an imaginary line that joins the two end points of the cutting edge. In this case, the direction would be normal to a line joining points A and C as shown in Figure 2.9.

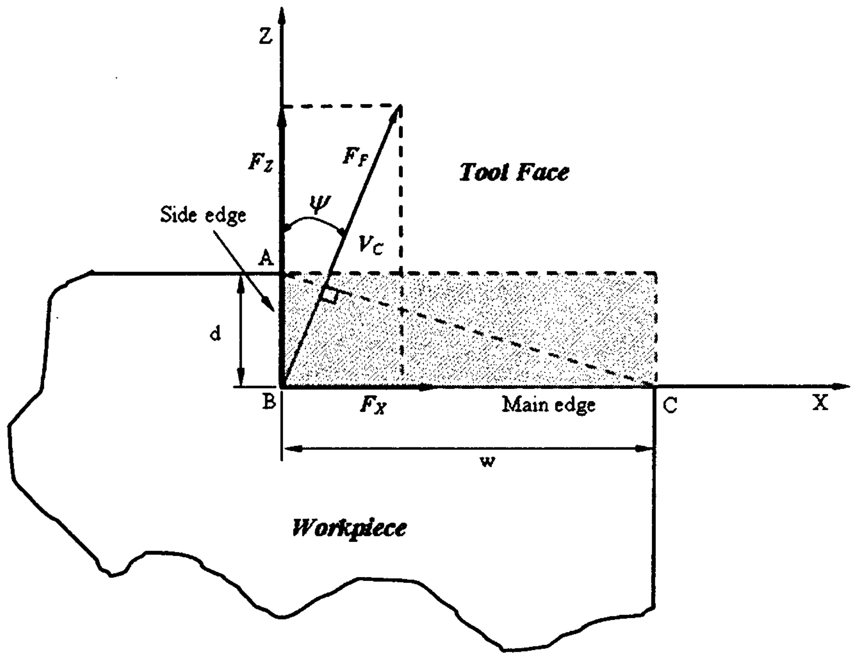

Figure 2-9. Simple flow rule applied to two-edge cutting

The chip flow rule lies between the upper bound estimate for the frictionless case and the case with friction for $C_f = 4$. These two bounds can be used in order to estimate the cutting forces in the two-edge cutting process.

2.3. An Upper-Bound Analysis of the Bandsawing Static Components of Force

In Section 2.2, a simplified two-edge cutting model was developed aiming to develop a basic understanding for the coupling between the cutting forces in multi-edged tools. This section presents a more comprehensive model that includes the effects of all the edges present in unbalanced cutting during bandsawing. In particular, the influence of the third cutting edge in bandsawing is studied. This edge is represented by line CD in Figure 2.1. Two simplifications have been made for the analysis: the hook angle on the blade is zero and the radial angle is also zero. The idealized geometry for this situation is presented in Figure 2-10, and is similar to that presented in Figure 2.1.

2.3.1. Geometry of the Three-Edge Cutting Model

The width of the cut is K_W. The tooth is removing a depth equivalent to one bite with its main edge. The length of the side load applied to the tooth is represented by the distance shown between points A and B and the lateral displacement is Δ. The material flows onto the tool (or vice-versa) with velocity V_0 and is sheared along edges AC, CD and DF. Hodograph 1 represents the shear process along edge CD, at the main shear plane which location in space is given by angle ϕ_M. The material flows along the main shear plane and then reaches the vertical component of velocity of the chip, V_{CY}. A similar situation occurs on the side edge AC where the incoming material must shear and reach an outgoing velocity V_{CX}. The final chip velocity will lie on the face of the tool with direction ψ.

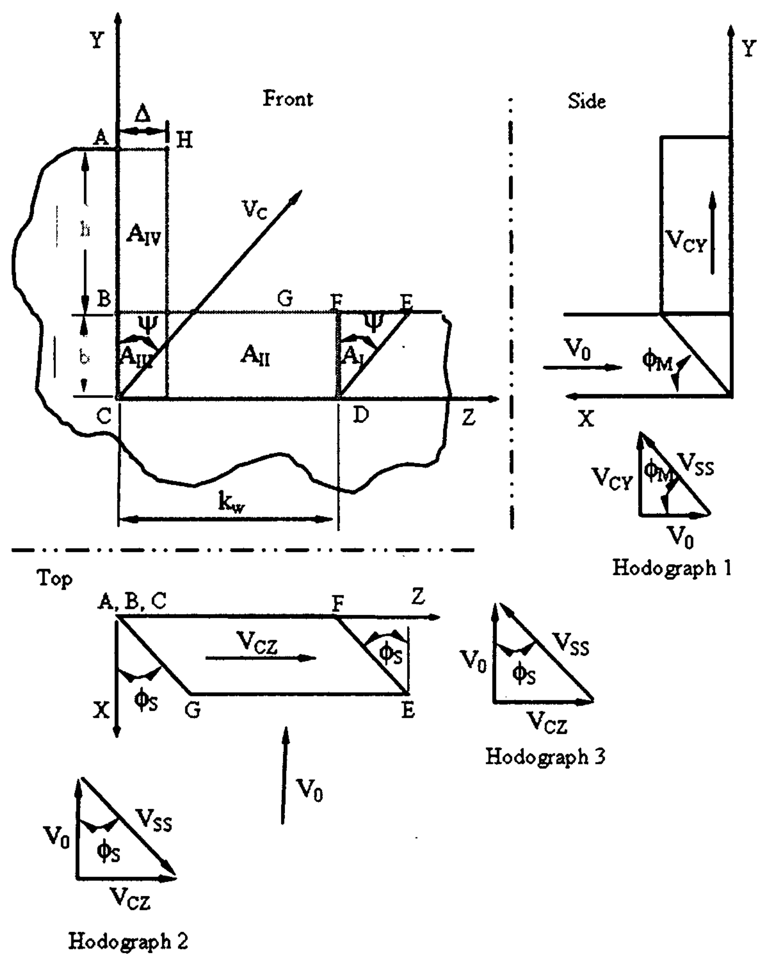

Figure 2-10. Geometry of the three-edge cutting process in bandsawing for $\tan\psi \le \dfrac{bite}{\Delta}$

The areas for this geometry need to be calculated for two different cases. First, as shown in Figure 2-10, when the tangent of the chip flow angle is less than $\frac{bite}{\Delta}$, the total shear can be calculated by adding sub-areas A_I through A_{IV}, and it can be easily shown that,

$$A_I = A_{DEF} = \frac{b^2 \cot\psi}{2\sin\phi_S} \tag{2.24}$$

$$A_{II} = A_{CDEG} = \frac{K_W b}{\sin\phi_M} \tag{2.25}$$

$$A_{III} = A_{BCG} = \frac{b^2 \cot\psi}{2\sin\phi_S} \tag{2.26}$$

$$A_{IV} = A_{ABGH} = \frac{h\Delta}{\sin\phi_S} \tag{2.27}$$

The second case occurs when $\tan\psi > \frac{bite}{\Delta}$ as it is shown in Figure 2-11 below,

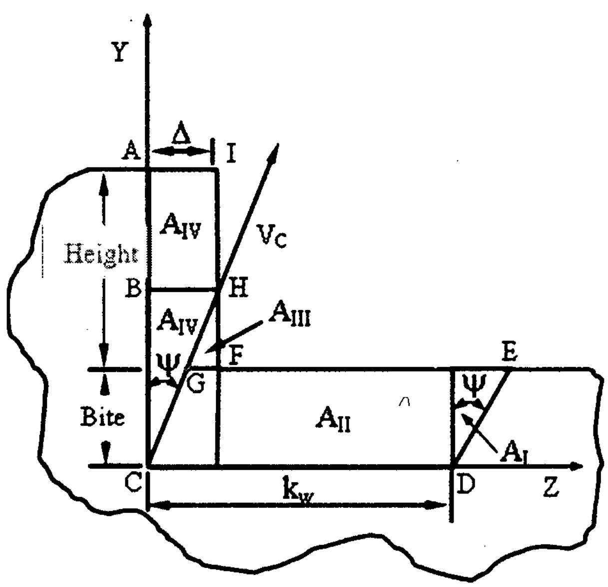

Figure 2-11. Geometry of the three-edge cutting process in bandsawing for $\tan\psi > \frac{bite}{\Delta}$

For this case, the areas are given by the following expressions,

$$A_I = \frac{\Delta(2b - \Delta \tan \psi)}{\sin \phi_S} \tag{2.28}$$

$$A_{II} = \frac{\Delta^2 \tan \psi}{2 \sin \phi_S} \tag{2.29}$$

$$A_{III} = \frac{\Delta^2 \tan \psi}{2 \sin \phi_M} \tag{2.30}$$

$$A_{IV} = \frac{(K_W - b)b + \dfrac{b^2 \cot \psi}{2}}{\sin \phi_M} \tag{2.31}$$

$$A_V = \frac{b^2 \cot \psi}{2 \sin \phi_S} \tag{2.32}$$

The change of velocity in all the planes must be equal since the material enters the cutting region with uniform velocity and leaves as a rigid body. The velocities can be estimated in a similar way to that presented in Section 2.2. The shear velocity can be estimated from the following expression,

$$|Vs| = V_0 \sqrt{\sec^2 \phi_S + \tan^2 \phi_M} = V_0 \sqrt{\sec^2 \phi_M + \tan^2 \phi_S} \tag{2.33}$$

The geometry proposed for the first case presented yields,

Case a: $$\frac{w}{V_0 k} = \sqrt{\sec^2 \phi_M + \tan^2 \phi_S} \left[\frac{b^2 \cot \psi}{2 \sin \phi_S} + \frac{K_W b}{\sin \phi_M} + \frac{b^2 \cot \psi}{2 \sin \phi_S} + \frac{h\Delta}{\sin \phi_S} \right] \tag{2.34}$$

Case b: $$\frac{w}{V_0 k} = \left[\frac{\Delta(2b - \Delta \tan \psi)}{\sin \phi_S} + \frac{\Delta^2 \tan \psi}{2 \sin \phi_S} + \frac{\Delta^2 \tan \psi}{2 \sin \phi_M} + \frac{(K_W - b)b + \dfrac{b^2 \cot \psi}{2}}{\sin \phi_M} + \frac{b^2 \cot \psi}{2 \sin \phi_S} \right] \ldots$$

$$\sqrt{\sec^2 \phi_M + \tan^2 \phi_S} \tag{2.35}$$

In order to implement a numerical solution, the minimum of equations 2.34 and 2.35 was found for every step and the lowest of power from both of them taken as the local solution. This solution is presented in Section 2.3.3 with respect to ϕ_S and ϕ_M.

2.3.2. Friction Considerations in Three-edge Cutting

In Section 2.2, the friction in the cutting process was added by considering an area of friction contact proportional to the uncut chip thickness area. This is only one of the approaches that can be used in order to account for the power spent in the friction process in cutting. A more general assumption that can be used is that the area of plastic contact on the face of the tool is proportional to the total shear plane area as follows,

$$F_f = C_f A_T k_{fc} \tag{2.36}$$

The constant can be found empirically from orthogonal cutting data. The model can be calibrated to yield a more accurate prediction of the cutting force. The experiments to find the value of this constant are presented in the third chapter of this thesis. This consideration for the friction yields the following additional term that must be added to the power expression 2.34 and 2.35,

$$w_f = C_f A_T k V_c \tag{2.37}$$

Where w_f is the power spent on friction in the cutting process, C_f is an empirical constant, A_T the total area in all the shear planes and V_c the velocity of the chip.

2.3.3. Cutting Force Calculation in Three-edge Cutting

It was discussed in Section 2.2 that the cutting force on the face of a tool with zero hook angle has two has two components. One first term is due to the friction of the chip sliding on the face of the tool. The second term is due to the edge forces and is proportional to the length of the cutting edge. Therefore it can be stated that,

$$F_Y = F_Y + F_{eY} \tag{2.38}$$

And,

$$F_Z = F_{cZ} + F_{eZ} \tag{2.39}$$

Where, the subscript c stands for cutting force and e for edge force. The cutting force terms in each direction depend on the friction force and its orientation as shown in Figure 2.10, which can be obtained from the upper-bound formulation presented in Sections 2.3.1 through 2.3.2.

$$F_L = F_f \sin\psi + F_{eL} \tag{2.40}$$

And,

$$F_Y = F_f \cos\psi + F_{eY} \tag{2.41}$$

Equation 2.36 could be used in order to estimate the friction force. However, the total area of shear is a parameter that can only be conveniently estimated inside the upper-bound formulation. It is more practical to reformulate the friction force in terms of the uncut chip area in order to allow for simple formulas to be used. Therefore, equation 2.36 will be used for power estimation and the following formula will be used to force calculations,

$$F_f = k_{fc} A_c \tag{2.42}$$

Where A_C is the uncut chip area given by,

$$A_c = h\Delta + bk_w \tag{2.43}$$

It is convenient to express the force in a non-dimensional form in order to arrive at a general solution. The cutting component of the lateral force in the X direction will be finally calculated from the following equation,

$$\frac{F_{CL}}{k_{fc}bk_w} = \left(\frac{h}{b}\frac{\Delta}{k_w} + 1\right)\sin\psi \tag{2.44}$$

Equation 2.44 allows the estimation of the lateral cutting force in a bandsawing process with 0 hook angle once the bite, the kerf width and the orthogonal cutting constants are known. From this point, the result obtained from this equation will be referred to as non-dimensional lateral cutting force.

2.3.4. Simulation Results for the Three-Edge Cutting Process

In order to summarize the results obtained by the model in this section, the geometry of the process has been described in terms of three independent non-dimensional parameters. The first is $\frac{b}{K_w}$, which represents the depth of the cut is with respect to the width of the tooth. The second parameter, $\frac{h}{b}$, determines the relation between the size of the balanced cut region to the lateral unbalanced cut taken. Finally, $\frac{\Delta}{K_w}$, relates the total width of the tooth to the lateral displacement experienced by the sawblade. Figure 2-12 presents the simulation results obtained for the chip flow angle.

The results for the chip flow angle show great sensitivity for the initial side engagement of the saw tooth. The range of $\frac{\Delta}{K_W}$ between 0 and 0.025 shows how the chip flow angle increases suddenly from zero to 10 - 20 degrees for all the simulation cases studied. In a bandsaw, with a typical width of kerf of 0.100 – 0.250 inches, this range corresponds to a maximum lateral displacement of 0.0025 – 0.00625 inches, which is typically found in washboarding patterns as seen in Section 2.1. After $\frac{\Delta}{K_W} = 0.050$, the sensitivity of the chip direction to the lateral deflection of the blade seems to decrease.

Ψ vs $\dfrac{\Delta}{K_w}$ for $\dfrac{b}{K_w} = 0.25$

a)

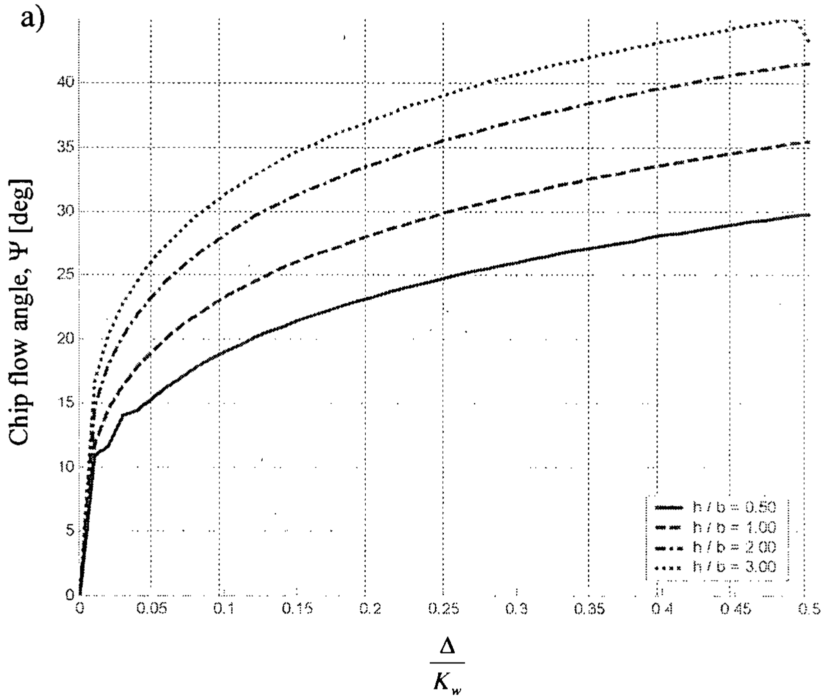

Ψ vs $\dfrac{\Delta}{K_w}$ for $\dfrac{b}{K_w} = 0.50$

b)

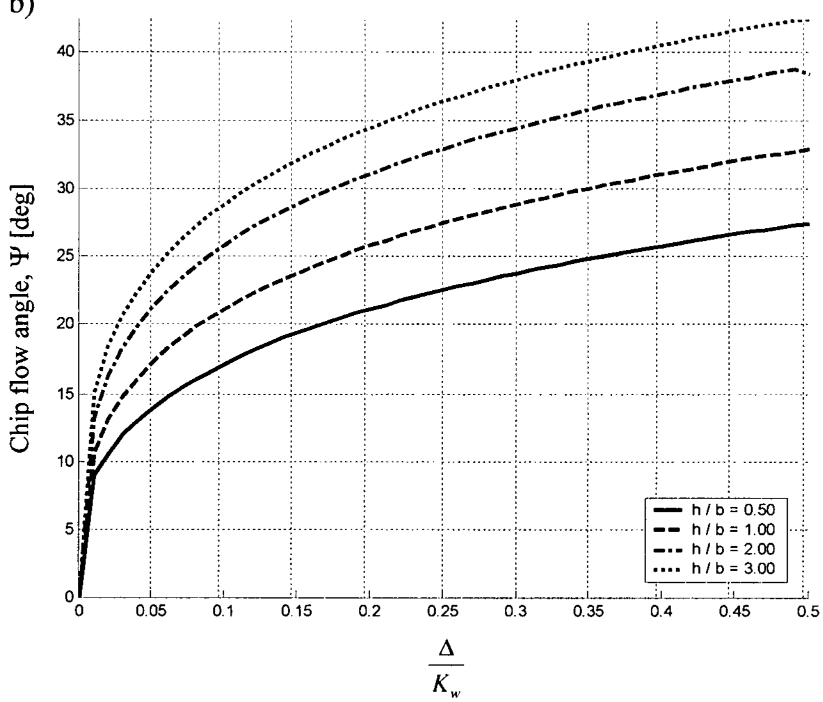

Figure 2.12 (a). Chip flow angle solution for the three-edge cutting. a) $\dfrac{b}{K_w} = 0.25$, b) $\dfrac{b}{K_w} = 0.50$

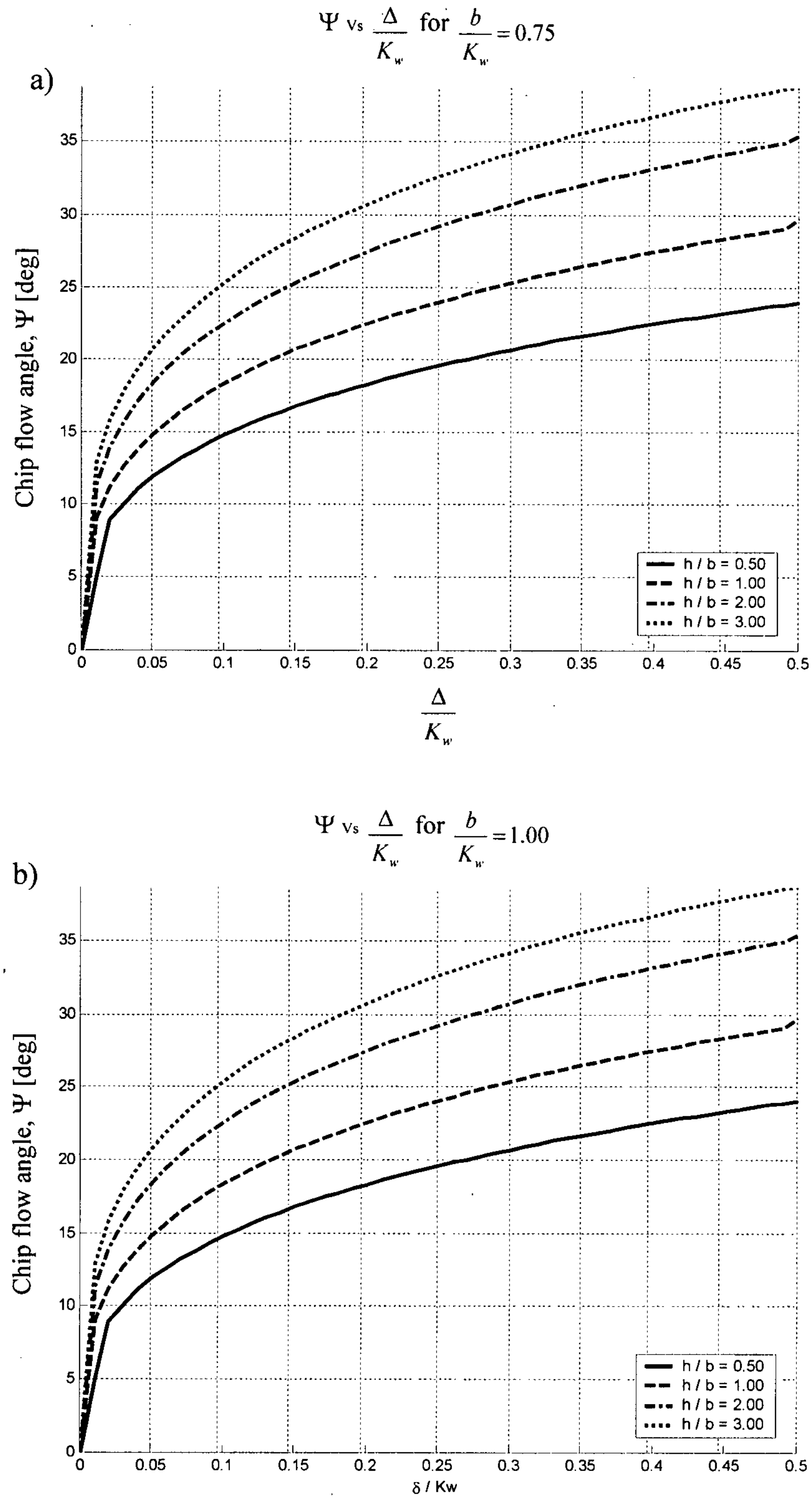

Figure 2.12 (b). Chip flow angle solution for the three-edge cutting. a) $\frac{b}{K_w} = 0.75$, b) $\frac{b}{K_w} = 1.00$

The right hand side term of equation 2.44 has been evaluated as well and the results are presented in Figure 2.13. It can be seen that in a similar fashion to the solution for the chip flow angle, the non-dimensional cutting force presents two regions that are approximately linear. The influence of the bite with respect to the width of the kerf seems to be small compared to other effects. The length of the extra side-cutting edge increases the stiffness of the process in a non-linear manner.

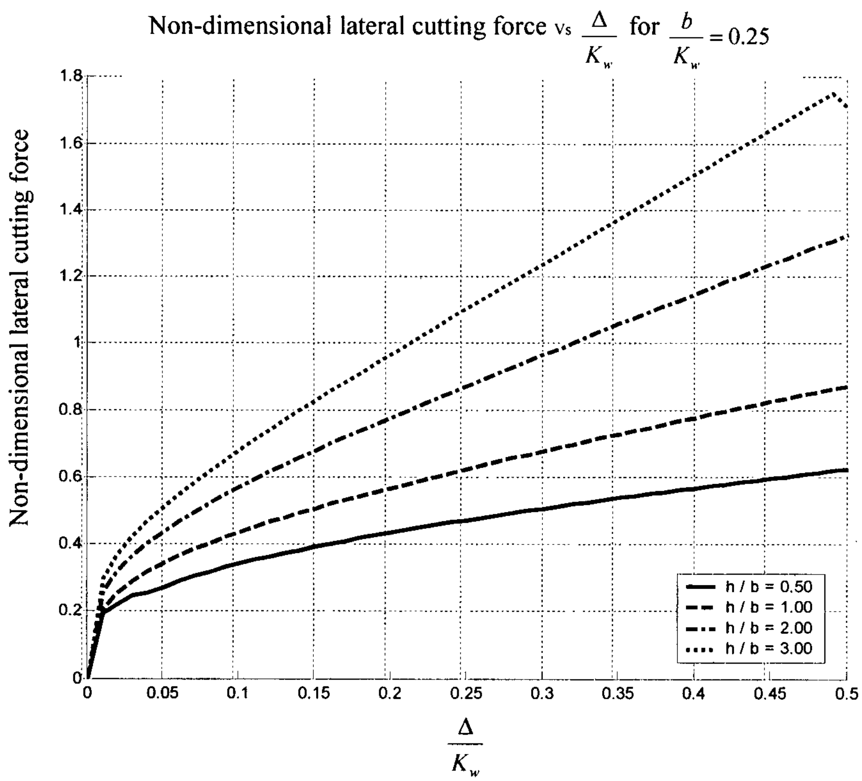

Figure 2-13 (a). Non-dimensional lateral cutting force for three-edge cutting for $\frac{b}{K_w} = 0.25$

Non-dimensional lateral cutting force vs $\dfrac{\Delta}{K_w}$ for $\dfrac{b}{K_w} = 0.50$

a)

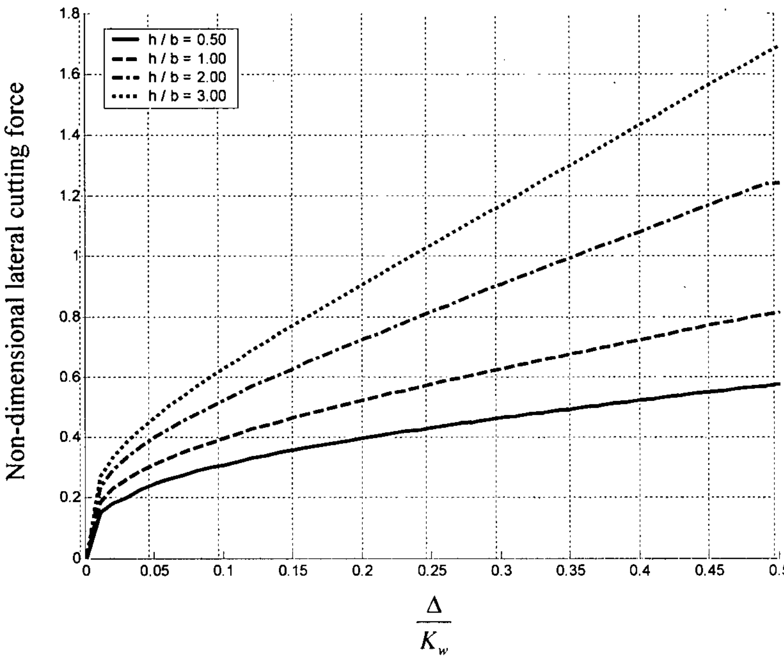

Non-dimensional lateral cutting force vs $\dfrac{\Delta}{K_w}$ for $\dfrac{b}{K_w} = 0.75$

b)

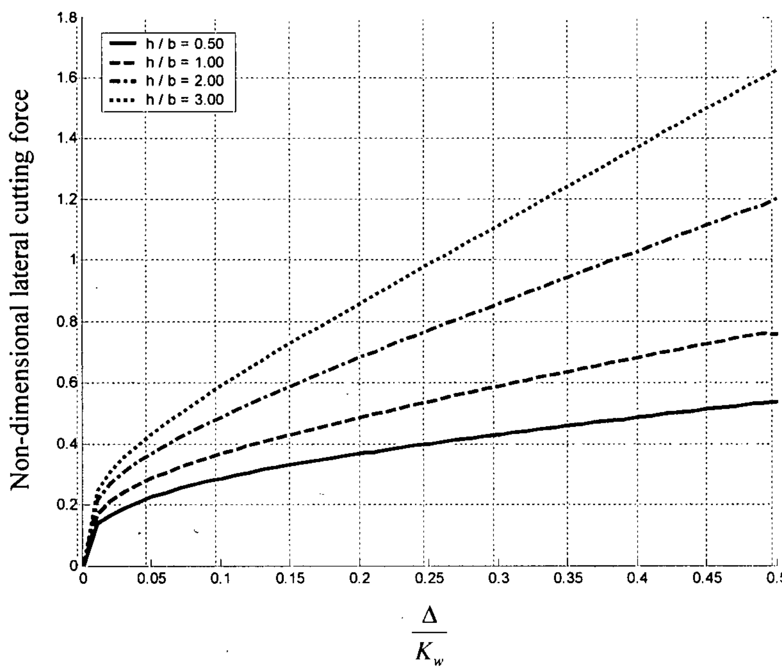

Figure 2-13 (b). Non-dimensional lateral cutting force for three-edge cutting. a) $\dfrac{b}{K_w} = 0.50$, b) $\dfrac{b}{K_w} = 0.75$

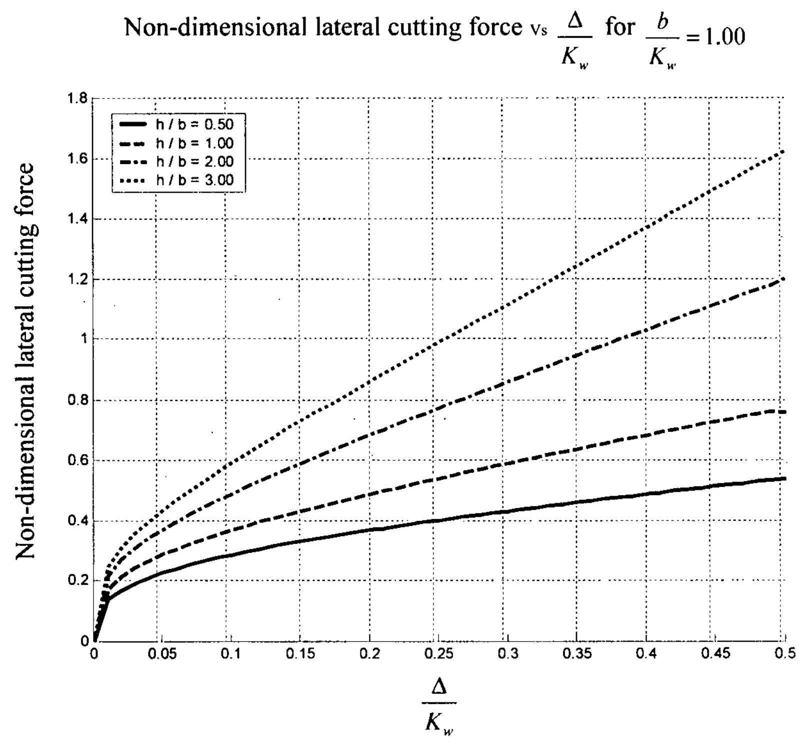

Figure 2-13 (c). Non-dimensional lateral cutting force for three-edge cutting for $\frac{b}{K_w} = 1.00$

This concludes the analysis for the three-edge cutting case presented. The following section will focus on the issue of the influence of the hook angle on the lateral cutting forces.

2.4. Analysis of the Two-edge Cutting Process for a General Hook Angle

Sections 2.2 and 2.3, present a series of upper-bound models that yield a basic understanding of the simple case of unbalanced multi-edge cutting when the hook angle is zero. However, those models do not address the effect of induced obliquity that the hook angle has over the side edges of the bandsaw. Obliquity will most likely have an effect on the lateral stiffness of the process which is not understood at this point. In order to model this change in the lateral forces introduced by variations on the hook angle it is important to understand the chip creation process under the constraints induced by this three-dimensional geometry. The model proposed for this analysis is presented in Figure 2-14.

2.4.1. Geometry of the Two-edge Cutting Process for a General Hook Angle

The hook angle in a bandsaw introduces obliquity in the lateral cutting process. Obliquity This occurs when the velocity vector and a cutting edge are not normal. This is likely to have an influence in the magnitude of the lateral cutting forces produced in sawing. The model presented in Section 2.2 of this chapter does not address this issue and therefore needs to be extended in order to gain understanding of this effect. The object of this section is to conduct an analysis of the influence that varying the hook angle has on the stiffness of the lateral cutting process in bandsawing.

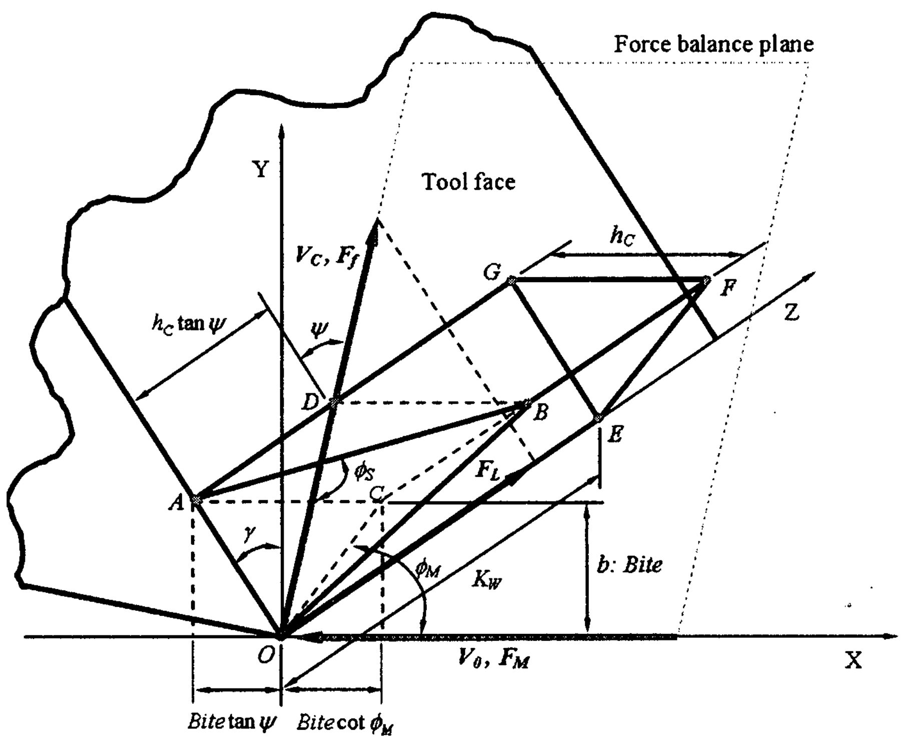

Figure 2-14. Three-dimensional cutting geometry for a saw tooth for a non-zero hook angle

Figure 2-14 is a general representation of the specific case presented in Figure 2-7. The face of the tool lies on a plane that contains the X axis as shown, where the main edge is located. The hook angle γ, is measured with respect to the Y axis shown and defines the orientation of the face in space. The lateral cutting edge corresponds to line OA. The width of the tooth is K_W, and the depth of the cut is one bite. OAGE is the projection of the uncut chip thickness geometry on the face of the tool.

Two shear planes are assumed in the process, the lateral one is ABO and the main BOEF. The lateral shear angle is measured on the plane XZ from the Z axis. The main shear angle is referenced from the Z axis on plane YZ to line OC. The lateral shear angle is referenced from line AC, which is parallel to the Z axis. The chip slides on the face of the tool with direction ψ and velocity V_C measured on that same plane with respect to the side edge AO.

2.4.2. Shear Areas in the Two-edge Cutting Process for a General Hook Angle

The shear planes on this case become more complex than the ones in the models presented previously. In order to simplify the analysis, vector algebra can be used to calculate the shear areas. Plane ABO can be described by vectors OA and OB which are defined as follows,

$$O\vec{A} = (-b\tan\gamma, b, 0) \tag{2.45}$$

And,

$$O\vec{B} = (b\cot\phi_M, b, h_c \tan\phi_S) \tag{2.46}$$

Hence area of ABO can be calculated as half the norm of the cross product of vectors AO and BO,

$$A_{ABO} = \frac{|A \times B|}{2} = \frac{b}{2}\sqrt{b^2(\cot\phi_M + \tan\gamma)^2 + h_C^2 \tan^2\phi_S(\tan^2\gamma + 1)^2} \tag{2.47}$$

The area of the main shear plane can be calculated from the difference between the areas of plane OCFE and OCB, where this latter area is defined by vectors OC and OB. Using cross products it can be easily shown that,

$$A_M = A_{OCFE} - A_{OCB} = \frac{bK_W}{\sin\phi_M} - \frac{b}{2}\frac{(\tan\gamma + \cot\phi_M)}{\sin\phi_M}\tan\phi_S \tag{2.48}$$

Finally, the total area is,

$$A_T = \frac{bK_W}{\sin\phi_M} - \frac{b}{2}\frac{(\tan\gamma + \cot\phi_M)}{\sin\phi_M}\tan\phi_S + \frac{b}{2}\sqrt{b^2(\cot\phi_M + \tan\gamma)^2 + h_C^2\tan^2\phi_S(\tan^2\gamma + 1)^2}$$

Where,

$$h_C = b(\tan\gamma + \cot\phi_M) \tag{2.49}$$

2.4.3. Velocity Hodographs in the Two-edge Cutting Process for a General Hook Angle

Given that the chip is constrained to leave as a rigid body, the incoming material, with velocity V_0, must shear on the lateral and main shear plains in the way presented by the hodographs in Figure 2-14. The final velocity of all the material must be V_C and therefore the shear velocities induced on each of the shear planes must be V_{SM} and V_{SS} as shown.

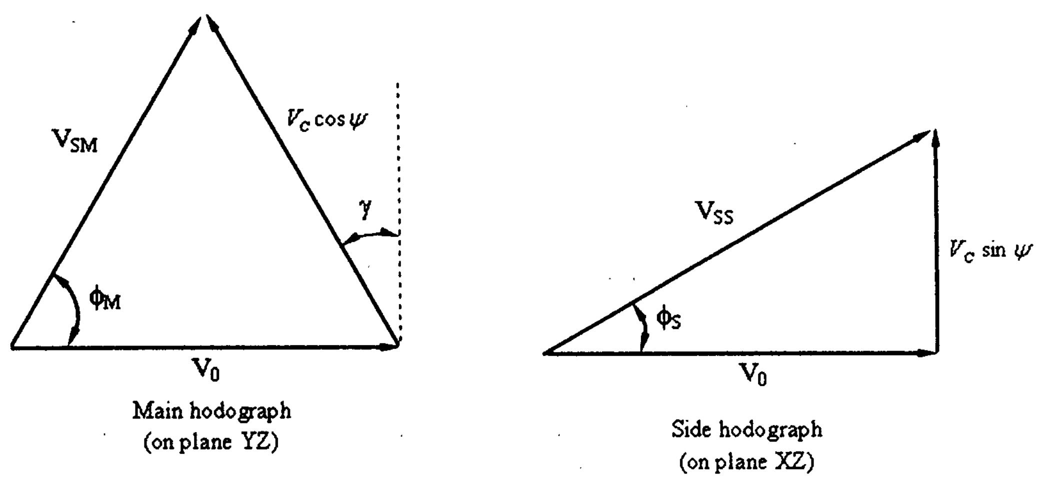

Figure 2-15. Process hodograph for the general two-edge cutting process shown in Figure 2-14

The magnitude of the total shear velocity in plane ABO is the norm of the resultant vector from the addition of $V_c\cos\psi$ and V_{SS} and can be expressed as,

$$V_{SST} = V_0\sqrt{\frac{\cos^2\gamma}{\cos^2(\phi_M - \gamma)} + \tan^2\phi_S} \tag{2.50}$$

Similarly, the velocity on shear plane BFEO can be expressed as,

$$V_{SST} = V_0 \sqrt{\frac{\sin^2 \phi_M}{\cos^2(\phi_M - \gamma)} + \frac{1}{\cos^2 \phi_S}} \tag{2.51}$$

2.4.4. Forces in the Two-edge Cutting Process for a General Hook Angle

In Section 2.3 a series of assumptions for the friction force in the cutting process were introduced and used in order to estimate the cutting forces. It will be considered here again that the friction force is proportional to the total area of shear and therefore,

$$F_f = C_f k A_T$$

The main cutting force can be readily calculated from the upper bound solution presented given that,

$$F_m = \frac{w}{V_0} \tag{2.52}$$

A convenient way to conduct the force balance for this case is to take the projection of the forces in a plane that contains the main force and the friction force vectors and treat the forces as a 2D system. This geometry is illustrated in Figure 2.14 and the corresponding force diagram shown in Figure 2.16 below. The angle θ_{mf} shown is measured between F_f and the Z axis on the plane of force projection.

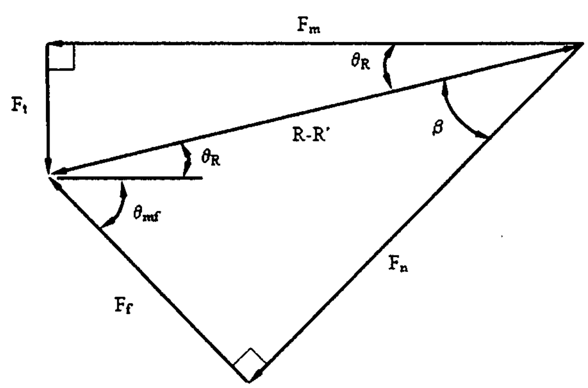

Figure 2-16. Force balance for process presented in Figure 2-14

Given that the magnitude and direction of $\boldsymbol{F_m}$ and $\boldsymbol{F_f}$ are known, the system can be solved and therefore the thrust force, $\boldsymbol{F_t}$ found since that direction of all the forces has already been defined in Figure 2-14. Given that the systems of force F_m- F_t and F_f -F_n are equivalent, the following expression can be obtained for θ_R.

$$\tan\theta_R = \frac{\cos\theta_{mf} - \dfrac{\dfrac{C_f A_T}{w}}{V_0 k}}{\sin\theta_{mf}} \tag{2.53}$$

Where the angle θ_{mf} can be found using the definition of dot product between a unit vector along the Z axis and $O\bar{D}$. If the unit vector is defined as $\hat{k} = (0,0,1)$, then we have,

$$\cos\theta_{mf} = \frac{O\bar{D}.\hat{k}}{|O\bar{D}||\hat{k}|} \tag{2.54}$$

Where $O\bar{D} = (h_c \tan\phi_S, b, b\tan\gamma)$ (2.55)

And finally,

$$\cos\theta_{mf} = \frac{\tan\gamma}{\sqrt{(\tan\gamma + \cot\phi_m)^2 + \tan\gamma + 1}} \tag{2.56}$$

2.4.5. Simulation Results for Two-edge Cutting Process for a General Hook Angle

Figure 2.17 shows the solution for the chip flow angle obtained from the upper-bound formulated in this section. The independent variable taken was the ratio of the bite to the kerf width. This is a measure of the amount of side edge in the cut with respect to the main edge

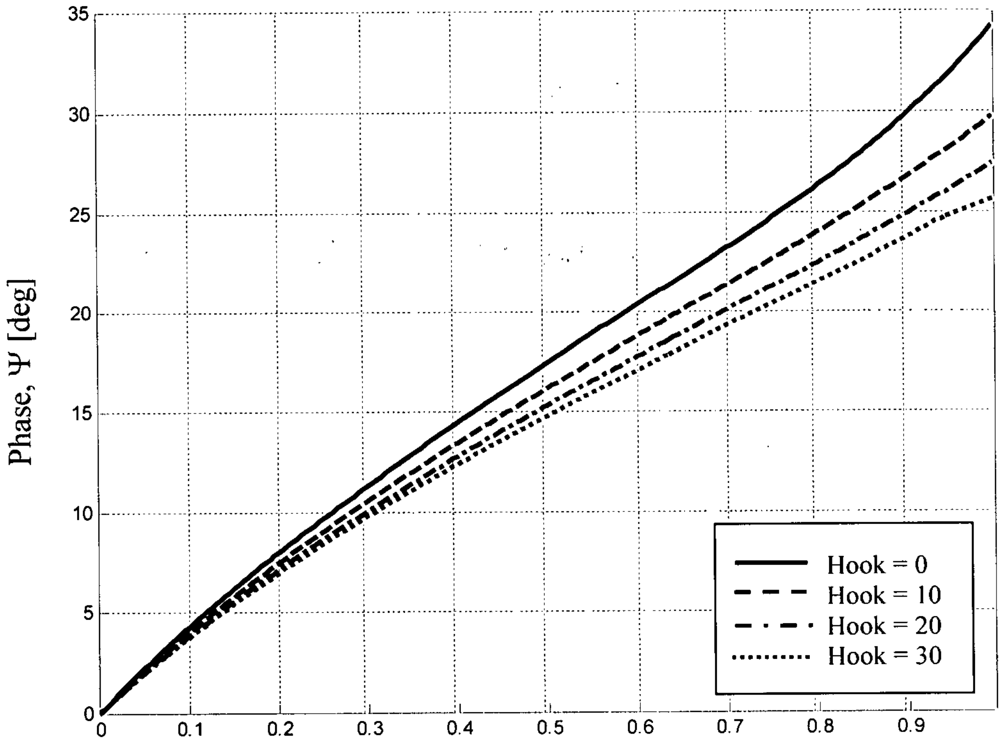

$$\frac{Bite}{K_w}$$

Figure 2-17. Simulation results for the chip flow angle in two-edge cutting for various values for the hook angle

The solid line represents a tool with zero hook angle, which is the case studied in Section 2.1. The solution corresponds to the one obtained in that previous section closely, when the friction constant $C_f = 2$, which is a reasonable value. The other lines in Figure 2.17 correspond to the solutions for tools with different amounts of hook. It can be seen that as the hook angle increases, ψ becomes less sensitive to the influence of the lateral cutting edge. The influence of this effect in the cutting forces has been simulated as well and it can be seen in Figures 2-18 through 2-20.

Figure 2-18 shows the increase in the non-dimensional main cutting force as the lateral cut is introduced. The force has been formulated in the form,

$$\frac{F}{kA} = f\left(\frac{b}{k_w}\right) \tag{2.57}$$

Where $f\left(\dfrac{b}{k_w}\right)$ is the function presented in Figures 2-18 through 2-20. This formulation allows the study of the effect of the departure of the cutting process from orthogonallity without accounting the increase in the uncut chip area. This is to say the solution presented actually corresponds to the increments in process stiffness.

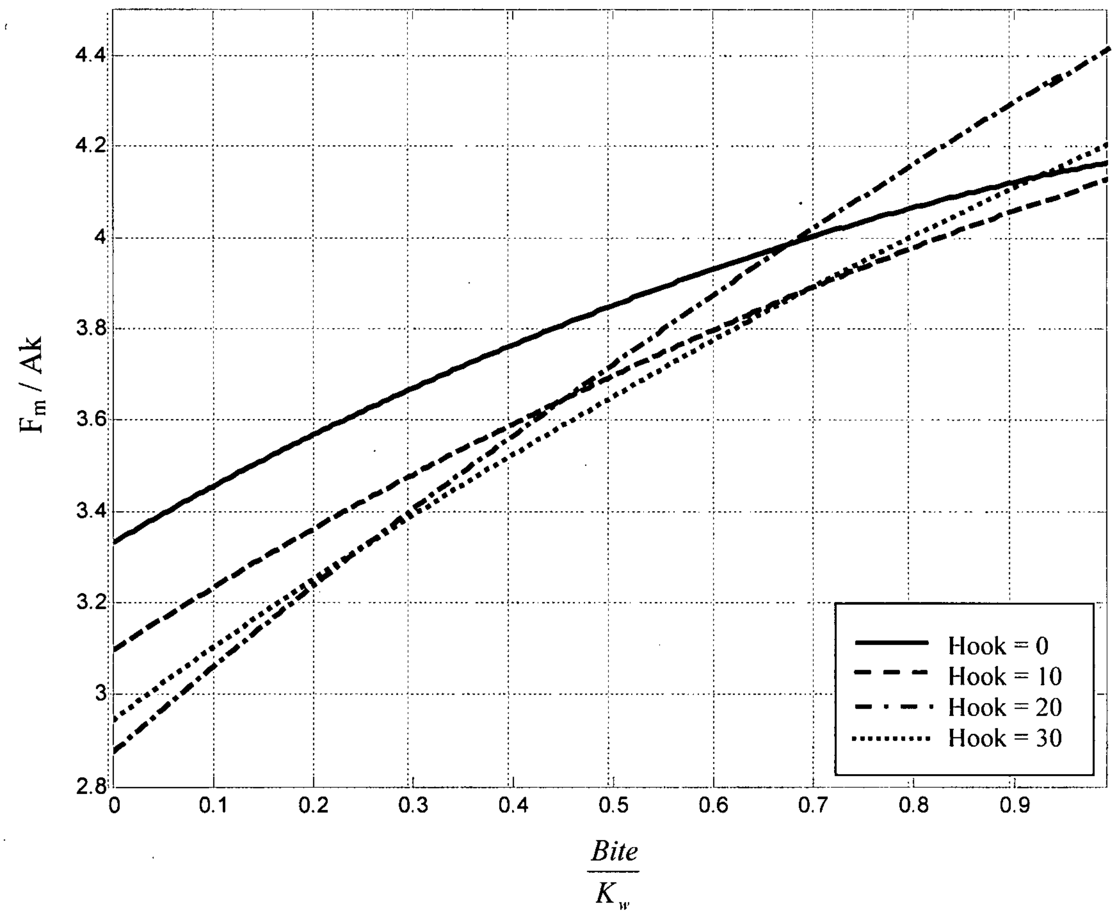

Figure 2-18. Simulation results for the non-dimensional main cutting force coefficient in two-edge cutting for various values for the hook angle

It can be seen that the main cutting force is lower for the tool with the highest hook angle when the cut is orthogonal. However, at the same time, this tool will develop the highest main cutting force when the size of the main and side cutting edge is equal.

The feed force seems to have little sensitivity to the addition of the side cutting edge as can be seen in Figure 2-19. Therefore it is expected that in bandsawing the lateral cut will create only a small amount of coupling between the feed cutting force and the lateral force.

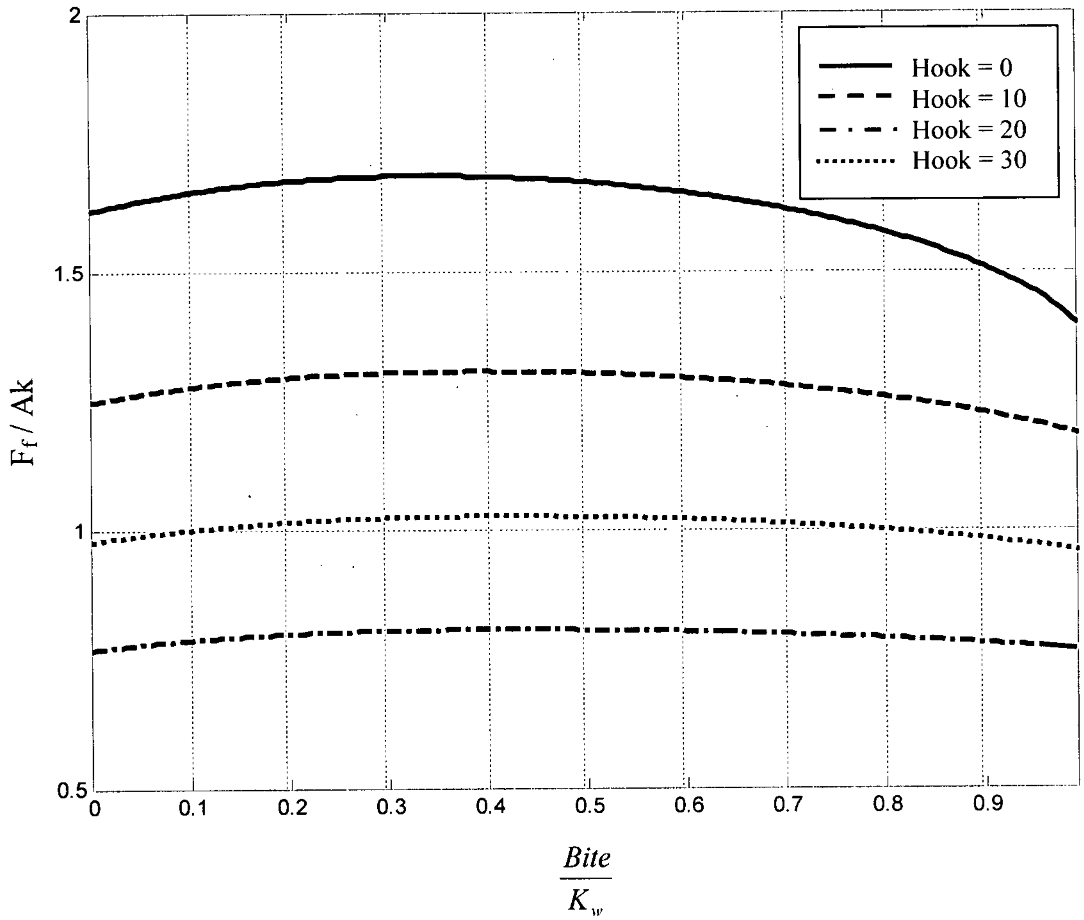

Figure 2-19. Simulation results for the non-dimensional feed cutting force coefficient in two-edge cutting for various values for the hook angle

Figure 2-20 shows the result for the lateral cutting force. It can be seen that 0 hook tool presents higher lateral stiffness than the 30 degree hook tool. It can be concluded that the increasing the hook angle in a sawblade most likely decreases the lateral cutting stiffness of the sawing process.

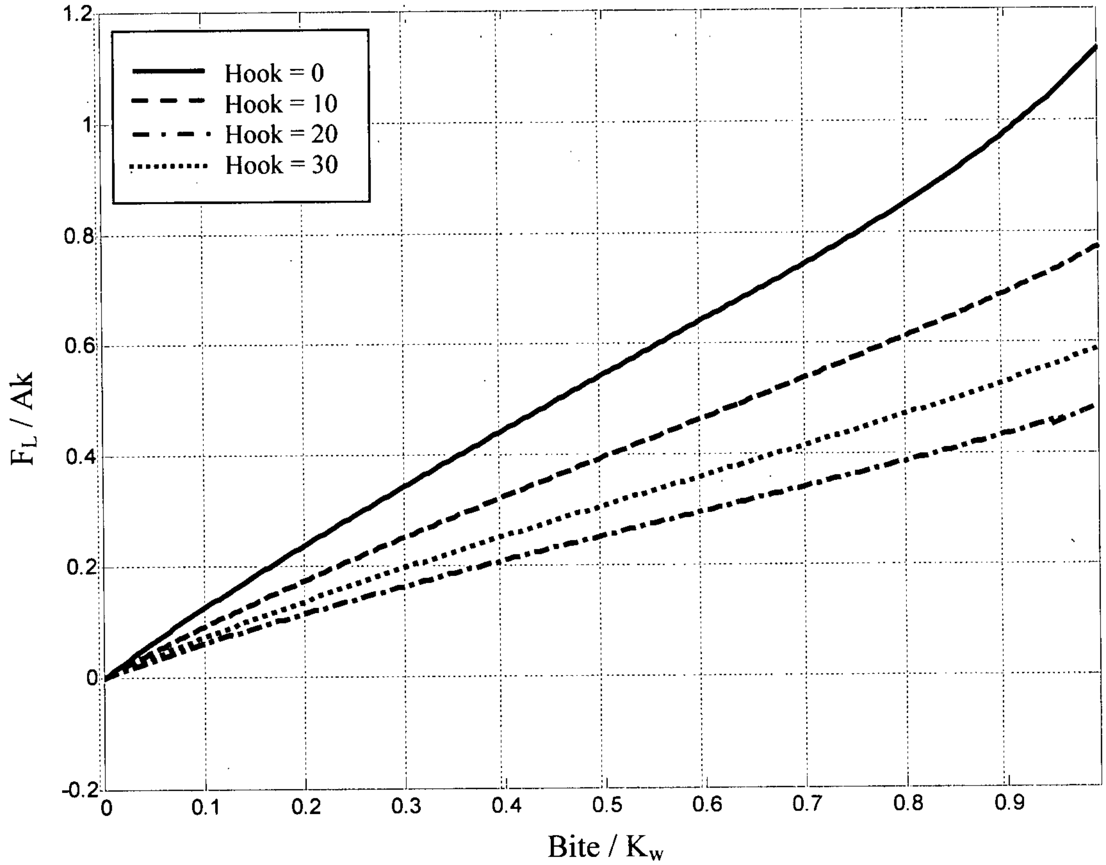

Figure 2-20. Simulation results for the non-dimensional lateral cutting force coefficient in two-edge cutting for various values for the hook angle

2.5. Summary

The following points summarize the most important findings of the study conducted in this chapter:

- The lateral cutting forces in the bandsawing process depend not only on the extra side cutting area but also on the length of the extra lateral cutting edge

- The cutting forces in bandsawing can be predicted if the influence of the lateral cut on the chip flow is known and a series of orthogonal cutting experiments are conducted in order to evaluate the stiffness of the process

- A series of upper-bound models have been developed in order to predict the chip flow angle on the face of the tool and therefore the cutting forces

- The lateral cutting force is non-linear with respect to the lateral cutting area

- The stiffness of the lateral cutting process decreases as the hook angle increases

CHAPTER III

"An expert is a man who has made all the mistakes which can be made in a very narrow field."

- Niels Bohr

3. ANALYTICAL DEVELOPMENT OF A DYNAMIC CUTTING FORCE MODEL FOR BANDSAWING

The second chapter of this thesis presented an analysis which addressed the modeling of the cutting forces created by saw teeth under static cutting conditions (constant chip load). It is to be expected that the velocities of the tool also have an effect on the cutting forces. This chapter presents a study of these effects through the development of an upper-bound model of the dynamic cutting process. The formulation includes the development of a simple model for the effects of a non-zero cutting edge radius. The final goal of the development presented here is to establish a methodology that can be used for the modeling of the dynamic sawing process. The dynamics of sawing are unique because of the fact that the vibrations of the tool occur in a direction that is perpendicular to the feed velocity.

3.1. An Upper-Bound Analysis of the Ploughing Process

The portion of the cutting forces which is related to the influence of the cutting edge is usually termed *"the ploughing component"*. This edge-related process plays an important role in chatter vibrations. When the speeds of cut are low as in, steel machining; the surface slopes left behind by the vibrating tool are significant when compared to the clearance angle of the tool. Under this condition, process damping is created by the interaction between the clearance face and the workpiece surface. Chatter vibrations are less likely to occur in this case. On the other hand, when the cutting speeds are higher as in machining of aluminum or wood, the slopes present in the dynamic cutting process are small compared to the clearance. In this case, the damping induced by the flank of the tool is low and chatter vibrations are likely to arise.

It is worthwhile to conduct a detailed examination of the application of the upper-bound method to the modeling of the edge forces in orthogonal cutting before examining the more complex issue of dynamic cutting. Therefore this section presents an analysis of the ploughing process. The model assumes an edge radius on the cutting tool. The presence of this hone introduces some deformation under the edge of the tool. Force equilibrium is used in order to estimate the length of plastic contact on the rake face.

3.1.1. Geometry Model Proposed for the modeling of the Ploughing Forces

Manjunathaiah and Endres [33] presented a model for orthogonal cutting in which the influence of an edge-radius on the tool is explicitly accounted for in the force expressions. The proposed geometry is shown in Figure 3.1. The material enters the cutting region with velocity V_0 and shears along plane AB. After that, the material flows as a whole inside ABP. Angle θ defines the separation point P, which determines the penetration depth δ for a given tool radius. All material above this point will flow up and become chip. All material below P will be deformed further through shear along BP and BC and will finally become part of the freshly cut surface.

Manjunathaiah and Endres obtained a solution for the value of ϕ as a function of δ. However no analytical expression is available for the calculation of the depth of penetration that allows a direct solution for the forces. It is proposed here that the model presented in [33] be extended including an estimate of the depth of penetration using the upper-bound approach.

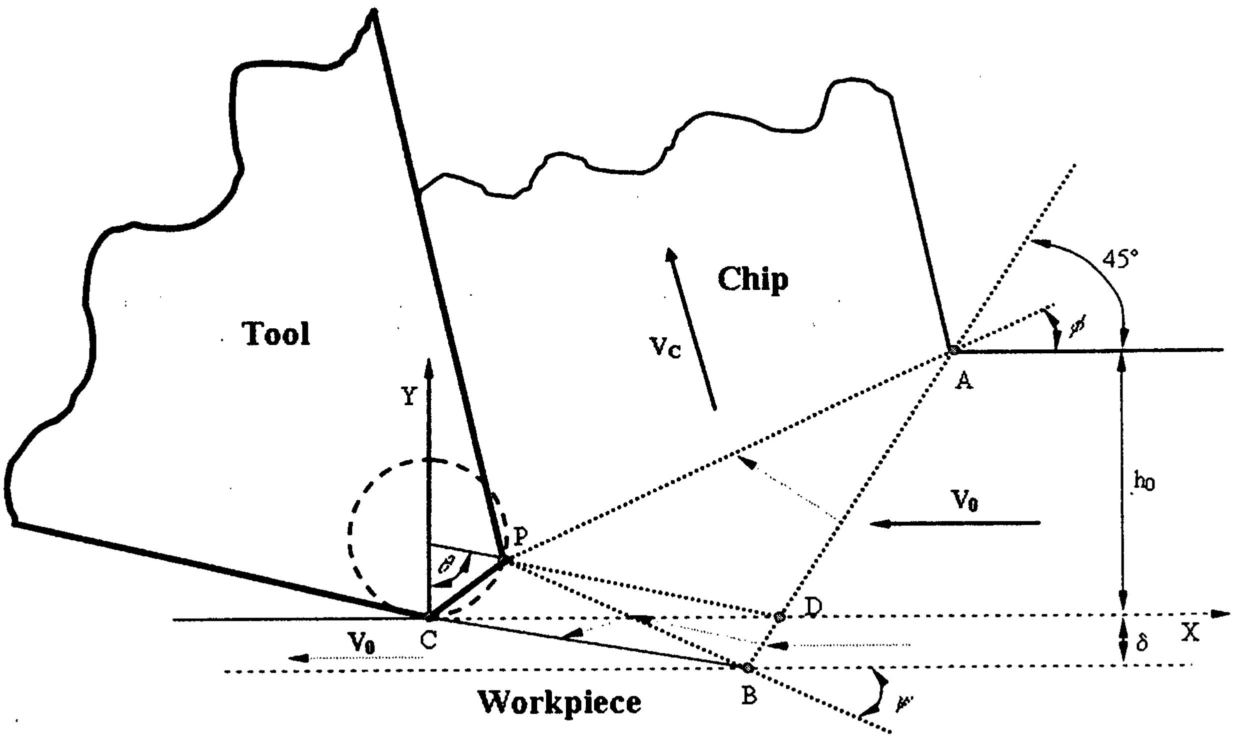

Figure 3-1. Manjunathaiah and Endres' model

The geometry shown in Figure 3-2 illustrates the idealization proposed for the analysis. A tool with some wear on the edge is removing material with constant chip thickness, h_0. The workpiece moves towards the tool with speed of cut V_0. The wear on the tool has been approximated to a straight line between points C and D as shown. The clearance angle is α and the hook angle γ. The plastic deformation zone extends below the cutting edge by amount δ, which will be referred to as *penetration depth*. The arrows in Figure 3.2 illustrate the material flow in the cutting model.

The following are the considerations made for this model:

1. All assumptions made for the model presented in section 2.2.

2. The edge nose of the tool is approximated to a straight line between points C and D

3. Shear plane BC is collinear with the face of the tool

Initially, all the incoming material yields on plane AB entering triangle ABC. Inside this region all the material flows with velocity V_{ABC}. Point C is a stagnation point, which divides the flow in two different directions. Any material above C will become chip after shearing on plane AC. Any material below C will shear again on plane BC entering region BCD, where it will have velocity V_{BCD}. Finally this portion of the flow will become part of the workpiece again by shearing on plane BD.

In Figure 3.2 only ϕ and L are independent variables. The solution proposed requires the minimization of the power with respect to these two variables.

After defining all the magnitudes for the deformation geometry, the penetration depth can be now written in terms of the hook angle and the nose radius of the tool as,

$$\delta = L\cos\gamma - r(1+\sin\gamma) \tag{3.1}$$

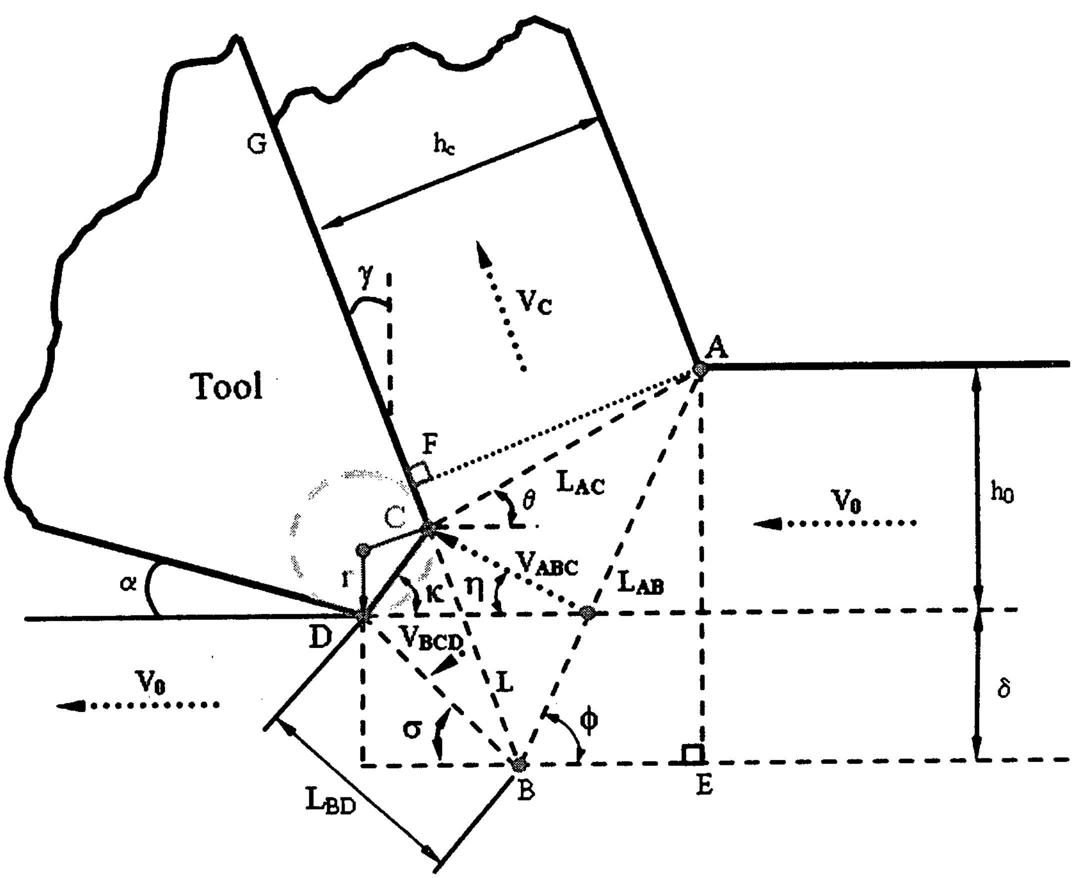

Figure 3-2. Geometric model proposed for the upper-bound solution of the ploughing forces in cutting with an edge-radiused tool

In the first part of the analysis, the specific case of a frictionless tool will be considered. In this case the power on the process will be the sum of the power expenditure in each of the shear planes considered. In order to find these quantities, the area of shear for all the planes must be calculated as well as the velocity across them.

The shear areas can be found using simple geometry by considering the triangles defined by points A, B, C, D and F in Figure 3.2. The width of cut is considered to be unity.

It can be seen by considering triangle ABE that the length of the shear plane AB is,

$$L_{AB} = \frac{h_0 + \delta}{\sin\phi} \tag{3.2}$$

Angle θ can be found as a function of ϕ and L considering triangle ABC,

$$\tan\theta = \frac{h_0 + \delta - L\cos\gamma}{L\sin\gamma + L_{AB}\cos\phi} \tag{3.3}$$

From ABC, the length of AC can be obtained as,

$$L_{AC} = L_{AB}\frac{\cos(\phi - \gamma)}{\cos(\theta - \gamma)} \tag{3.4}$$

The angle κ is assumed to be an effective negative hook angle at the nose of the tool. This parameter is only affected by the main hook angle and it can be expressed as,

$$\kappa = \tan^{-1}\left(\frac{1+\sin\gamma}{\cos\gamma}\right) \tag{3.5}$$

The assumed length of the nose of the tool is then,

$$L_{CD} = \frac{r\cos\gamma}{\cos\kappa} \tag{3.6}$$

Angle σ defines the orientation of line BD and is given by,

$$\sigma = \tan^{-1}\left(\frac{\delta}{\delta\cot\phi + L\sin\gamma}\right) \tag{3.7}$$

Length BD can be found using triangle BCD,

$$L_{BD} = \frac{\delta}{\sin\sigma} \tag{3.8}$$

3.1.2. Velocity Hodograph for the Ploughing Process

Lines AB, BC, AC and BD all define velocity discontinuities where the material is assumed to shear instantaneously. A hodograph, showing the proposed kinematics of the solution for the cutting process is presented in Figure 3-3.

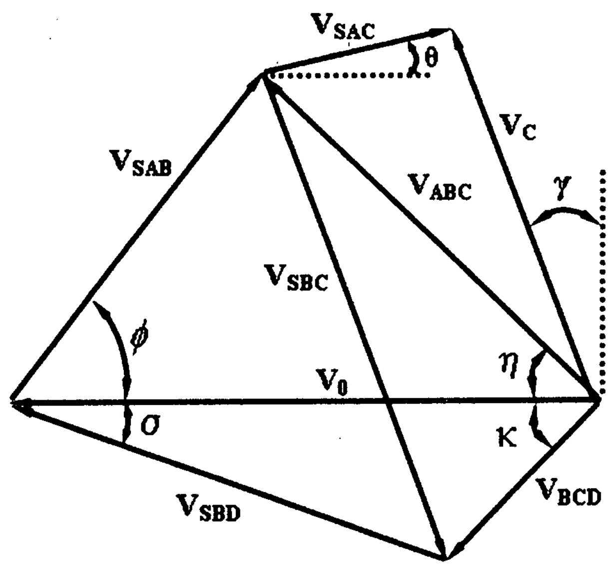

Figure 3-3. Velocity hodograph for the ploughing model

In order to comply with volume continuity the incoming flow to the cutting region must be the same as the outgoing flow. In order to meet this constraint, the value for angle η must be,

$$\eta = \arctan\left(\frac{r(1+\sin\gamma)}{\delta\cot\phi + L\sin\gamma}\right) \tag{3.9}$$

The velocity on the shear plane AB is,

$$V_{SAB} = V_0 \frac{\sin\eta}{\sin(\eta+\phi)} \tag{3.10}$$

The velocity for all the material inside region ABC is,

$$V_{ABC} = V_0 \frac{\sin\phi}{\sin(\eta+\phi)} \tag{3.11}$$

And on shear plane AC it is seen that,

$$V_{SAC} = V_{ABC} \frac{\cos(\gamma+\eta)}{\cos(\gamma-\theta)} \tag{3.12}$$

The velocity of the chip can be easily found from volume continuity and is given by,

$$V_C = V_{SABC} \frac{\sin(\eta+\theta)}{\cos(\theta-\gamma)} \tag{3.13}$$

The velocity of the material inside region BCD is,

$$V_{BCD} = V_0 \frac{\sin\sigma}{\sin(\sigma+\kappa)} \tag{3.14}$$

Since BG is a line of velocity discontinuity, the shear velocity on shear plane BC must be in the same direction as the chip velocity and therefore the following relation can be established,

$$V_{SBC} = V_{ABC}\sin(\eta-\gamma) + V_{BCD}\sin(\kappa-\gamma) \tag{3.15}$$

Finally, the velocity on shear plane BD is found to be,

$$V_{SBD} = V_0 \frac{\sin\kappa}{\sin(\sigma+\kappa)} \tag{3.16}$$

The shear work rate is the product of the shear force and the shear velocity. The overall work rate is the sum of the shear work in planes AB, AC, BC and BD. For the frictionless case the expression for the power is,

$$w = w_{SAB} + w_{SAC} + w_{SBC} + w_{SBD} \tag{3.17}$$

Where each of the power expressions is given by,

$$w_{AB} = L_{AB}V_{SAB} = \frac{(h_0 + P)}{\sin\phi}\frac{\sin\eta}{\sin(\eta+\phi)}kwV_0 \tag{3.18}$$

$$w_{AC} = L_{AC}V_{SAC} = \frac{(h_0 + P)}{\cos(\theta-\gamma)}\frac{\cos(\phi-\gamma)}{\sin(\eta+\phi)}\frac{\cos(\gamma+\eta)}{\cos(\gamma-\theta)}kwV_0 \tag{3.19}$$

$$w_{BC} = Lkw\left[V_{ABC}\sin(\eta-\gamma) + V_{BCD}\sin(\kappa-\gamma)\right] \tag{3.20}$$

$$w_{BD} = \frac{\delta}{\sin\sigma}\frac{\sin\kappa}{\sin(\sigma+\kappa)}kwV_0 \tag{3.21}$$

The upper-bound solution requires that the work rate is minimized. This minimum leads to the specification of unique values for the penetration depth δ and the shear angle ϕ. Because this work is aimed at examining more complex problems, from the start the system has been modeled using a numerical analysis package to allow rapid determination of minimum values.

3.1.3. Friction Considerations in the Analysis of the Ploughing Process

In order to include the effect of friction in this process, it is assumed that the boundary ACF on the chip meets force equilibrium. F is a separation point, which defines the end of the friction contact on the face of the tool. A free-body diagram of the chip is shown in Figure 3-4.

The shear force for a unit width of cut is equal to the product of the shear yield stress and the shear area assuming unit width is,

$$F_S = kL_{AC} \tag{3.22}$$

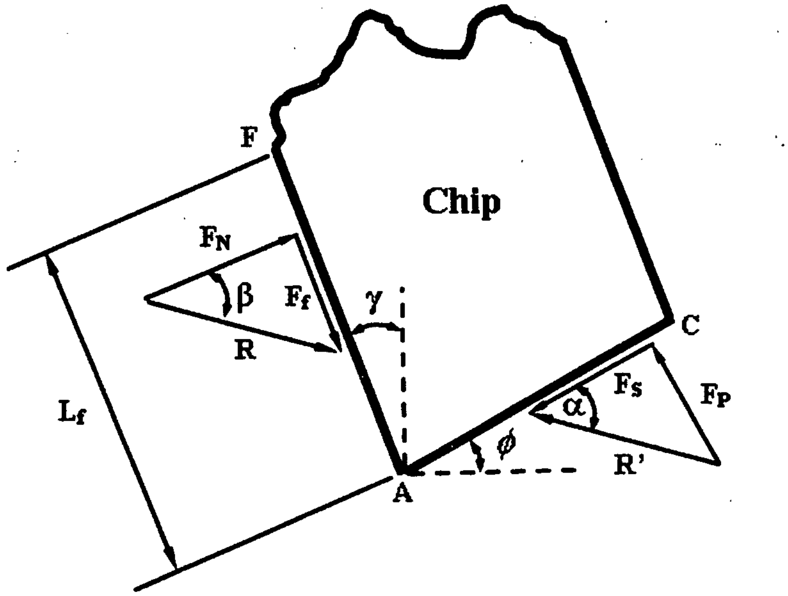

Figure 3-4. Force balance on the chip for the ploughing model with edge penetration

To maintain force equilibrium, the normal force on the shear plane must be related to the shear force by the angle α as follows,

$$F_P = F_S \tan\alpha$$

Where,

$$\alpha = \phi + \beta - \gamma \tag{3.23}$$

Seethaler and Yellowley [29] considered the friction coefficient to be the ratio of two plastic stresses by assuming an ideal rigid-plastic material and sticking friction on the hook face of the tool. The following expression was presented for the friction angle,

$$\tan\beta = \frac{1}{1 + \frac{\pi}{2} - 2\gamma} \tag{3.24}$$

The resultant force can also be expressed in terms of the shear force and α,

$$R = \frac{F_S}{\cos\alpha} = \frac{F_S}{\cos(\phi + \beta - \gamma)} \tag{3.25}$$

The friction on the face of the tool will be a combination of elastic and a plastic component. However it will be assumed that all the friction is plastic and therefore the force can be expressed as the product of the shear yield stress, k, and the plastic contact area,

$$F_f = kL_f \tag{3.26}$$

The friction can also be expressed in terms of the resultant force as follows,

$$F_f = R\sin\beta = \frac{F_S \sin\beta}{\cos(\phi + \beta - \gamma)} \tag{3.27}$$

Hence, substituting equations (3.22) and (3.26) in equation (3.27) yields an expression for the plastic contact length,

$$L_f = L_{AC}\frac{\sin(\beta)}{\cos(\theta + \beta - \gamma)} \tag{3.28}$$

Finally, replacing the value for L_{AC} from equation 3.4 it is seen that,

$$L_f = \frac{h_0}{\sin\phi}\frac{\cos(\varepsilon - \phi)}{\cos(\theta - \varepsilon)}\frac{\sin\beta}{\cos(\theta + \beta - \gamma)} \tag{3.29}$$

The friction work done along boundary CF can be calculated as the product of the velocity of the chip and the friction force on the face of the tool. The final expression for this quantity is,

$$w_{f,face} = \frac{\sin\beta}{\cos(\theta - \gamma)\cos(\theta + \beta - \gamma)}V_0 h_0 \tag{3.30}$$

The expression presented above has been added to the power calculated in section 3.1.2 and a numerical solution for the shear angle, ploughing angle and non-dimensional cutting force is presented in the following section.

3.1.4. Results for the Ploughing Geometry

Figure 3-5 shows the resulting shear angle, ϕ for four different hook angle configurations as a function of the radius of the nose of the tool. It can be seen from the figure that the ploughing process does affect the main shear process by changing the orientation of the main shear plane.

For the tool with 30° hook angle, it can be observed that over the range of tool radius shown, the shear angle changes 12 degrees. In contrast, for the 0° tool, the shear angle only changes by 5° over the same range. It can therefore be concluded from this model that tools with a large positive hook angles are more sensitive to ploughing those with a smaller hook.

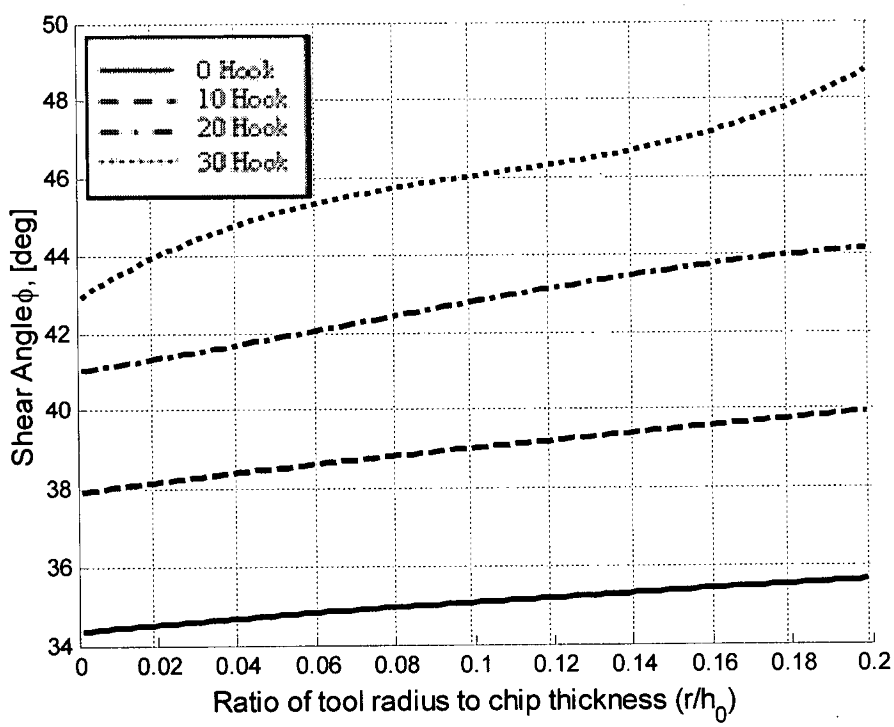

Figure 3-5. Solution for the shear angle, $h_0 = 1.0$

Figure 3-6 shows the penetration depth below the edge of the tool as a function of the nose radius. Surprisingly this model predicts that no penetration will occur. This also implies no flow and therefore no relative motion of the portion CBD with respect to the tool. This is known as built-up edge and it is known to occur in the cutting of metals and wood.

The finding that the material in front of the tool will only stick to the edge and not flow under the tool to create a new surface eliminates the need to assume the direction of BC to be collinear with the face of the tool. The model in the following section assumes zero penetration as a starting point, and allows the upper-bound to find the direction of the stress field in front of the face of the tool.

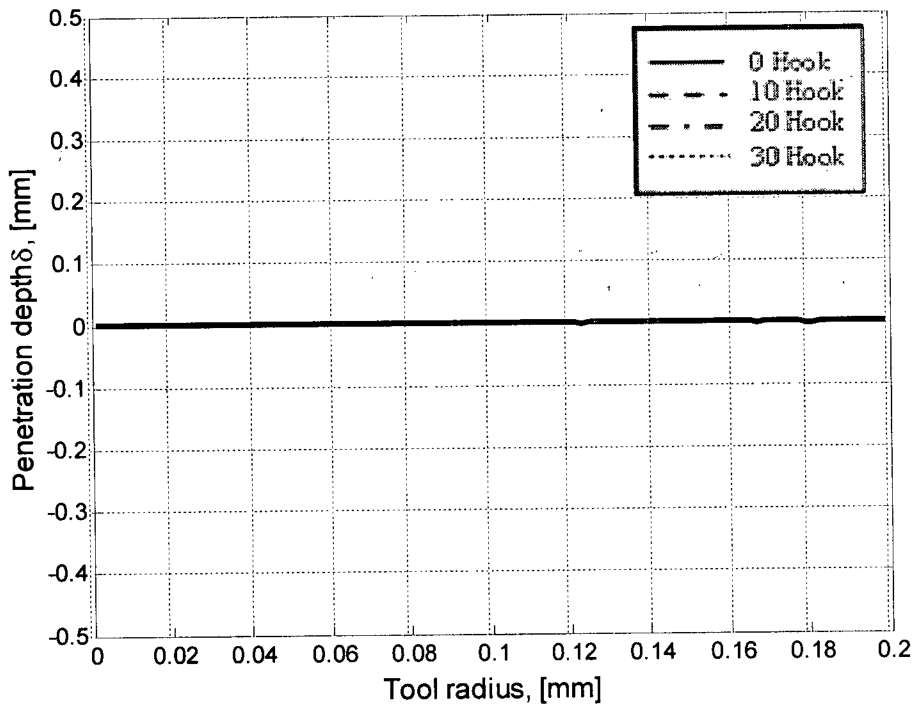

Figure 3-6. Penetration depth δ (below the edge of the tool)

3.2. A Built-up Edge Analysis of the Ploughing Process

The model developed so far predicts the existence of a built-up edge on the tool. Based on this a new, more simple ploughing analysis can be proposed. Assumption number three in section 3.1.1 can be eliminated and the geometry of the cutting region can be studied with respect to a new variable that will be called *Ploughing Angle* in this section. It is assumed again that the presence of the nose radius on the tool distorts the cutting field from the orthogonal cutting situation. The stress below the surface of the tool creates a feed component that adds to the cutting force in the feed and main directions.

3.2.1. Proposed Geometry for the Built-up Edge Analysis of the Ploughing Process

The geometry proposed is shown in Figure 3-7. The tool is cutting material with an intended chip thickness h_0. The edge of the tool presents a honed region that has a built-up edge in front. As the tool moves along, the incoming material shears along the first shear plane AB and its velocity changes to V_{ABC}. This velocity is parallel to line BC, which defines the boundary of the ploughing region CBG. Shear occurs again when the material reaches plane AC. Finally the material leaves the primary cutting region and travels along the face as chip with velocity V_C.

In order to calculate the power spent on the cutting process, the lengths of the shear planes need to be derived in terms of the proposed geometry. The independent variables in this model are the shear angle ϕ and the ploughing angle ε and therefore all the magnitudes will be derived as a function of them.

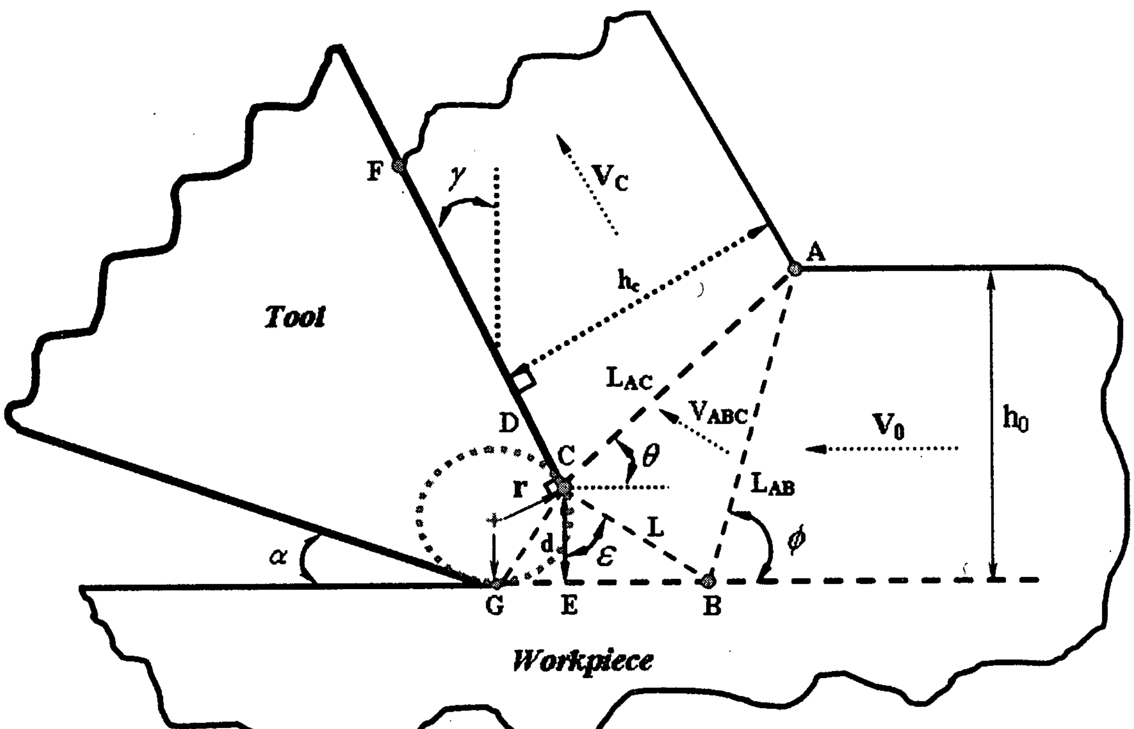

Figure 3-7. Built-up edge model geometry

Length L, can be expressed as a function of the ploughing angle ε, the hook angle γ and the radius of the nose of the tool r. From triangle BCE in Figure 3-7 it can be shown that,

$$L = \frac{r(1+\sin\gamma)}{\cos\varepsilon} \tag{3.31}$$

The length of the main shear plane AB is can be calculated in terms of the shear angle and the uncut chip thickness as follows,

$$L_{AB} = \frac{h_0}{\sin\phi} \tag{3.32}$$

The length of the secondary shear plane AC can obtained considering triangle ABC,

$$L_{AC} = L_{AB}\frac{\cos(\varepsilon-\phi)}{\cos(\theta-\varepsilon)} \tag{3.33}$$

The chip thickness can be found in terms of the uncut chip thickness as,

$$h_C = \frac{h_0}{\sin\phi}\frac{\cos(\varepsilon-\phi)\cos(\theta-\gamma)}{\cos(\theta-\varepsilon)} \tag{3.34}$$

Angle θ is a function of ε, ϕ and the ratio L_{ab}/L and it is given by,

$$\tan\theta = \frac{\frac{L_{AB}}{L}\sin\phi - \cos\varepsilon}{\sin\varepsilon + \frac{L_{AB}}{L}\cos\phi} \tag{3.35}$$

The distance along the bottom boundary of the ploughing regions, L_{BG} is given by,

$$L_{BG} = r(1+\sin\gamma)\tan\varepsilon + r\cos\gamma \tag{3.36}$$

Equations 3.31 through 3.34 provide all the lengths needed in order to calculate the power in the cutting process. The next step requires proposing an admissible velocity field for the problem.

3.2.2. Velocity Hodograph for the Built-up Edge Analysis of the Ploughing Process

The incoming velocity is V_0 and the shear velocities are V_{SAB} and V_{SAC}. The addition of the incoming and shear velocities vectors must equal the outgoing chip velocity V_C as represented in the following figure.

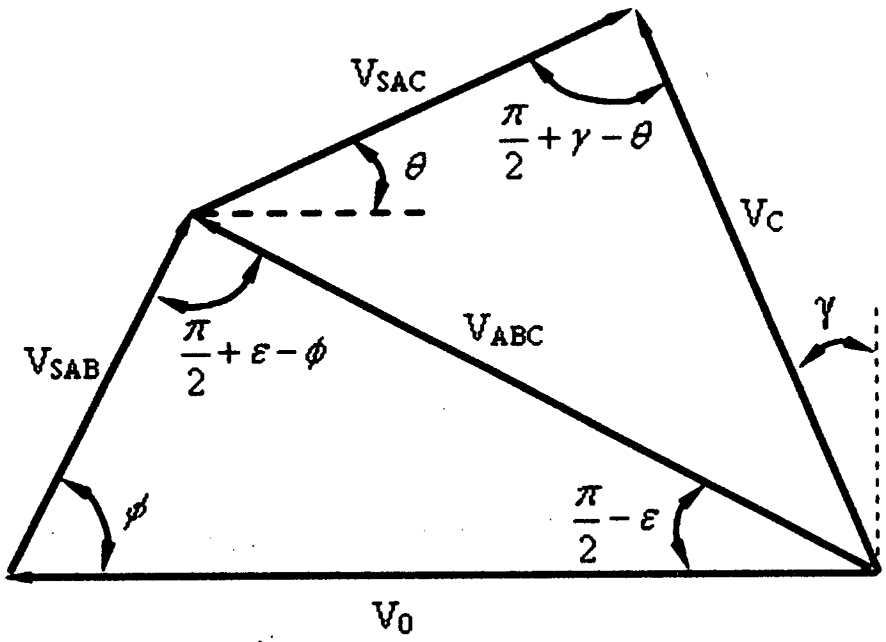

Figure 3-8. Velocity hodograph for the ploughing model in Figure 3-7

Given that ϕ and ε are considered independent variables, the velocity in region ABC can be calculated as,

$$V_{ABC} = \frac{\sin\phi}{\cos(\varepsilon-\phi)} V_0 \tag{3.37}$$

The shear velocities can also be easily found from the hodograph as follows,

$$V_{SAB} = \frac{\cos\varepsilon}{\cos(\varepsilon-\phi)} V_0 \tag{3.38}$$

$$V_{SAC} = \frac{\sin\phi\sin(\varepsilon-\gamma)}{\cos(\varepsilon-\phi)\cos(\theta-\gamma)} V_0 \tag{3.39}$$

Where θ can be obtained from equation 3.35

The chip velocity can be found from volume continuity along boundary ABCD and is given by,

$$V_C = \frac{\sin\phi\cos(\theta-\varepsilon)}{\cos(\varepsilon-\phi)\cos(\theta-\gamma)} V_0 \tag{3.40}$$

3.2.3. Power Spent in the Frictionless Ploughing Process

Shear power in this process is spent in shear planes AB and AC and also along the built-up edge boundary on BC and BG. The expressions for the power spent can be obtained by taking the product between the force and the velocity along the planes considered. If it is assumed that the boundaries of the cutting region are stressed to the yield point, then it is possible to obtain the following expressions for the power,

$$w_{SAB} = kwL_{AB}V_{SAB} = \frac{\cos\varepsilon}{\sin\phi`\cos(\varepsilon-\phi)}kwh_0V_0 \tag{3.41}$$

$$w_{SAC} = kwL_{AC}V_{SAC} = \frac{\sin(\varepsilon-\gamma)}{\cos(\theta-\varepsilon)\cos(\theta-\gamma)}kwh_0V_0 \tag{3.42}$$

$$w_{SABC} = kwLV_{ABC} = \frac{\sin(\varepsilon-\gamma)}{\cos(\theta-\varepsilon)\cos(\theta-\gamma)}kwh_0V_0 \tag{3.43}$$

$$w_{BG} = kwL_{BG}V_0 = kwV_0\left[r(1+\sin\gamma)\tan\varepsilon + r\cos\gamma\right] \tag{3.44}$$

The total power spent in the frictionless process will be the sum of equations 3.41 through 3.44. The value of k, w and V_0 is irrelevant to the solution since they are constants present in all the terms and therefore will not affect the minimization of the work function.

Further considerations will be made in section 3.2.5 in order to find a reasonable estimate of the friction in the cutting process. This needs to be done to include a friction term in the final solution to the model. For now, the frictionless case will be studied in section 3.2.4.

3.2.4. Frictionless results for the Built-up Edge Analysis of the Ploughing Process

Given that the goal of this analysis is to obtain a simple ploughing model that can be used to estimate actual cutting conditions in dynamic cutting, a numerical approach has been used from the beginning to obtain the values for the ploughing and shear angles. Figure 3-9 shows the solution for the shear angle as a function of the tool radius for four different values of hook angle.

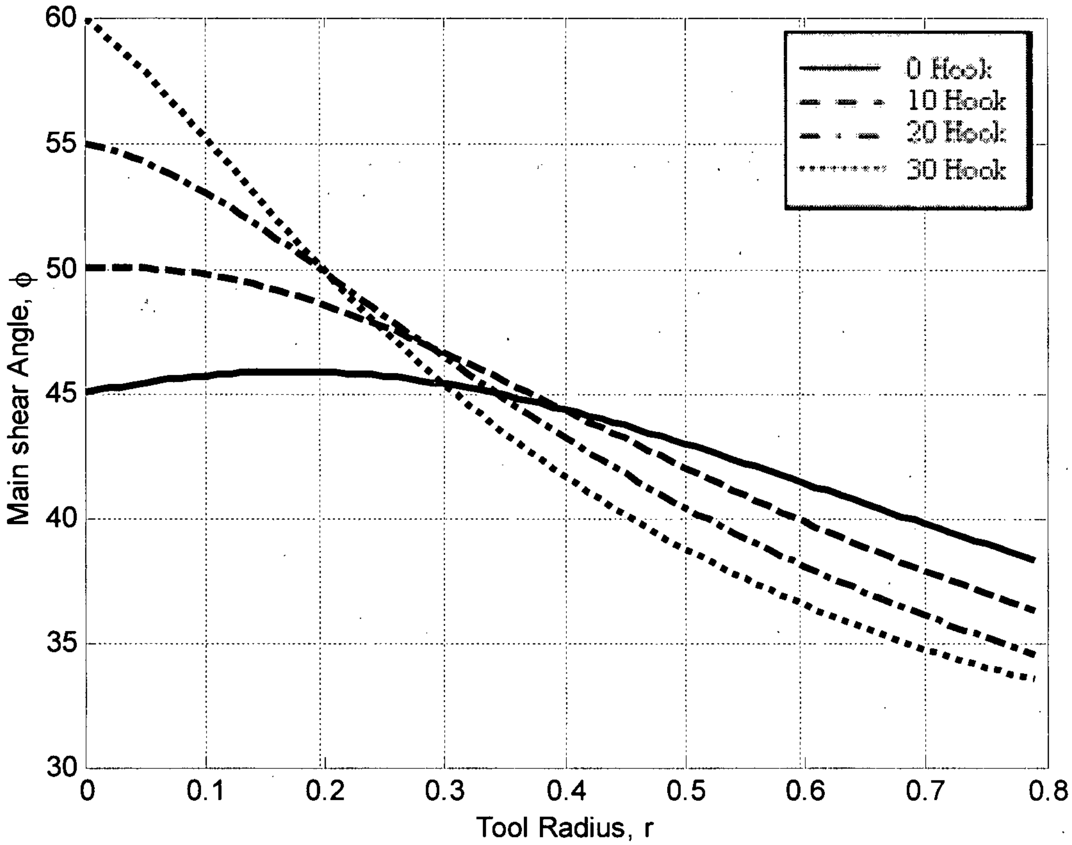

Figure 3-9. Main shear angle, φ for frictionless process, h_0=1.0

It can be seen in Figure 3-9 that the model predicts the same value as merchant model (equation 1.4) for the frictionless case, which serves as a simple way to verify that the solution obtained is correct.

The model shows great sensitivity of the main shear angle with respect to the nose radius of the tool. For the zero hook tool the shear angle seem to increase slightly up to $r = 0.2$ and then decrease. For all the other cases, the nose radius decreases the shear angle which is a similar effect to that of introducing friction in the process.

When compared to Figure 3-5, the figure above seems to show that the solution obtained for this model varies significantly to that found in section 3.2. This is due to the assumption on the extension of the hook of the tool below the cutting edge made in the previous model, which is not employed in this case.

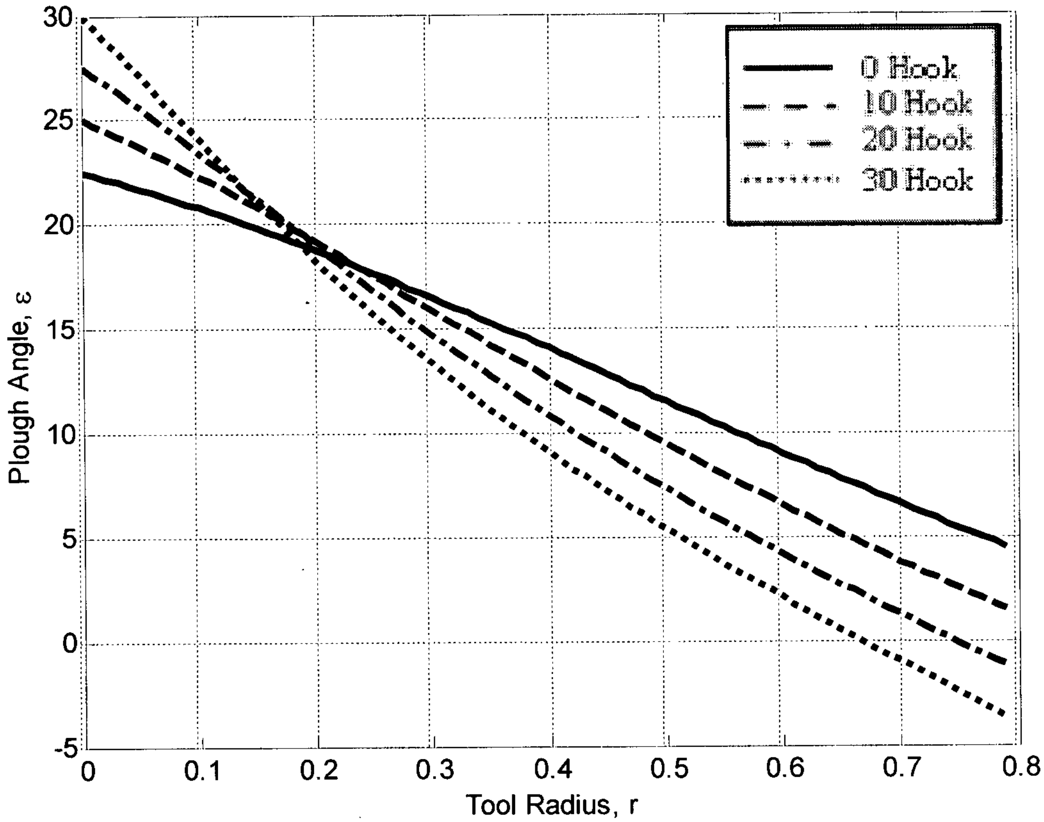

Figure 3-10. Ploughing angle, ε for frictionless process, h_0=1.0

Figure 3-10 shows the results obtained for the ploughing angle versus the radius of the nose of the tool. Significant sensitivity can be observed. For the case γ = 30° it can be seen that for zero nose radius on the tool, planes BC and the face of the tool are collinear. However, as the radius increases the slope of line BC seems to be smaller than that of the hook face going down to even negative values for the ploughing angle. This is evidence that the assumption made for the previous model might not be correct. It is also found in the result above that a tool with a larger positive hook angle is more sensitive to the influence of the nose radius over the cutting forces.

Figure 3-11 shows the non-dimensional main cutting force plotted versus the tool nose radius. For all cases the force increases with the radius of tool. However, the effect on the 30 degree hook tool seems to be less linear than that of the other three tools.

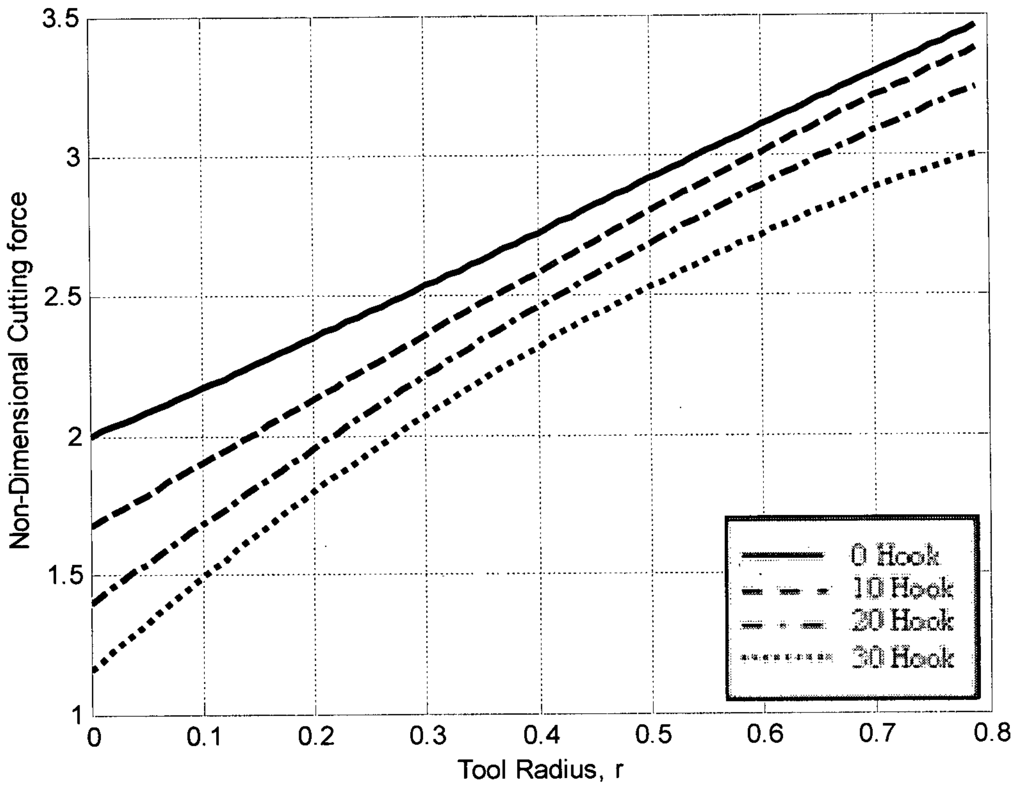

Figure 3-11. Non-dimensional cutting force for frictionless process, h_0=1.0

3.2.5. Adding Friction to the Analysis of the Ploughing Process

The formulation presented for the process friction in section 3.1.3 will be followed once more in order to add an estimate of the friction force in the cutting process,

$$F_f = R\sin\beta = \frac{F_S \sin\beta}{\cos(\phi+\beta-\gamma)} \tag{3.27, repeated}$$

Therefore, the following term must be added to the internal power spent in the process,

$$w_f = \frac{F_S \sin\beta}{\cos(\phi+\beta-\gamma)} \frac{\sin\phi\cos(\theta-\varepsilon)}{\cos(\varepsilon-\phi)\cos(\theta-\gamma)} V_0 \tag{3.45}$$

3.2.6. Results for the Built-up Edge Analysis of the Ploughing Process Considering Friction Effects

Figure 3-12 shows the main shear angle ϕ plotted as a function of the tool nose radius for four values of the hook angle.

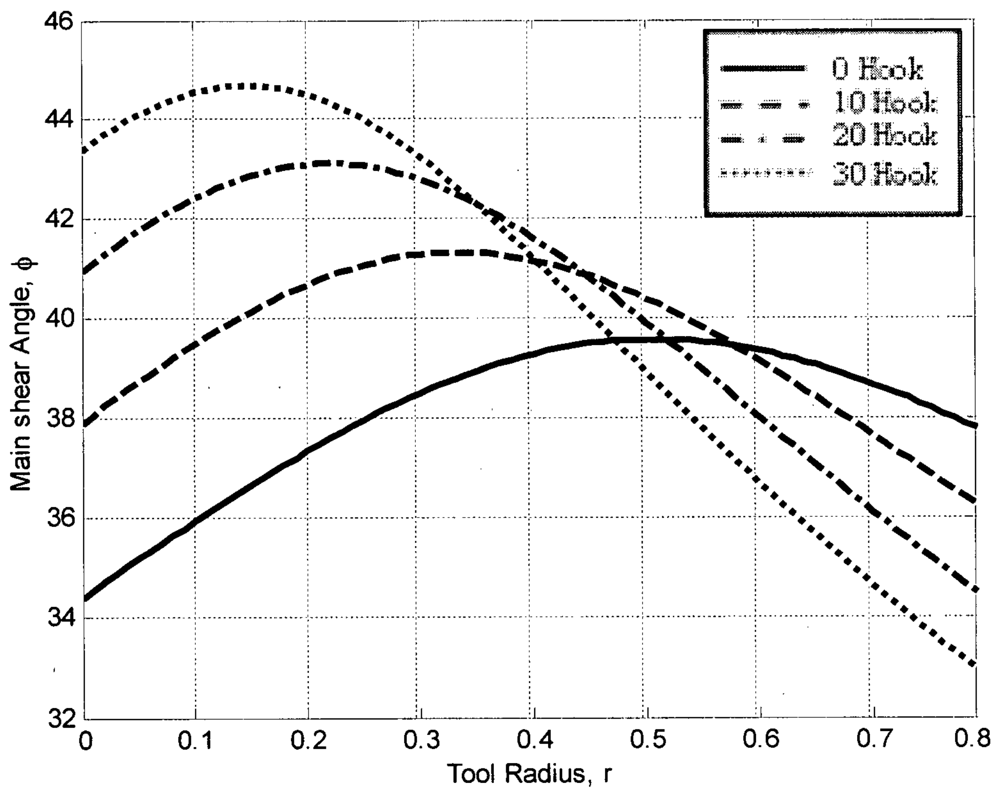

Figure 3-12. Main shear angle, φ, for the case with friction, h_0=1.0

Figure 3-13 shows the ploughing angle ε plotted as a function of the tool nose radius for four values of the hook angle. It can be seen that the shear angle increases with the increment of the tool radius initially and then decreases.

The ploughing angle decreases consistently with the increase in tool radius for all values of hook angles. It can be seen that as the hook is increased, the ploughing angle becomes more sensitive to the size of the nose of the tool.

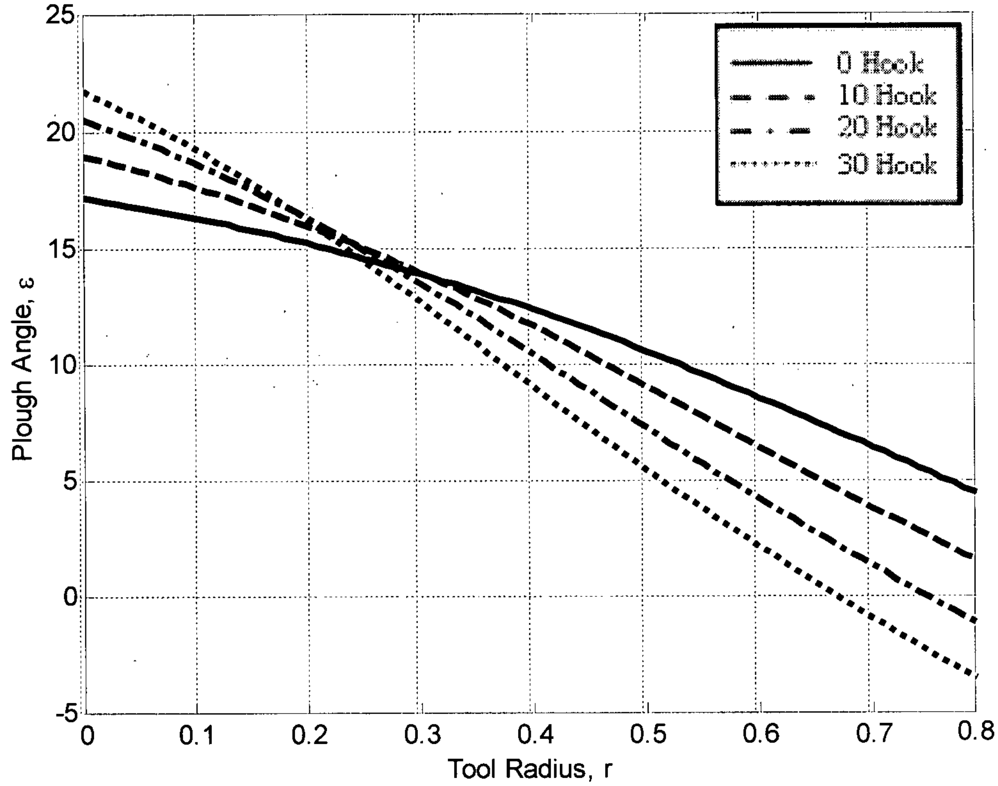

Figure 3-13. Ploughing angle, ε, for the case with friction, h_0=1.0

Figure 3-14 shows the non-dimensional cutting force plotted as a function of the tool nose radius for four values of the hook angle. In a similar way to that seen in Figure 3.11, the specific energy required to remove the material increases consistently with the increment in the nose radius, which confirms that the solution obtained is correct.

This section and the previous have provided an analysis of the ploughing process in cutting. The goal of this work is to obtain a model that can be applied to the analysis of the dynamic cutting process by using the upper-bound approach.

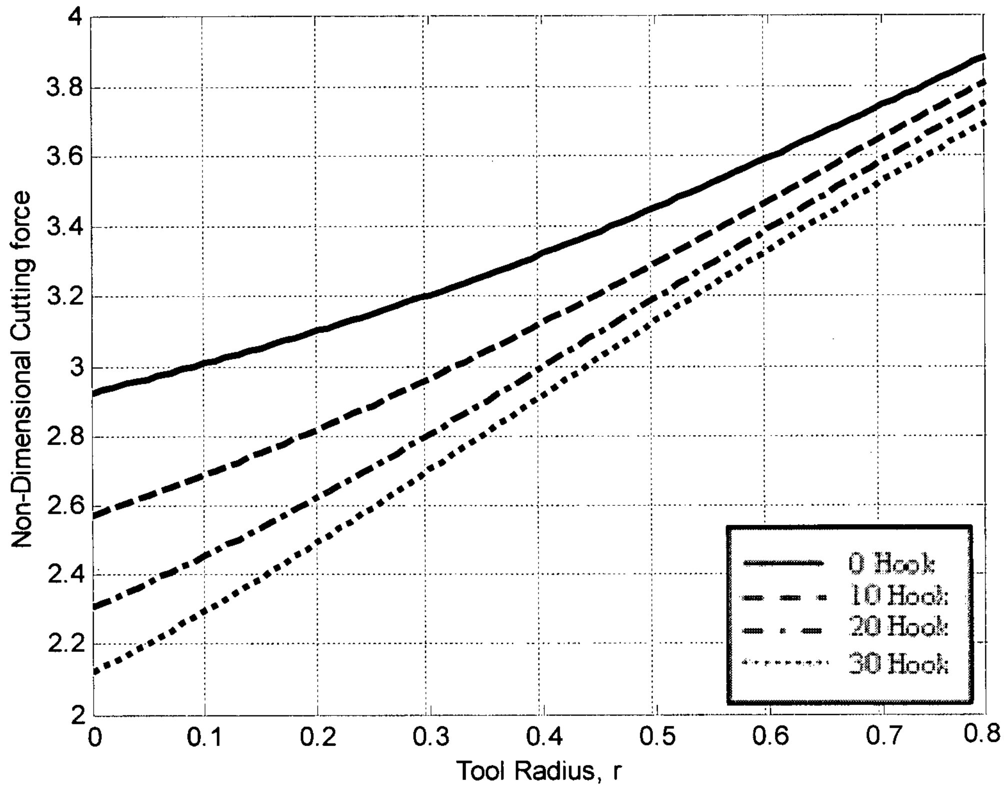

Figure 3-14. Non-dimensional cutting force for the case with friction, h_0=1.0

3.3. An Analysis of the Cutting Region Geometry in Wave Cutting

The analysis presented in this section aims to develop a basic understanding of the effect of the inner surface modulation in wave cutting. This is of importance for the interpretation of the results that will be obtained later in this chapter. The case shown in Figure 3-15 is similar to the one shown in Figure 3-7 only differing by the fact that the bottom surface presents a slope due to a vertical velocity component on the tool.

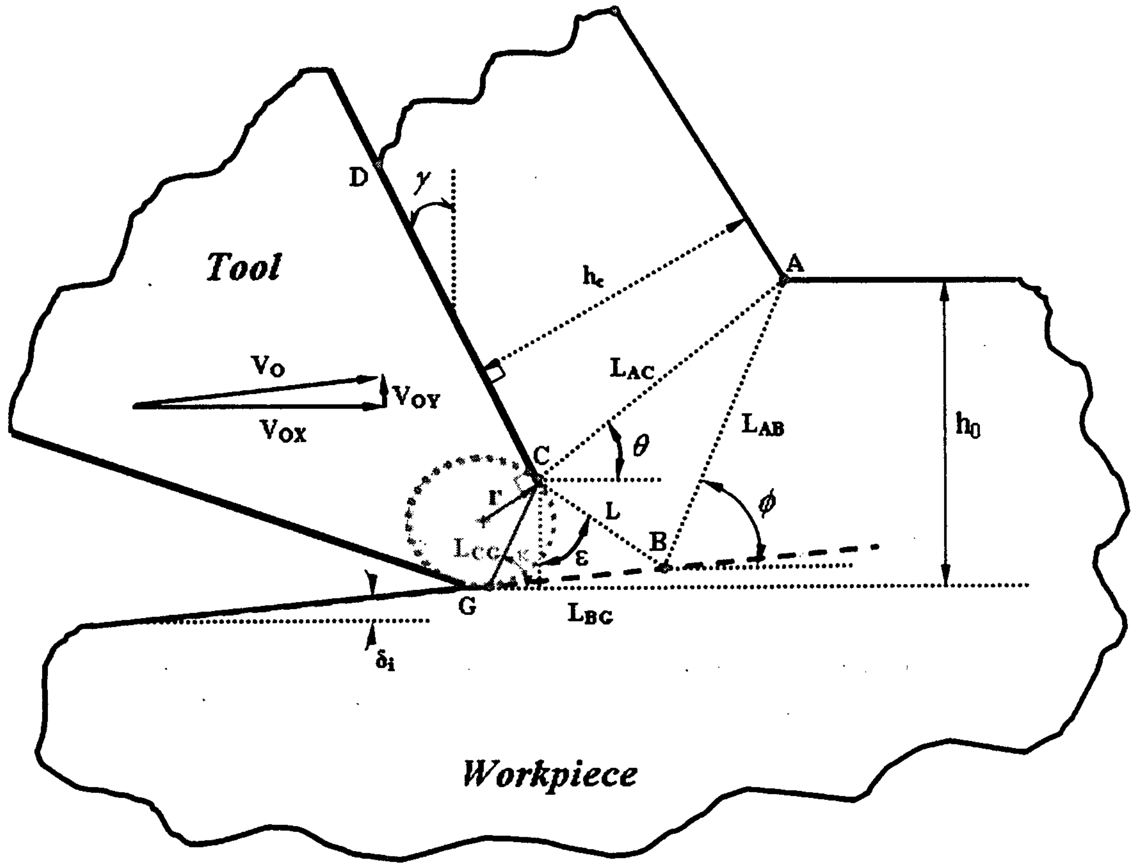

Figure 3-15. Orthogonal cutting with tool having a vibration velocity in the feed direction

Line CG, which is assumed to be the nose of the tool, which makes angle κ with the horizontal and given by,

$$\tan\kappa = \frac{\cos\delta + \sin\gamma}{\sin\delta + \cos\gamma} \tag{3.46}$$

The length of the nose of the tool is L_{CG} and can be found from,

$$L_{CG} = r\sqrt{2(1+\sin(\gamma+\delta))} \tag{3.47}$$

The lengths of the shear planes can be found using a similar procedure to that shown in section 3.2. Equations 3-47 through 3-50 are used to calculate these magnitudes,

$$L = L_{CG}\frac{\sin(\kappa+\delta)}{\cos(\varepsilon+\delta)} \tag{3.48}$$

$$L_{BG} = L_{CG} \frac{\cos(\varepsilon - \kappa)}{\cos(\varepsilon + \delta)} \tag{3.49}$$

$$L_{AB} = \frac{h_0}{\sin\phi} \tag{3.50}$$

$$L_{AC} = L_{AB} \frac{\cos(\varepsilon - \phi)}{\cos(\theta - \varepsilon)} \tag{3.51}$$

Knowing the area of the shear planes, it is now required to find the shear velocities in order to obtain the power expressions for the process.

3.3.1. Velocity Hodograph for the Wave Removing Process with a Bottom Surface Slope

The velocity hodograph for the process is presented in Figure 3-15. It can be seen that a vertical component of velocity, V_{0y}, has been added in order to account for the tool vibration.

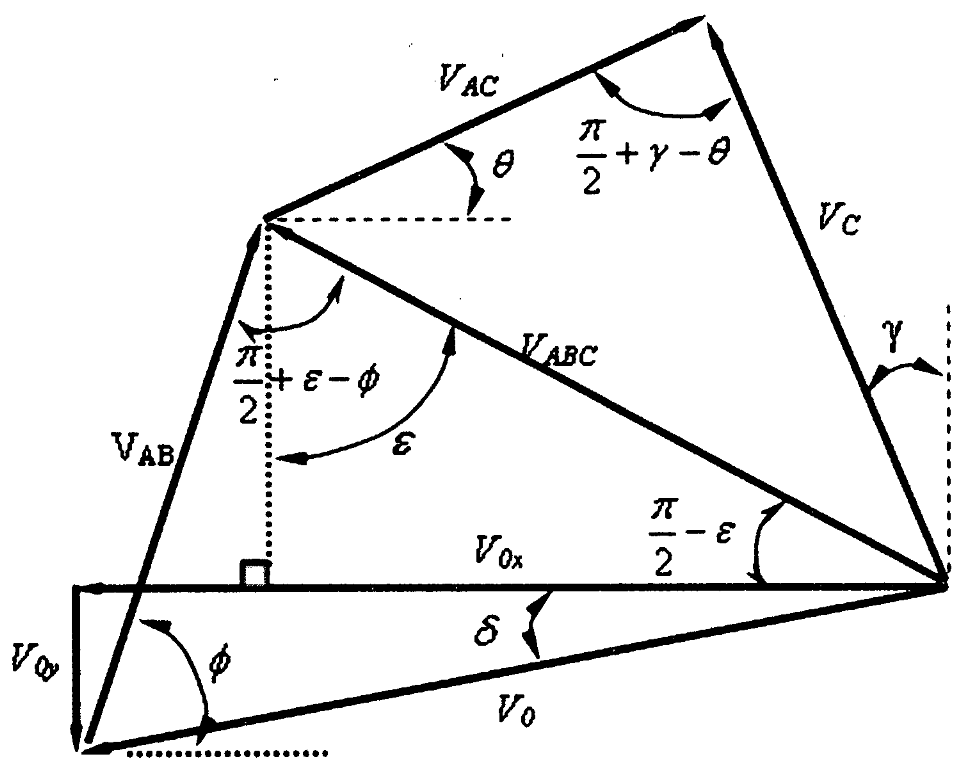

Figure 3-16. Velocity hodograph for the process shown in Figure 3-15

The following velocity equations can be derived from the hodograph in Figure 3-16,

$$V_0 = \frac{V_{0x}}{\cos(\delta)} \tag{3.52}$$

$$V_{AB} = V_0 \frac{\cos(\delta - \varepsilon)}{\cos(\varepsilon - \phi)} \tag{3.53}$$

$$V_{ABC} = V_0 \frac{\sin(\phi - \delta)}{\cos(\varepsilon - \phi)} \tag{3.54}$$

$$V_{AC} = V_0 \frac{\sin(\phi - \delta)}{\cos(\varepsilon - \phi)} \frac{\sin(\varepsilon - \gamma)}{\cos(\gamma - \theta)} \tag{3.55}$$

$$V_C = V_0 \frac{\sin(\phi - \delta)}{\cos(\varepsilon - \phi)} \frac{\cos(\theta - \varepsilon)}{\cos(\gamma - \theta)} \tag{3.56}$$

The final power expression is given by the following equation in terms of the shear plane lengths and shear velocities,

$$w = V_0 L_{BG} + V_{ABC} L_{CB} + V_{SAB} L_{AB} + V_{SAC} L_{AC} + V_c L_f \tag{3.57}$$

The length of plastic contact L_f can be obtained from equation 3.29 in page 63.

3.3.2. Simulation results for the Wave Cutting Process with a Bottom Surface Slope

A numerical solution has been implemented to find the minimum energy solution. These results are presented in Figure 3.17 below for tool hook angles of 0, 10, 20 and 30 degrees. Also various ratios of the radius of the tool nose to the uncut chip thickness are considered. This non-dimensional parameter is used in order to quantify size of the wear or imperfection on the nose of the tool.

It can be seen that for all the tools studied, the bottom surface slope has no effect on the position of the shear angle. As the nose radius of the tool increases, the effect of ploughing in the wave cutting process becomes evident. Also, the effect of the slope in the ploughing angle is smaller when the nose radius is zero than when it is larger.

This provides evidence that that previous models that did not consider the nose of the tool did not account for all the energy expenditure in dynamic cutting given that a portion of this energy is being consumed in the localized effects within the ploughing region.

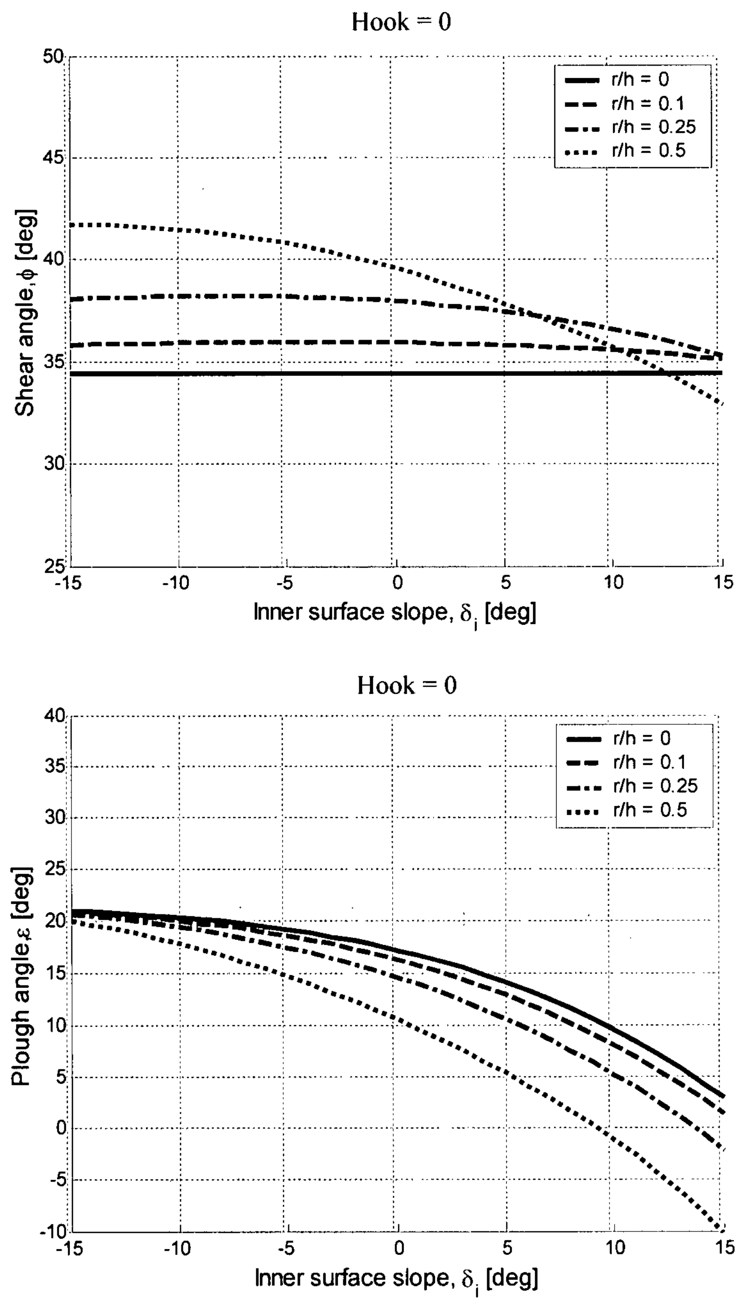

Figure 3-17 (a). Simulation results for the ploughing process with a bottom surface slope for a tool with 0^{o} hook angle.

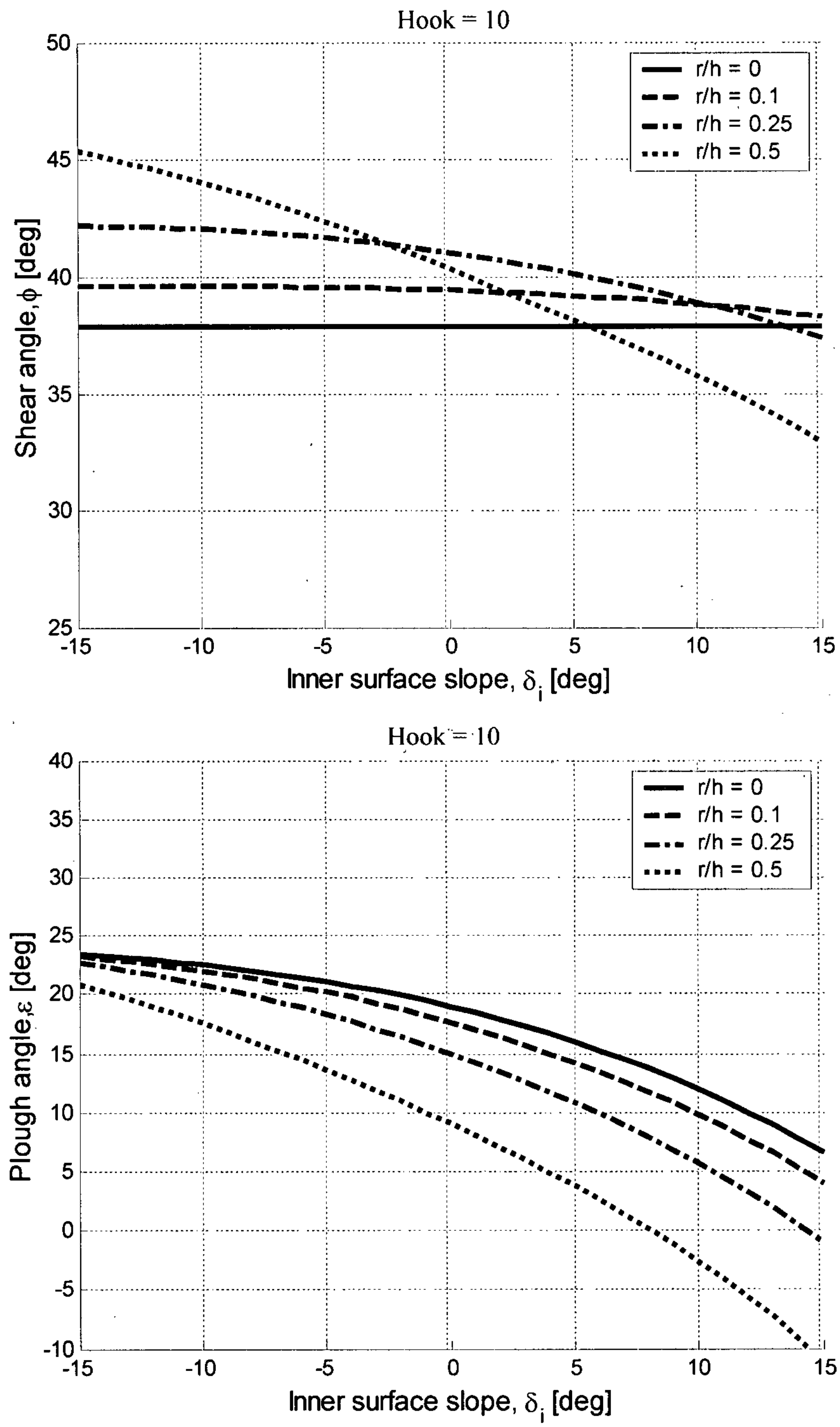

Figure 3-17 (b). Simulation results for the ploughing process with a bottom surface slope for at tool with 10° hook angle

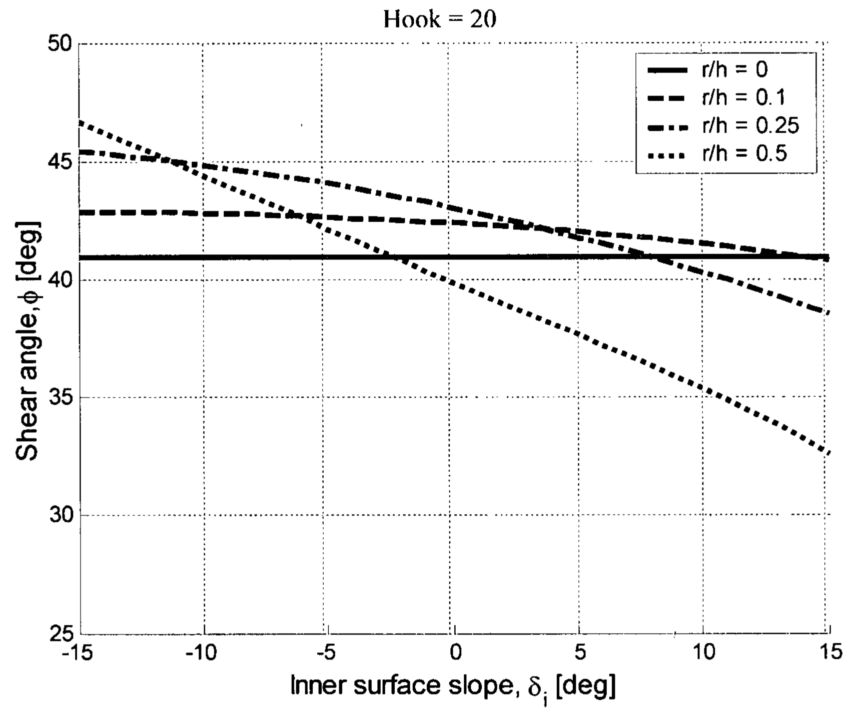

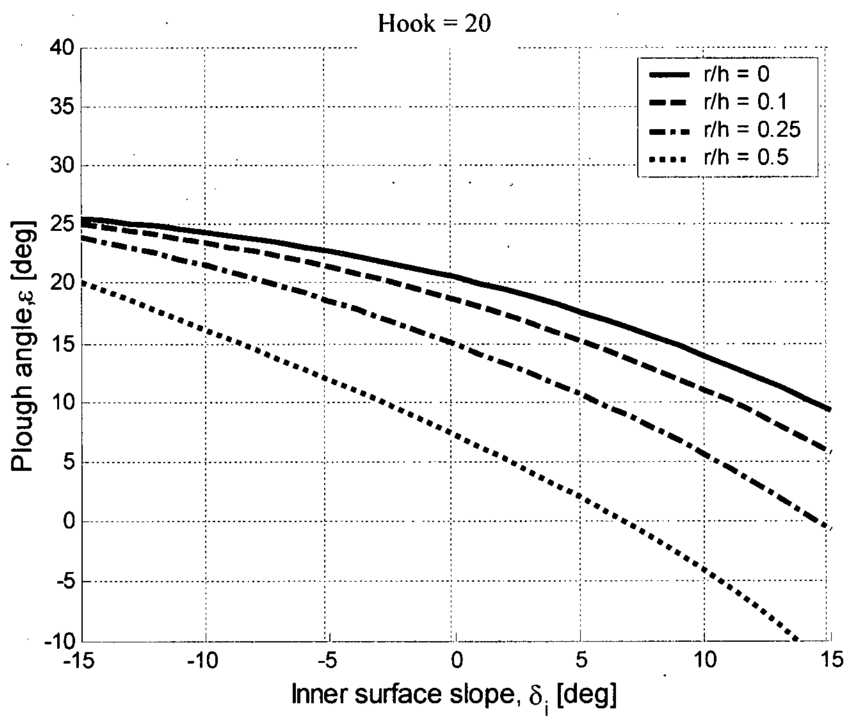

Figure 3-17 (c). Simulation results for the ploughing process with a bottom surface slope for at tool with 20° hook angle.

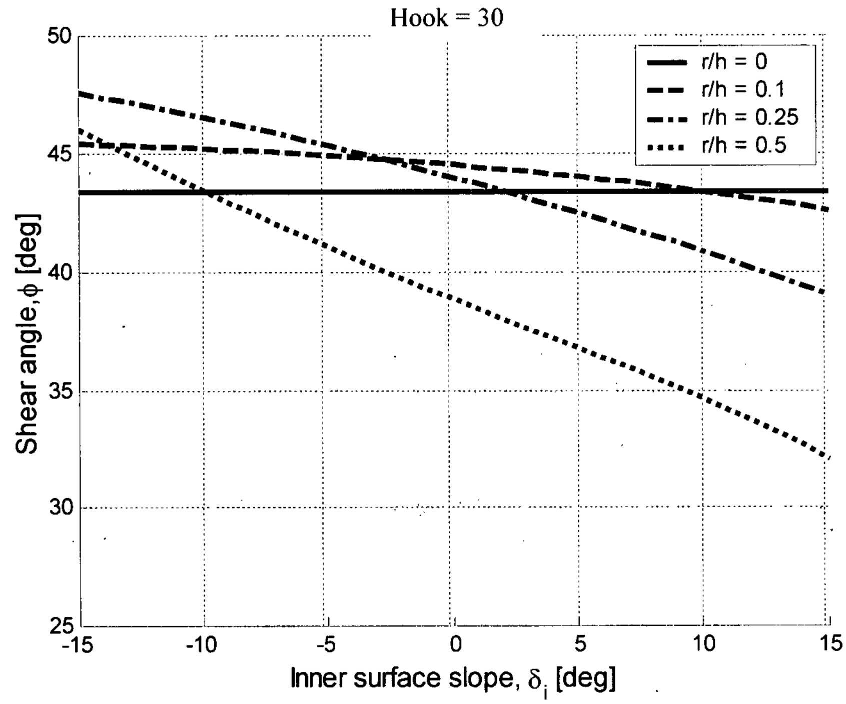

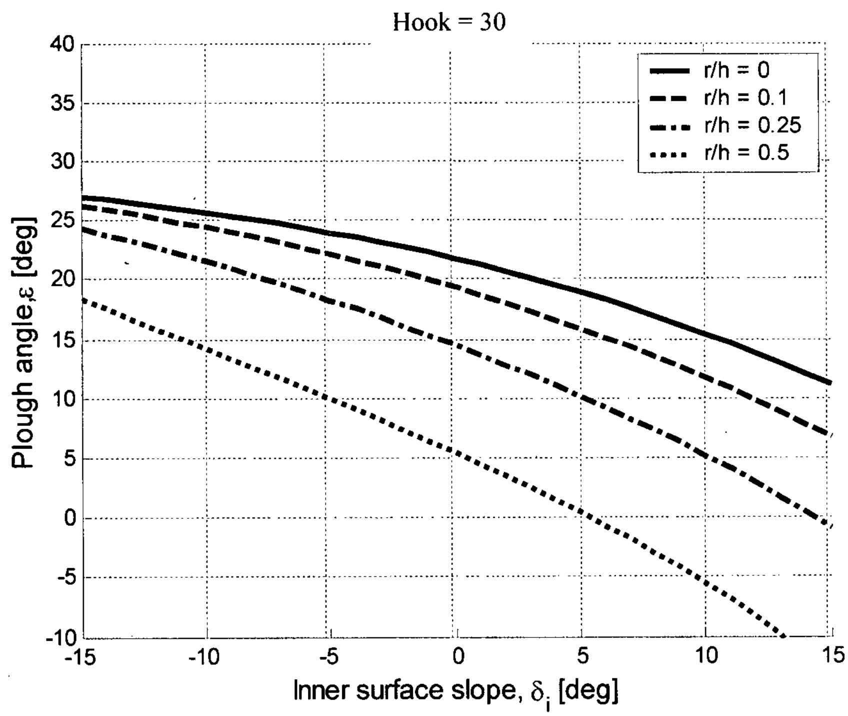

Figure 3-17 (d). Simulation results for the ploughing process with a bottom surface slope for at tool with 30° hook angle.

This model of the wave cutting process that considers the defects of the size of the nose of the tool provides a solid foundation for the next section of thesis. This section will deal with the more complex issue of analyzing the full dynamic cutting process in depth and the modeling of the effect of different tool parameters in the dynamic cutting forces obtained from the process.

3.4. An Upper-bound Model of the Dynamic Cutting Process Considering Ploughing Effects

The prediction of cutting forces under dynamic cutting conditions is a very important component of the study of machine tool chatter. This study has classically been divided in two parts in order to simplify its understanding. These parts are: 1) wave cutting, the process in which a vibrating tool removes material from a workpiece with a flat surface and, 2) wave removing, where an undulated surface is removed with a rigid tool. More attention has been given in the past to the wave removing process since it has been considered to contain some of the fundamental mechanisms for dynamic instabilities. The wave cutting process has proven very difficult to analyze both analytically and experimentally. Nevertheless, it is of fundamental importance to improve the understanding of wave cutting in order to provide solutions for stopping dynamic instabilities in machine tools.

Sections 3.2 and 3.3 presented the development of an upper-bound study of the ploughing process. It was concluded that a simple built-up edge model can be used for the analysis of the edge forces in orthogonal cutting. This model can also be used in an upper-bound to study the effect of tool vibration during cutting. The development of such model is the object of this section.

3.4.1. Background on the Study of the Dynamic Cutting Process

Das and Tobias [34] formulated a model for dynamic cutting based on static cutting data. The formulation proposed that the oscillating cutting force magnitude and phase could be estimated from a simple orthogonal cutting database. The results presented were compared to experimental data obtained by Shumsheruddin [35]. The model proved reasonably applicable for the case of wave removing, showing in most cases accurate predictions for both magnitude and phase as a function of the vibration frequency of the tool. However, the estimations for the case of wave cutting were not accurate in either magnitude or trend.

Nigm, Sadek and Tobias [36] presented an analysis that overcomes the problems of the previous model proposed by Das. The model predicts the force magnitude and phase by making use of an extensive database of orthogonal cutting data that includes information about the influence of cutting temperature and work hardening effects on the specific material. Results from Shumsheruddin [35] were also used in order to validate this model. The agreement with the experimental data shown by this development was very good in both magnitude and phase. However, the applicability of the model is limited given the large amount of data required for the force predictions and the fact that a new set of experiments is needed for each type of material, tool and lubricant.

Wu [23] considered the effect of ploughing on dynamic cutting by assuming that there is a separation point on the nose of an edge-radiused tool. Below this point, all the material is elastically deformed, flowing under the clearance face of the tool and back into the workpiece. Wu assumed that the force produced is proportional to the total volume of work material displaced below the separation point. The main shortcoming of this work is that that the primary shear process ahead of the tool will most likely be affected by the ploughing. This will introduce additional dynamic effects on the main shear plane, which need to be considered.

In order to improve the understating of this complex process, and propose a simple model that allows the prediction of the cutting forces under dynamic conditions, the plastic deformation effect at the nose of the tool must be included. Therefore the study conducted here focuses on finding a solution for force estimation based on simple orthogonal cutting data and that includes the ploughing effect produced by the nose of the tool.

3.4.2. Geometry of the Model Proposed for the Analysis of the Wave-on-Wave Cutting Process

Figure 3.18 shows the geometry for the analysis presented in this section. The tool shown removes material from a workpiece in a way similar to that presented in previous sections. However in this case, the tool is vibrating and therefore producing a wavy surface. At the same time a previous sinusoidal surface is been removed. A primary shear plane is assumed along AB and a secondary shear plane along AC. Region BCG is the built-up edge in front of the edge similar to that described in sections 3.3.

The equations for the outer and inner surfaces are presented in the figure. The phase between the waves is α. It is assumed that the slopes of the surfaces are small. This consideration allows for line BG to be approximated as a straight line with slope equal to that of the point on the inner surface sinusoid at point G. This set of assumptions allows solving for the areas of shear planes AB, AC, CB and BG.

Considering the geometry of the nose of the tool it can be seen that,

$$\tan\kappa = \frac{\cos\delta_i + \sin\gamma}{\sin\delta_i + \cos\gamma} \tag{3.58}$$

The effective length of the nose of the tool CG is a function of the inner surface slope and the hook angle of the tool,

$$L_{CG} = r\sqrt{2(1+\sin(\gamma+\delta_i))} \tag{3.59}$$

The length of plane CB is,

$$L = L_{CG}\frac{\sin(\kappa-\delta_i)}{\cos(\varepsilon-\delta_i)} \tag{3.60}$$

The length of plane BG can be obtained from,

$$L_{BG} = L_{CG}\frac{\cos(\varepsilon-\kappa)}{\cos(\varepsilon-\delta_i)} \tag{3.61}$$

Coordinate x is measured with respect to point P shown. Y is measured with respect to the mean chip thickness of the bottom surface. It is possible to calculate the coordinates of points G and B from the lengths already found as follows,

$$[x_G, y_G] = \left[r\sin\delta_i, A_i \sin\left(\frac{2\pi}{\lambda}(x + r\sin\delta_i)\right)\right] \tag{3.62}$$

$$[x_B, y_B] = \left[r\cos\gamma + L_{CB}\sin\varepsilon, A_i \sin\left(\frac{2\pi}{\lambda}(x + r\sin\delta_i)\right) + L_{BG}\sin\delta_i \right] \tag{3.63}$$

The equation of line AB is known from the coordinates of point B and its slope.

$$y_{AB} = \tan\phi x + y_B - \tan\phi x_B \tag{3.64}$$

At point A, line AB meets the outer sine wave and therefore the following equation can be solved numerically to find its coordinates,

$$\tan\phi x - A_0 \sin\left(\frac{2\pi}{\lambda} x + \alpha\right) + y_B - \tan\phi x_B - h_0 = 0 \tag{3.65}$$

L_{AB} and L_{AC} become,

$$L_{AB} = \frac{x_A - x_B}{\cos\phi} \tag{3.66}$$

$$L_{AC} = L_{AB}\frac{\cos(\varepsilon - \phi)}{\cos(\theta - \varepsilon)} \tag{3.67}$$

Where,

$$\tan\theta = \frac{L_{AB}\sin\phi - L_{AC}\cos\varepsilon}{L_{AB}\cos\phi + L\sin\varepsilon} \tag{3.68}$$

The equations above provide a way to calculate all the necessary lengths for the solution of the upper-bound. It is now required to propose an admissible velocity field in order to find the power spent in the process.

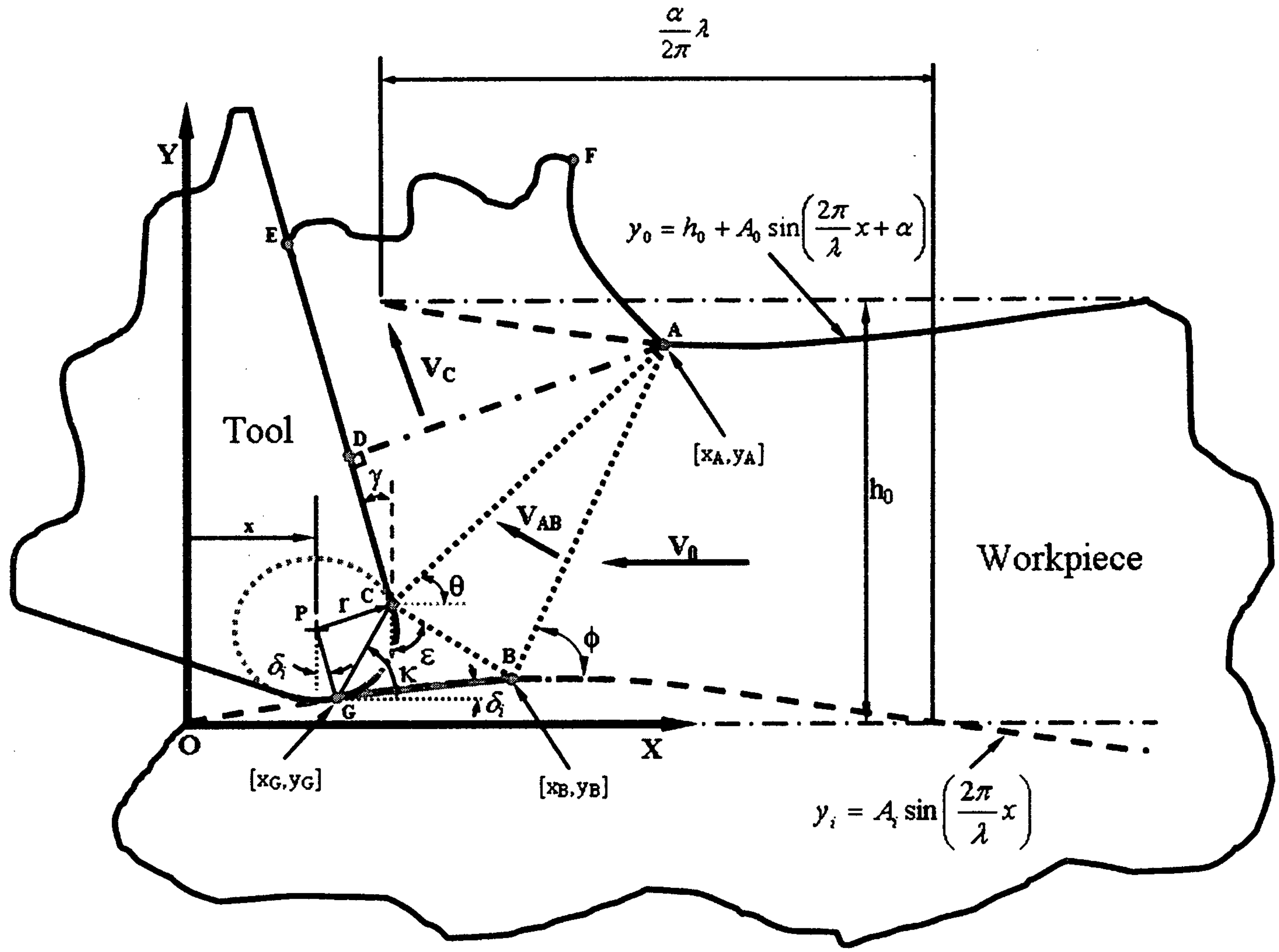

Figure 3-18. Geometry model for the dynamic cutting process

3.4.3. Velocity Hodograph for the Wave-on-Wave Cutting Process

The hodograph for the wave-on-wave cutting process is presented below. The cutting velocity is V_{0X}. However, the vibrations of the tool add an extra velocity component V_{0Y} and the resultant incoming velocity is therefore V_0.

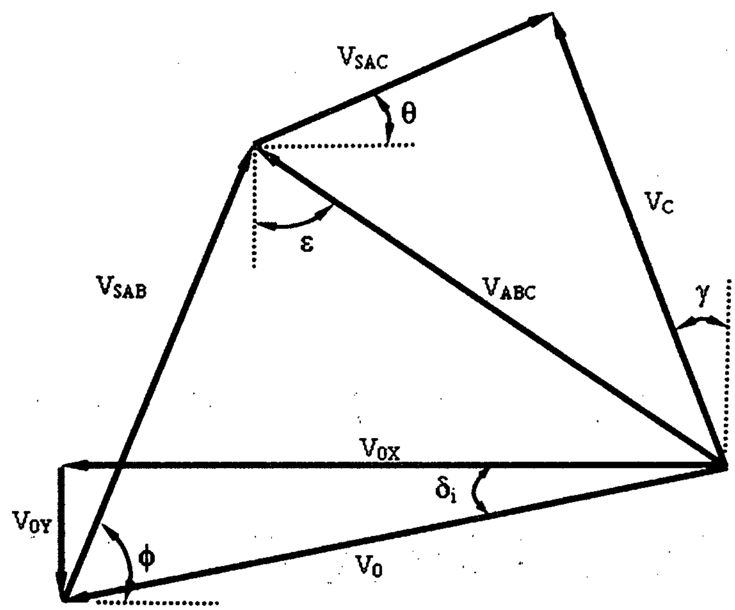

Figure 3-19. Process hodograph for wave-on-wave Cutting

The magnitude of the incoming velocity is,

$$V_0 = \frac{V_{0X}}{\cos\delta_i} \tag{3.69}$$

It can be seen from Figure 3-19 that the velocity on shear planes AB and AC is,

$$V_{AB} = V_0 \frac{\cos(\varepsilon - \delta)}{\cos(\varepsilon - \phi)} \tag{3.70}$$

$$V_{ABC} = V_0 \frac{\sin(\phi - \delta)}{\cos(\varepsilon - \phi)} \tag{3.71}$$

$$V_{AC} = V_{ABC} \frac{\sin(\varepsilon - \gamma)}{\cos(\theta - \gamma)} \tag{3.72}$$

Finally, the velocity of the chip is,

$$V_C = V_{ABC} \frac{\cos(\theta - \varepsilon)}{\cos(\gamma - \theta)} \tag{3.73}$$

3.4.4. Friction Considerations in Dynamic Cutting

Following an analysis similar to that of section 3.1.3, the friction force can be estimated. For this case, force a balance of the chip is used to calculate the friction force. The resultant force expression is,

$$F_f = L_{Ac} kw \frac{\sin\beta}{\cos(\theta + \beta - \gamma)} \tag{3.74}$$

Where,

$$\tan\beta = \frac{1}{1 + \frac{\pi}{2} - 2\gamma} \tag{3.75}$$

Equations 3.73 and 3.74 allow the estimation of the power spent on friction on the face of the tool, which affects the solution for the shear geometry.

Finally, the power spent in the dynamic cutting process can be calculated using the equations obtained above,

$$\frac{w}{bk} = L_{AB}V_{AB} + L_{AC}V_{AC} + LV_{ABC} + L_{bg}V_0 + F_f V_c \tag{3.76}$$

The minimization of equation 3.75 with respect to ε and ϕ allows a solution for the cutting geometry which is necessary in order to estimate the cutting forces in the process presented in Figure 3-18.

3.4.5. Forces in the Wave-on-Wave Cutting Process

The forces applied to the tool can be evaluated considering force balance on the chip if quasi-static equilibrium is assumed. Boundary ABCGEF can be considered for this analysis. The tool exerts forces F_m and F_t along line CE. Shear planes GB and AB experience compressive and shear forces which are shown in Figure 3-20.

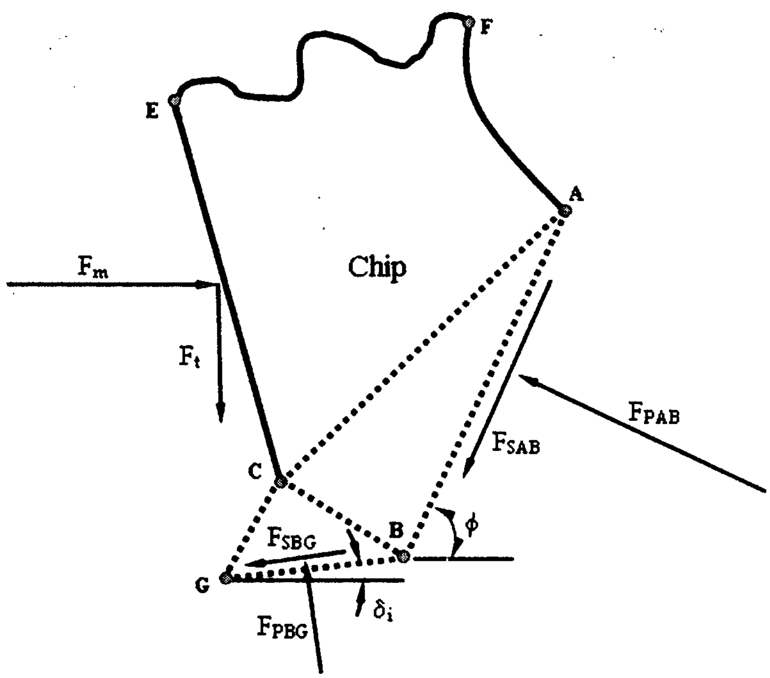

Figure 3-20. Force balance for the dynamic cutting process

The main force, F_m shown in Figure 3-20 can be estimated from the power expression used to solve the upper-bound problem (equation 3.75) since this force can be expressed as the total power spent divided by the instantaneous magnitude of the cutting velocity,

$$F_m = \frac{w}{V_0} \tag{3.77}$$

The shear forces on AB and BG can be considered to be the product of the yield stress times the area of the plane,

$$F_{SAB} = kbL_{AB} \tag{3.78}$$

And,

$$F_{SBG} = kbL_{BG} \tag{3.79}$$

This leaves Ft, F_{PAB} and F_{PBG} as unknowns in the process. The equilibrium conditions on the chip will provide two equations and therefore one more assumption will be needed in order to find the forces. Boundary ABG is a slip-line where the material is stressed up to the yield point. Since flow occurs on both sides of the line, Hencky's equations must provide a reasonable estimate of the ratio of plastic stresses along this boundary. Since only one more equation needs to be established, the assumption will be only applied to line BG yielding the following expression for the force perpendicular to the shear plane as a function of the inner surface slope,

$$F_{PBG} = (1 + \frac{\pi}{2} - 2\delta_i + 2\delta_o)F_{SBG} \tag{3.80}$$

Taking summation of force along the x direction it is possible to obtain the following expression for the normal force on shear plane AB,

$$F_{PAB} = \frac{F_m - F_{SAB}\cos\phi - F_{SBG}\cos\delta_i - F_{PBG}\sin\delta_i}{\sin\phi} \tag{3.81}$$

The feed force, F_f can be obtained now by taking summation of forces along the y direction,

$$F_{PAB} = L_{BG}\sin\delta_i - L_{AB}\sin\phi + \left(1 + \frac{\pi}{2} - 2\delta_i + 2\delta_o\right)L_{BG}\cos\delta_i + F_{PAB}\cos\phi \tag{3.82}$$

Equations 3.76 through 3.81 allow the computation for the cutting forces for the dynamic cutting case shown in Figure 3-18. A computer simulation can be used in order to study the effect that the different variables involved in the process have on the cutting forces. This analysis permits the evaluation of the performance of the cutting process in terms of the geometry, cutting conditions and material the shear stress of the material.

3.5. Simulation Results for the Dynamic Cutting Model

Nigm and Sadek [27] reported a thorough experimental study of the dynamic cutting process. The cutting tests were conducted on a lathe with the tool cutting orthogonally on the end of a tubular workpiece. The tool was forced to vibrate in a controlled manner normal to the cut surface by means of an electrohydraulic actuator, the useful frequency range of which it was 0 to 300 Hz. The tool was mounted on a two-component dynamometer which measured the force components parallel and normal to the cutting direction. Wave cutting and wave removing tests were carried out in the same run by forcing the tool to vibrate during one revolution of the workpiece and holding it still during the next revolution to remove the wave previously generated.

The work material used was hot finished mild steel. The material was in tube form, with an outside diameter of 194 mm and a thickness of 3.5 mm. The shear stress for this material is provided by Tobias in [34] as $k = 4133$ bar. The cutting tools used were throwaway carbide tips ISO P30.

Table 3-1. Cutting Conditions Studied by Nigm and Sadek in [27]

Series	Variable studied	Range	Value for other variables
A	Frequency	60 to 300 Hz on four steps	Average chip thickness : 0.19 mm Cutting speed : 140 m/min Hook angle : 5 degrees Chip thickness modulation : 0.05 mm
B	Amplitude of chip thickness modulation	0.05 to 0.18 mm peak on four steps	Average chip thickness : 0.19 mm Cutting speed : 140 m/min Hook angle : 5 degrees Frequency : 120 Hz
C	Average chip thickness	0.095 to 0.245 mm on four steps	Frequency : 120 Hz Cutting speed : 140 m/min Hook angle : 5 degrees

			Chip thickness modulation : 0.05 mm
D	Hook angle	0 to 10 on three steps	Frequency : 120 Hz Cutting speed : 140 m/min Average chip thickness : 0.19 mm Chip thickness modulation : 0.05 mm

3.5.1. Effect of Frequency of Chip Thickness Modulation in Dynamic Cutting

The effect of frequency on the cutting forces is of special interest in the study of the dynamics of the cutting process. The following set of figures shows the results from the computer simulation obtained from the model proposed in this section when the frequency is varied between 50 and 300 Hz. The magnitude of the dynamic cutting force component as well as its static component and phase are shown in Figure 3-21. A series of nose radiuses for the tool have been used in the simulation and they have been plotted in different line types in order to observe the effect of this variable on the process as well.

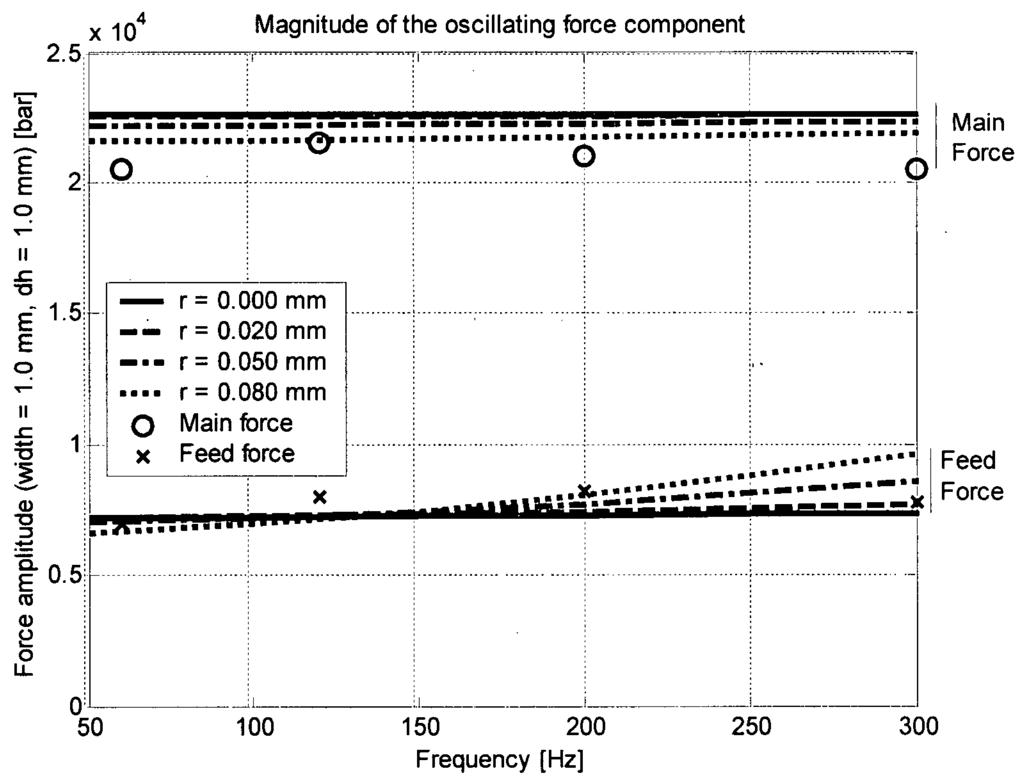

Figure 3-21 (a). Effect of frequency on wave cutting

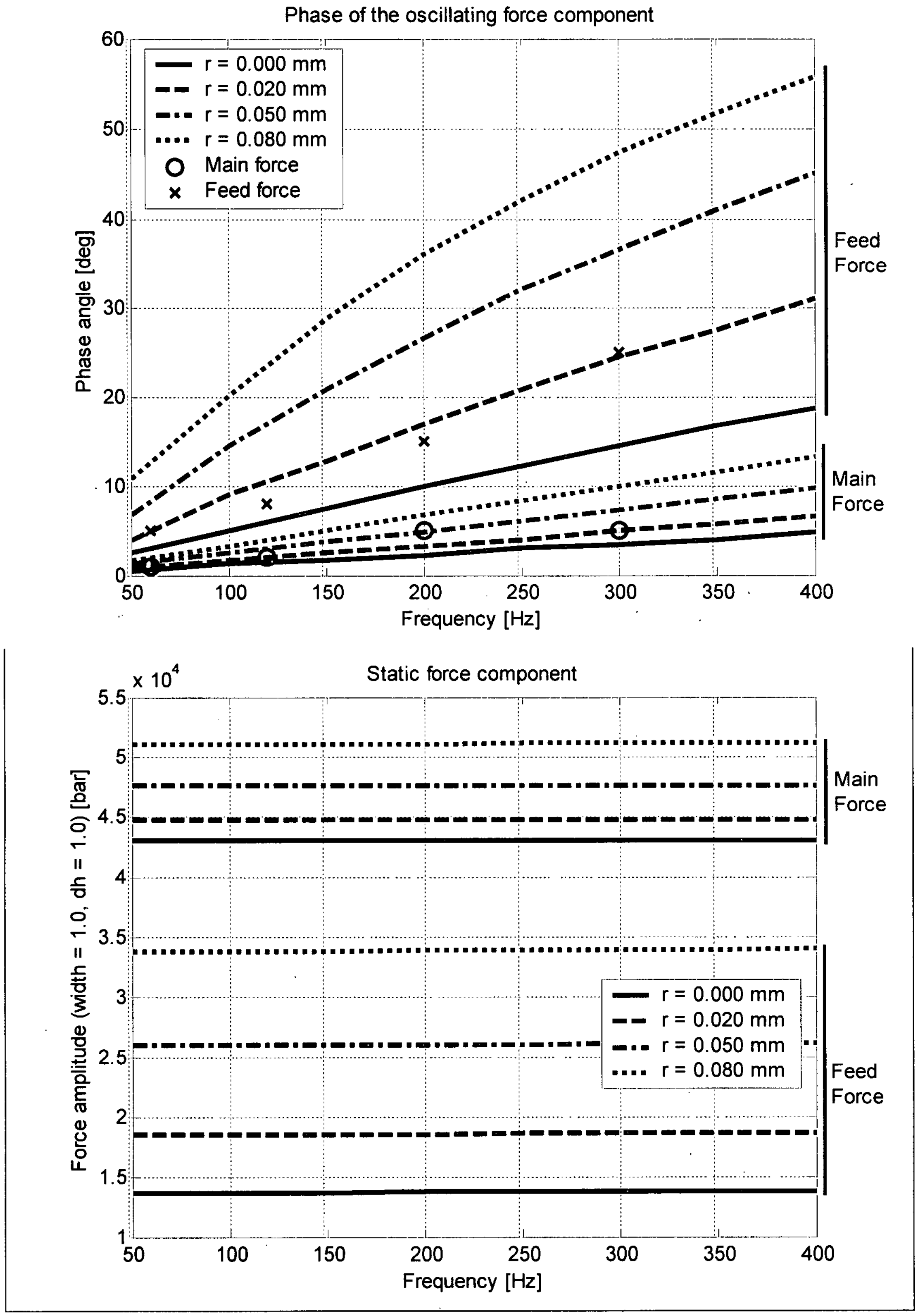

Figure 3-21 (b). Effect of frequency on wave cutting

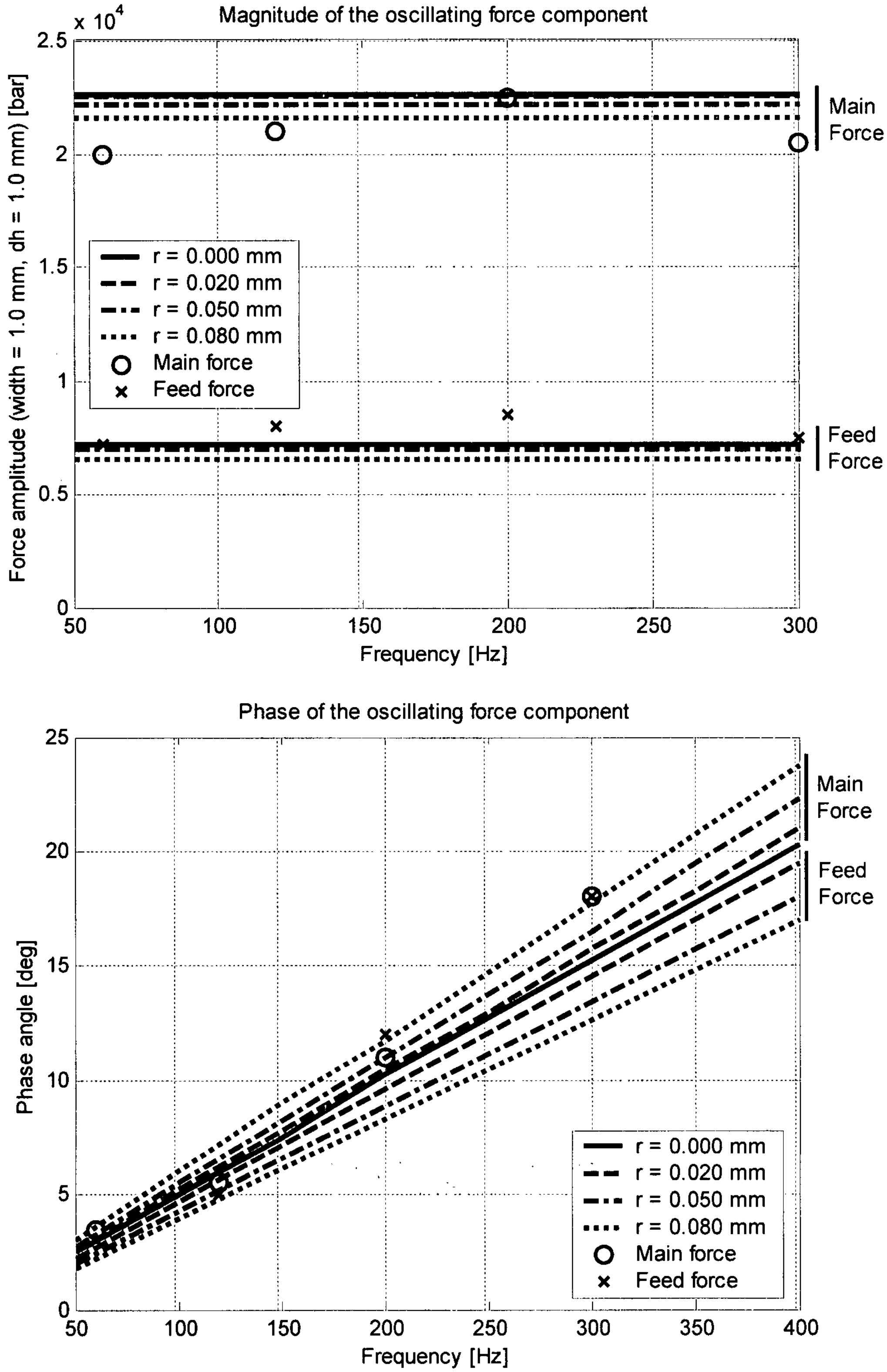

Figure 3-22 (a). Effect of frequency on wave removing

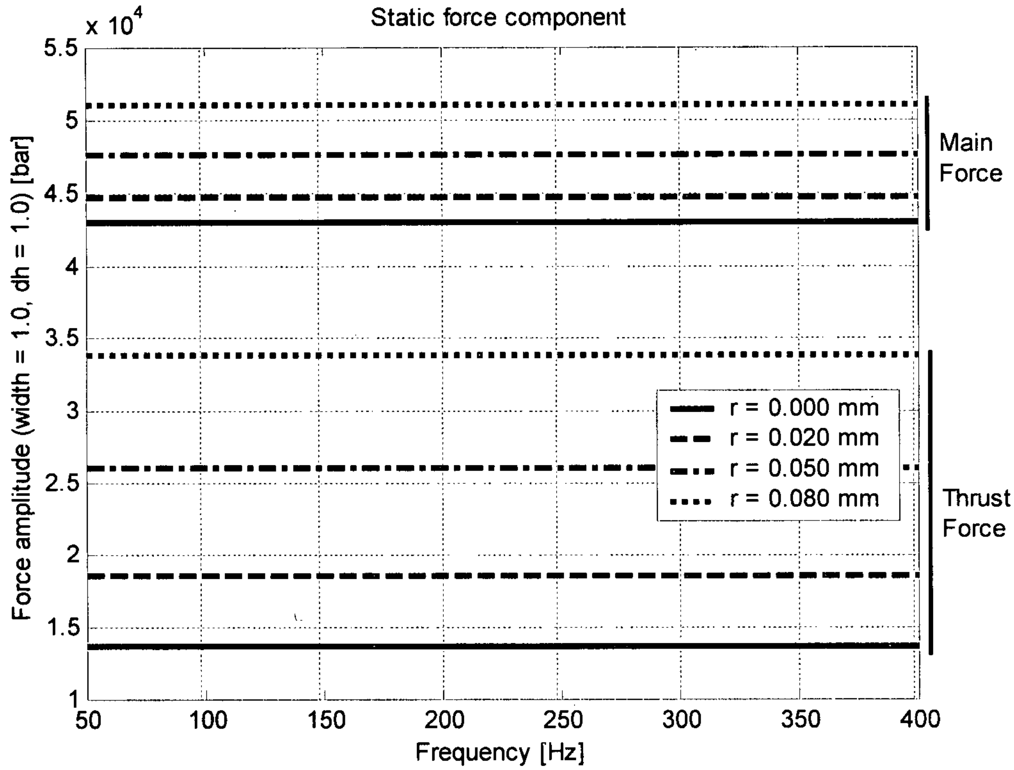

Figure 3-22 (b). Effect of frequency on wave removing

Nigm and Sadek did not control the nose radius as a parameter in their experimental study and therefore this value was not given. However an edge radius of 20 μm is typical for turning tools. Therefore it is to be expected that the dashed lines representing this radius value in Figure 3.21 would be the most approximate case of all the ones plotted.

It can be seen that for a perfectly sharp tool, the magnitude of the cutting force is constant throughout the frequency range studied for both wave cutting and removing. The experimental results appear to be in agreement with the model estimation for the main cutting force in this respect. However, the simulation predicts that for the feed force, an increase approximately linear will occur when a nose radius is introduced on the tool. The experimental data supports the model since the data points show an increasing trend for the magnitude of the feed force as well.

It can be concluded that even though an increasing trend exists, the effect of frequency on the amplitude of the forces is more likely small. On the other hand, the phase in the cutting forces leads with respect to the position of the tool and seems more sensitive to frequency, increasing linearly for both cases studied. Good agreement is found again in this sense between the model and the experimental data for the wave cutting case. It can be seen in Figure 3-21 that for wave removing the simulation results are close to the experimental data for the main cutting force but the phase for the feed force seems to have been slightly underestimated.

3.5.2. Effect of Hook Angle in Dynamic Cutting

The simulations and experimental results shown in Figure 3-22 suggest that the dynamic cutting forces decrease with the increase of the hook angle. It can therefore be seen that increasing the hook angle of the tool, the dynamic stiffness can be decreased. This concept can be used in tool design, when a reduction in the dynamic forces coefficients needs to be achieved.

With respect to the phase, it can be concluded that the hook angle has a very small effect in the phase of the main cutting force in wave cutting but it plays a more important role for the feed force phase, which increases in an almost linear fashion with the increase of the hook angle. In the case of wave removing, the effect of the hook angle proves small for both the feed and main forces.

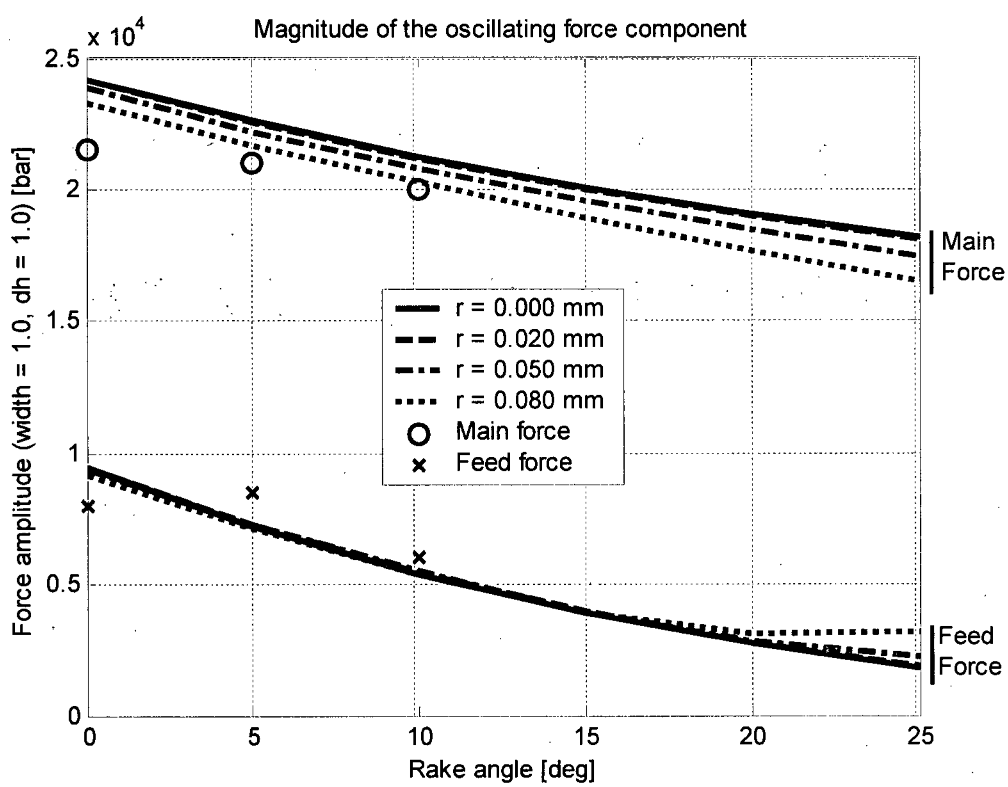

Figure 3-23 (a). Effect of hook angle on wave cutting

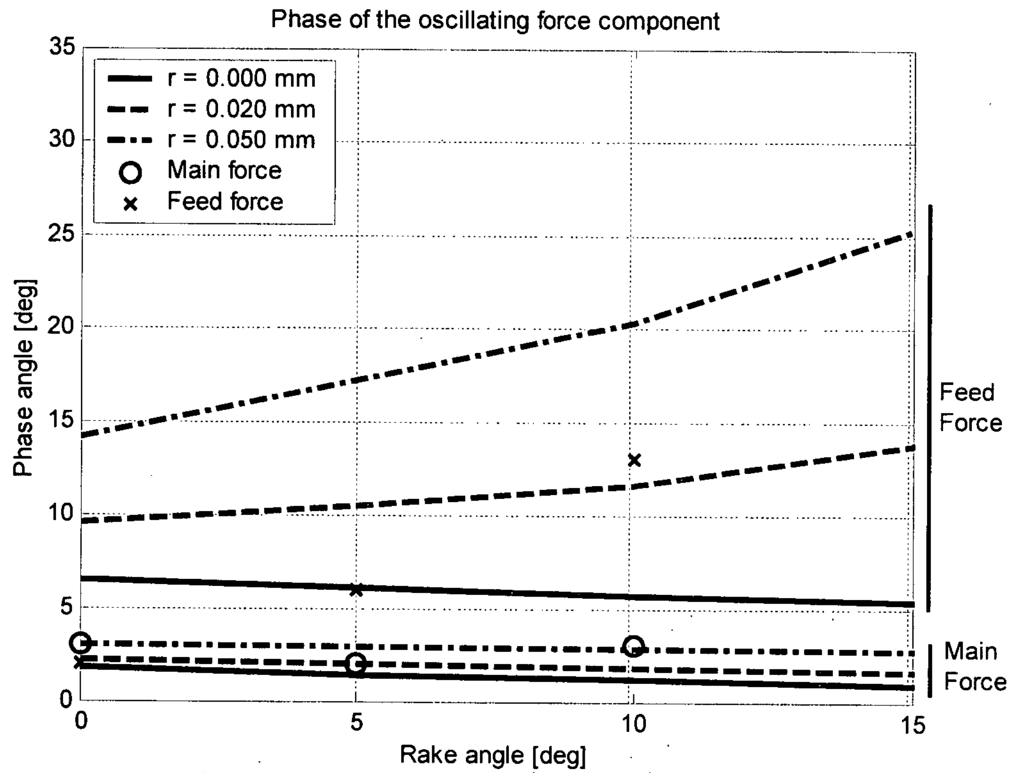

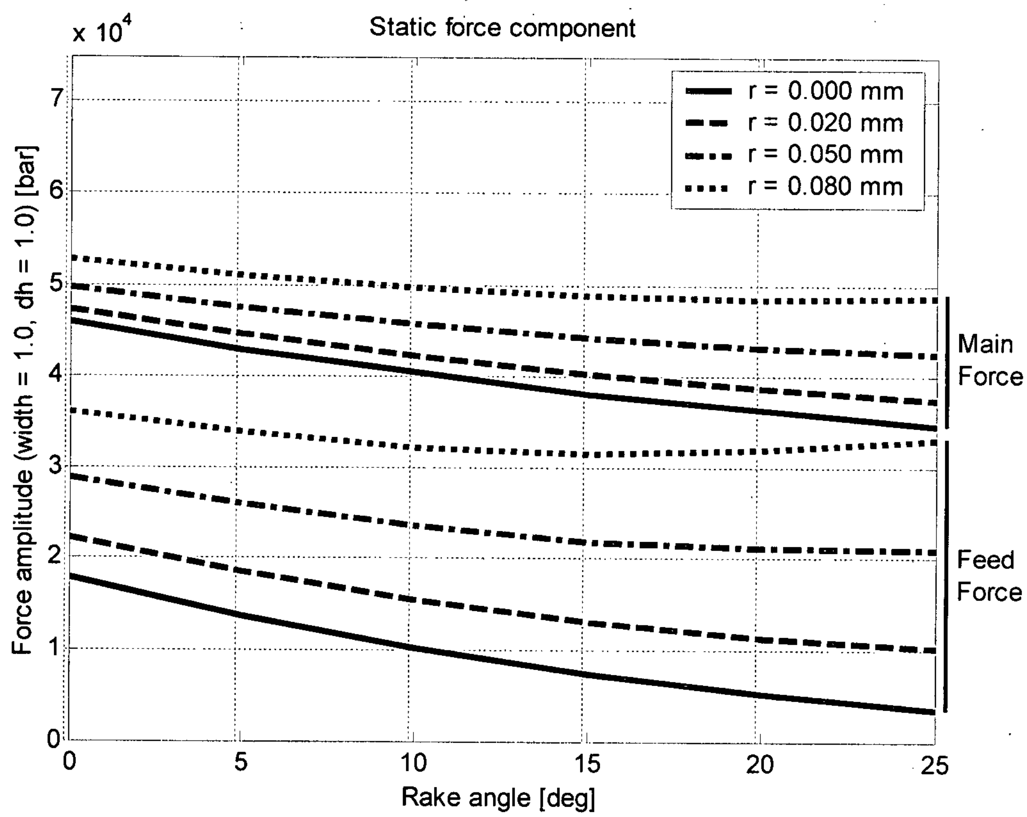

Figure 3-23 (b). Effect of hook angle on wave cutting

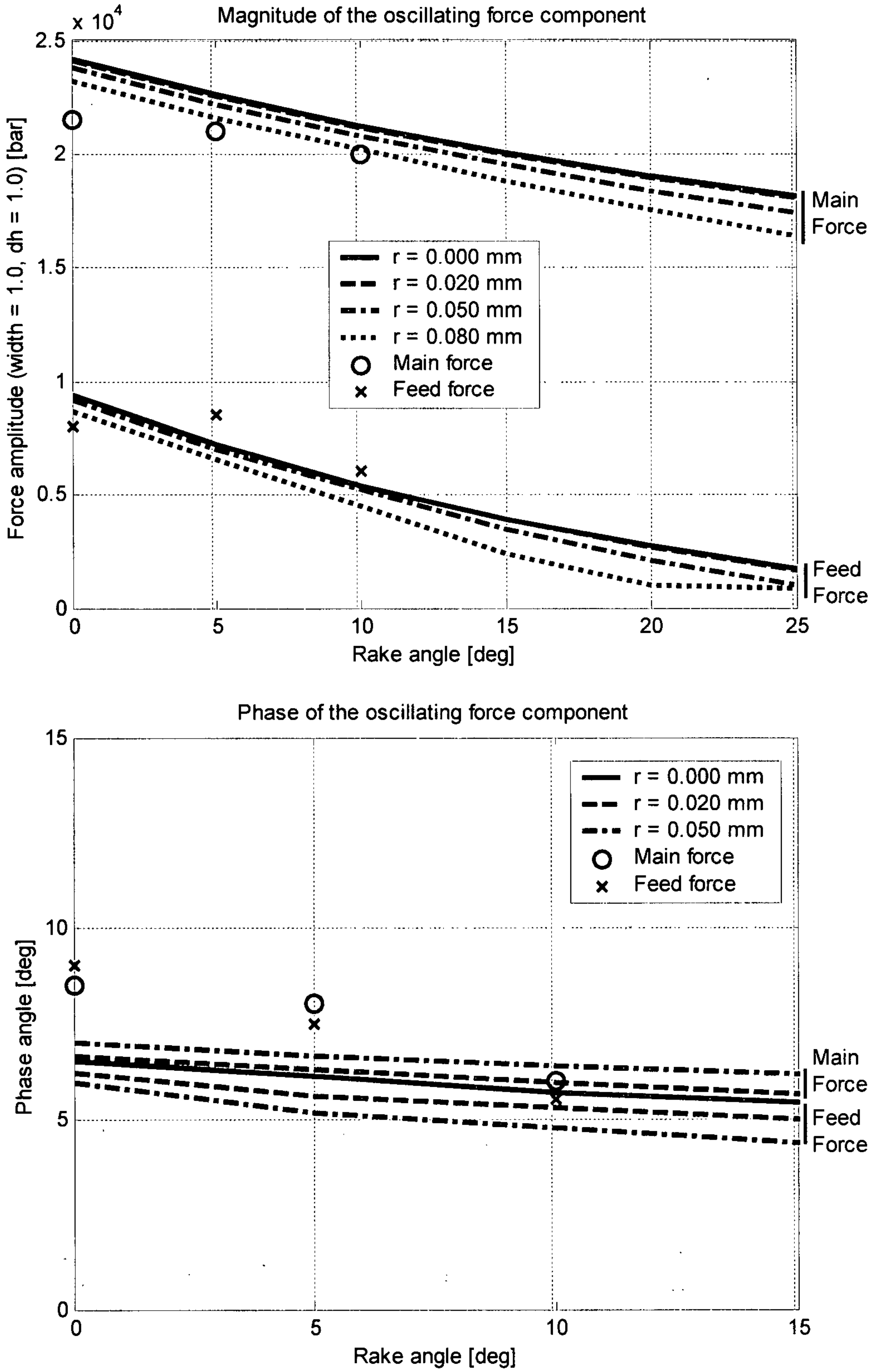

Figure 3-24 (a). Effect of hook angle on wave removing

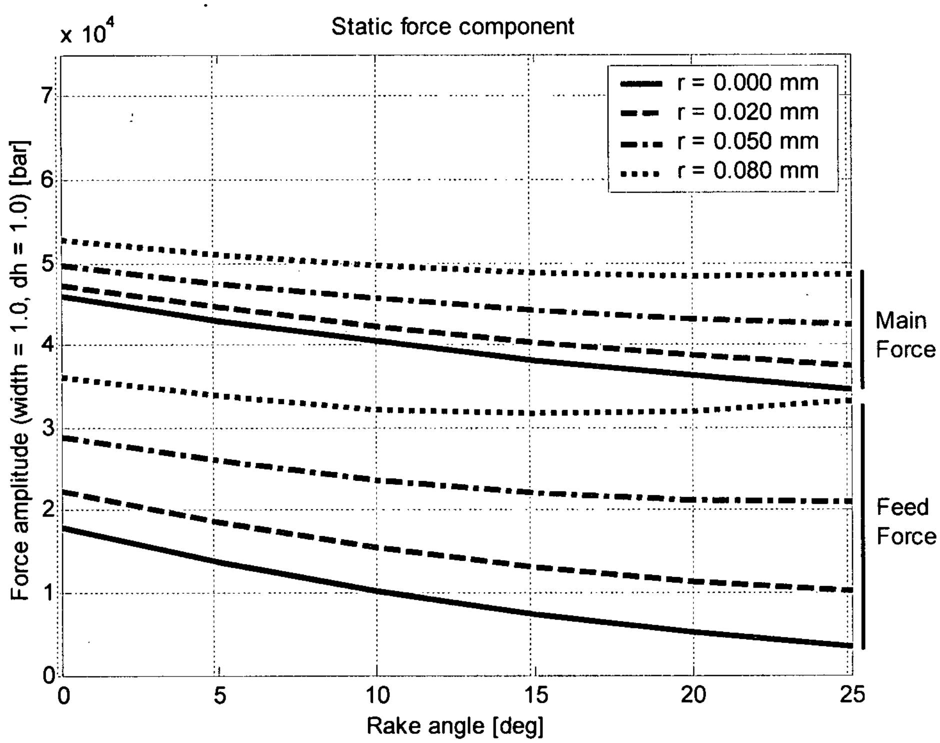

Figure 3-24 (b). Effect of hook angle on wave removing

It can be concluded from the discussion and results above that the upper bound approach proposed can also be used to estimate the effect of the hook angle in the phase and amplitude of the dynamic cutting forces for isotropic materials.

3.5.3. Effect of Feed Rate in Dynamic Cutting

The effect of the feed rate in dynamic cutting was studied using the simulation developed and the results are presented in Figure 3-25. It can be seen that experimental result shows a decrease in the magnitude of the feed force which cannot be explained using the model developed. The model also predicts a small increase in the magnitude of the main cutting force in wave cutting and wave removing. The experimental result is close to the model prediction but it is not possible to tell if an increasing trend exists or not due to the limited amount of data.

As for the phases it can be said that the prediction and experiments show a lead of the force with respect to the tool for both wave cutting and wave removing. The trend shows that the phase of the feed force is more sensitive to changes in the feed rate than the phase of the main force.

It can be concluded that the upper bound developed is a good predictor for the effects of the feed rate in the dynamic cutting process but that the effect on the magnitude of the feed force need further investigation.

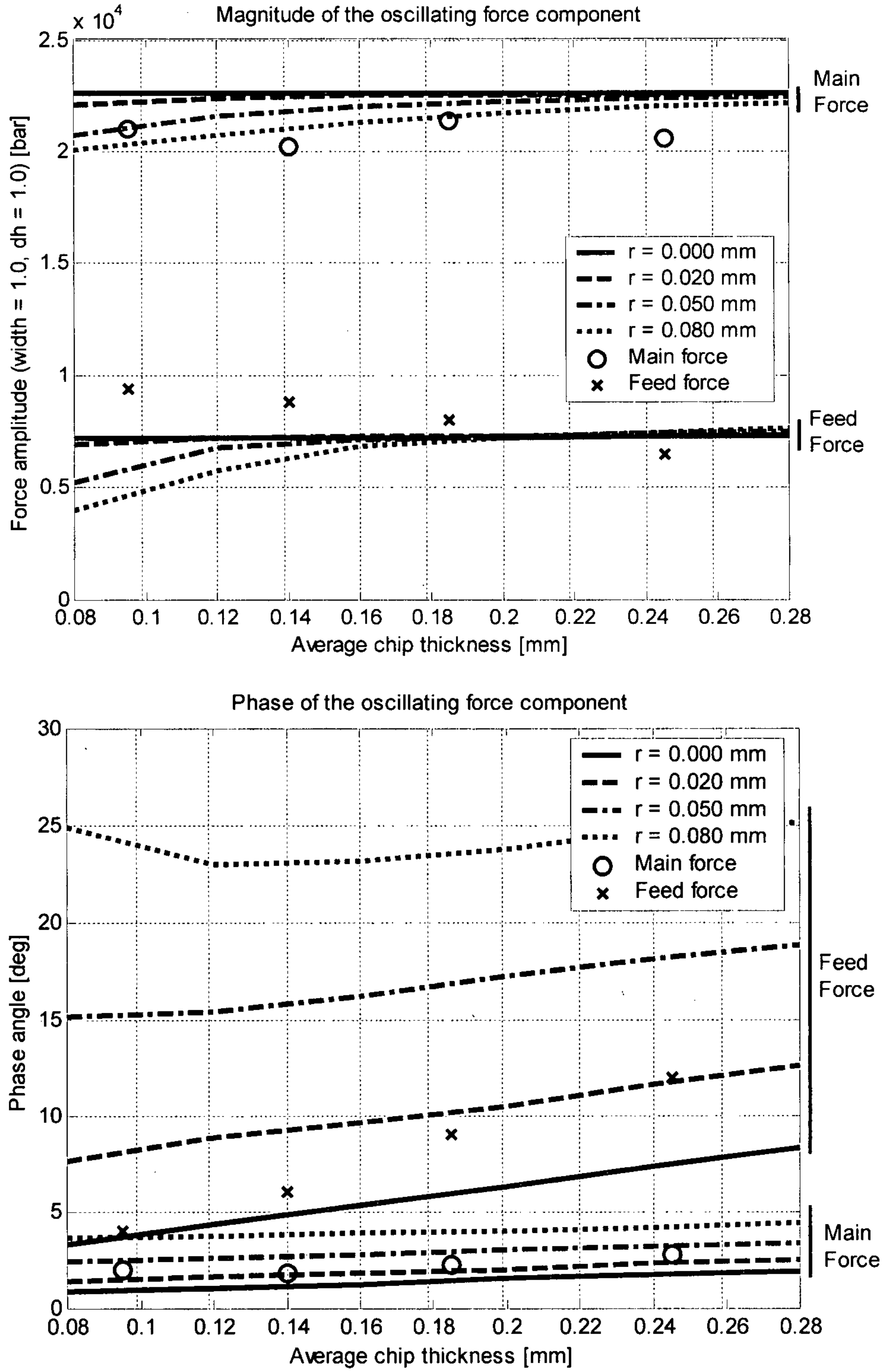

Figure 3-25 (a). Effect of the feed on wave cutting

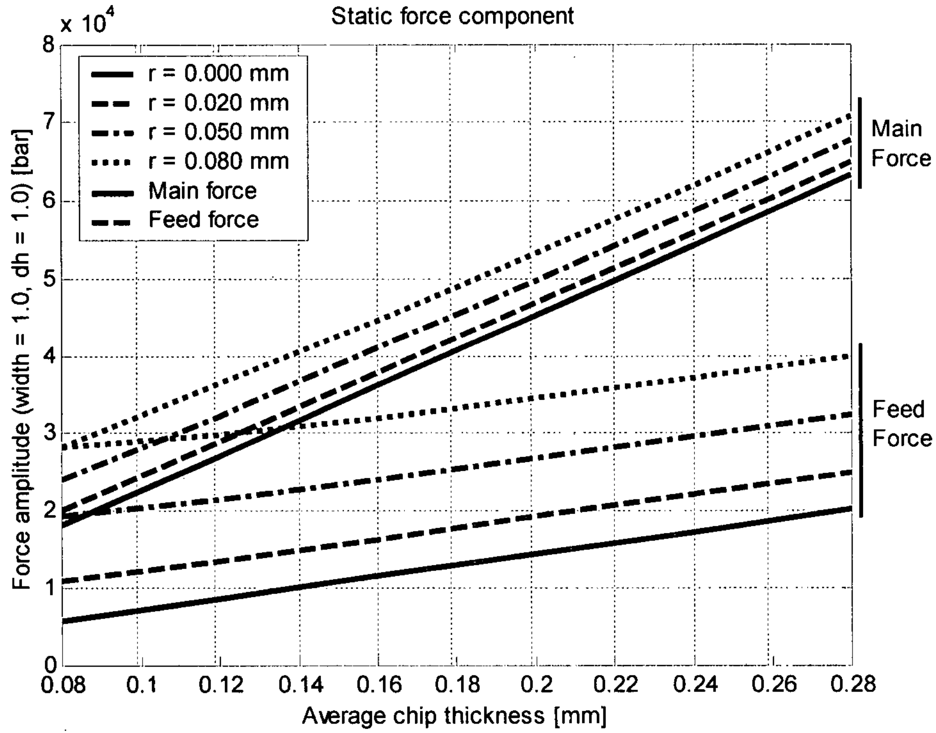

Figure 3-25 (b). Effect of the feed on wave cutting

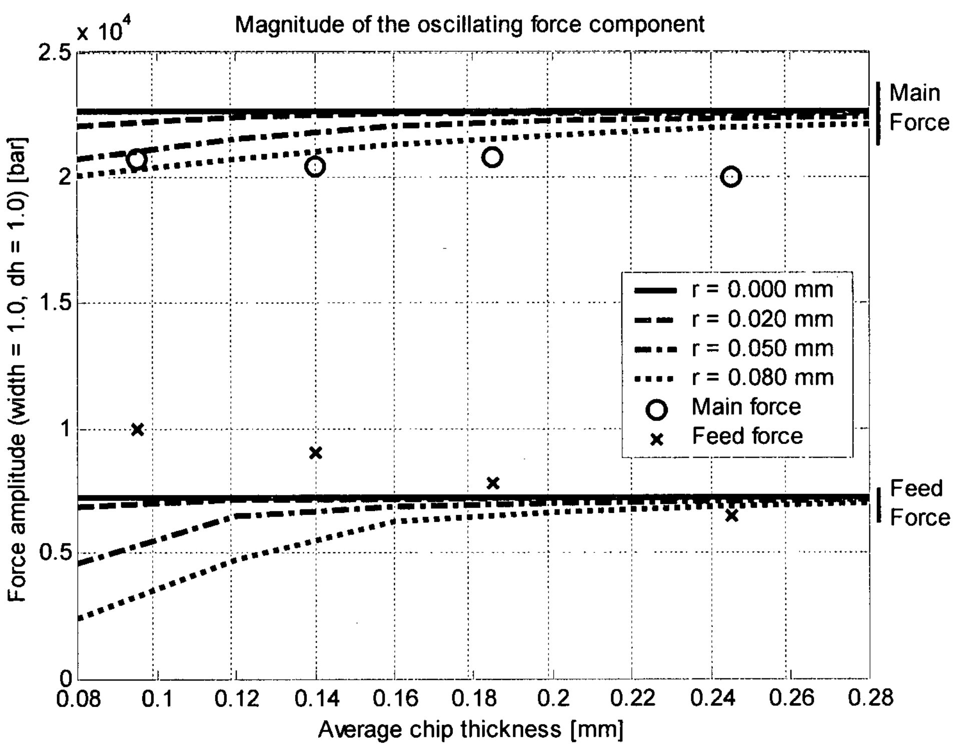

Figure 3-26 (a). Effect of the feed on wave removing

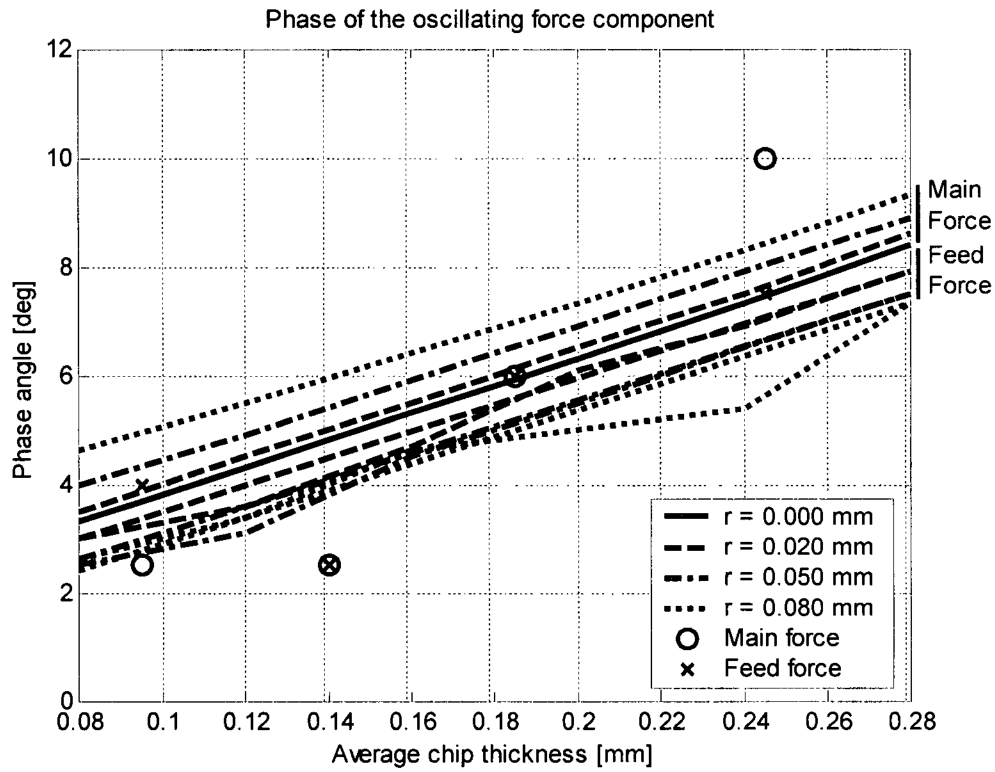

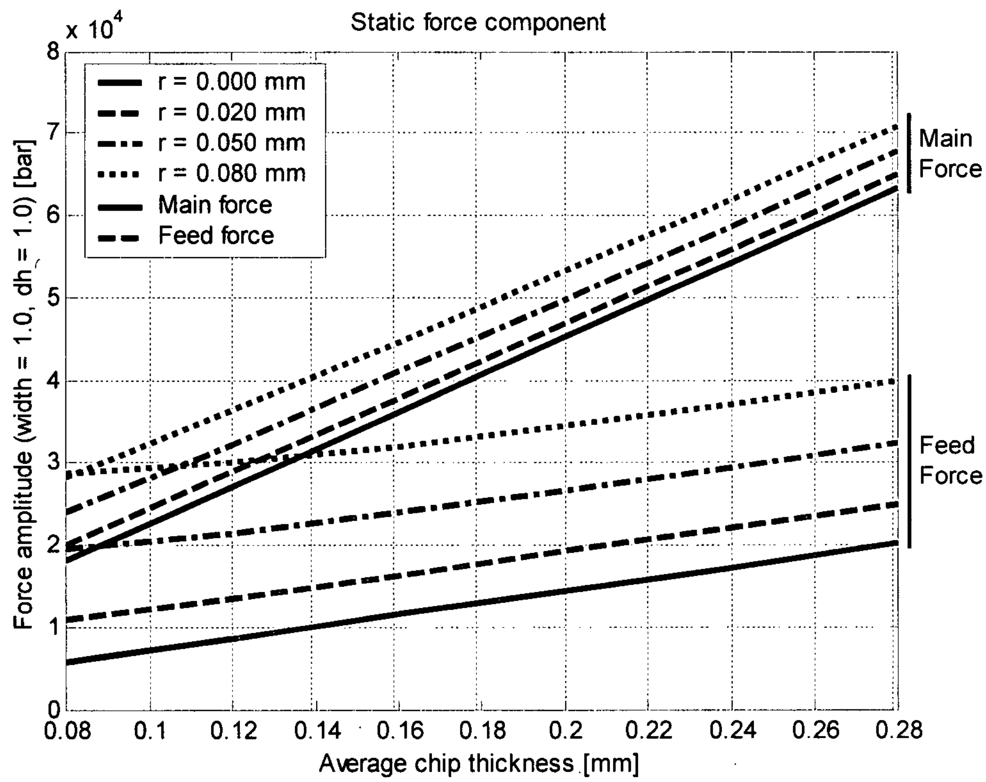

Figure 3-26 (b). Effect of the feed on wave removing

3.5.4. Effect of Vibration Amplitude in Dynamic Cutting

It can be seen from the experimental results shown in Figure 3.24 that the effect of the amplitude of vibration in the dynamic cutting coefficients is similar to that of the feed. However, in this case the upper-bound model developed predicts the decreasing trend of the amplitude of the feed force more closely then for the case of the feed effect. The phase of the forces with respect to the tool increases in all the cases shown, being more sensitive in wave removing than in wave cutting.

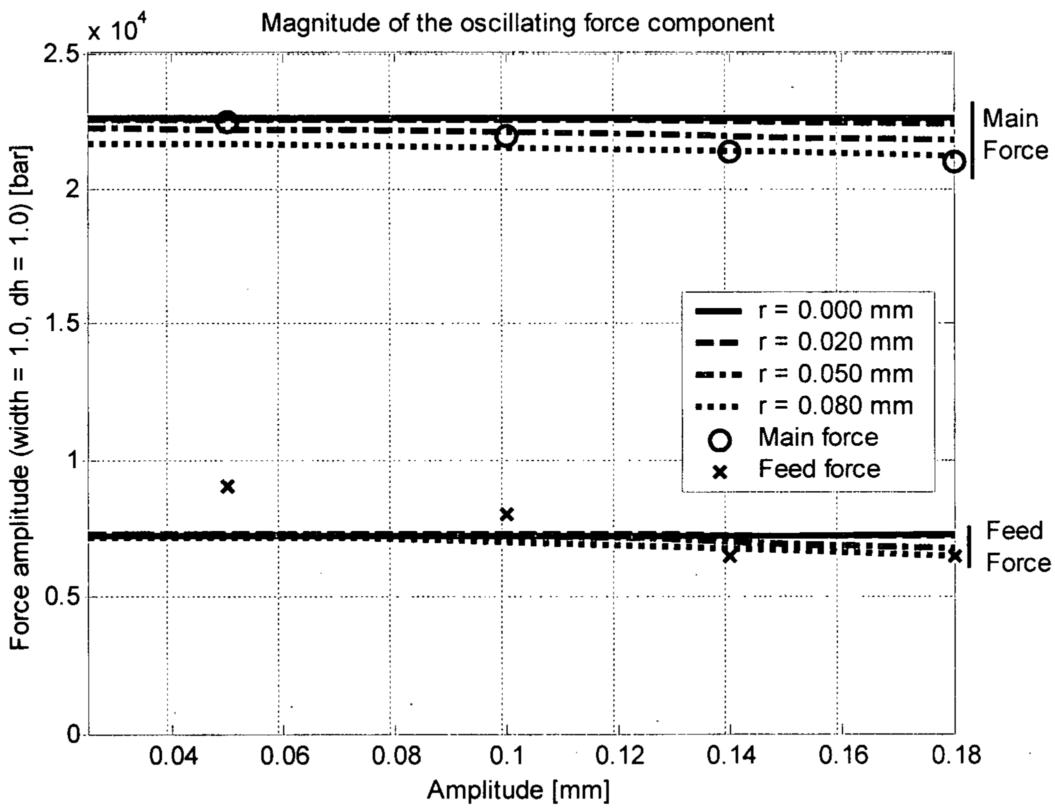

Figure 3-27 (a). Effect of vibration amplitude on wave cutting

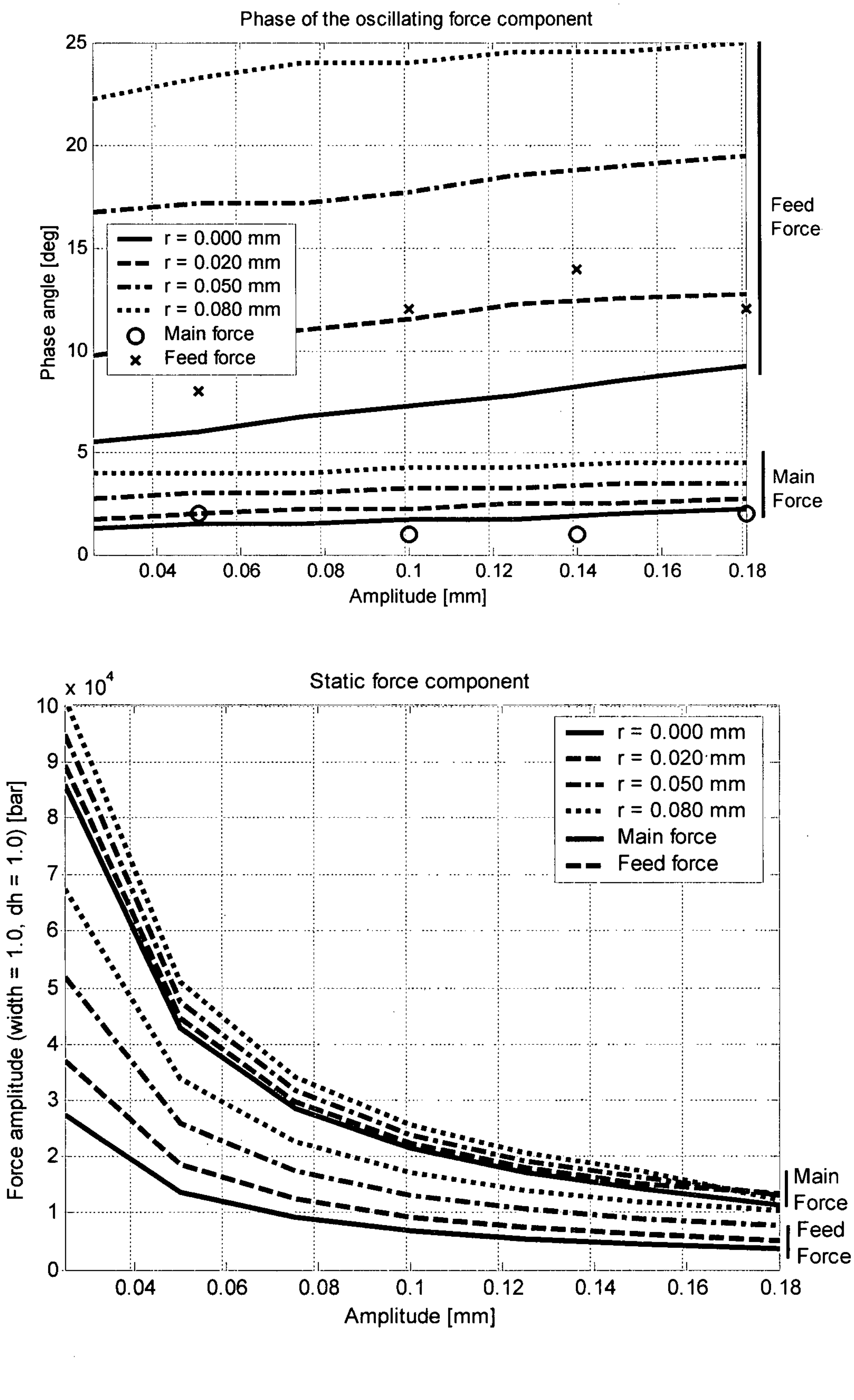

Figure 3-27 (b). Effect of vibration amplitude on wave cutting

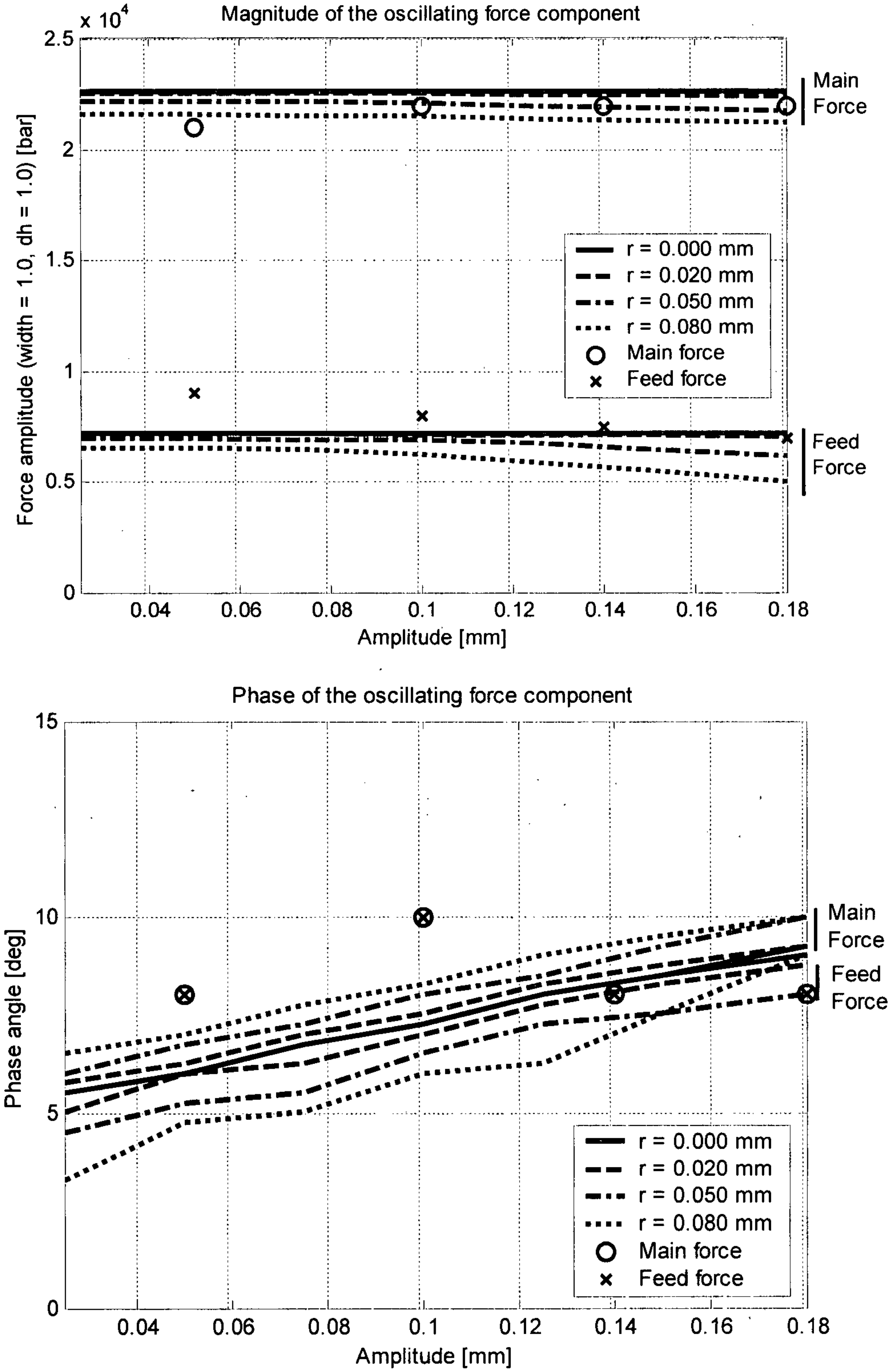

Figure 3-28 (a). Effect of vibration amplitude on wave removing

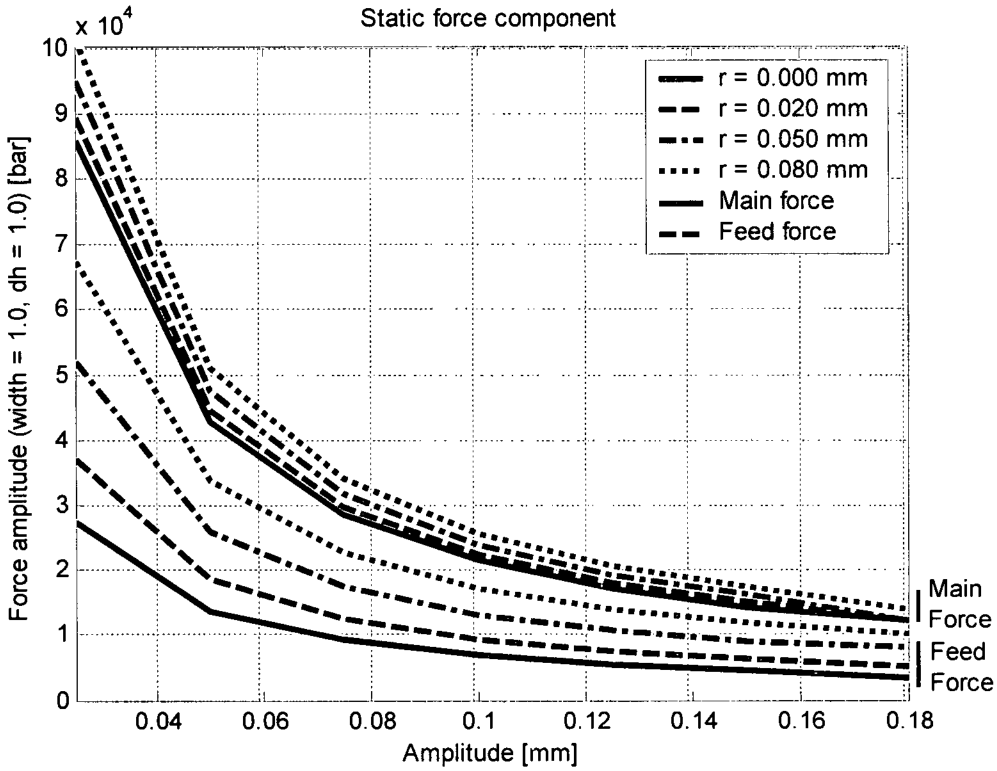

Figure 3-28 (b). Effect of vibration amplitude on wave removing

3.6. Summary

- A model for estimation of influence of the ploughing process on the mechanics of cutting has been presented.

- A model of the dynamic orthogonal cutting process has been developed. The results have been compared to the experimental results presented in the literature and it is found that the new theory predicts the magnitude and phase of the dynamic cutting forces.

- The influence of various tool and process parameters in the dynamic cutting process has been studied using the model developed and it was found that the prediction of the main trends in the process can be predicted using the new theory

CHAPTER IV

> "Engineering is the art of modeling materials we do not wholly understand, into shapes we cannot precisely analyze so as to withstand forces we cannot properly assess, in such a way that the public has no reason to suspect the extent of our ignorance."
>
> - Dr A.R. Dykes, British Institution of Structural Engineers, 1976

4. EXPERIMENTAL INVESTIGATION INTO THE LATERAL CUTTING FORCES IN BANDSAWING

The objective of the experimental work reported here is to develop an understanding of the mechanisms that contribute to lateral cutting forces in the bandsawing process. These forces have been identified as one of the causes for the washboarding problem. An experimental rig available at the CAD/CAM laboratory in the University of British Columbia has been instrumented and used to conduct several cutting tests in wood samples with the purpose of validating the static portion of the cutting model developed in the second chapter of this thesis work.

Douglas fir in saturated and dry condition was used for the work conducted. A series of cutting tools were made of high-speed-steel for the cuts with three hook angles, 0, 20 and 40 degrees. The experiments conducted are summarized as follows:

1) Orthogonal cutting forces in saturated and dry Douglas fir with various hook angles

2) Two-edge cutting forces in saturated and dry Douglas fir with various hook angles

3) Simulated sawing cuts with a bandsaw tooth in saturated and dry Douglas-fir

4.1. Experimental Setup for Static Cutting Experiments

The objective of this section is to provide a description of the experimental apparatus and procedures used for the static cutting experiments reported in this thesis. The instrumentation used is described along with the settings used, as well as the frequency characteristics of the cutting-rig structure, the calibration of the cutting force dynamometer and the wood samples.

The high frequency nature of washboarding makes it difficult to directly study the excitation forces from the bandsawing process. The setup required for measuring these forces would need a flat transfer function up to at least 1000 Hz. Previous research in the Wood Sawing Laboratory attempted to measure the high frequency components of the lateral forces in circular sawing but it was found that the dynamometer-workpiece-wood carriage system being used had a flat transfer function only up to 150 Hz making any measurements above this frequency not reliable. This work was reported by Montgomery in [30].

A setup available at the CAD/CAM laboratory at UBC was adapted to conduct a series of static cutting force experiments that simulate the cuts taken by a bandsaw during regular operation. The apparatus consists of a metallic frame made of 2-inch square tubular section and a pendulum arm that is suspended from a couple of bearings located on the top of this frame. The whole system resembles the machine used for the Charpy impact test. Figure 4-1 shows this structure, indicating all of its main parts. A coordinate system is shown to define the directions of the cutting forces measured by the dynamometer.

The procedure followed for the experiments was as following:

1) A tool was mounted at the end of the pendulum arm on a tool holder
2) A wood workpiece of known width was mounted on top of the dynamometer
3) The workpiece was machined with the tool until a flat top surface was obtained to be used as a zero reference for the chip thickness measurements.

4) The desired chip thickness was set by moving the tool forward in a tool-holder equipped with a dial gauge. This device has an accuracy of 25 microns.
5) The arm was lifted to a set height and then released.
6) The forces produced during the cut are measured using the 3D dynamometer installed at point 4 shown.
7) The forces were recorded using a Tektronix TDS 420A oscilloscope that computes the average force during the cut.
8) The forces were recorded manually in a log-book

The cutting speed was kept constant for all the tests at 2 m/s by controlling the height to which the arm was lifted.

The dynamic characteristics of this structure are of importance in the experimental work reported here. The chip thickness must remain constant during the cut to at least 1 thousand of an inch and therefore any vibrations of the tool with respect to the workpiece holder are undesirable if they exceed this value.

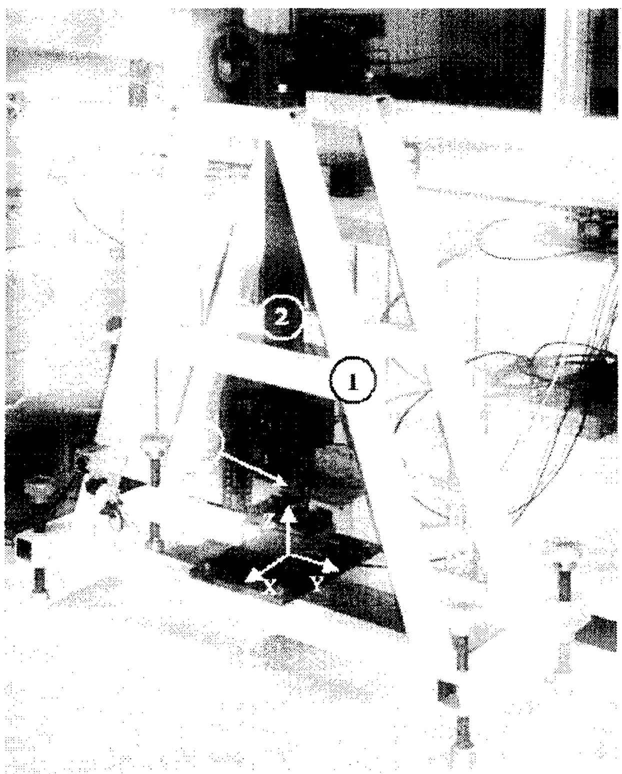

Figure 4-1. Pendulum cutting apparatus. 1: Frame, 2: Pendulum arm, 3: Tool, 4: Dynamometer

4.1.1. Sample Cutting Force Results Obtained with the Pendulum setup

A series of orthogonal cutting tests were conducted on saturated Douglas fir in order to adjust the settings of the instrumentation used. The main and feed cutting forces were measured. Figure 4-2 is a schematic representation of the orthogonal cutting process and shows the conventions used for the measurements.

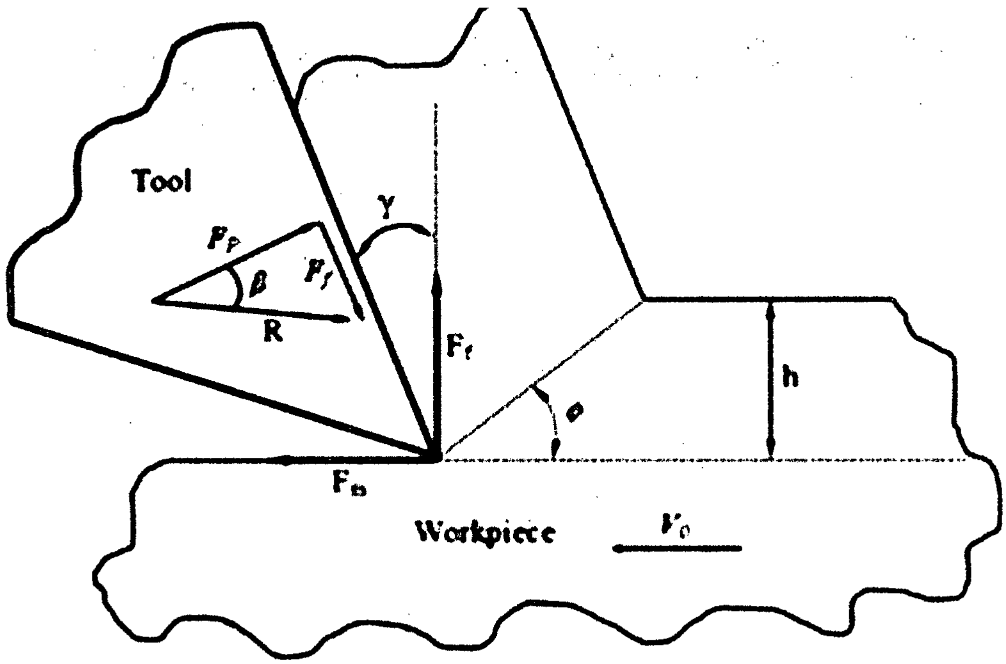

Figure 4-2. Schematic diagram of the orthogonal cutting experiment

Figure 4.3 shows a sample cut measured using the pendulum setup. This data has been low-pass filtered at 200 Hz in order to eliminate any noise and dynamic effects from the structure in the signal.

It can be seen that the duration of the cut is approximately 25 milliseconds. Therefore, the effect of filtering at 200 Hz will only have a slight effect on the mean force value recorded from the oscilloscope.

For each cut in the main direction an average value from the beginning to the end of the cut was taken as an actual estimate of the cutting force in the process. In the feed direction, the value of the force in the middle of the cut was used. This procedure was used for all the results presented in the cutting force plots in this thesis.

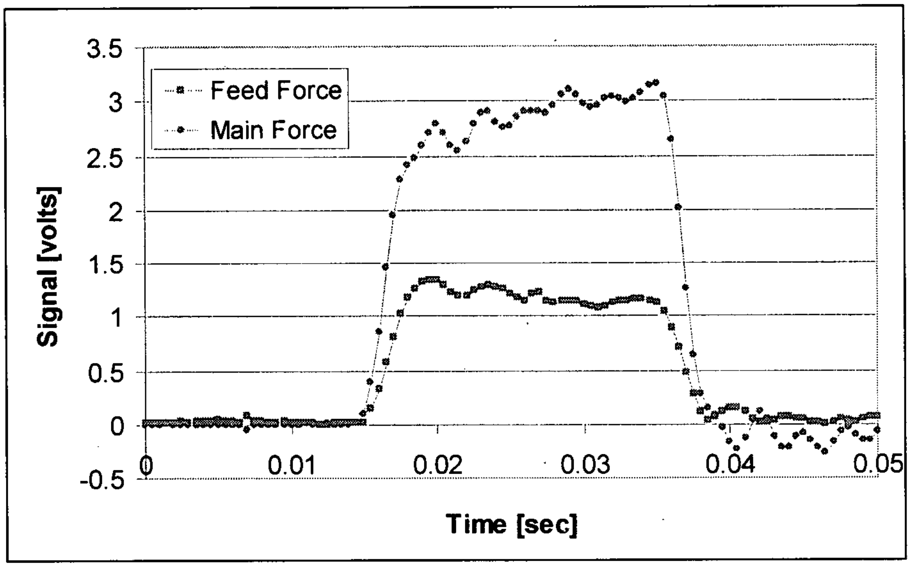

Figure 4-3. Sample orthogonal cut along the grain. Rake angle: 0 degrees, no lubrication, material: Douglas fir

4.1.2. Transfer function of the pendulum structure

The experiments reported in this chapter aim at measuring the average forces in a typical wood machining process under various conditions. In order to guarantee that the forces measured are accurate, the stiffness and frequency response characteristics of all the components in the experimental apparatus must be within acceptable ranges. It is known that the excitation forces to the structure during cutting range from 0 to 200 Newtons in the X and Y directions.

Appendix A shows the displacement transfer function of the experimental rig used. The structure was reinforced in order to minimize its vibrations and free the frequency range of interest from any structural resonancies. It can be seen that the structure is free from resonant modes up to 250 Hz in the feed and main directions. The signal in these two directions has therefore been low-pass filtered at 200 Hz using a 4^{th} order Butterworth filter. The lateral direction in the structure seems to be more flexible, showing modes at 30 and 48 Hz. Therefore some interference in the signal is expected at these frequencies and therefore the lateral force signal was notch-filtered to eliminate these modes.

4.1.3. Three-dimensional force dynamometer

A three-dimensional cutting force dynamometer was used for the measurement of the cutting forces. The frequency response of the device was verified and it was found that it presents a flat response up to 500 Hz, which is more than the specification required for the measuring the forces in the pendulum rig.

The dynamometer was set on a flat table for calibration and then loaded in its three orthogonal directions by using pulleys and weights. The output voltages were registered with an oscilloscope. The device was calibrated between 0 and 160 Newton's, which is the range of forces measured during the experiments conducted. The output of the device in this range seems to be highly linear, as expected. Figures 4-2 shows the calibration curves for the dynamometer.

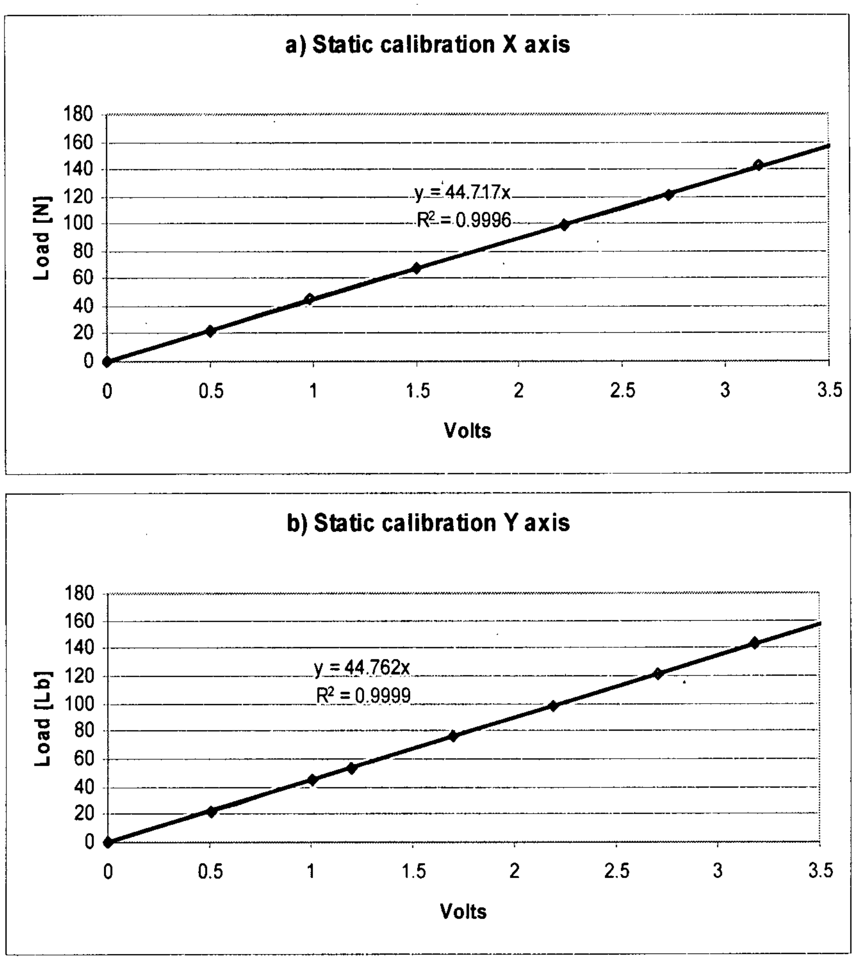

Figure 4-4 (a). Static Calibration of the three-dimensional dynamometer used for the experimental work. a) X axis, b) Y axis

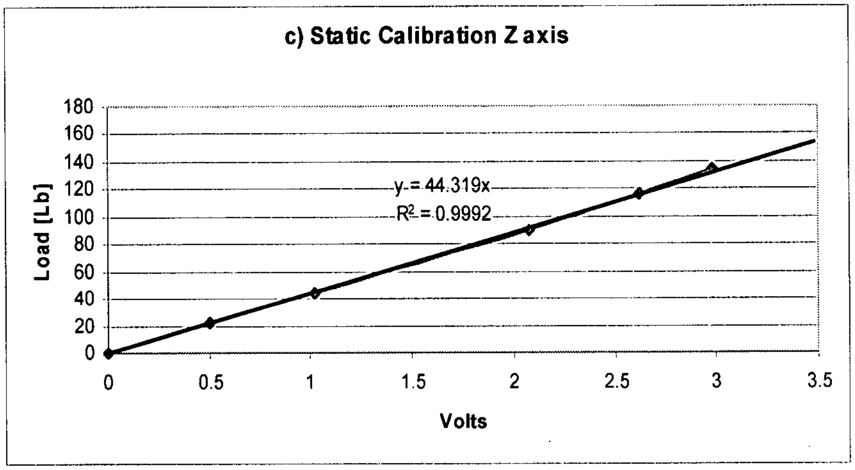

Figure 4-4 (b). Static Calibration of the three-dimensional dynamometer used for the experimental work. c) Z axis

4.1.4. Data Acquisition and Signal Conditioning

Charge amplifiers are a required part of the dynamometer system. Since the force transducers in the dynamometer are piezoelectric, the charge amps must be used to convert the static charge to an analog output, which can be read as a signal in volts. Long-range charge settings are used with the following sensitivities for each component of force.

Table 4-1 Charge Amplifier Settings Used for the Cutting Experiments

Axis	Mechanical Units per V	Sensitivity (pC/V)
X	100	3.05
Y	100	3.00
Z	100	1.65

A Krohn-Hite 3905B multi-channel low-pass filter was used to eliminate noise on all the channels coming from the dynamometer. This is an analog sixth order Butterwoth filter. The cut-off frequency was set at 200 Hz for the experiments. This value for the cut-off frequency has been chosen so that it is above any frequency components of interest.

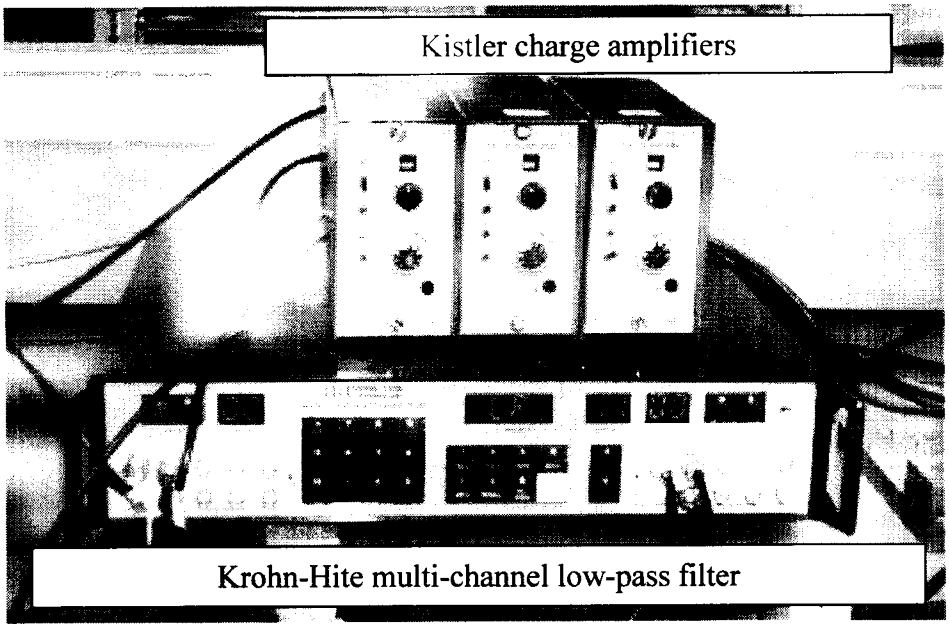

Figure 4-5. Charge amplifiers and analog filter used for the cutting Experiments

All data acquisition on the experiments conducted was done with a Tektronix TDS 420A. This is a 200 MHz 4-channel digitizing oscilloscope with floppy disk facilities.

4.1.5. Wood Samples

A number of wood samples were made to be used in the experiments. All the samples were 75 mm long, 38 mm high and had 7.6 mm width (± 0.5 mm). The material used for the samples was Canadian Douglas fir. These specimens were obtained from a batch that was used to conduct washboarding experiments at Forintek. Two moisture content levels were used on this experimental work. A set of samples was left uncovered for about three week indoors in the CAD/CAM laboratory and its equilibrium moisture content was measured to be 7%, these samples are the material referred to as "dry Douglas fir" in the experimental results shown. Another batch of samples was kept in containers with enough water to keep them just above the saturation point; these will be called "saturated Douglas fir" here. All these samples were planed to obtain uniform thickness. The knots were removed and the direction of the fiber has been set to be straight along the length of the sample for uniformity of the results.

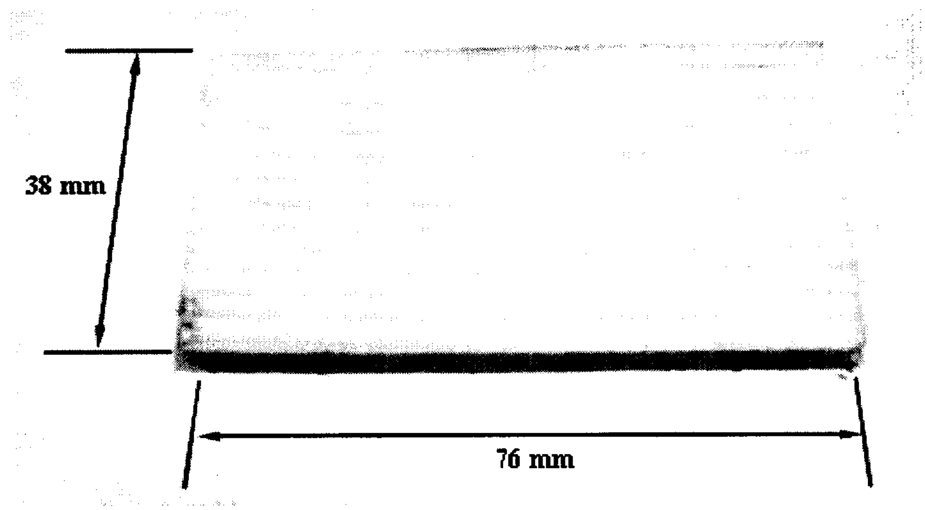

Figure 4-6. Typical Douglas fir sample used in the cutting experiments conducted

Density is an in important variable when cutting forces are studied. More dense wood pieces require higher cutting forces in all directions than lighter ones. While the influence of the density in the cutting forces was not studied in this work, the workpieces were chosen to have similar density in order to minimize the variability in the experimental results. The density of a population of 40 samples for each batch, dry and saturated was measured and the average is presented in the following table:

Table 4.2 Average Density for the Wood Samples Used

Material	**Density [gm/cm^3]**
7% Moisture Content	0.5365
Saturated	0.6412

4.2. Orthogonal Cutting Experiments

The second chapter of this thesis presents a series of analytical developments for improving the current understanding and allowing the prediction of the static and dynamic components of force in bandsawing. These models require sets of orthogonal cutting data that need to be obtained experimentally. The results presented in this section will be used to validate the cutting models presented throughout this thesis.

The study covers three different directions of cutting defined by the orientation of the wood fibers with respect to the tool. The convention here followed was originally defined by Koch in [10] and is summarized in the following table:

Table 4-3. Name convention for the cutting direction with respect to the wood grain

90-90	Cutting across the fibers with the main cutting velocity perpendicular to them. This cutting process is also known as ripsawing
0-90	Cutting parallel to the fibers with the main velocity of the tool perpendicular to them. This process is also called veneer cutting.
90-0	Cutting along the fibers. The main cutting velocity vector is parallel to the fibers but the tool edge is perpendicular to them. This process is also known as planing.

The following cases were studied:

1) Saturated and dry Douglas fir

2) 90-0 cutting or planing and 90-90 cutting or ripsawing

3) Hook angle of 0, 20 and 40 degrees

All the tools used had a clearance angle of 15^0. The width of the cuts was 7.6 mm (± 0.5 mm).

A typical plot of the orthogonal cutting forces as a function of the chip thickness is shown in Figure 4.7. It can be seen that the trend for both, the main and feed force is approximately linear over the range shown. Linear regression of this experimental data was performed in order to obtain a series of orthogonal cutting constants, whose definition and physical significance have been summarized in table 4-3.

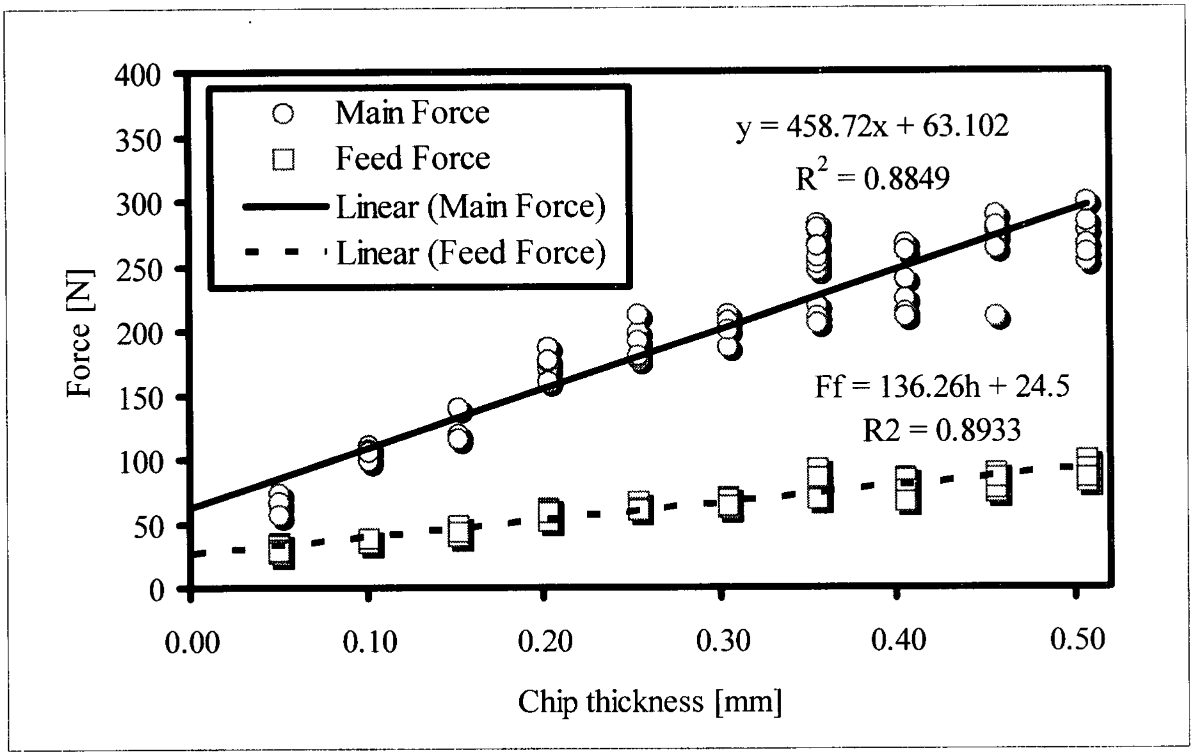

Figure 4-7. Orthogonal cutting forces, a typical experimental result (along the grain)

Appendix B presents all the data obtained from the orthogonal experiments conducted. A compilation of these results is can be seen in table 4-5. These results will be used throughout this chapter for the validation of the static models presented for bandsawing.

It can be seen from the results that the stiffness of the cutting process is lower for saturated wood than for dry wood. In the case of a tool with a zero degree hook, the main cutting force doubles with respect to the dry state and the feed force increases by 37%. It is believed that the saturated state is a closer approximation to the bandsawing conditions in primary manufacturing since the logs are sawn in fresh state, meaning that the wood will still have most of its original moisture.

Table 4-4. Definitions for the orthogonal cutting constants used

Constant	Definition
K_{mc}	Main specific cutting pressure: Pressure required for the cutting process in the direction of the main force.
K_{me}	Main edge constant: Stiffness of the edge localized process in the main direction. This term has units of [N/mm]
K_{fc}	Feed specific cutting pressure: Pressure required for cutting in the direction of the feed force.
K_{fe}	Feed edge constant: Stiffness of the edge localized process in the feed direction. This term has units of [N/mm]
r_c	$\frac{k_{fc}}{k_{mc}}$, ratio between the cutting force required in the feed and main directions
r_e	$\frac{k_{fe}}{k_{me}}$, ratio between the edge force required in the feed and main directions

Increasing the hook angle greatly decreases the specific cutting pressure in the main and feed directions. It can be seen that in cutting along the grain, that a change in the hook from 0 to 40 degrees, causes the pressure to decrease 75%. The edge cutting constants decrease with this change as well. In planing, varying the hook angle from 0 to 20 degrees decreases the main cutting pressure by 55% and in ripsawing, the change is 50%, which suggests that changes in this variable has similar impact in different directions of cut.

It is also to be noted from the results that the feed specific cutting pressure changes from a positive value into a negative when the hook angle is 20 degrees or more. It can be concluded that at some point between 0 and 20 the stiffness of the process must be zero.

Table 4-5. Orthogonal Cutting Constants Obtained from the Cutting Tests

Material	Rake angle [deg]	Direction of cut	K_{mc} [Mpa]	K_{me} [N/mm]	K_{fc} [Mpa]	K_{fe} [N/mm]	r_c	r_e
Saturated Douglas Fir	0	90-0	30.884	7.518	12.464	3.947	0.40	0.52
7% Moisture Content Douglas Fir	0	90-0	58.858	8.429	18.236	3.268	0.31	0.39
Saturated Douglas Fir	20	90-0	27.417	2.882	-3.321	1.066	-0.12	0.37
Saturated Douglas Fir	40	90-0	12.352	1.761	-6.294	0.450	-0.51	0.26
Saturated Douglas Fir	20	90-90	52.039	5.009	-1.720	1.482	-0.03	0.30
Saturated Douglas Fir	40	90-90	26.199	4.250	-2.373	1.641	-0.09	0.39

No experiments were conducted in the 0-90 direction due to unavailability of cutting samples with this fiber geometry. Also, attempts to obtain experimental results for the 90-90 cutting direction with a zero degree rake tool showed that under these conditions cutting was not feasible, showing only fiber ripping and extremely high, unsteady cutting forces. Therefore no results are reported here for either of these cases.

4.3. Two-Edge Cutting Experiments

A three-dimensional cutting model was presented in section 2.1 of this thesis. The model proposes, that based on a set of orthogonal constants for the wood cutting process, the chip flow and cutting forces can be predicted for a 0 degree rake tool. The purpose of the experiment presented here is to validate the model proposed. The geometry of the cut was the same as that shown in Figure 2-1. The cutting conditions used are listed in table 4-6.

Table 4-6. Cutting Conditions for the Two-edge Cutting Experiments

Tool Material	High Speed Steel
Rake angle	0 degrees
Clearance angles	7° on both cutting edges
Speed of cut	2 m/sec
Lubrication	None

The specific procedure followed was as described in section 4-1 of this chapter. The following Figure illustrates the experiment conducted. The goal is to reproduce the process represented in Figure 2-6. To achieve this, a corner of the tool is used to perform the cut and the dimensions of both edges are controlled in order to achieve the desired chip geometry.

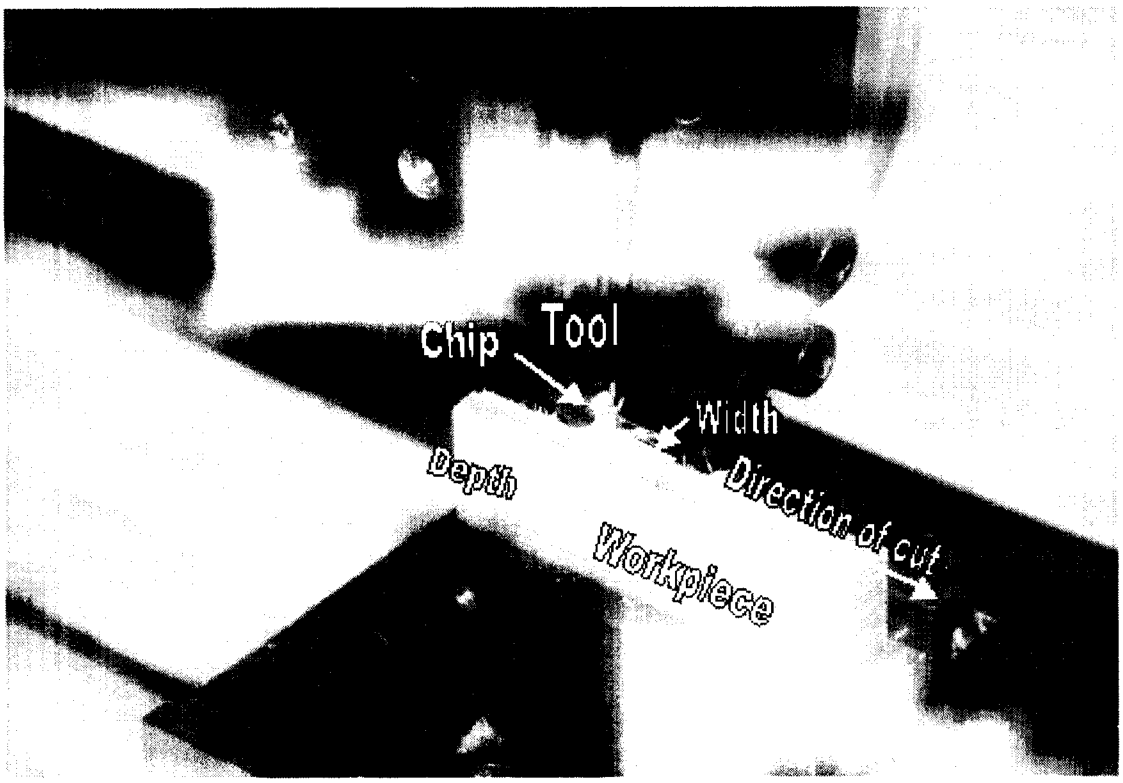

Figure 4-8. Illustration of the two-edge experiment conducted

Figure 4-9 shows the prediction for the lateral cutting force in two-edge cutting as a solid line which was obtained from the model proposed in formula 2.6. The triangles represent experimental data points. It can be seen that there is good agreement between the model proposed and the experimental result. Some scatter is present in the data which is typical in experimental results for wood cutting. However, the trends are conclusive in favor of the applicability of the cutting force model developed.

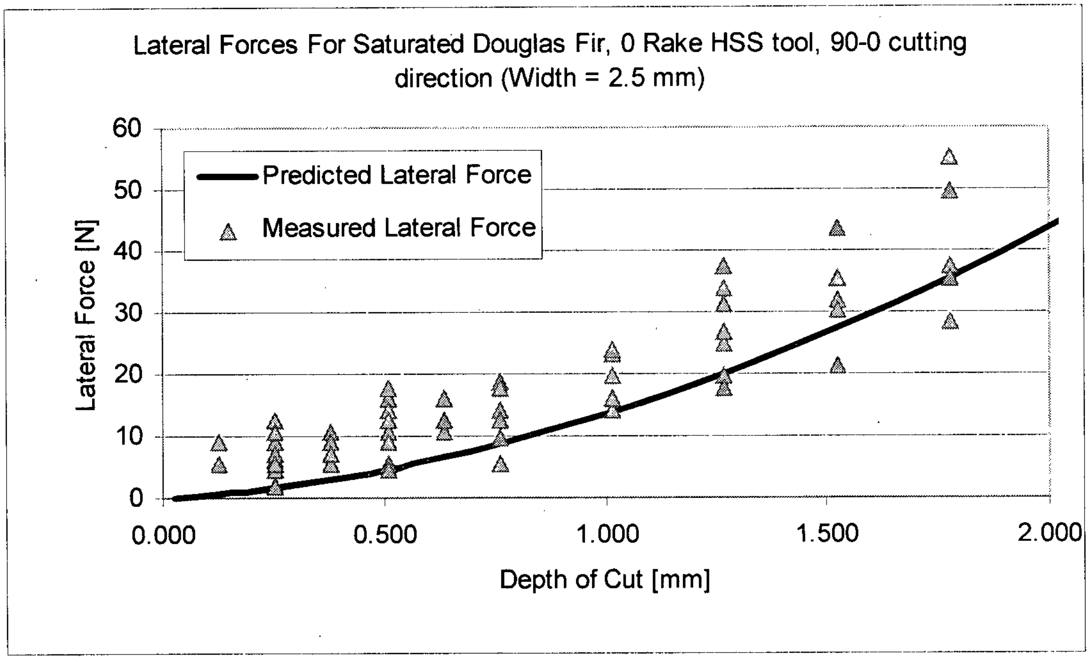

Figure 4-9. Measured and predicted lateral forces for saturated Douglas fir in planing

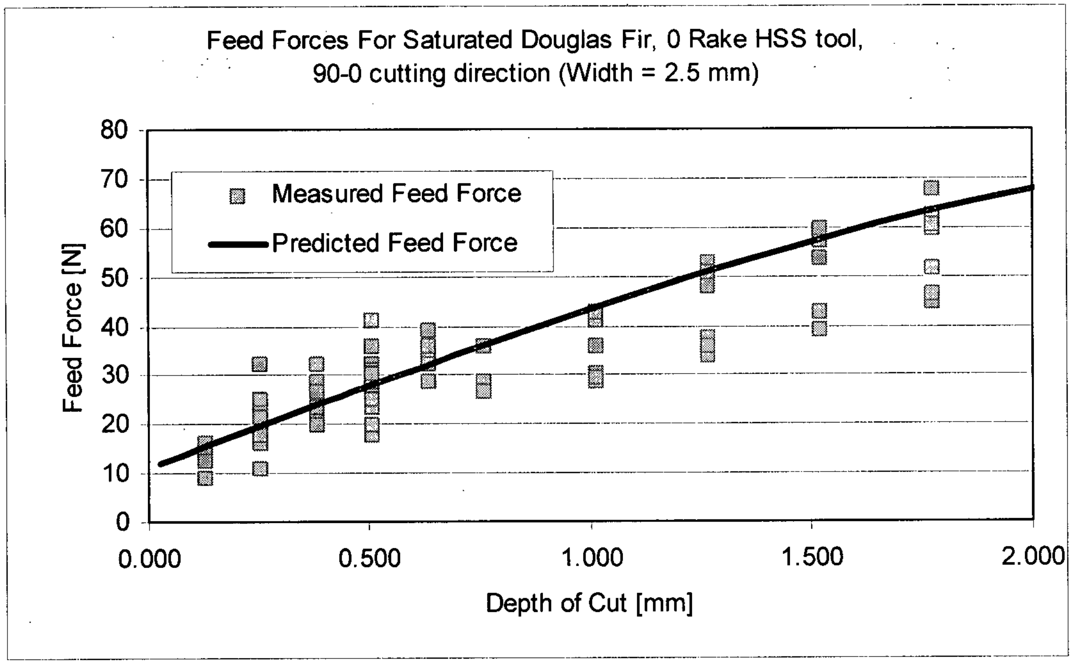

Figure 4-10. Measured and predicted feed Forces for saturated Douglas fir in planing

Figure 4-10 shows the prediction for the feed cutting force in two-edge cutting as a solid line which was achieved by using the model proposed in formula 2.7. It is again seen that the model is able to predict the correct trend for the cutting forces and that the actual magnitude of the force is also comparable to the experimental result.

Figure 4-11 below shows the predictions for the lateral cutting force and the experimental results obtained for dry Douglas fir. Saturated material tends to create a more homogeneous chip and this is usually reflected in the consistency of the cutting force measurements during experimentation. However, even when the experimental results seem somewhat scattered, the model seems to predict the force trend in an average sense throughout the range studied.

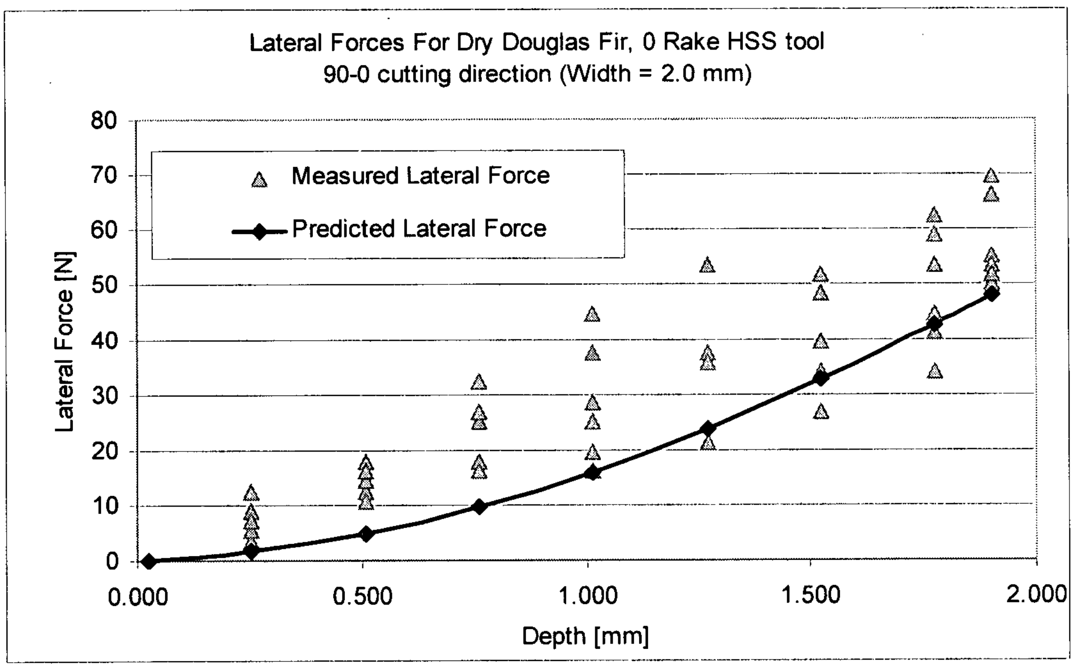

Figure 4-11. Measured and predicted lateral forces for dry Douglas fir in planing

The same that was stated for Figure 4-11 is applicable to Figure 4-12. The mathematical model can be considered a good average predictor of the feed cutting force.

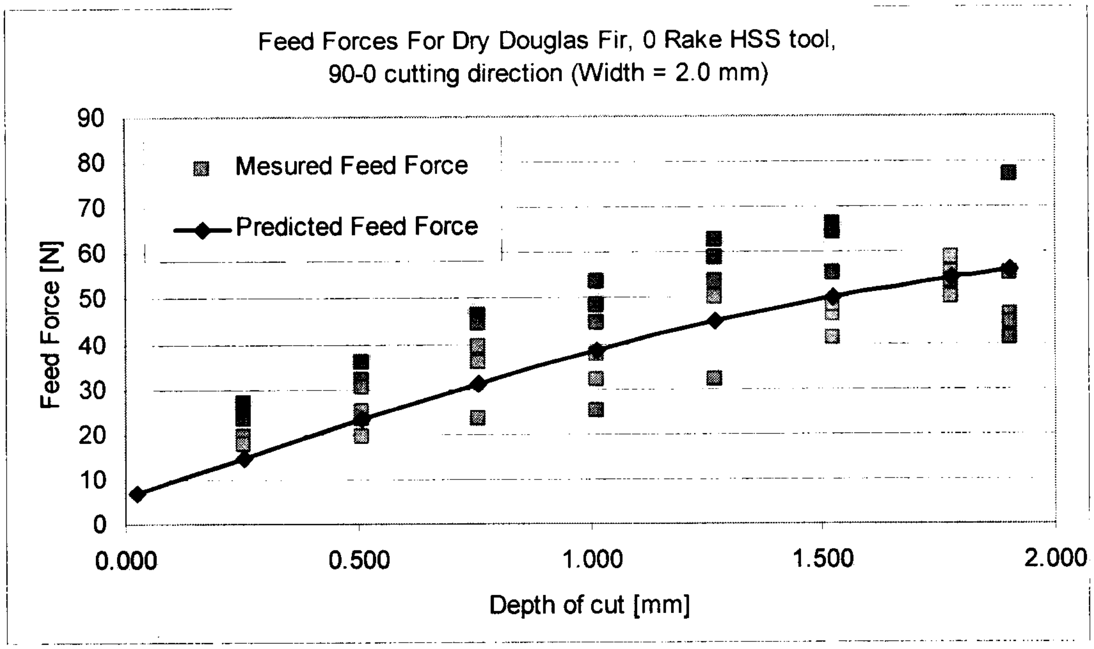

Figure 4-12. Measured and predicted feed forces for dry Douglas fir in planing

It can be concluded from the experimental data obtained that the assumptions made for the model proposed are reasonable for cutting of saturated wood in the 90-0 direction. In the case of dry wood, the variability of the data obtained increases but the model also seems to be a good predictor of the average value for the data obtained.

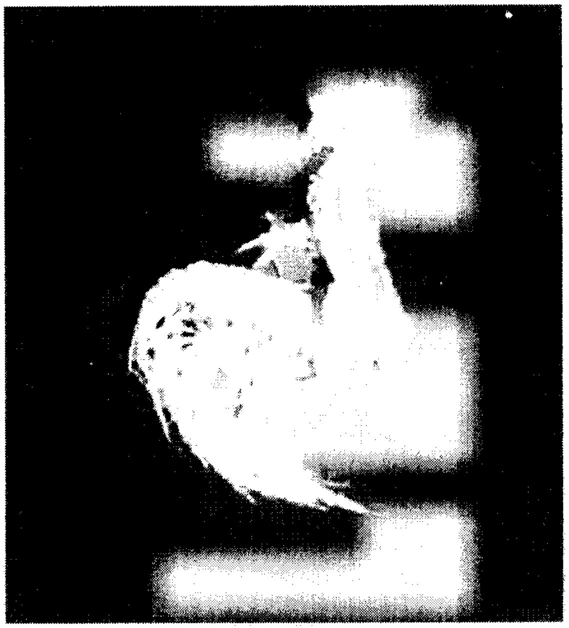

Figure 4-13. Helical chip obtained from a two-edge cut in saturated Douglas fir

Also, it is noteworthy that the chip obtained from the experiments in saturated and dry Douglas fir had a spiral like geometry, which is shown in Figure 4-13. This is similar to the chip formation that can be observed in turning of metals for a tool with a nose radius and suggests that there is lateral shear occurring in the cutting process.

4.4. Cutting Forces on a Saw Tooth

The experiments reported here have the object of identifying the cutting forces in the bandsawing process under "perfect" cutting conditions. This is, the tool used has been properly ground, the alignment of successive teeth is perfect and the workpiece is free of defects. The value registered for the lateral force corresponds to the average value during each cut.

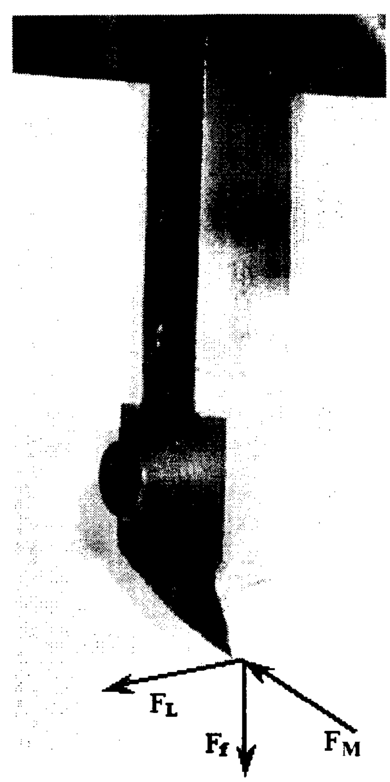

Figure 4-14. Saw tooth used for the experiments showing the three directions of force measured and convention for the force sign

For this experiment, a saw tooth in good condition was cut from a bandsaw, sharpened and installed on the arm of the pendulum setup in order to measure the cutting forces acting upon it. Figure 4-14 shows the tooth used, the direction of the three orthogonal components of force measured on the experiment and the directions taken as positive for convention. The following table presents all the information about the saw tooth used.

Table 4-7. Specifications for the saw tooth used in the experiments

Parameter	Value
Hook angle	30°
Clearance angle	16°
Sharpness angle	44°
Tangential angle	6°
Radial Angle	7°
Kerf	0.110 in
Thickness blade	0.050 in
Side Clearance	0.030 in
Wear condition	Moderate

Cuts were conducted in the three major directions identified in wood machining, 90-90, 0-90 and 90-0. The material used was Douglas fir, in the saturated and dry conditions.

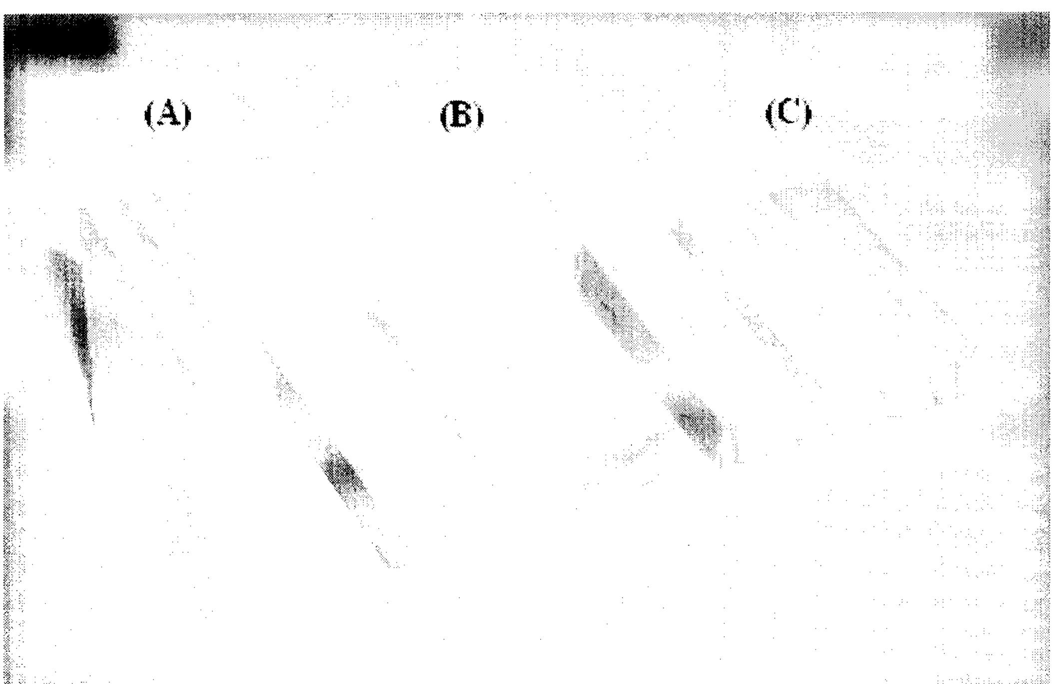

Figure 4-15. Samples cut in three different directions with respect to the Fibers. A) 90-90 direction, B) 0-90, C) 90-0

Figure 4-15 shows the slots cut from the samples after the experiment was conducted. The workpiece shown on (A) was cut against the grain, or 90-90 direction, which is the usual direction of cut in bandsawing. (B) was cut on the 0-90 direction and (C) was cut along the grain or 90-0 direction.

A typical set of results is presented in Figures 4-16 through 4-18. The results follow a linear trend for the feed and main force in a similar fashion to the orthogonal cutting case.

It can be seen in Figure 4-18 that the lateral cutting force is non-zero, even though the load presented to the tooth is balanced. There is no obvious trend to be specified for the lateral cutting forces in this case. However, the force can be statically described in a simple way by calculating the envelope of the maximum force expected in relation with a given chip thickness. This will give an equation for the lateral forces that defines a maximum limit for them. The sign, as seen from the experiments can be either positive or negative.

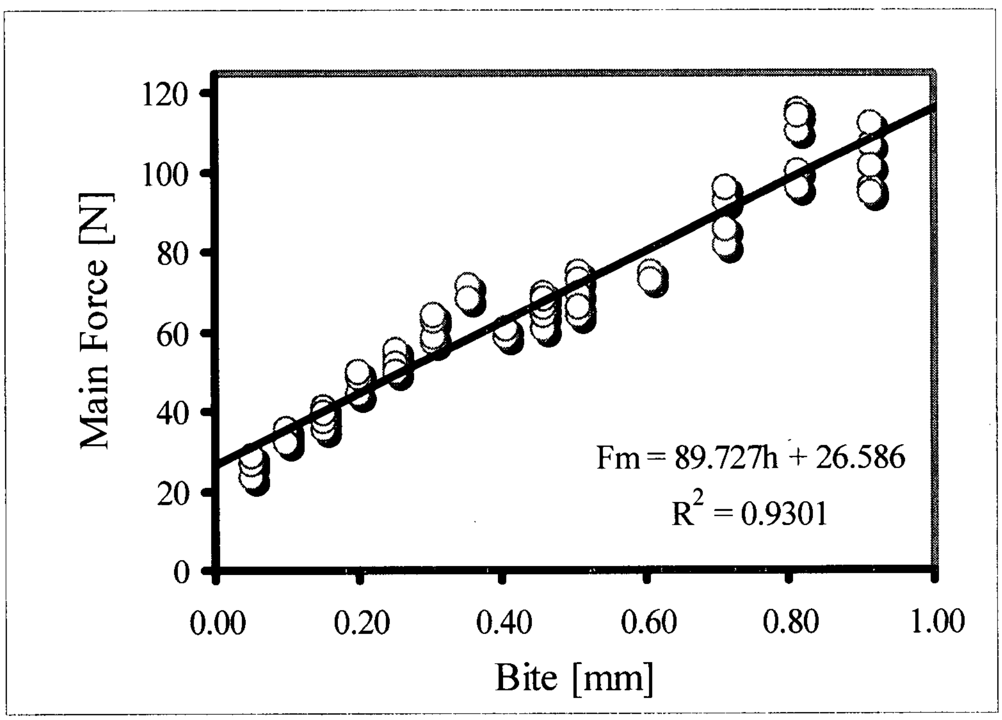

Figure 4-16. Typical main cutting force plot obtained in single tooth sawing

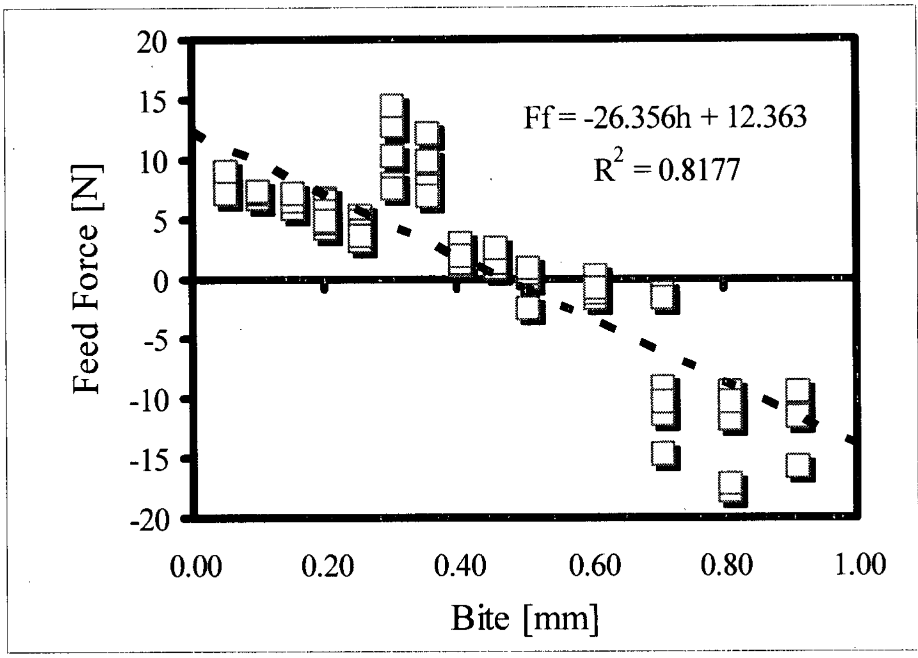

Figure 4-17. Typical feed cutting force plot obtained in single tooth sawing

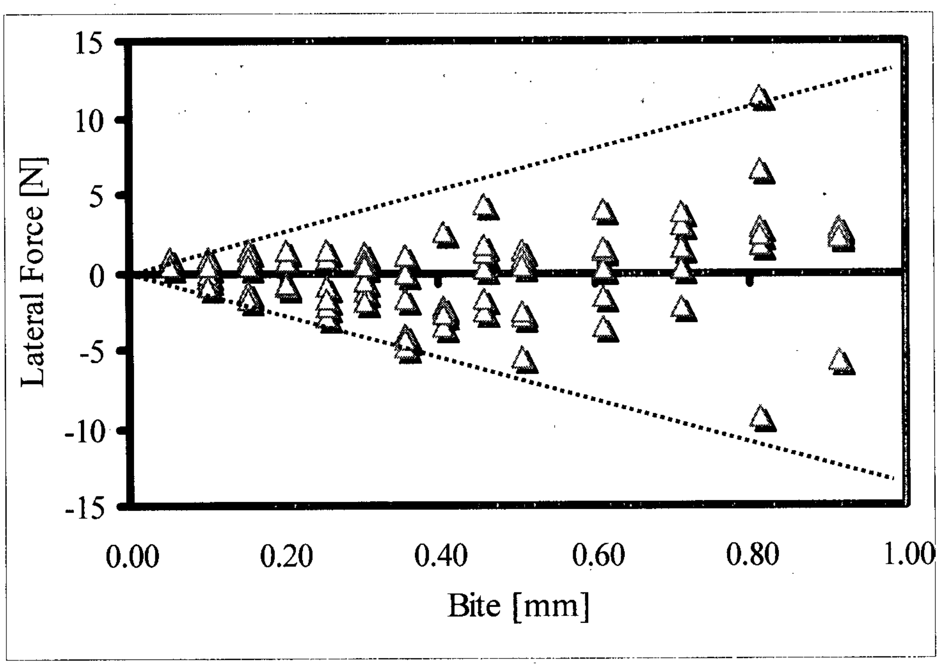

Figure 4-18. Typical lateral cutting force plot obtained in single tooth sawing

All the results obtained are shown in appendix C and summarized in table 4.8. The lateral force is described as negative or positive due to the behavior shown in Figure 4-18. The sub index "*e*" added to a direction of force corresponds to the edge component of that force.

Table 4-8. Cutting constants obtained from the single-tooth sawing experiment

Material	**Direction of cut**	**F_m [N/mm]**	**F_{me} [N]**	**F_f [N/mm]**	**F_{fe} [N]**	**F_L [N/mm]**
Saturated Douglas Fir	90-90	89.72xbite	26.58	-26.35xbite	12.36	±14xbite
7% Moisture Content Douglas Fir	90-90	110.27xbite	24.61	-19.79xbite	7.13	N/A*
Saturated Douglas Fir	90-0	66.47xbite	5.60	-18.88xbite	5.90	±17xbite
7% Moisture Content Douglas Fir	90-0	94.37xbite	0.1195	-25.22xbite	6.08	±17xbite
Saturated Douglas Fir	0-90	159.63xbite	-8.28	-49.68xbite	12.46	±30xbite
7% Moisture Content Douglas Fir	0-90	135.39xbite	2.29	-38.26xbite	11.00	±19xbite

* In this case, the experimental data yielded no correlation between the lateral force and the bite used. This result can be seen in Appendix C, plot D-2.

The Experimental results show that under "perfect" cutting conditions the maximum peak of the lateral cutting forces reaches 30 Newton's (Appendix C). One explanation for the existence of these lateral forces is density gradients within the piece of wood used. These gradients are the result of the difference in properties between early-wood and late-wood. For each hard ring in Douglas fir there is a soft ring. This creates a field in which the lateral forces in the sawtooth will never be balanced. However, as seen from the experiment it is possible to define limits for the possible lateral forces in a saw tooth as a unction of the bite used.

As for the mains and feed cutting forces, it can be seen that they follow a fairly linear trend with respect to the bite as mentioned before. The spread of the data is approximately 20%, which seems reasonable in wood cutting. One possible explanation for this variability is the fact that successive cuts are taken in positions of the workpiece separated by a bite distance. The material in these two positions will most likely have a different ring configuration or average density and this will impact the forces in the same way that was explained in the discussion for the lateral forces.

According to the experimental results presented, the stiffest direction of cut is 0-90. This is an expected result since two edges of the saw-tooth are cutting across the fibers in this direction. The softest direction of cut is, as expected, along the grain. One interesting finding is that even when this direction presents the lowest stiffness, the edge forces are the highest compared to the other two directions.

The feed force results show that for the tool geometry that was used on the experiments, the tooth is pulled onto the wood during cutting in the feed direction.

4.5. Summary

The following points summarize the findings of this chapter:

- A series of experiments was conducted in order to validate the static portion of the cutting model proposed for bandsawing in this thesis work
- The experimental procedures and instruments used for the research conducted were described
- A set of orthogonal cutting data was obtained. This data can be used in the cutting models developed in order to predict the cutting forces in complex cutting processes such as bandsawing
- A model to predict the cutting forces in two-edge cutting was validated. It was found that the theory developed is a good predictor for the cutting forces in this process
- A series of experiments that simulate cuts taken by a bandsaw were conducted. The results show the trends followed by the feed, main and lateral cutting forces with respect to the size of the bite
- A model was proposed to find the bounds for the lateral cutting force for a sawtooth

CHAPTER V

CONCLUSIONS AND RECOMMENDATIONS

The forces applied to a saw tooth subjected to unbalanced chip loads during bandsawing have been investigated theoretically using an upper-bound approach. A detailed examination of the process in the presence of tool vibration has been carried out again, using the upper bound approach. Finally, the static model proposed was validated experimentally using a simple cutting rig available at the CAD/CAM laboratory at the University of British Columbia.

The following points summarize the main findings of this research:

I. Analytical Development of a Static Cutting Force Model for Bandsawing

- The cutting forces in bandsawing can be predicted if the influence of the lateral cut on the chip flow is known and a series of orthogonal cutting experiments are conducted in order to obtain the orthogonal cutting constants for the material used

- The lateral cutting forces in the bandsawing process depend not only on the extra side cutting area between consecutive teeth but also on the length of the extra lateral cutting edge and the radius of the cutting edge. This extra component of force is known as a parasitic or edge force.

- A series of upper-bound models have been developed in order to predict the chip flow angle on the face of the tool and therefore the cutting forces

- The stiffness of the lateral cutting process decreases as the hook angle increases

II. Analytical Development of a Dynamic Cutting Force Model for Bandsawing

- A model for estimation of the influence of the ploughing process has been presented. This development is based upon the findings of previous researchers in the area of tool wear and has been formulated in order to model the effects of the nose of the tool during washboarding.

- A model for the orthogonal dynamic cutting process has been developed. The results have been compared to the experimental results presented in the literature. It is found that the new theory predicts the magnitude and phase of the dynamic cutting forces reasonably well.

- The influence of various tool and process parameters in the dynamic cutting process has been studied using the model developed and it was found that the prediction of the main trends in the process can be achieved using the new theory

III. Experimental Investigation into the Lateral Cutting Forces in Bandsawing

- A series of experiments was conducted in order to support the theory presented for the static portion of the cutting model proposed for bandsawing in this thesis work

- A set of orthogonal cutting data was obtained. This data can be used in the cutting models developed in order to predict the cutting forces in complex cutting processes such as bandsawing

- A model to predict the cutting forces in two-edge cutting was validated. It was found that the theory developed is a good predictor for the cutting forces in this process

- A series of experiments that simulate cuts taken by a bandsaw were conducted. The results show the trends followed by the feed, main and lateral cutting forces with respect to the size of the bite

- A simple model was proposed to estimate the bounds for the lateral cutting forces in sawing for balanced ship loads

IV. Recommendations

The analysis conducted on the geometry of a bandsaw tooth and its cutting interactions yields a series of recommendations that can be used in order to help stop the washboarding problem. Figure 5.1 shows a modification that can simply be made to a sawtooth. The dashed lines correspond to the profile of a tooth with the geometry currently used in saw mills. This shape is reached by either swaging to blade or using stellite inserts which are purchased and welded onto the blades made locally. The new geometry is shown in solid lines superimposed in the drawing. The idea proposed is to reduce the flank interaction of a saw tooth by decreasing the size of the inserts used. In the old geometry, the excess side flank BC is readily available to produce undesirable interactions with the workpiece. In contrast, the flank for the new geometry has been moved to the position shown by line BD.

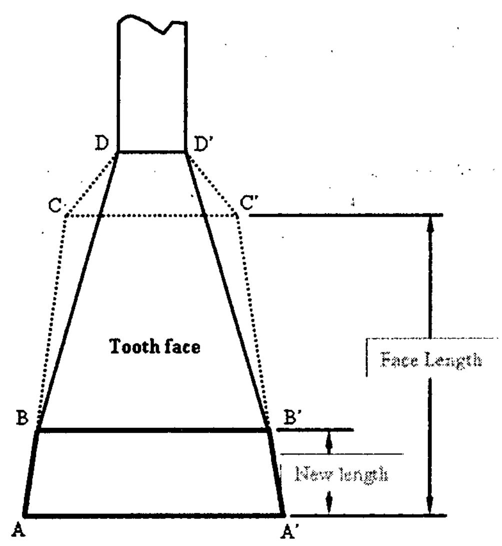

Figure 5-1. Short-faced saw tooth geometry

Ideally, if the new face length shown in the figure is as small as one bite, most of the side interaction between the saw tooth and the workpiece in subsequent cuts will be avoided.

Another idea that will be proposed here is related to the finding in the dynamic cutting model developed that changes in the rake angle of the tool can decrease the dynamic cutting coefficients. A saw tooth with hollow face is shown in Figure 5-2. This geometry is similar to the one found in a freshly swaged saw-tooth with the difference that in this case, the lateral edges have been sharpened as well as the main edge. The main cutting edge has been preserved on the tooth in order to avoid an increase in the main cutting force by conducting this modification. The side hook angle for this tool is γ_L shown in the top view of the saw tooth. If the value of this angle is as high as 30 degrees, the lateral stiffness coefficient will decrease significantly.

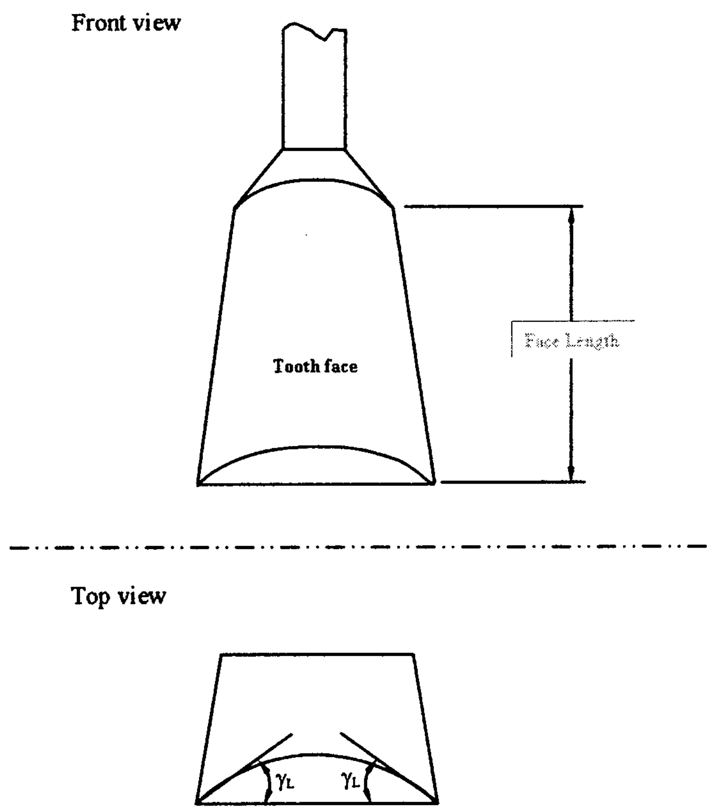

Figure 5-2. Hollow face geometry for a bandsaw tooth

V. Recommended Further Research

The theory presented in the body of this work can be used as the foundation for further developments in the knowledge about the mechanics of cutting in bandsawing and the eventual solution of the washboarding problem. The following points correspond to further work that could be conducted to extend the theories and developments contained in this thesis:

- Experimental validation of the three-edge cutting model presented in section 2.3 of the second chapter of this thesis.
- Experimental validation of the static model for two-edge cutting with variable hook angle.
- Analytical development of a three-edge cutting model with variable hook angle.
- Analytical development of a dynamic cutting model for two and three edge cutting based on the developments presented in sections 2.2, 2.3, 3.2 and 3.5 of this thesis.
- Experimental validation of the dynamic cutting model proposed for wood machining processes and the extended model of multiple-edge dynamic cutting
- Implementation of the new saw tooth geometries proposed above and testing in a bandsaw blade for washboarding resistance

BIBLIOGRAPHY

[1] Luo, Z., "*Parametric Vibrations of Traveling Plates and Mechanics of Washboarding in Bandsaws*", 2001, PhD Dissertation, Department of Mechanical Engineering, University of British Columbia, Vancouver, B.C., Canada

[2] Simmonds, A., "*Wide Bandsaws*", 1980, Stobart & Son, London

[3] Tian, J., "*Self-Excited Vibrations of Rotating Discs and Shafts With Applications to Sawing and Milling*", 1998, PhD Dissertation, Department of Mechanical Engineering, University of British Columbia, Vancouver, B.C., Canada.

[4] Tobias, S.A., Fishwick, W., "*A Theory of Regenerative Chatter*", 1958, The Engineer, London, V. 205, pp. 199-203.

[5] Tlusty, J., Polacek, M., 1963, "*The Stability of Machine Tools Against Self-Excited Vibrations in Machining*", ASME *International Research in Production Engineering*, pp. 465-474.

[6] Merritt, H.E., 1965, "*Theory of Self-Excited Machine Tool Chatter*", ASME *Journal of Engineering for Industry*, Vol. 87, pp. 447-454.

[7] Lehmann, B.F., "*The Cutting Behavior of Bandsaws*", 1993, PhD Dissertation, department of Mechanical Engineering, University of British Columbia, Vancouver, B.C., Canada.

[8] Franz, N.C., "*An Analysis of the Wood-Cutting Process*", 1958, The University of Michigan Press, Ann Arbor

[9] McKenzie, W.M., "*Fundamental Analysis of the Wood Cutting Process*", 1961, The University of Michigan Press, Ann Arbor

[10] Koch, P., "*The Utilization of the Southern Pines*", 1972, U.S. Department of Agriculture Forest Service

[11] Koch, P., *"Wood Machining Processes"*, 1964, The Ronald Press Company, New York

[12] St-Laurent, A, *"Effects of Saw Tooth Edge Defects on Cutting Forces and Sawing Accuracy"*, 1970, Forest Products Journal, Vol. 20, No. 5, pp. 33-40

[13] McKenzie, W.M., *"Wood is easy to cut – or is it?"* 1993, Proceedings of 11th International Wood Machining Seminar, pp. 27-40

[14] Merchant M.E., *"Mechanics of the Cutting Process"*, Journal of applied physics, 1945, Vol. 16, pp 267 and 318

[15] Armarego E.J.A., Brown, R.H., *"The machining of metals"*, 1969, Prentice-Hall, Englewood Cliffs, New Jersey

[16] Lee, E. H. Schaffer B. W., *"Theory of Plasticity Applied to the Problem of Machining"*, 1951, Journal of Applied Mechanics, Vol. 18

[17] Shaw, M. C., Cook, N. H., Finnie, I., *"Shear Angle Relationship in Metal Cutting"*, Transactions of the ASME, 1953, Vol. 75

[18] Oxley, P. L. B., *"A Strain Hardening Solution for the Shear Angle in Orthogonal Metal Cutting"*, 1961, International Journal of Mechanical Engineering Science, Vol. 3

[19] Tobias, S.A., *"Machine Tool Vibration"*, 1965, Blackie & Son, Glasgow

[20] Albrecht, P., *"Dynamics of the Metal Cutting Process"*, Journal of Engineering for Industry, November 1965 pp. 429-441

[21] Tlusty, J., *"Analysis of the State of Research in Cutting Dynamics"*, Annals of the CIRP, 1978, No. 27 Vol. 2 pp. 583-589

[22] Wu, W.D., *"Governing Equations of the Shear Angle Oscillation in Dynamic Orthogonal Cutting"*, 1986, Journal of Engineering for Industry, Vol. 108, pp. 280–287.

[23] Wu, W.D., "*Comprehensive Dynamic Cutting Force Model and its Application to Wave-Removing Processes*", 1988, Journal of Engineering for Industry, Vol. 110, pp. 153 –161

[24] Wallace P.W., Andrew, C., "*Machining Forces: Some Effects of Tool Vibration*", 1965, Journal of Mechanical Engineering Science, Vol. 7, pp. 152-162

[25] Wallace P.W., Andrew, C., "*Machining Forces: Some Effects of Removing a Wavy Surface*", 1966, Journal of Mechanical Engineering Science, Vol. 8, pp. 129-139

[26] Nigm, M. M., Sadek, M. M., "*Experimental Investigation of the Characteristics of Dynamic Cutting Process*", 1977, Journal of Engineering for Industry, ASME, No. 99, pp. 410-418

[27] Nigm, M. M., Sadek, M. M. and Tobias, S. A., 1972, "*Prediction of Dynamic Cutting Coefficients from steady-State Cutting Data*", 1972, Proceedings of the MTDR conference, pp. 3-12

[28] Usui, E., Hirota, A. and Masuko, M., "*Analytical Prediction of Three-dimensional Cutting Processes*", 1978, Trans. ASME, Journal of Engineering for industry, Vol. 100, pp. 222-253

[29] Seethaler, R. J., Yellowley, I., "*An Upper-Bound Cutting Model For Oblique Cutting Tools with a Nose Radius*", 1997, International Journal of Machine Tools and Manufacture, Vol. 37, No. 2, pp. 119-134

[30] Montgomery, D., "*Cutting forces in Circular Sawing*", 1988, unpublished, University of British Columbia, Vancouver, Canada.

[31] Field, M., and Merchant, M. E., "*Mechanics of Formation of the Discontinuous Chip in Metal Cutting*", 1948, Transactions of the ASME, Vol. 71

[32] St. Laurent, A., "*Influence des Noeuds sur les Forces de coupe dans le Sciage du Bois*", 1971, Canadian Journal of Forest Research, Vol. 1, pp. 43-56

[33] Manjunathaiah, J., Endres, W. J., *"A New Model and Analysis of Orthogonal Machining With an Edge-Radiused Tool"*, 2000, Journal of Manufacturing Science and Engineering, V. 122, pp. 384-390.

[34] M. K. Das and Tobias, S.A., *"The Relation Between the Static and Dynamic Cutting of Metals"*, 1967, International Journal of Machine Tool Design and Research, V. 7, pp. 63-89.

[35] Shumsheruddin, A. A., *"Dynamic Orthogonal Metal Cutting"*, 1964, Ph.D. Thesis, Birmingham University.

[36] Nigm, M. M., Sadek, M. M. and Tobias, S. A., "Prediction of dynamic cutting coefficients from steady-state cutting data", 1972, Proceedings of the Thirteenth International MTDE Conference, p.3.

[37] Hosford, W.F., Cadell, R.M., *"Metal Forming; Mechanics and Metallurgy"*, 1993, Prentice-Hall, Englewood Cliffs, New Jersey

Appendix A

Transfer Function of the Experimental Setup

This appendix shows the dynamic characteristics of the setup used for the experimental work reported in chapter 4. Figure A-1 shows the convention for the coordinate system used for the measurements. The transfer function was measured by setting an accelerometer at point 3 and impacting with a test hammer at that same location.

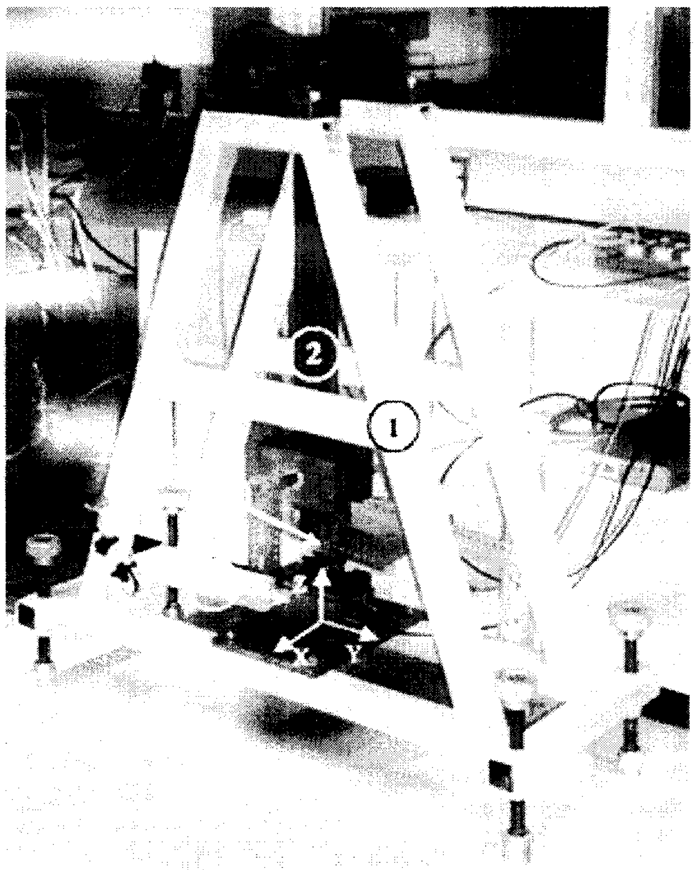

Figure A-1. Pendulum Cutting Apparatus. 1: Frame,
2: Pendulum arm, 3: Tool, 4: Dynamometer

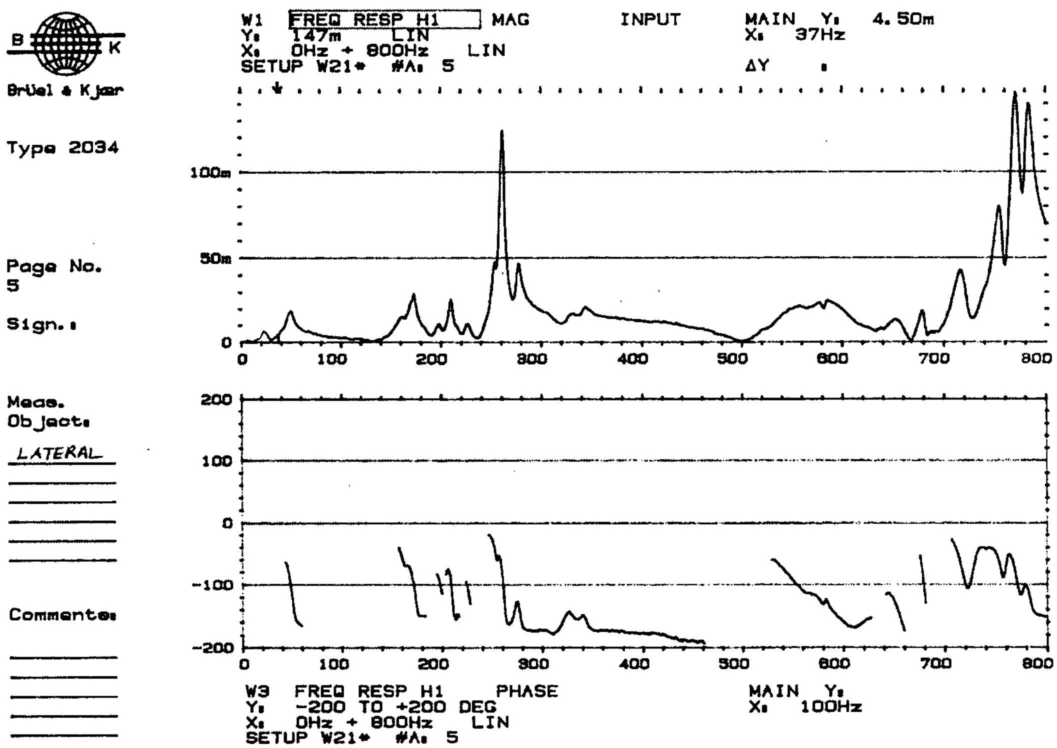

Figure A-2. Transfer function of the pendulum setup in the lateral force direction

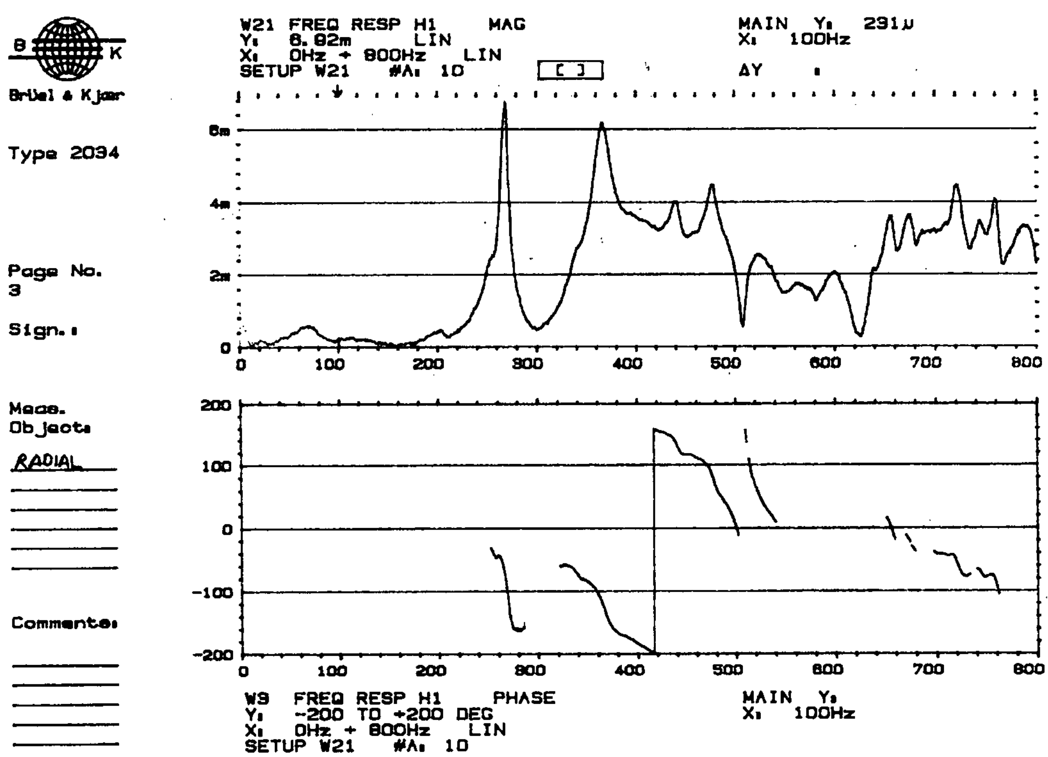

Figure A-3. Transfer function of the pendulum setup in the direction of the feed force

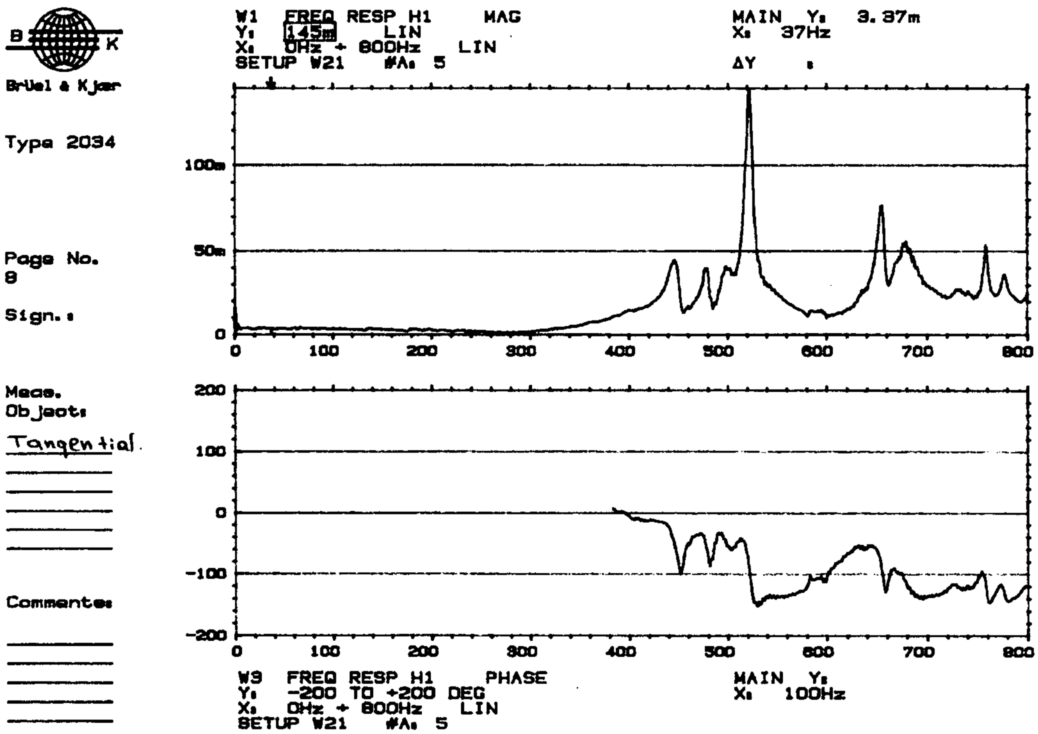

Figure A-4. Transfer function of the pendulum setup in the direction of the main force

Appendix B

Orthogonal Cutting Results

The cutting models developed in this thesis require orthogonal cutting data. The experimental results presented here provide all the information needed in order to validate the models proposed. The convention used for the direction of cutting with respect to the fibers is the one presented in Table 4-3. High-speed steel tools were used for all the tests. The width of cut was 8.4 mm in all cases. The wood species used was Canadian Douglas fir.

B.1. 90-0 Cutting Direction Results

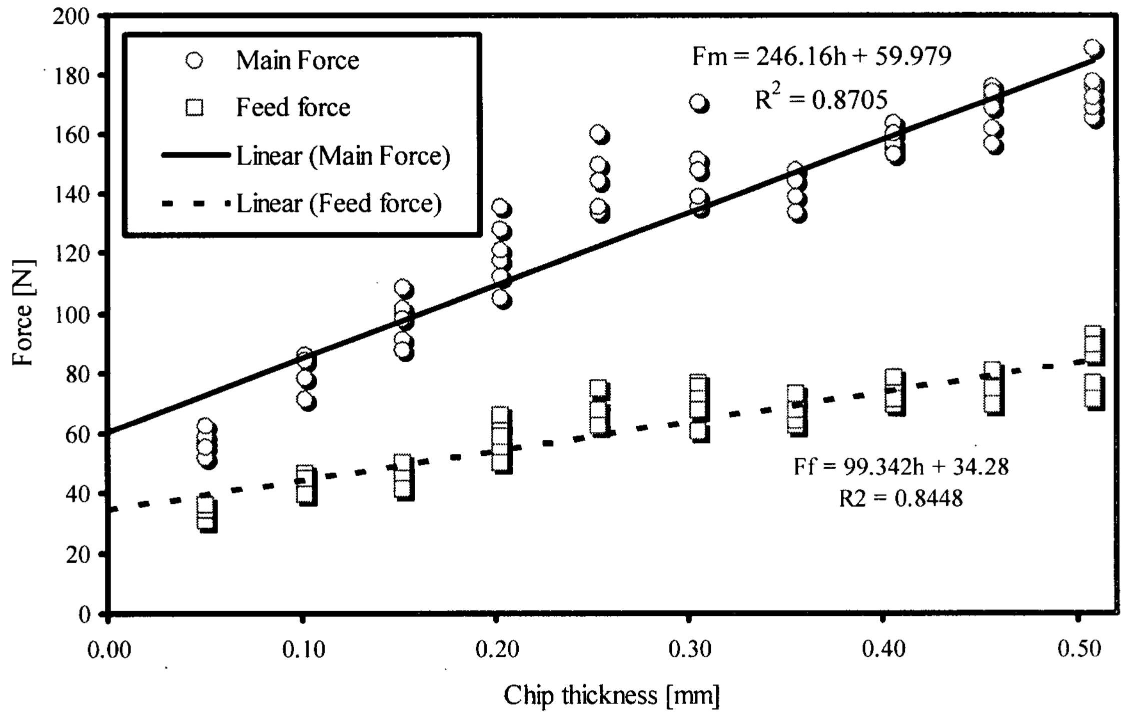

Figure B-1. Forces in orthogonal cutting along the grain.
Saturated Douglas fir. Hook angle = 0 degrees. Width = 8.4 mm.

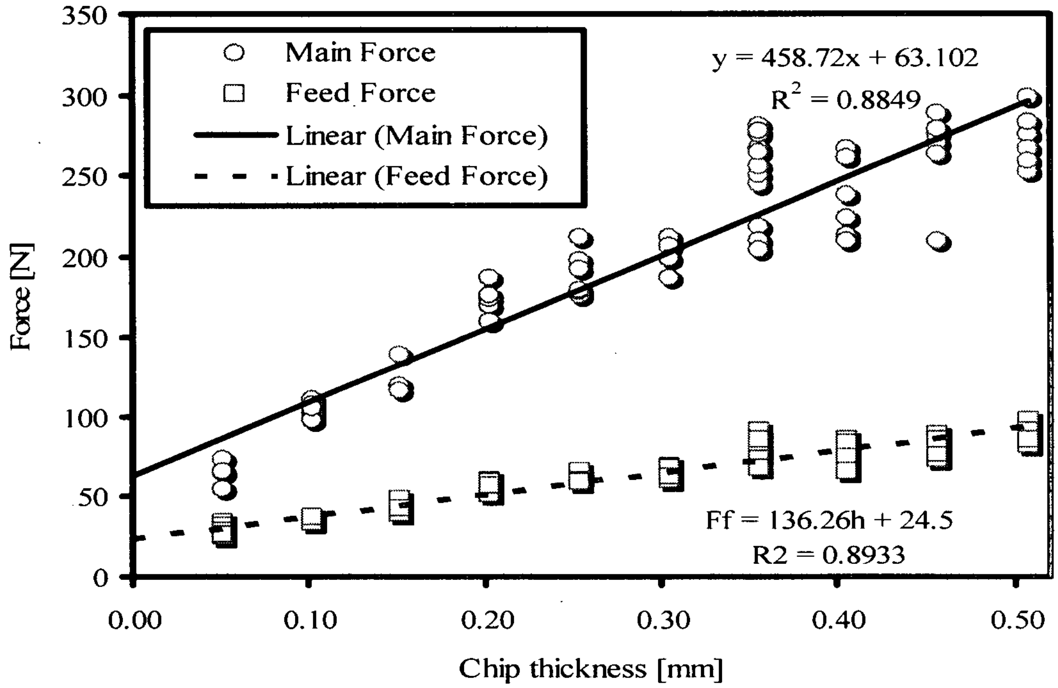

Figure B-2. Forces in orthogonal cutting along the grain.
Dry Douglas fir. Hook angle = 0 degrees. Width = 8.4 mm.

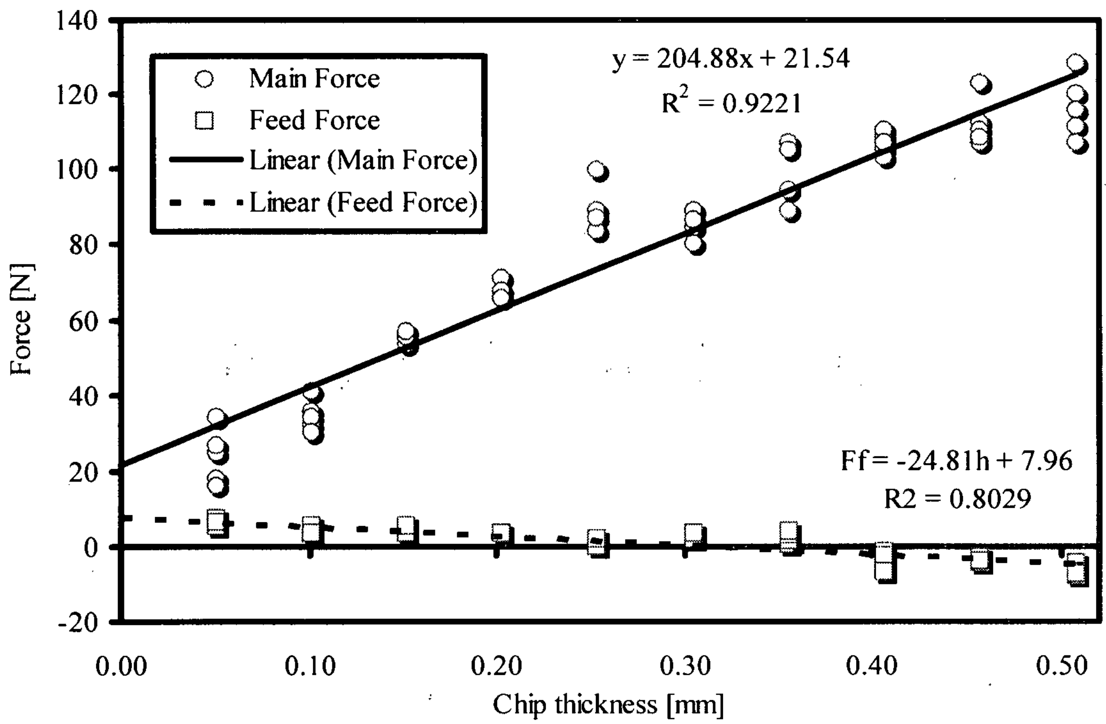

Figure B-3. Forces in orthogonal cutting along the grain.
Saturated Douglas fir. Hook angle = 20 degrees. Width = 8.4 mm.

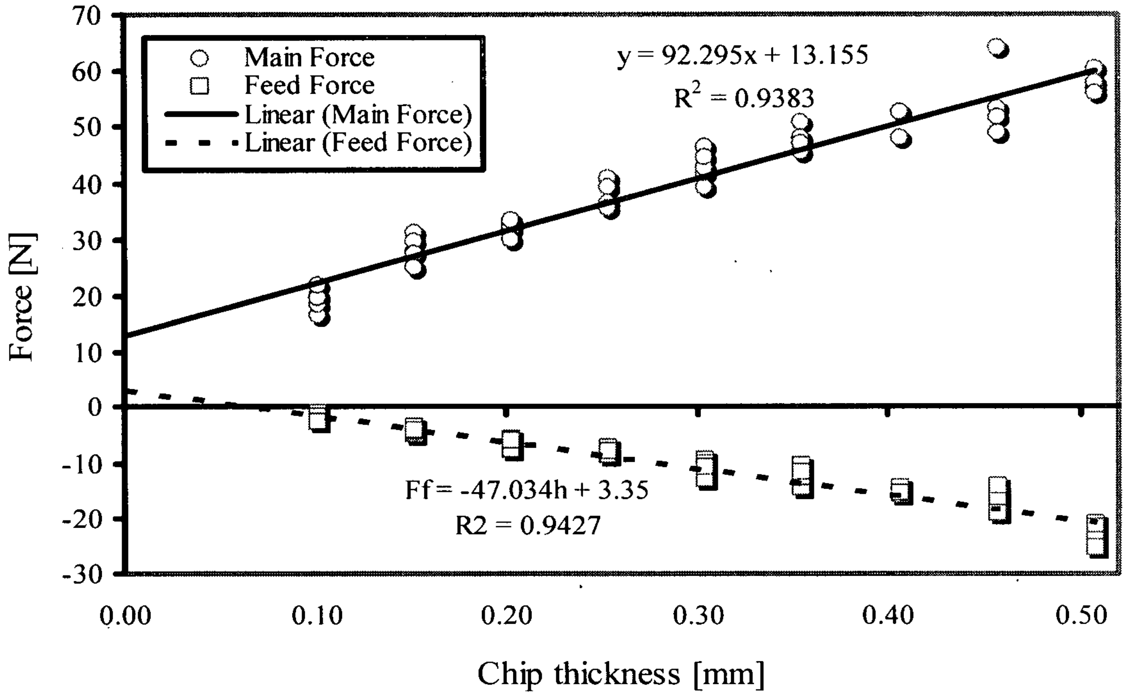

Figure B-4. Forces in orthogonal cutting along the grain.
Saturated Douglas fir. Hook angle = 40 degrees. Width = 8.4 mm.

B.2. 90-90 CUTTING DIRECTION RESULTS

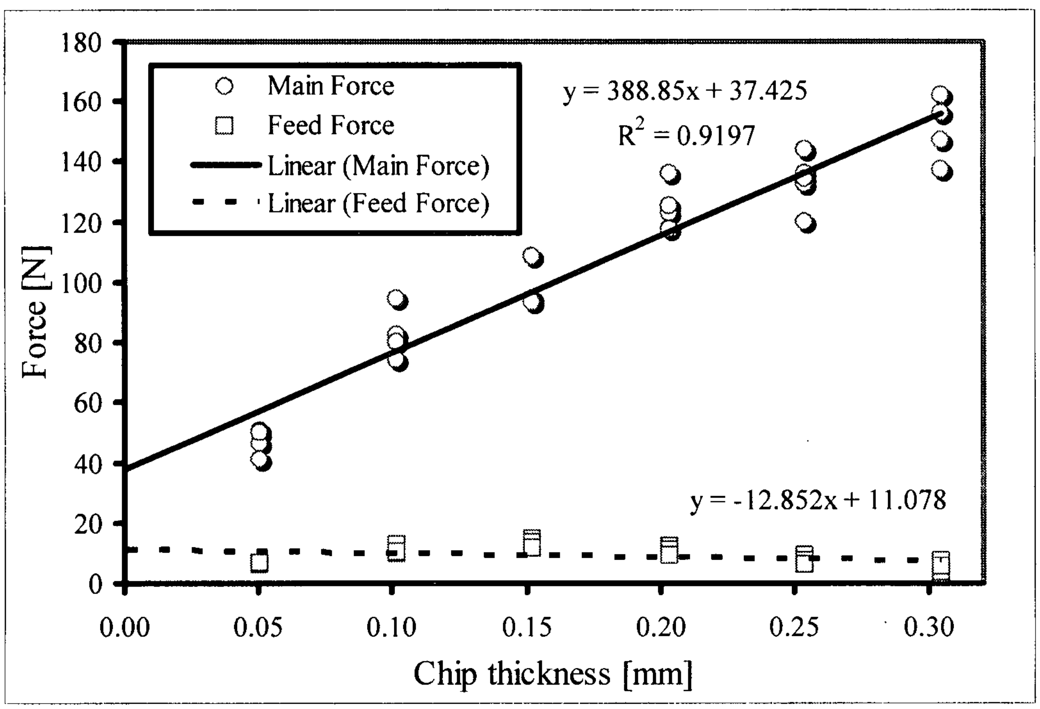

Figure B-5.Forces in orthogonal cutting across the grain.
Saturated Douglas fir. Hook angle = 20 degrees. Width = 8.4 mm.

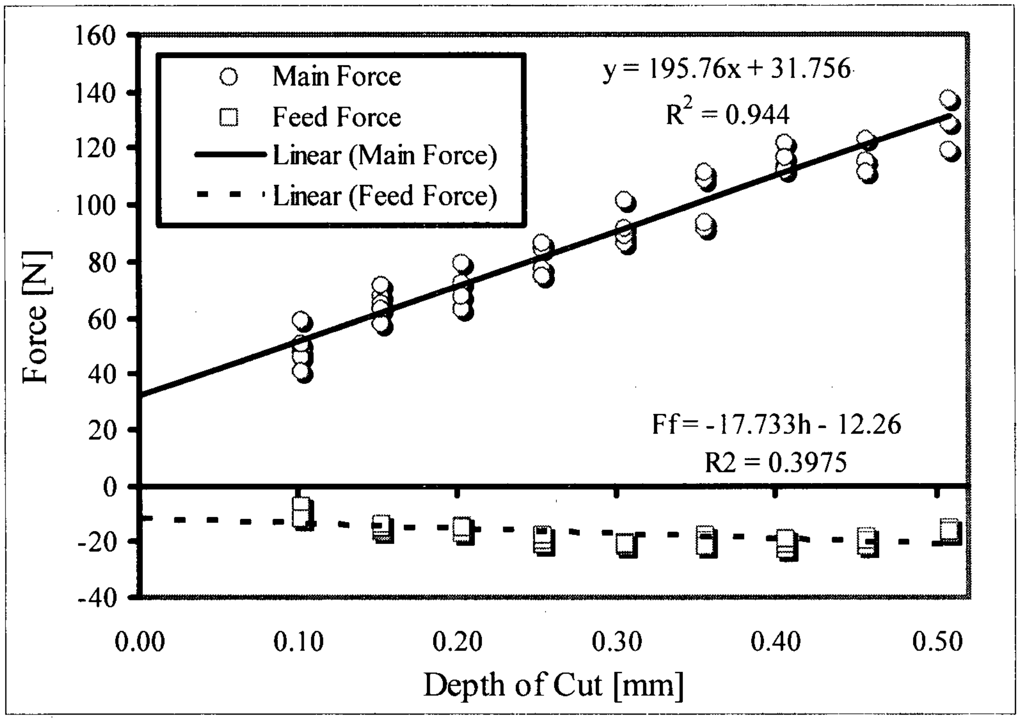

Figure B-6. Forces in orthogonal cutting along the grain.
Saturated Douglas fir. Hook angle = 40 degrees. Width = 8.4 mm.

Appendix C

Single-tooth Experimental Cutting Force Results

C.1. 90-90 Cutting Direction

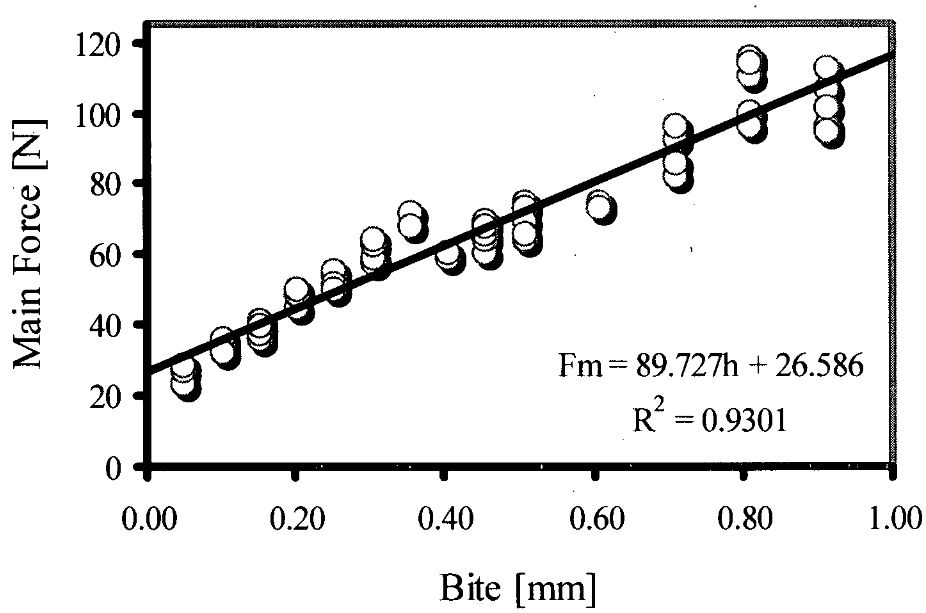

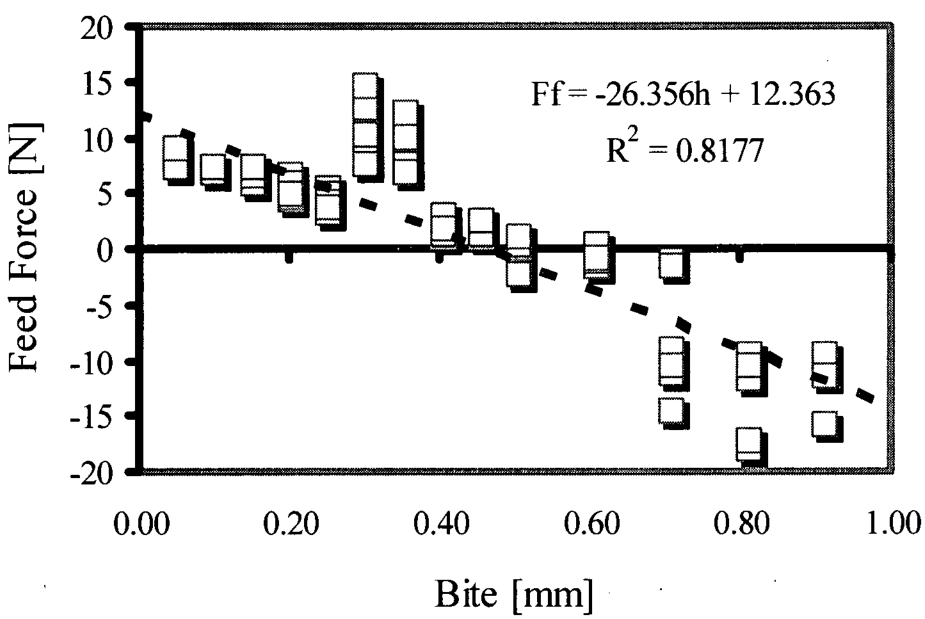

Figure C-1 (a). Cutting forces in a bandsaw tooth. Saturated Douglas fir

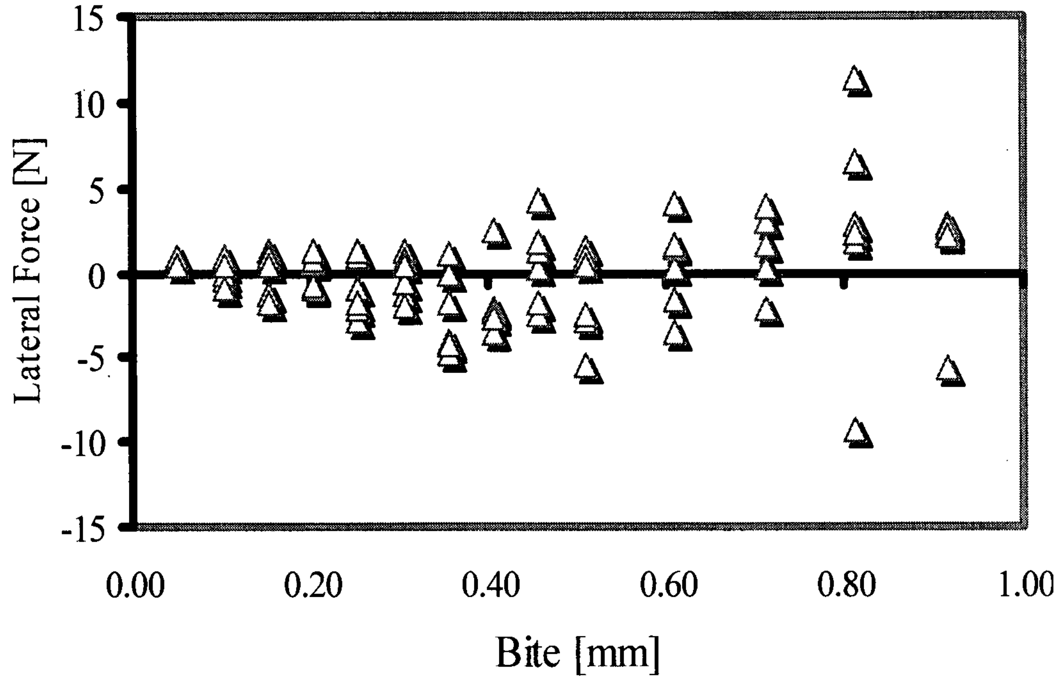

Figure C-1 (b). Cutting forces in a bandsaw tooth. Saturated Douglas fir

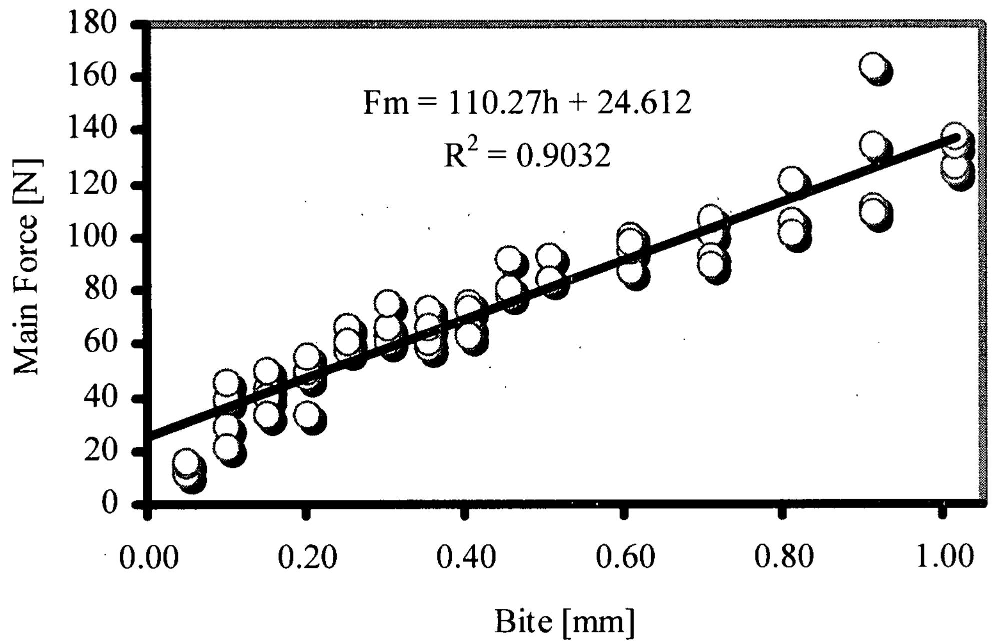

Figure C-2 (a). Cutting forces in a bandsaw tooth. Dry Douglas fir

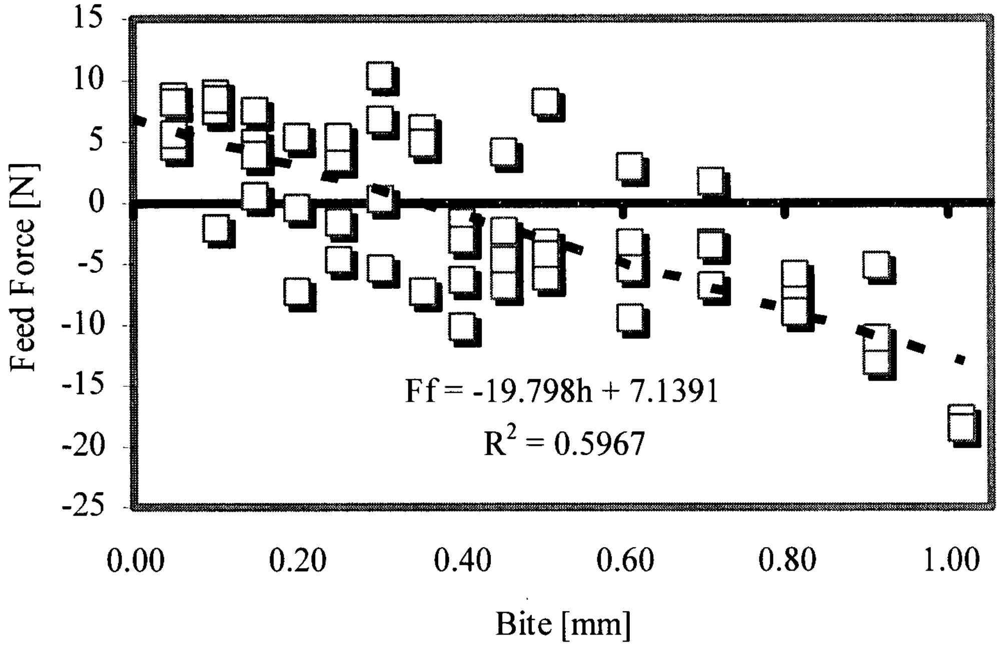

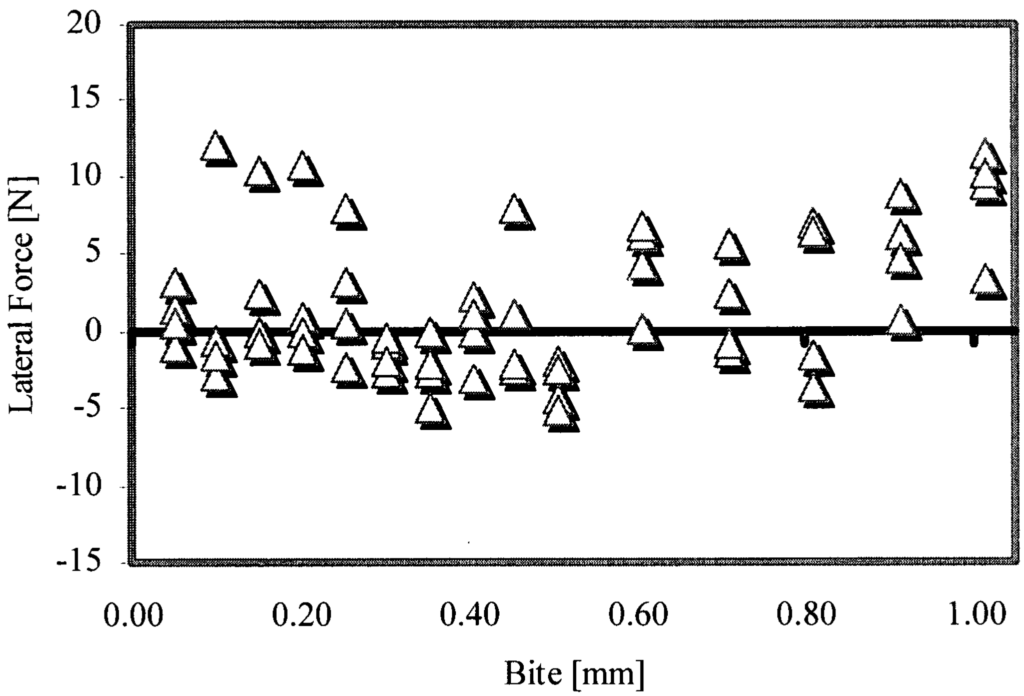

Figure C-2 (b). Cutting forces in a bandsaw tooth. Dry Douglas fir

C.2. 90-0 Cutting Direction

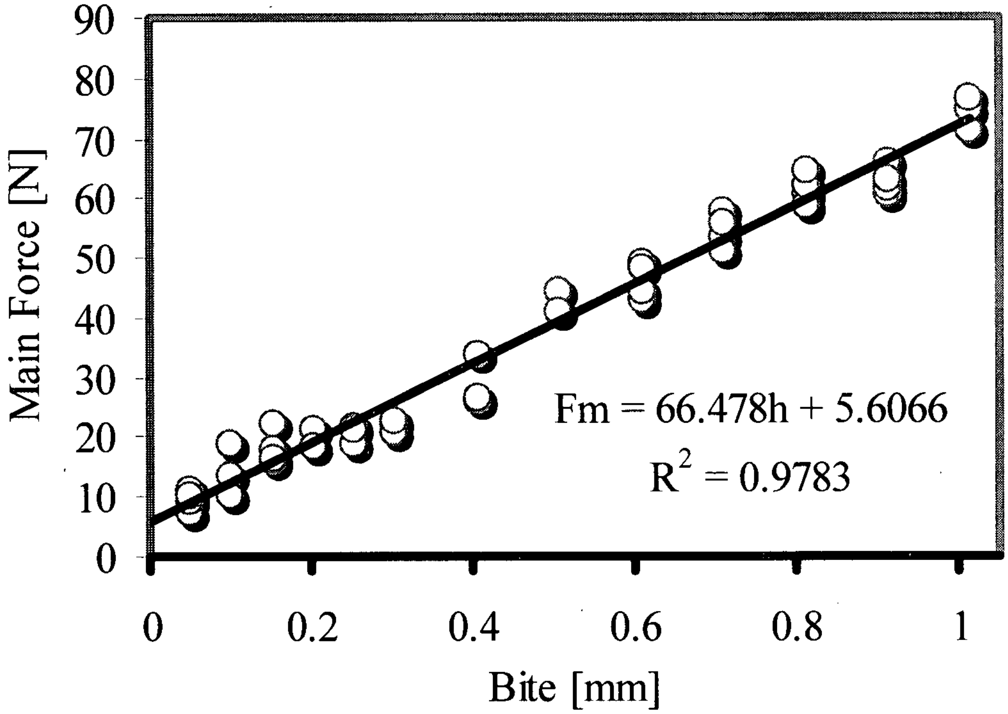

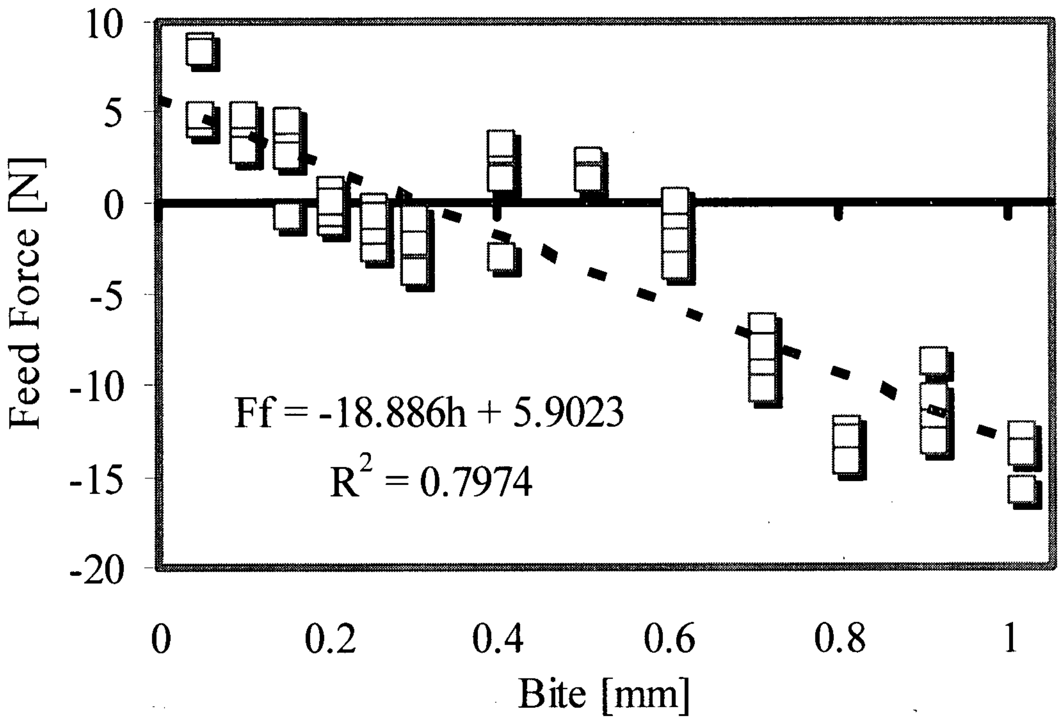

Figure C-3 (a). Cutting forces in a bandsaw tooth. Saturated Douglas fir

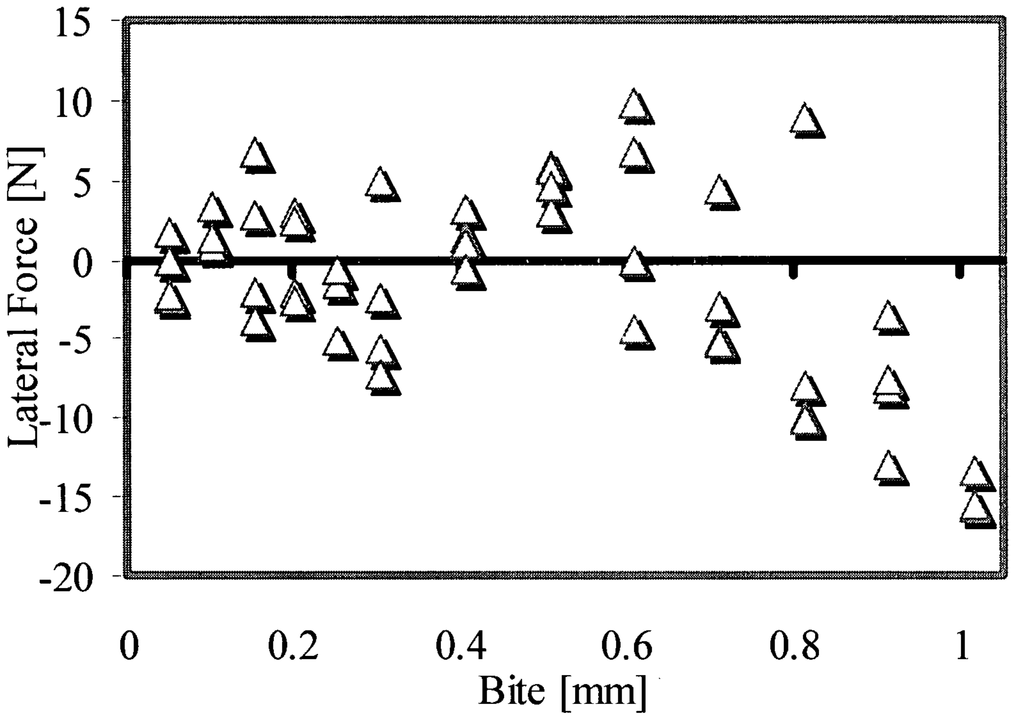

Figure C-3 (b). Cutting forces in a bandsaw tooth. Saturated Douglas fir

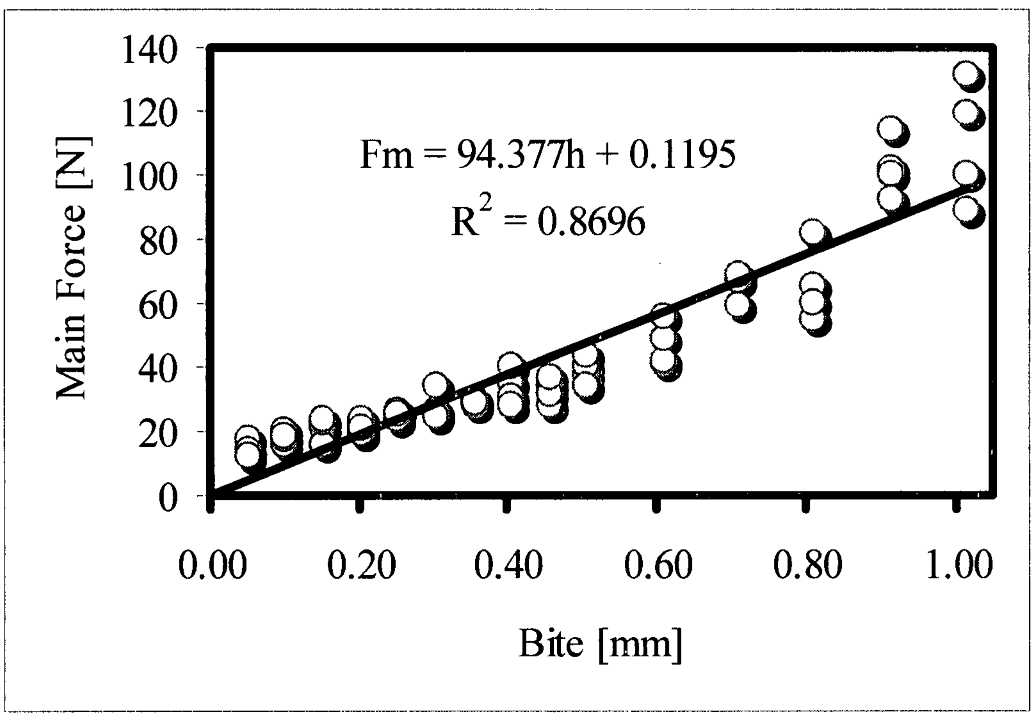

Figure C-4 (a). Cutting forces in a bandsaw tooth. Dry Douglas fir

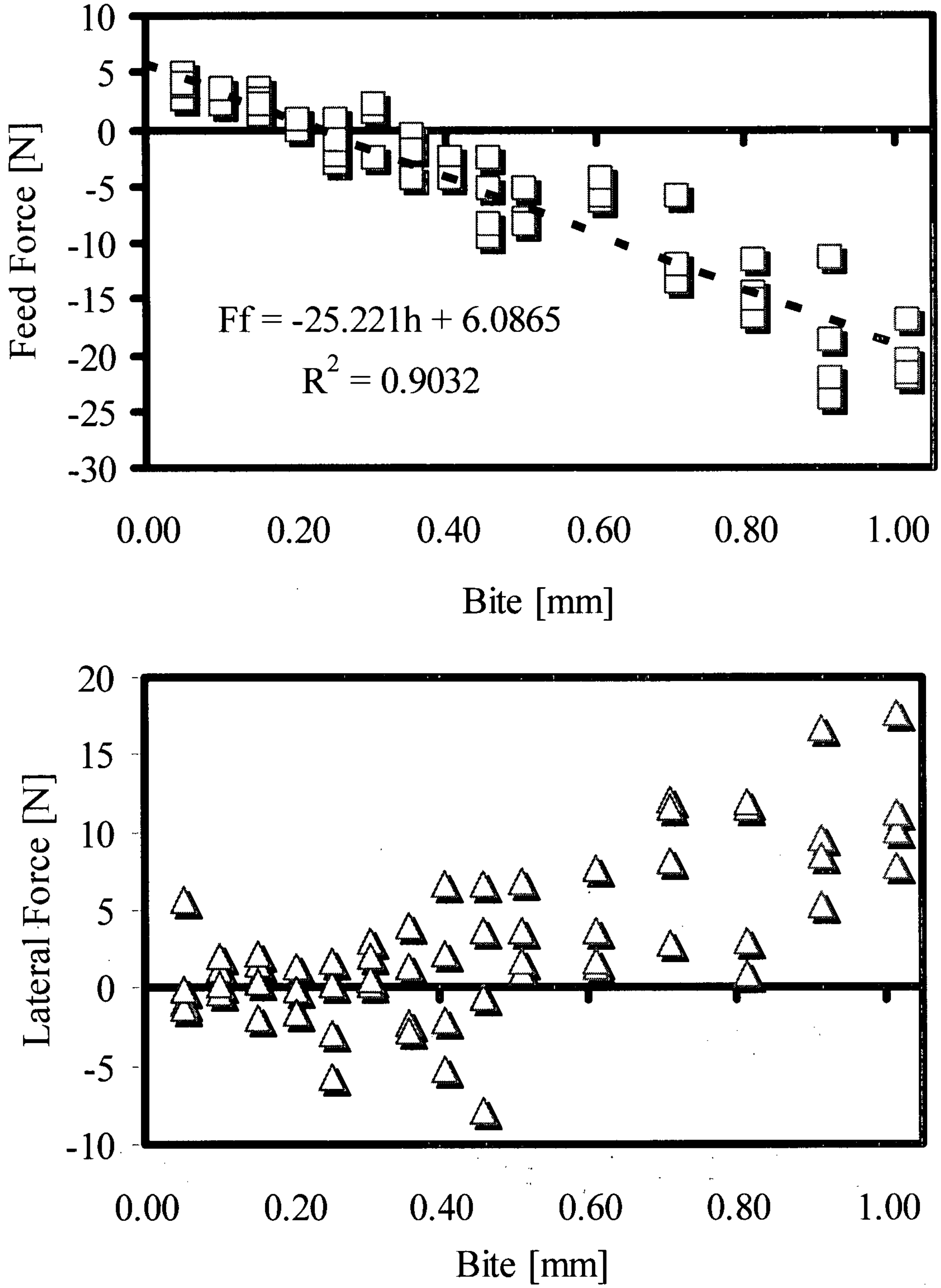

Figure C-4 (b). Cutting forces in a bandsaw tooth. Dry Douglas fir

C.3. 0-90 Cutting Direction

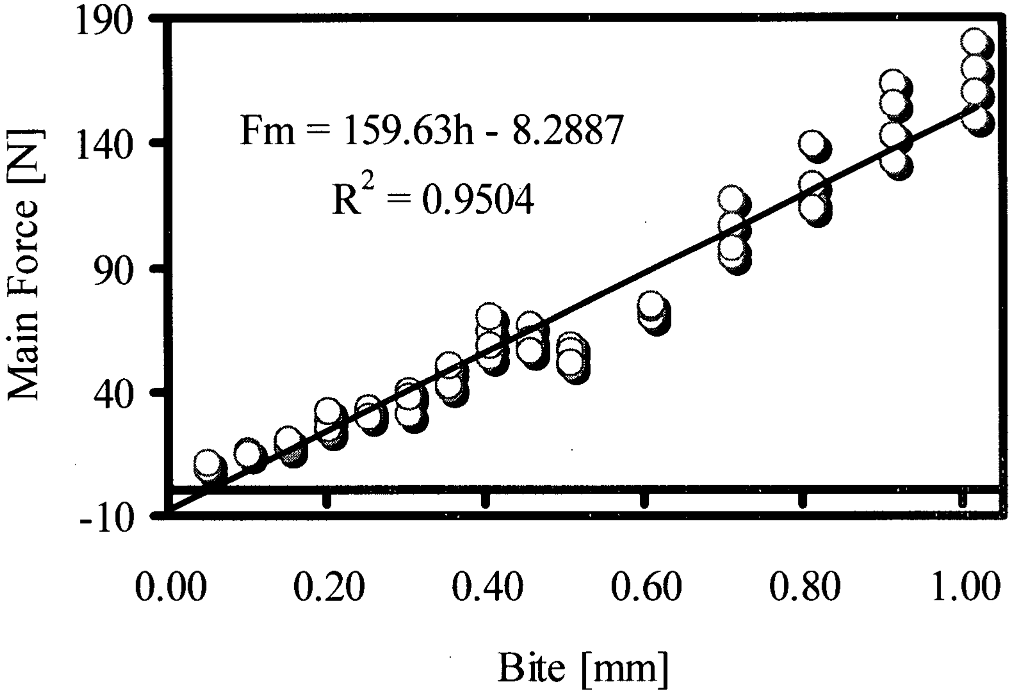

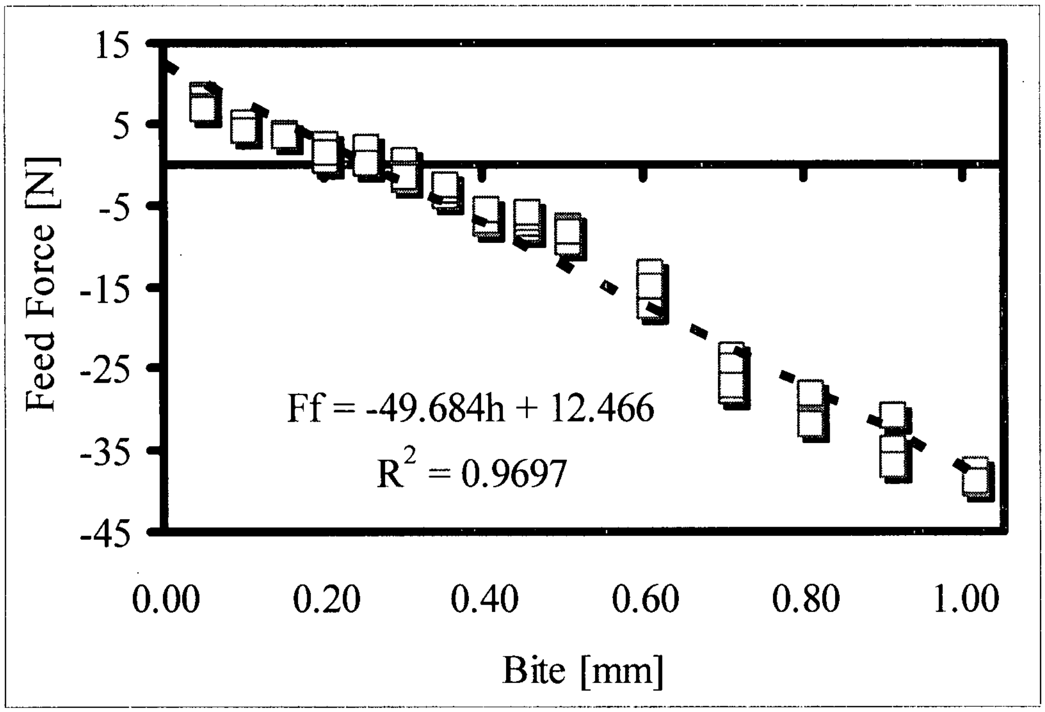

Figure C-5 (a). Cutting forces in a bandsaw tooth. Saturated Douglas fir

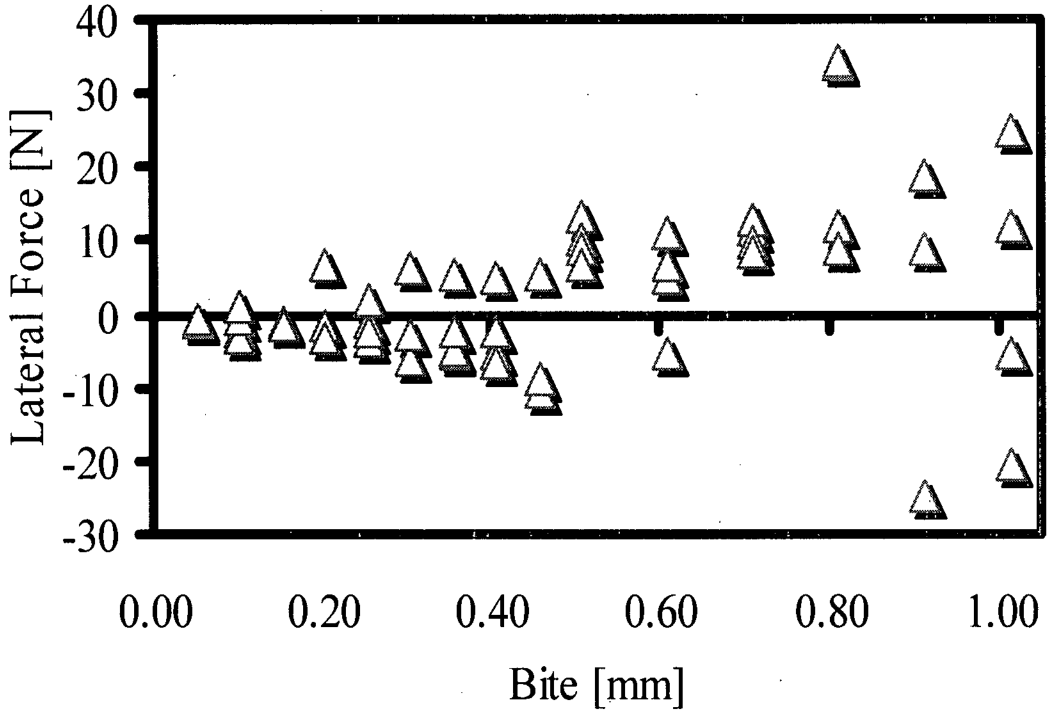

Figure C-5 (b). Cutting forces in a bandsaw tooth. Saturated Douglas Fir.

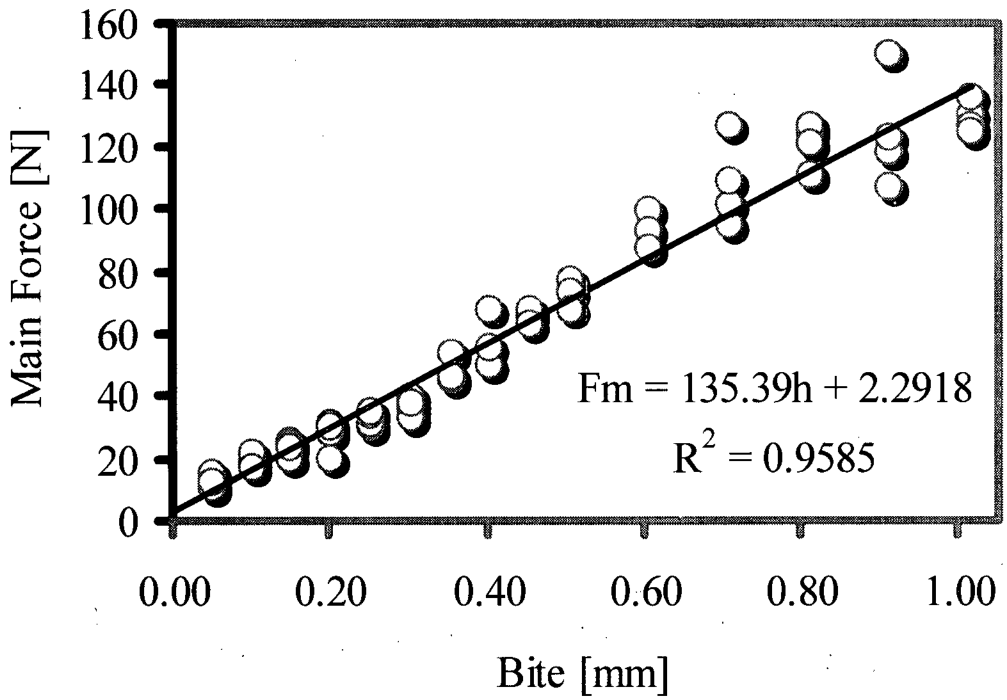

Figure C-6 (a). Cutting forces in a bandsaw tooth. Dry Douglas fir

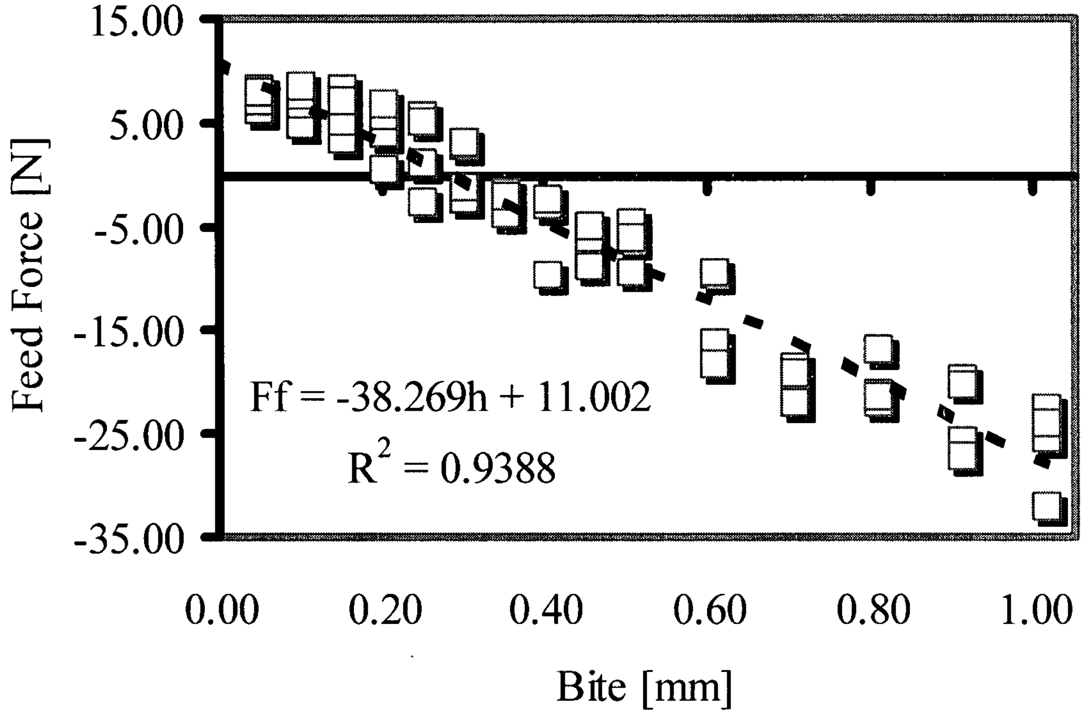

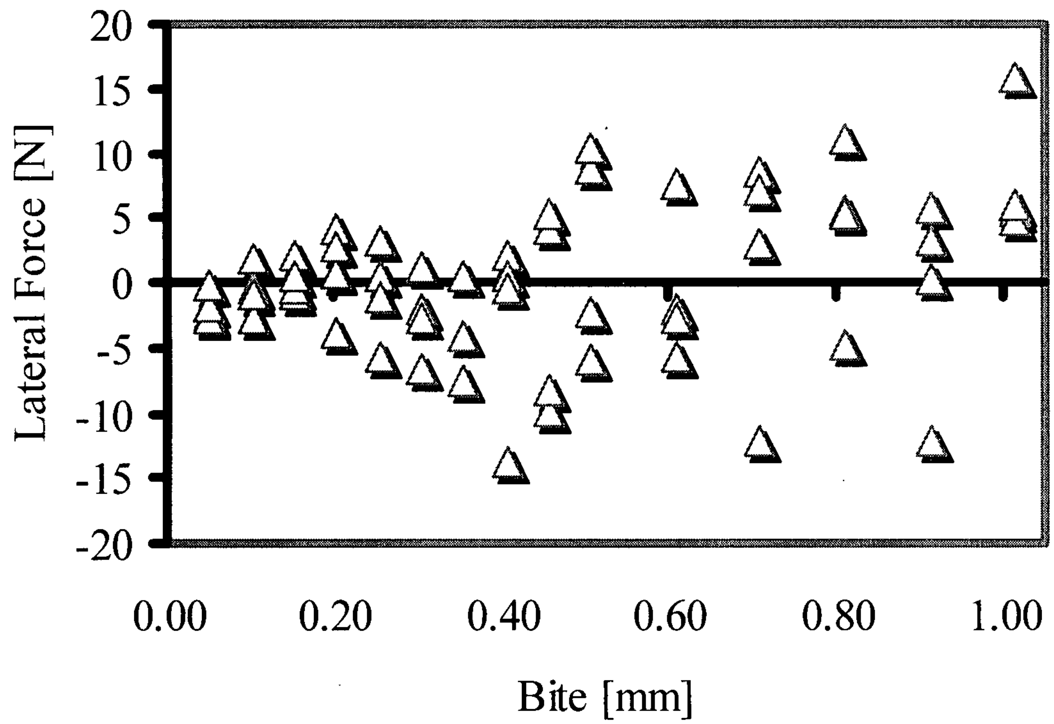

Figure C-6 (b). Cutting forces in a bandsaw tooth. Dry Douglas fir

Appendix D

Two-Edge Cutting Force Measurements for a Non-zero Hook angle

The results presented in this appendix were obtained using the procedure and apparatus described in chapter 4. This data is provided as reference for future research.

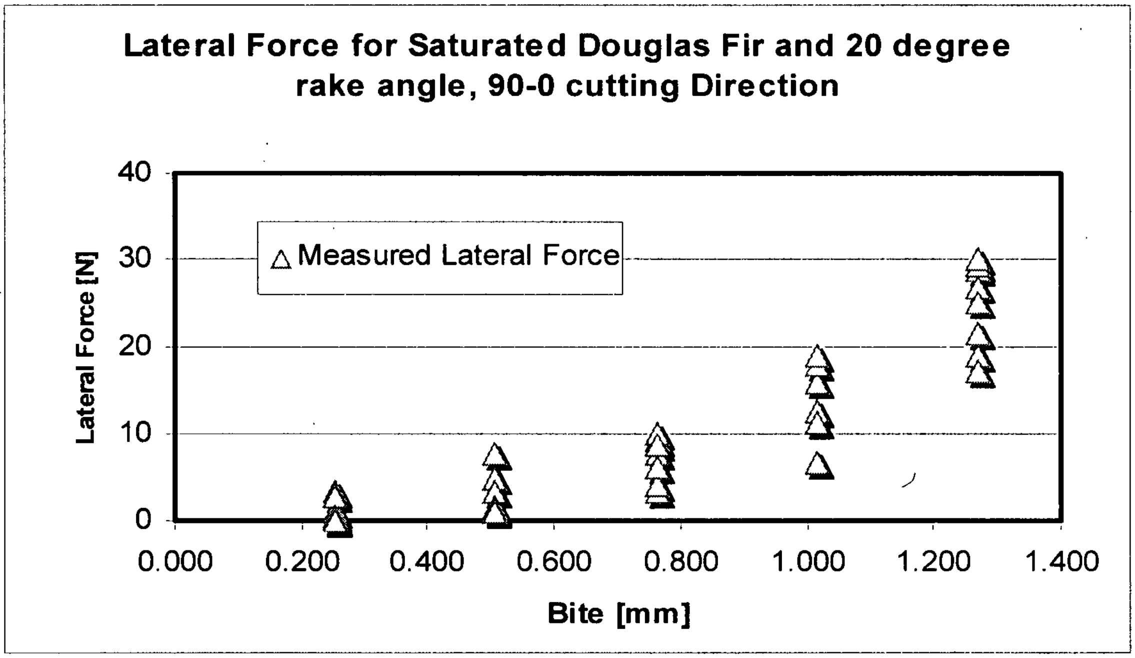

Figure D-1. Two-edge lateral cutting force for cutting in the 90-0 direction.
Tool hook angle = 20 degrees

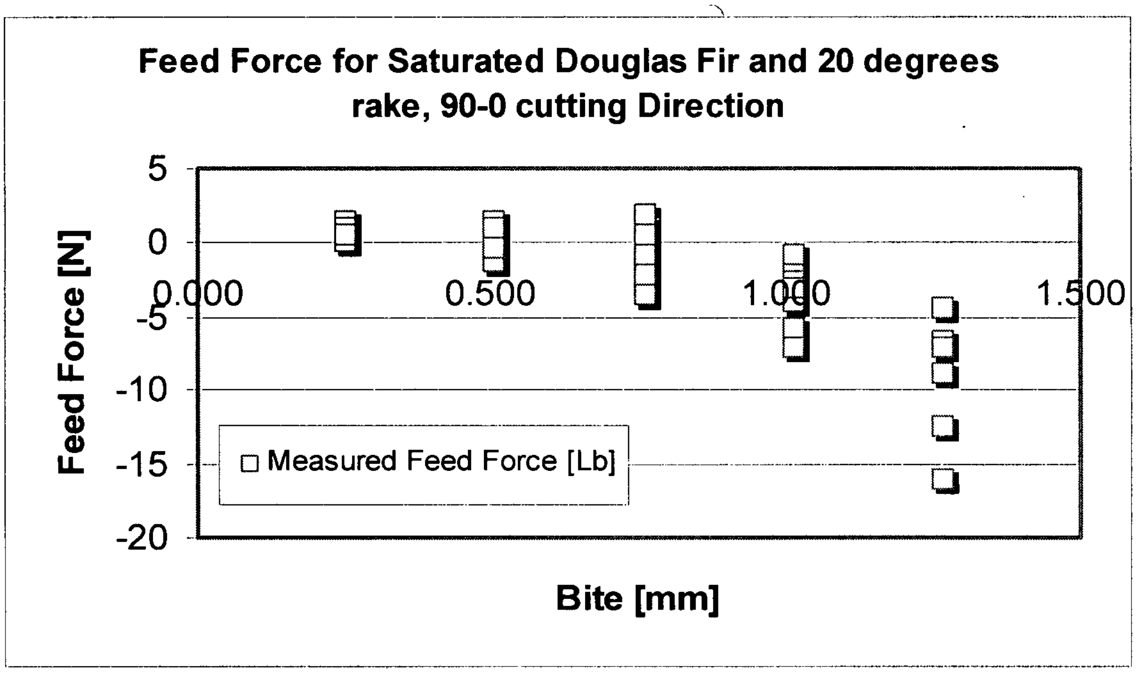

Figure D-2. Two-edge feed cutting force for cutting in the 90-0 direction.
Tool hook angle = 20 degrees

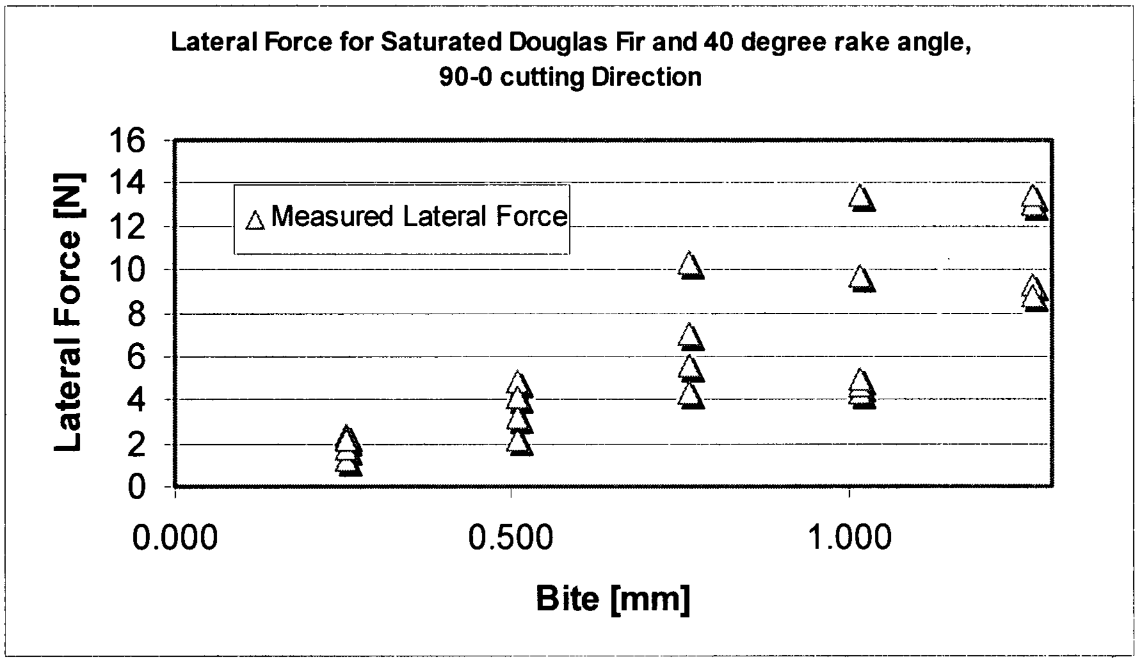

Figure D-3. Two-edge lateral cutting force for cutting in the 90-0 direction.
Tool hook angle = 40 degrees

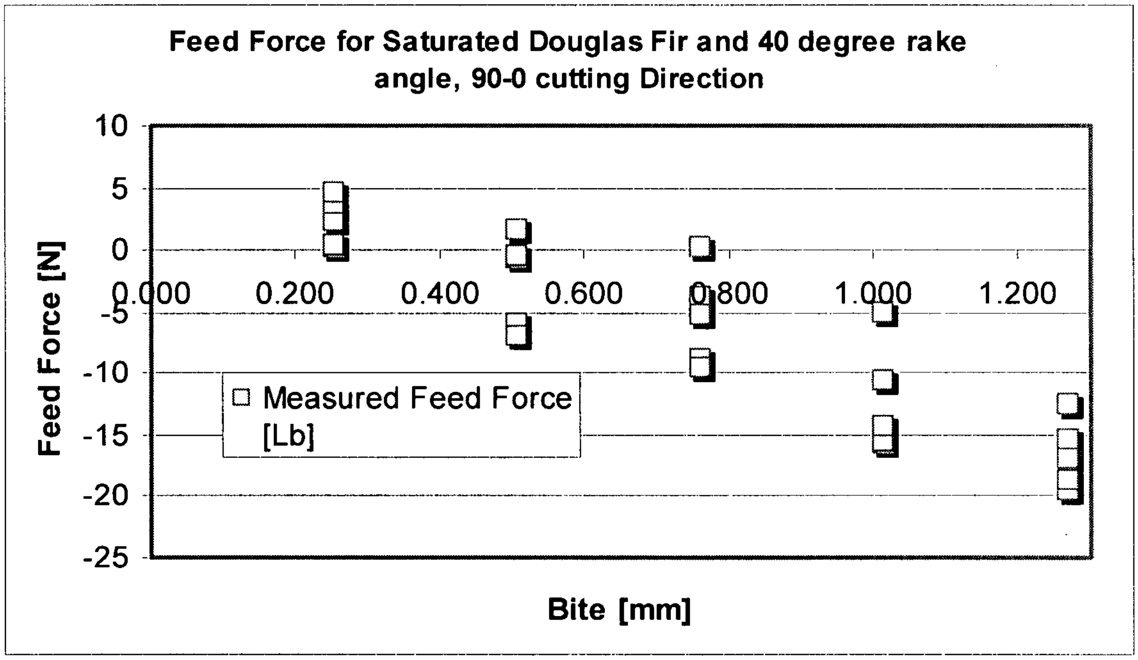

Figure D-4. Two-edge feed cutting force for cutting in the 90-0 direction.

Tool hook angle = 40 degrees

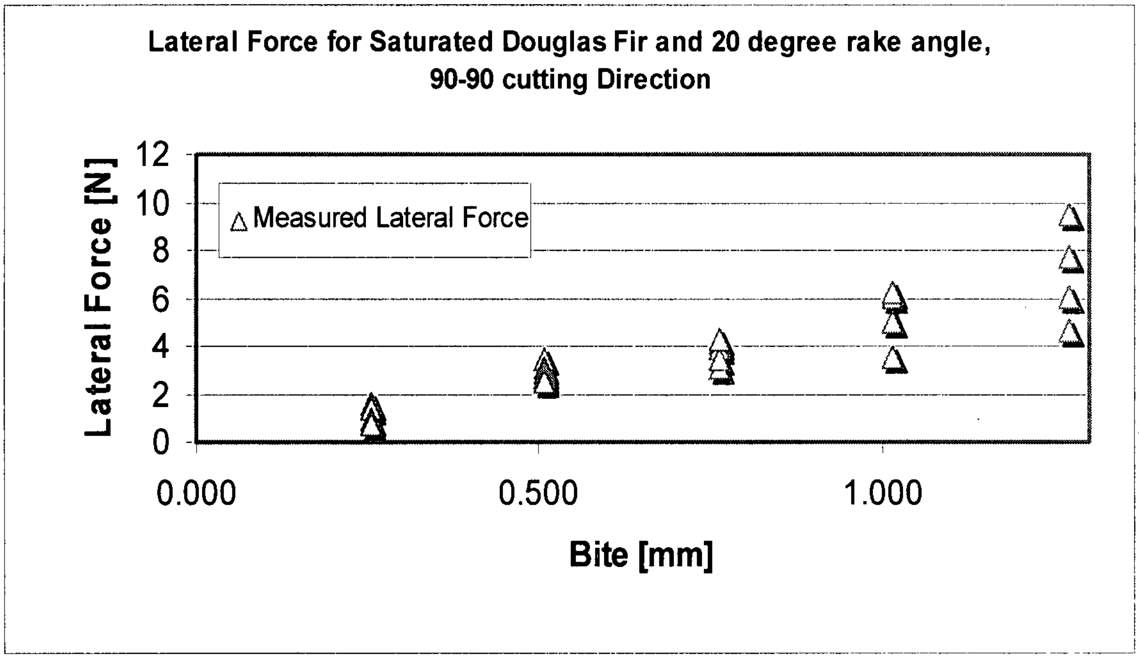

Figure D-5. Two-edge lateral cutting force for cutting in the 90-90 direction.

Tool hook angle = 20 degrees

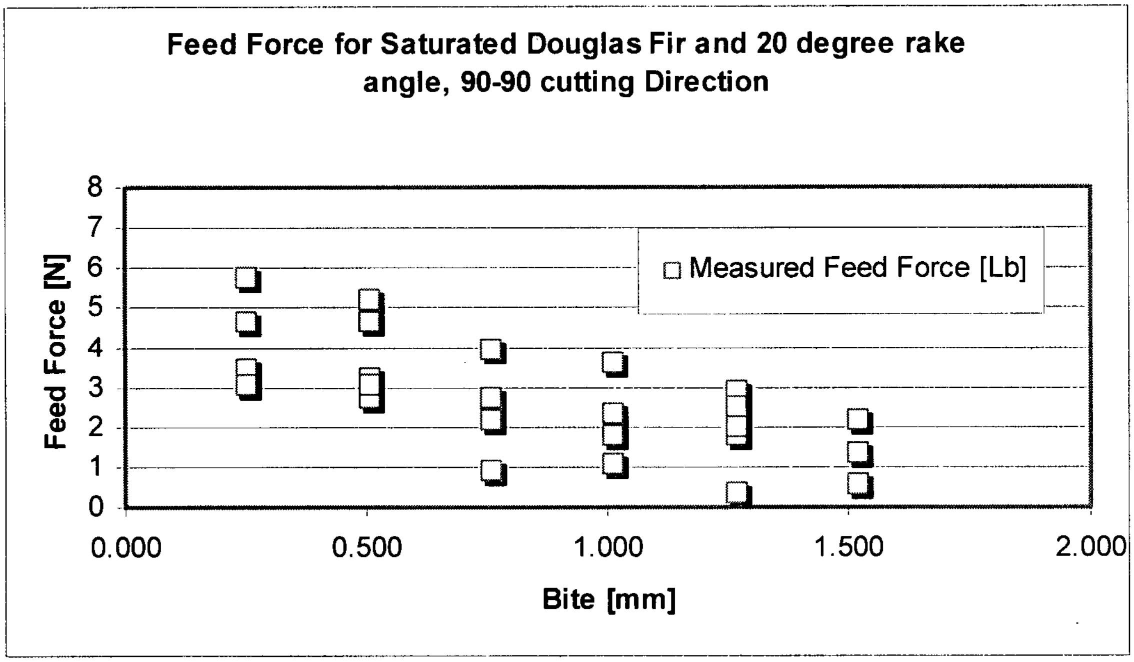

Figure D-6. Two-edge feed cutting force for cutting in the 90-90 direction.

Tool hook angle = 20 degrees

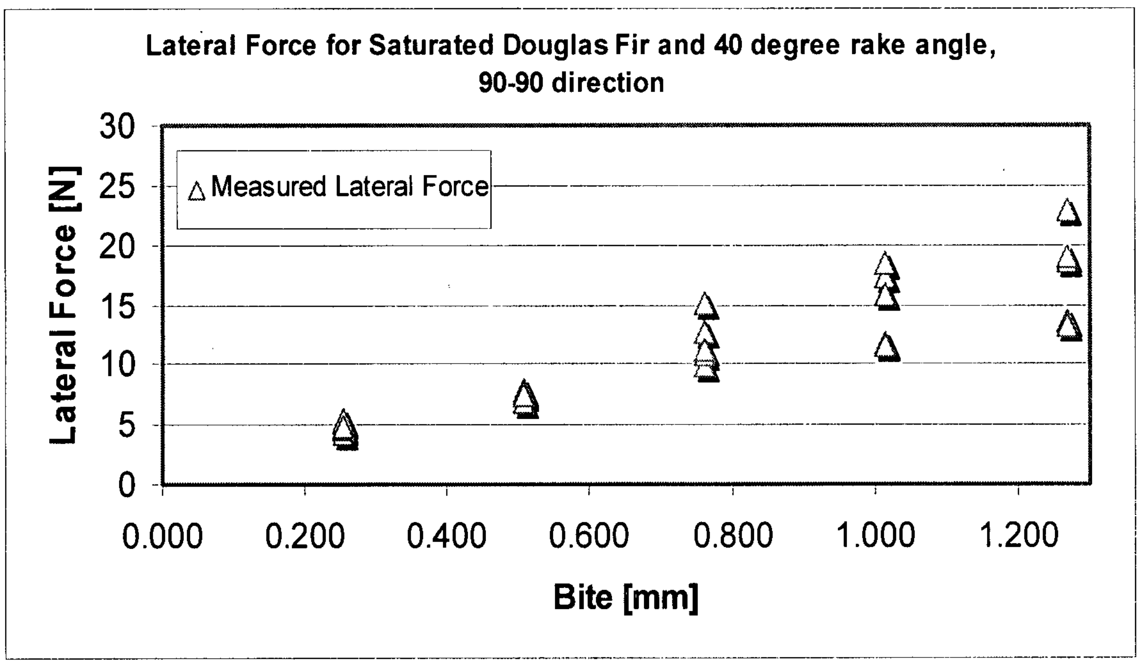

Figure D-7. Two-edge lateral cutting force for cutting in the 90-90 direction.

Tool hook angle = 40 degrees

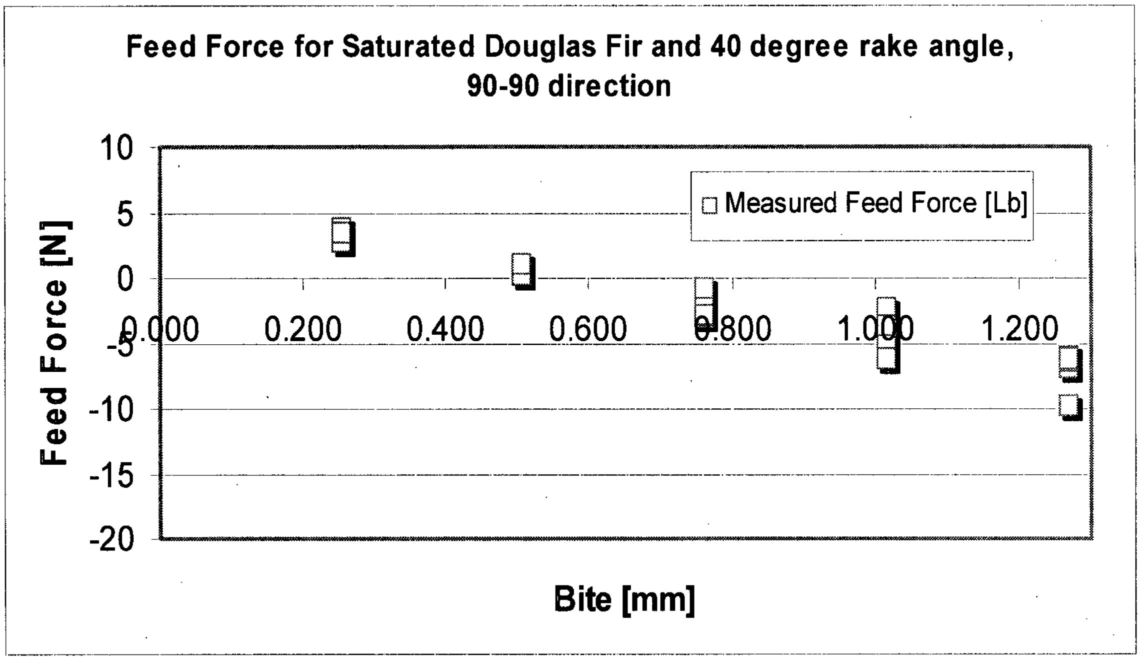

Figure D-8. Two-edge feed cutting force for cutting in the 90-90 direction.

Tool hook angle = 40 degrees

Appendix E

Influence of growth rings and knots in the cutting forces

E.I. Cutting Forces in Growth Rings

One observation made during the cutting experiments is that there is a strong oscillating force component at the ring passing frequency. This finding was made when setting up experiments on a milling machine at low speeds of cut (50 mm/sec). It was noticed that during the cutting, the main force peaks every time the tool cuts one of the dark rings on a sample as shown in the following figure. These two types of ring are known *as "early wood"* and *"late wood"*. The former presents a lighter color than the latter one.

The ring passing frequency in the bandsawing process is usually of higher order than the tooth passing frequency. There are usually between 3 and 20 rings between two consecutive teeth in a bandsaw (one pitch).

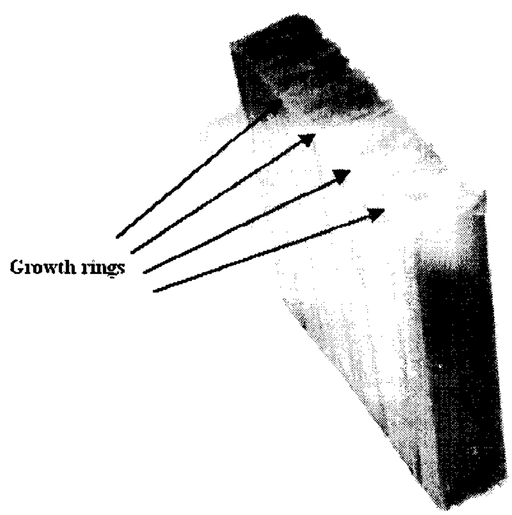

Figure E-1. Position of the growth rings on a wood sample

The orthogonal cutting forces measured on a sample with four growth rings are shown in the following two plots. Two different tools were used in the cuts, a 20-degree positive rake angle tool and a 40-degree rake tool.

It can be seen that the main force on the tool has a harmonic component at the ring passing frequency with amplitude of 150 Newton. Also, it can be seen that the lateral force has the same frequency content of the main force but presents small amplitude of about 10 Newton. The feed force presents a different behavior than the main and lateral forces. Its frequency content seems to be about three times that of the ring passing frequency. There is no explanation available at this point for this difference.

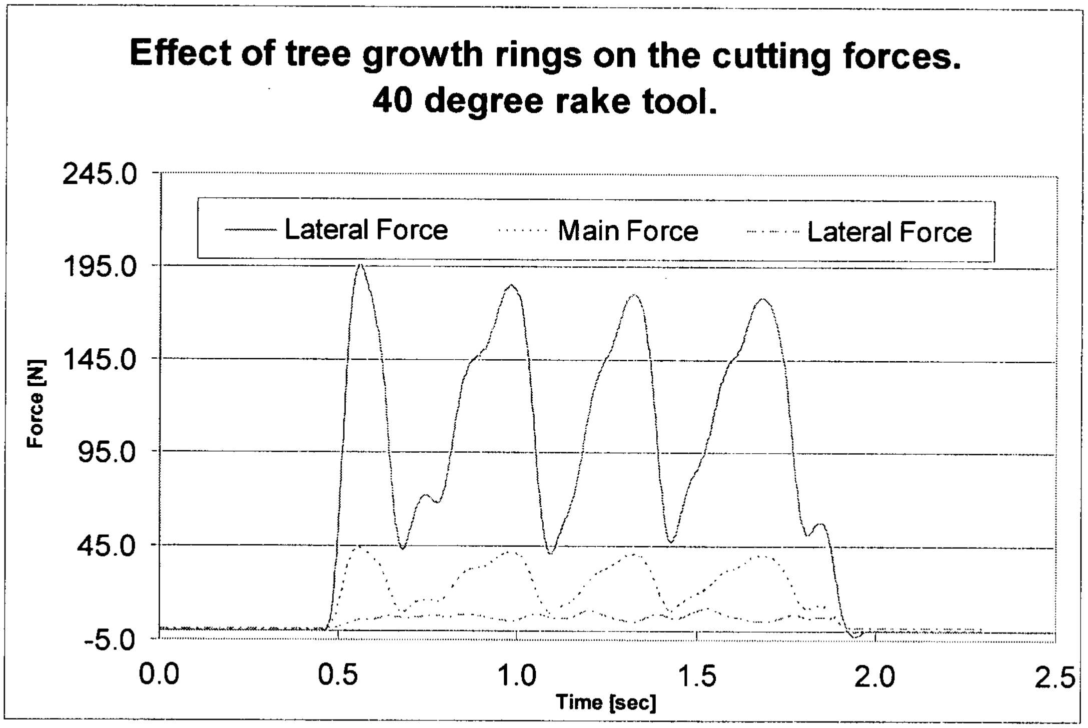

Figure E-2. Orthogonal cutting forces for 0.010" chip thickness, Dry Douglas fir, 90-90 cutting direction, four growth rings, 40^0 rake HSS tool

There is no experimental evidence that the washboarding problem is dependent on the characteristics of the rings on the workpiece being cut. Nevertheless, this experiment shows that the excitation forces in wood machining processes are dependent on issues such as the growth process of the tree originally cut and that the magnitude of these oscillations is large compared to the peak values of the forces.

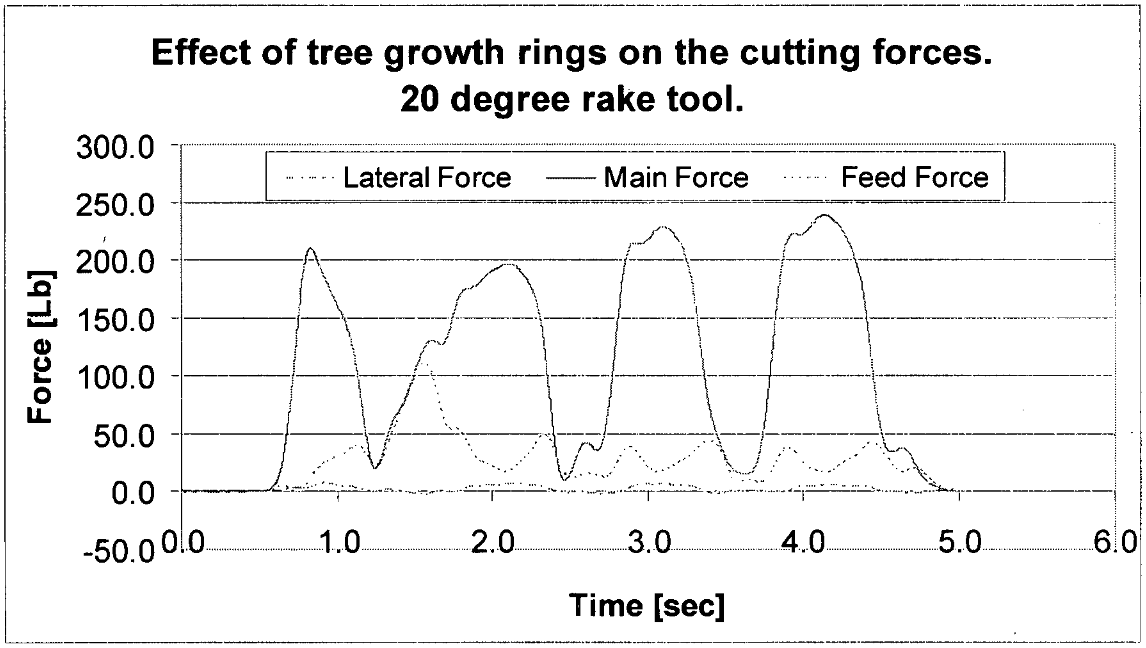

Figure E-3. Orthogonal cutting forces for 0.010" chip thickness, Dry Douglas fir, 90-90 cutting direction, four growth rings, 20^{O} rake HSS tool

E.2. Cutting forces in Knots

St. Laurent [30] examined the effect of knots on the cutting forces. In his experiments, a single tooth was mounted on a 3D force dynamometer. The three forces were recorded while a block of wood was pushed onto the wood cutting near or through a knot. For softwoods the average lateral force was about 20-30% of the tangential force in the surrounding clear wood, which corresponds to a value of force between 15 and 40 Newton. Also, in previous research in washboarding, evidence has been found that the lateral vibration response of the blade increases when a knot is cut.

The objective of the experiment presented here is to measure the process stiffness during cutting of a knot under simulated bandsawing conditions. For this purpose, two samples with knots were cut with the same saw tooth described on section 3.2 of this chapter. The bite was increased between cuts and the forces measured to obtain a series of plots similar to those in section 3.2. It was checked that the tooth was cutting through the knot for all the points where the forces were recorded.

The following figure shows a sample containing a knot that was used in the experiment.

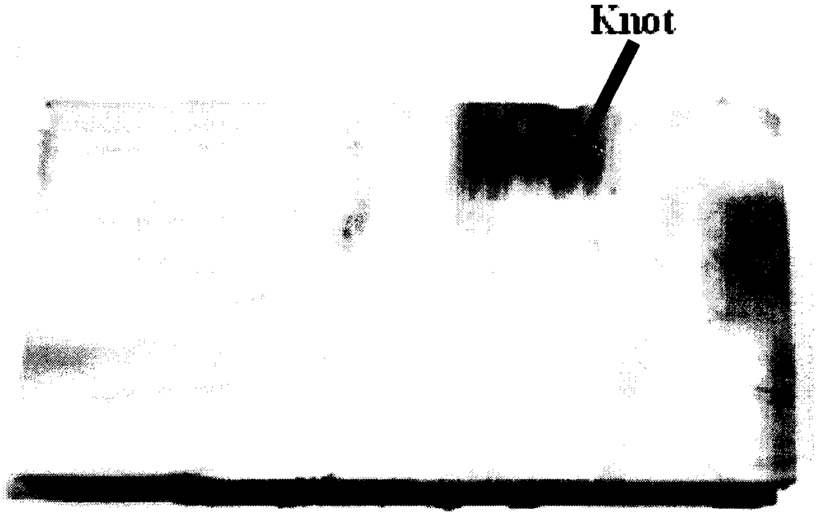

Figure E-4. Wood Sample containing a Knot used for experiments

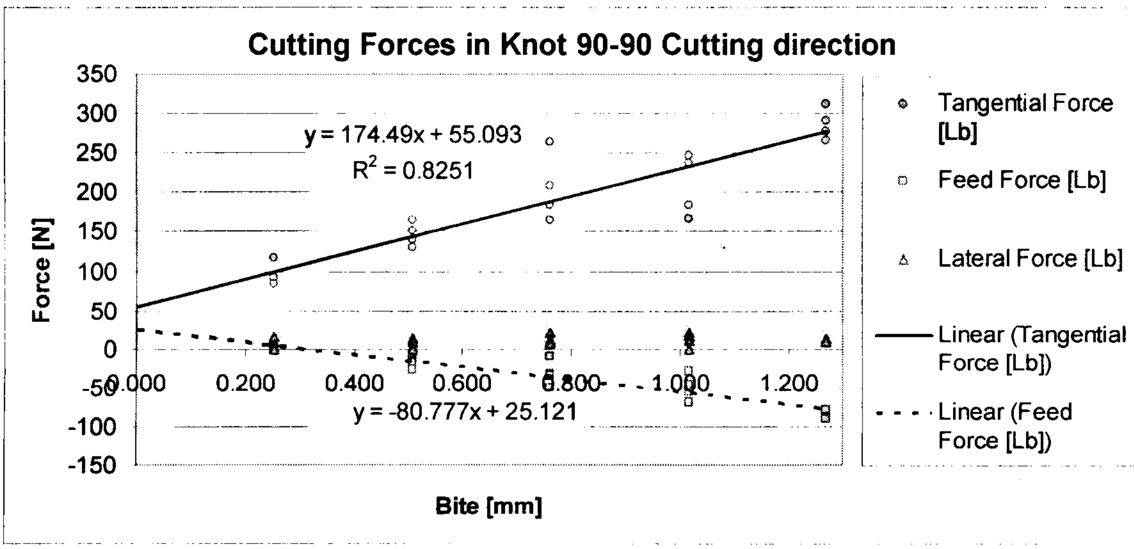

Figure E-5. Main and Feed cutting forces in knot #1, 90-90 direction, dry Douglas fir

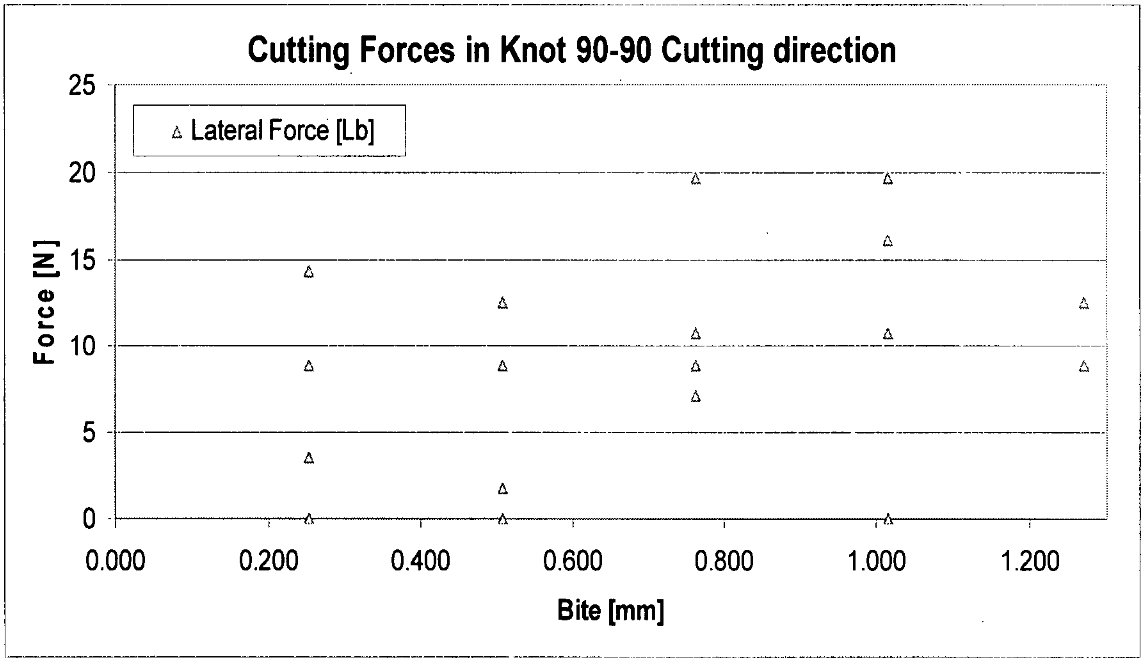

Figure E-6. Lateral cutting forces in knot #1, 90-90 direction, dry Douglas fir

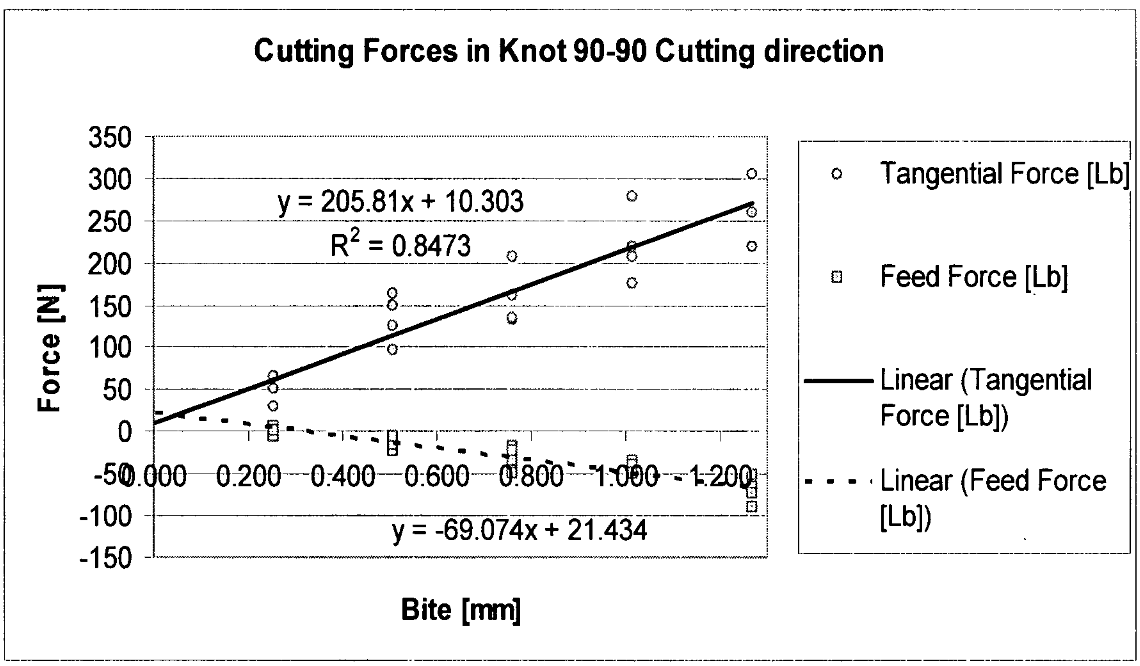

Figure E-7. Main and Feed cutting forces in knot #2, 90-90 direction, dry Douglas fir

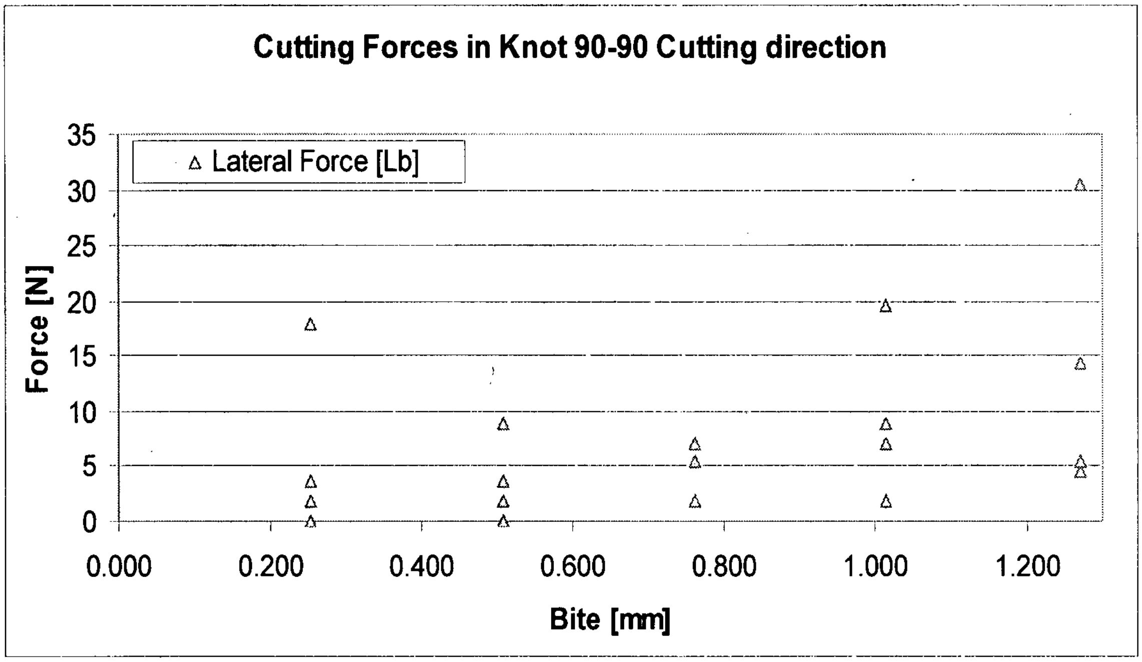

Figure E-8. Lateral cutting forces in knot #2, 90-90 direction, dry Douglas fir

Figures 3.19 and 3.20 were obtained under the same conditions as figure 3.11 in section 3.2 except for the presence of the knot in the sample. It can be seen that the process stiffness for the main force is 85% higher in Figure 3.21 than in the same experiment without the knot. The feed force increased 235%. For the second knot cut, the main force increased 57% and the feed force 292%.

This experiment does not provide evidence that cutting a knot increases the lateral forces. This is probably due to the fact that the chip load on both sides of the tooth was still balanced so even if the material being cut is harder, the net lateral force is still small. It is expected that the lateral forces would be much higher when cutting a knot if the tooth has any defects or if the alignment of consecutive teeth is not perfect.